UNIVERSIDADE NOVA DE LISBOA

Faculdade de Ciências e Tecnologia

CHEMICAL REACTION NETWORK OF FLAVYLIUM IONS IN HETEROGENEOUS MEDIA

RAQUEL GOMES

Dissertação apresentada para a obtenção do Grau de Doutor em Química, especialidade em Química-Física, pela Universidade Nova de Lisboa, Faculdade de Ciências e Tecnologia

Supervisor: Professor Doutor Fernando Pina

Co-supervisor: Professor Doutor A. Jorge Parola

LISBOA

2009

To my parents
Aos meus pais

"*O que a vida apresenta de pior não é a violenta catástrofe, mas a monotonia dos momentos semelhantes; numa ou se morre ou se vence, na outra verás que o maior número nem venceu nem morreu: flutua sem norte e sem esperança. Não te deixes derrubar pela insignificância dos pequenos movimentos e serás homem para os grandes; se jamais te faltar a coragem para afrontar os dias em que nada se passa, poderás sem receio esperar os tempos em que o mundo se vira.*"

Agostinho da Silva, *in "Textos e Ensaios Filosóficos"*

Acknowledgments

It's hard to sit down after all this time and think how many persons have given a contribution to this work. I will give it a try, but I will forget someone, so I apologize right before beginning.

First of all, I would like to thank my supervisor, Professor Fernando Pina, not only because he has believed in me, but most of all for the moments he didn't. For all the discussions, for all the fights and the moments when he was away which made me grow-up. For giving me all the opportunities… And because I will never forget that the experimental part, the Lab work, I have learned directly from him…

Professor Jorge Parola, my dear co-supervisor, I thank you for letting me think alone before giving me the solution, for all the synthetic help and for making me repeat experiments 1000 times – in the end it was really all right! I thank you for being the glue that keeps our group together and for calming down my nervous crisis. And I will never forget that paper we have written TOGETHER!

I thank all the photochemistry and supramolecular group for the technical support, for stimulation and for the good times we have been through. But allow me to name out a few persons whose help has been of crucial importance. Professor João Carlos Lima for the availability for all discussions, always questioning what seems obvious, and precious opinions and advices. Doctor César A. T. Laia, I thank you for all the cooperative work, the music, the friendship and the cigarettes we have smoked together, trying to domesticate our moods. Carlos Pinheiro, for all the fun and good times, for support and healthy competition. Doctor Vesselin Petrov, for the collaborative work, friendship and some experimental setups. Doctor Yoann Leydet is also acknowledged for the collaborative work and the French lessons!

I would like to thank Mestre Alexandre Jesus, for the work we have done together and all I have learnt from him in the synthesis Lab, besides a personal friendship. And Mestre Ana Marta Diniz, for being a good master student, for the strict collaboration we have developed and, most of all, for being always there. André Vidal Pinheiro has been an example of intelligence, persistence and integrity throughout these years. I acknowledge you for all the good talks, for listening to me and for precious advices.

I acknowledge Professor Luisa De Cola for accepting me for a short term period in the Westfälische Wilhelms-Universität Münster and for the fruitful discussions, and all the AG De Cola that has integrated me so well. We really had good times there! Particularly, I would like to thank Doctor Rodrigo Q. Albuquerque, for having supervised my work there, for giving me the motivation and the optimism I needed.

I also would like to acknowledge Professor Frank-Gerrit Klärner, Doctor Frank Bastkowski and Doctor Jolanta Polkowska, for providing us the molecular clips, for the collaborative work and for the fruitful discussions on the results.

Professor J. M. G. Martinho and Doctor A. Federov from IST are acknowledged for the time resolved fluorescence and fluorescence anisotropy measurements. BASF Corp. is acknowledged for the kind donation of Pluronic F127.

I deeply thank all my friends, for the help and support and for tolerating my absences and my bad moods. For having believed in me and kept me going forward. You know who you are and I won't make a list. But, particularly, André Pontes da Costa for the help and support in the initial phase of this thesis and Leonardo Mendes for some pictures' treatment.

Gabriele De Paoli, I would like to thank you for all the support, the talks (I am never tired of talking to you) and sorry for being so annoying while I was writing this thesis! You know how important you are and the reason why!

Finalmente, e seguramente com a maior importância, quero agradecer aos meus pais todo o seu incondicional apoio.

Raquel Gomes

Abstract

Flavylium compounds (2-phenyl-1-benzopyrylium) constitute a versatile family of molecules that illustrates the concept of multistate system, since different forms exhibiting diverse properties can be obtained by means of external inputs such as pH and light. Dramatic changes in the properties of the flavylium network can be observed in heterogeneous media due to specific interactions of some of the states with different chemical microenvironments. In this thesis, the effects of CTAB micelles (chapters 2 and 3), Pluronic micelles and gels (chapter 4) and encapsulation in molecular clips (chapter 5) and zeolite L (chapter 6) on the chemical reaction network of flavylium ions are reported.

Positively charged CTAB micelles, stabilizing *trans*-chalcone species, **Ct**, can be used to achieve efficient photochromism of flavylium compounds. 2-styryl-1-benzopyrylium salts, obtained by the introduction of a double bond between the benzopyrylium and the phenyl units, exhibit red shifted absorption maxima compared with flavylium analogues (up to 90 nm). This new family of compounds allows the design of photochromic systems based on CTAB micelles; in particular, switching from yellow to light blue using these derivatives of natural anthocyanins is possible. Flash photolysis experiments provided evidence for a singlet state isomerization process.

In Pluronic media, photochromic gels based on the flavylium network can be obtained. In chapter 4, the **Ct** photochromic mechanism was analyzed, using mainly fluorescence techniques such as steady-state, time-resolved and anisotropy. Evidences for **Ct** distribution among different sites within the Pluronic aggregate and for selective **Ct** photochemistry were found.

Finally, our approach focused on the encapsulation of flavylium salts. The association between a sulphate molecular clip and the several species from the network of a flavylium salt afforded water soluble host-guest complexes that were thoroughly studied. It was demonstrated that hydrophobic interactions between the molecular clips and the flavylium guest molecules are dominant; the other potential interactions, which certainly determine the structures of these host-guest complexes to a large extent, seem to be of minor importance for their stability. The hydration of the flavylium cation was found to be retarded in the presence of clip and the photochemically induced *trans-cis* isomerization seems essentially unaffected by the sulphate molecular clip.

Spectroscopic studies on flavylium compounds encapsulated into the one-dimensional channels of zeolite L revealed drastic changes on fluorescence behavior and it was shown that **Ct** can isomerize inside the channels of zeolite L.

Resumo

Os sais de flavílio (2-fenil-1-benzopirílio) constituem uma família versátil de moléculas que ilustra o conceito de sistemas multiestados, uma vez que formas diferentes, exibindo propriedades diversas, podem ser obtidas através de estímulos externos, tais como pH e luz. Mudanças dramáticas nas propriedades da característica rede de reacções dos compostos de flavílio podem ser observadas em meios heterogéneos, devido a interacções específicas de alguns dos estados com diferentes ambientes químicos. Nesta tese estuda-se o efeito na rede de reacções químicas dos flavílios de micelas de CTAB (capítulos 2 e 3), de micelas e géis de Plurónico (capítulo 4) e da encapsulação em clips moleculares (capítulo 5) e no zeólito L (capítulo 6).

As micelas de CTAB positivamente carregadas, estabilizando a *trans*-chalcona, **Ct**, podem ser utilizadas para obter fotocrosmismo eficiente com flavílios. Os sais de 2-estiril-1-benzopirílio, obtidos pela inserção de uma ligação dupla entre as unidades fenil e benzopirílio, exibem um desvio do comprimento de onda máximo de absorção para o vermelho, comparativamente aos flavílios análogos (até 90 nm). Esta nova família de compostos permite o design de sistemas fotocrómicos, baseados em micelas de CTAB; em particular, é possível mudar de amarelo para azul, usando estes derivados sintéticos das antocianinas. Utilizando fotólise de laser pulsado, pôde concluir-se que o processo de isomerização ocorre no estado excitado singuleto.

Na presença de Plurónico, géis fotocrómicos podem ser obtidos. No Capítulo 4, o mecanismo do fotocromismo da **Ct** foi analisado, usando sobretudo técnicas de fluorescência, tais como fluorescência de estado estacionário, resolvida no tempo e anisotropia. Foram encontradas provas experimentais para a distribuição de **Ct** por diferentes regiões dos agregados de Plurónico e para a ocorrência de fotoquímica selectiva.

Finalmente, a nossa abordagem concentrou-se na encapsulação de sais de flavílio. A associação entre o *clip* molecular sulfato e as diferentes espécies da rede de um flavílio, resulta na formação de complexos hospedeiro-hóspede que foram sistematicamente estudados. Foi demonstrado que as interacções hidrofóbicas entre os *clips* moleculares e os hóspedes de flavílio são dominantes; as outras interacções potenciais, que condicionam largamente as estruturas dos complexos hospedeiro-hóspede, parecem ter menor importância na sua estabilidade. A hidratação do catião flavílio é mais lenta e a fotoisomerização *trans-cis* parece não ser afectada na presença do *clip* sulfato.

Estudos espectroscópicos de compostos de flavílio encapsulados nos canais uni-dimensionais do zeólito L, revelaram mudanças drásticas nas propriedades de fluorescência e foi demonstrado que a **Ct** pode isomerizar dentro dos canais do zeólito L.

Résumé

Les ions flavyliums constituent une famille versatile de molécules et illustrent le concept de systèmes multi-états où différentes espèces dotés de propriétés singulières peuvent être obtenues par l'intervention de stimuli comme le pH ou la lumière. Des changements importants des propriétés de ce réseau moléculaire peuvent être obtenus dans des milieux hétérogènes du fait d'interactions spécifiques de certains états avec les différents microenvironnements chimiques. Dans cette thèse, les effets de micelles CTAB (chapitre 2 et 3) de micelles et gels pluroniques (chapitre 4), l'encapsulation dans des clips moléculaires (chapitre 5) et dans des zéolites L (chapitre 6) sur le réseau de réactions chimiques des ions flavyliums sont reportés.

Les micelles chargées positivement CTAB, qui stabilisent l'espèce *trans*-chalcone **Ct** peuvent être utilisées pour réaliser un photochromisme efficace des ions flavyliums. Des sels de 2-styryl-1-benzopyrylium, obtenus par l'introduction d'une double liaison entre les unités benzopyrilium et phenyl montrent des déplacements vers le rouge par rapport aux analogues flavylium (jusqu'à 90nm). Cette nouvelle famille de composés permet la conception de systèmes photochromiques basés sur des micelles CTAB; en particulier, un changement de couleur du jaune au bleu est possible en utilisant ces dérivés synthétiques des anthocyanines. Des expériences de spectroscopie d'absorption transitoire ont mis en évidence une photoisomérisation à l'état singulet.

Dans les milieux pluroniques, des gels photochromiques basés sur le réseau des ions flavyliums peuvent être obtenus. Dans le chapitre 4, le mécanisme du photochromisme de **Ct** a été analysé en utilisant principalement des techniques de fluorescence (*i*.e. spectroscopies stationnaires, d'anisotropie et résolues dans le temps). Une distribution de **Ct** sur différents sites au sein des agrégats pluroniques et une photochimie sélective ont pu être prouvées.

Finalement, notre approche a été étendue à l'encapsulation des ions flavyliums. L'association entre un clip moléculaire sulfaté et les différentes espèces du réseau ont permis la formation de complexes hôte-invité hydrosolubles. Leur étude a permis de démontrer que les interactions hydrophobiques entre les clips moléculaires et les espèces invités de type flavylium sont prédominantes ; les autres interactions potentielles qui déterminent la structure des complexes sont de moindres importances pour leur stabilité. Il a été démontré que la réaction d'hydratation des ions flavyliums est retardée en présence du clip moléculaire et que la réaction de photoisomerisation *cis*-*trans* n'est pas affectée dans le complexe.

Des études spectroscopiques sur les ions flavyliums encapsulés dans les canaux unidimensionnels des zéolites L ont révélé d'une part des changements importants des propriétés de fluorescence et d'autre part qu'une isomérisation *cis*-*trans* au sein des canaux de la zéolite L est possible

Abbreviations List

A	Absorbance
a.u.	Arbitrary unit
C_0	Total concentration of species
c	Speed of light
CMC	Critical micelle concentration
CMT	Critical micelle temperature
COSY	Correlation spectroscopy
CTAB	Cetyl trimethylammonium bromide
δ	Chemical shift
ε	Molar absorption coefficient
Φ_i	Quantum yield for a given process *i*
F	Fluorescence
I_0	Light intensity emitted by irradiation source at a selected wavelength
I	Intensity of emission
IC	Internal Conversion
ISC	Intersystem crossing
J	Coupling constant
k_j	Rate constant for a given process *j*, e. g. , k_{nr} = rate constant for non radiative processes
λ	Wavelength
λ_{em}	Emission wavelength
λ_{exc}	Excitation wavelength
λ_{irr}	Irradiation wavelength
λ_{max}	Wavelength of maximum emission or absorption
$\bar{\nu}$	Wavenumber
η	Viscosity
η_i	Efficiency for a given process *i*
NMR	Nuclear magnetic resonance spectroscopy
NOESY	Nuclear Overhauser effect spectroscopy
P	Phosphorescence
PSS	Photostationary state
r	Anisotropy
r_0	Fundamental anisotropy
T	Temperature
τ_l	Lifetime for a given process *l*
U.V.-Vis	Ultraviolet-Visible spectroscopy

$\mathbf{AH_2^{2+}}$	Protonated amino flavylium cation
$\mathbf{AH^+}$	Flavylium cation
A	Quinoidal base
A-	Ionized quinoidal base
B	Hemiketal
Cc	*Cis*-chalcone
$\mathbf{Cc^-}$	Ionized *cis*-chalcone
Ct	*Trans*-chalcone
$\mathbf{Ct^-}$	Ionized *trans*-chalcone
$\mathbf{CtH^+}$	Protonated amino *trans*-chalcone
CB	Conjugated bases (**A**, **B**, **Cc** and **Ct**)
K_{a+}	Equilibrium constant for the deprotonation of $\mathbf{AH_2^{2+}}$
$K_{a(1)}$	Equilibrium constant for the deprotonation of $\mathbf{AH^+}$
K_{a2}	Equilibrium constant for the deprotonation of **A**
K_{Ct+}	Equilibrium constant for the deprotonation of $\mathbf{CtH^+}$
$K_{Ct(1)}$	Equilibrium constant for the deprotonation of **Ct**
K_h	Equilibrium constant for the hydration of $\mathbf{AH^+}$
K_t	Equilibrium constant for the tautomerization of the **B**
K_i	Equilibrium constant for the isomerization of **Cc**
K'_a	Apparent equilibrium constant between $\mathbf{AH^+}$ and **CB**
k_a	Kinetic constant for the direct deprotonation reaction (formation of **A**)
k_{-a}	Kinetic constant for the inverse deprotonation reaction (the protonation of **A**)
k_h	Kinetic constant for the direct hydration reaction
k_{-h}	Kinetic constant for the inverse hydration reaction (the dehydration of **B**)
k_t	Kinetic constant for the direct tautomerization reaction
k_{-t}	Kinetic constant for the inverse tautomerization reaction
k_i	Kinetic constant for the direct isomerization reaction
k_{-i}	Kinetic constant for the inverse isomerization reaction
k_{-i+}	Kinetic constant for the inverse isomerization reaction (of $\mathbf{CtH^+}$)
…	…

Index

Scheme Index

Table Index

Figure Index

1. Introduction

This chapter is intended to serve as an introduction for the following chapters of this thesis. In a first part, the fundamental aspects of photophysics and photochemistry are summarized, as well as the experimental techniques that were applied. In the second part, the most important notions about the characteristic multiequilibria of flavylium salts in aqueous solutions and their applications are described.

1.1. Basic principles of photophysics and photochemistry

The aim of this subsection is to provide a very concise illustration of the processes taking place when light is absorbed by a molecule, and some of the associated measurements that were used throughout this thesis.

1.1.1. Light absorption

In photochemistry, focus is given on light, as an electromagnetic radiation (characterized by a wavelength, λ, a frequency, ν, and a velocity, c) in the region ranging from 100 to 1000 nm. However, it is the concept of light as stream of photons, without mass but with a specific energy, that explains the interaction of light with molecular systems – the interaction between one molecule and one photon is represented in equation 1.1:

$$\mathbf{A} + h\nu \rightarrow \mathbf{A}^* \qquad (1.1)$$

where **A** represents the ground state molecule, $h\nu$ is the photon and **A*** is the excited state molecule, that has extra energy $h\nu$. Indeed, the excited molecule must be considered a new chemical species with its own chemical and physical properties, often quite different from those of the excited state.

Molecules possess well-defined electronic states, a direct consequence of the separation between electronic and nuclear motions, known as the Born-Oppenheimer approximation. This is based on the difference of masses between protons and electrons, so that electrons can be considered the fast subsystem and protons the slow one. Two orbitals are of the particular importance for the absorption of light: the HOMO (Highest Occupied Molecular Orbital) and the LUMO (Lowest Unoccupied Molecular Orbital). Absorption of a photon with an appropriate energy can promote an electron from a lower energy orbital (frequently the HOMO) to a higher energy orbital (often the LUMO). For instance a transition of an electron from a π orbital to an antibonding π^* orbital can take place ($\pi \rightarrow \pi^*$ transition), or from a non bonding electron in an n orbital to a π^* orbital ($n \rightarrow \pi^*$ transition). The energy of the electronic transitions generally

follows the order: $n \rightarrow \pi^* < \pi \rightarrow \pi^* < n \rightarrow \sigma^* < \sigma \rightarrow \pi^* < \sigma \rightarrow \sigma^*$. The $n \rightarrow \pi^*$, for instance considering a carbonyl group, implies that an electron is removed from the oxygen atom and goes into the π^* orbital localized half on the carbon atom and half on the oxygen atom, meaning that this transition has a charge transfer (CT) character and implying a change in the dipole moment of the molecule.[1] Compounds are called solvatochromic when the position of their absorption (and emission) spectra depend on solvent polarity, a consequence of the preferential stabilization of the ground or excited state orbitals. A bathochromic (red) shift and a hypsochromic (blue) shift with increasing solvent polarity relate to positive and negative solvatochromism, respectively. Such shifts of appropriate solvatochromic compounds in solvents of various polarities can be used to construct empirical polarity scales.[1]

Experimentally, the efficiency of light absorption is characterized by absorbance (A) or transmittance (T):

$$T = \frac{I}{I_o} \tag{1.2}$$

$$A = -\log\frac{I}{I_0} = -\log T \tag{1.3}$$

where I_0 and I are light intensities of the beams entering and leaving the absorbing medium, respectively. In many cases, the absorbance of a sample follows the Beer-Lambert Law:

$$A = \varepsilon b[X] \tag{1.4}$$

where ε is the molar absorption coefficient (M^{-1} cm^{-1}), [X] is the concentration of a given species $\boldsymbol{X}$ (M) and b is the optical path length (cm). Failure to obey this linear dependence of absorbance with concentration may be related to the formation of aggregates or the presence of other absorbing species.[1] The ε expresses the ability of a molecule to absorb light in a given medium. Considering a molecule as an oscillating dipole, the *oscillator strength f*, related to the integral of the absorption band, is given by:

$$f = \frac{4.32\times10^{-9}}{n}\int \varepsilon(\bar{\nu})d\bar{\nu} \tag{1.5}$$

where n is the refractive index, $\bar{\nu}$ is the wavenumber (in cm^{-1}) and f values are normalized, so at its maximum it is 1 (for the harmonic oscillator). For $n \rightarrow \pi^*$ the values of ε are equal or less than a few hundreds and f value no bigger than 10^{-3}, and for $\pi \rightarrow \pi^*$ transitions these values are in principle much higher (f is close to 1 for some compounds - ε in the order of 10^5).[1]

Two major selection rules stand for absorption transitions:

1) Spin forbidden transitions: transitions between states of the same spin multiplicity are allowed, like singlet (S) → singlet or triplet (T) → triplet, and those transitions between states of different multiplicity are forbidden, (S → T) or (T → S). These transitions may be observed due to spin-orbit coupling, however with low ε. Crossing between the first singlet excited state (S_1) and the first triplet excited (T_1), intersystem crossing ISC, is possible thanks to spin-orbit coupling.

2) Symmetry forbidden transitions: the transition dipole moment is given by an integral dependent of the product of initial orbital and the final orbital functions. If this product is zero, the integral vanishes and the transition is forbidden, meaning that there is no spatial superposition between the two orbitals. Group theory is particularly useful predicting these cases.[2] A symmetry forbidden transition can nevertheless be observed because the molecular vibrations cause some departure from perfect symmetry (vibronic coupling).[1]

The geometry of a molecule in its ground state represents one stationary point (all forces acting on the nuclei are zero) on a 3*N*-6 dimensional potential hypersurface (3N-5 in the case of linear molecules). It corresponds to a local minimum − all displacements of nuclei from their equilibrium positions lead to a rise in the potential energy. Other stationary points on the ground-state potential energy hypersurface may represent different conformations of the same molecule or different molecules (including dissociation fragments or isomers). Each excited state has a similar potential hypersurface associated with it, exhibiting also stationary points that will not generally coincide with those on the ground-state surface. Scheme 1.1 shows a one-dimensional cross section of the ground state, S_0, and two excited-state potential surfaces, one of which is bound like the ground state, S_1, and the other of which is unbound, S_2.[3]

On bound surfaces, the vibrational motion is also quantized. The spacing of the vibrational energy levels is such that at room temperature most of the molecules are in the lowest vibrational state (according to the Boltzmann distribution). In addition, rotational motion of the molecule about its center of mass is also quantized and the spacing of the rotational energy levels depends inversely on the moment of inertia. For large molecules or in solution, the rotational structure is not resolved and at room temperature a number of rotational levels will be populated. The range of structures in the ground vibrational state is given by the vibrational wave function shown for the lowest vibrational level of S_0 in Scheme 1.1. The time required to excite the electron (10^{-15} s) is very short compared to vibrational periods ($>10^{-13}$ s), so the transitions occur without changing the nuclei position – Franck Condon principle. In Scheme 1.1 it is illustrated the range of structures from which *vertical* excitation may take place if the energy of the photon corresponds to the approximate energy difference between the ground-state lowest vibrational level and some vibrational level of an excited state potential energy surface. In general, the excited state reached by vertical excitation from the ground state will be

hot (vibrationally excited) and may dissociate if the vibrational mode of the excited state corresponds to bond stretching.[3]

In general, the population of an excited state results in bond weakening, because this new orbital has antibonding character, which has two consequences: excited state minima are often less deep than the corresponding for ground state, so that small amplitude vibrations in the excited state have lower frequencies and smaller energy spacing; large-amplitude motions along relatively flat pathways leading to highly distorted geometries will be found more frequently in the excited state.[4]

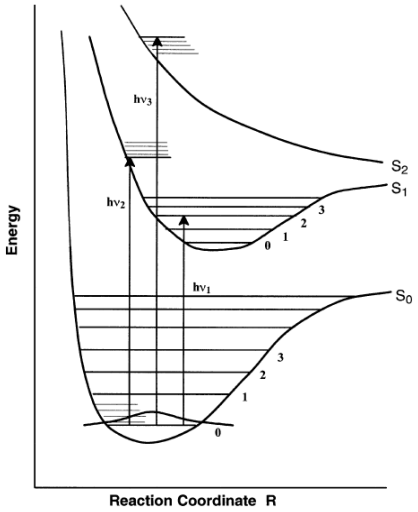

Scheme 1.1 – Potential energy surfaces for bound states, S_0 and S_1, and a dissociative state, S_2.[3]

To summarize, the width of an absorption spectrum is due to the existence of a continuous set of vibrational sublevels in each electronic state, and broadening can be also obtained from fluctuations in the solvation shell of the absorbing species.

1.1.2. Fate of the excited state

A representation of the sequence of events taking place after photoexcitation is given by a Jablonski diagram, Scheme 1.2. In the next lines, a brief summary of each process following the photoexcitation is given.

1) Internal conversion (IC): non-radiative transition between two excited states of the same spin multiplicity. When a molecule is excited to an energy level higher than the lowest vibrational level of the first electronic state, vibrational relaxation (and internal conversion if the singlet excited state is higher than S_1) leads the excited molecule towards the 0 vibrational level of the S_1 singlet state with a time-scale of 10^{-13}-10^{-11} s. The excess vibrational energy is transferred to the solvent during collisions of the excited molecule with the surrounding solvent molecules. As vibrational relaxation is so fast compared to the other processes taking place after photoexcitation of a molecule, the excited states can be considered thermally equilibrated states

and the laws of thermodynamics can be applied. From S_1, internal conversion to S_0 is possible but is less efficient than conversion from S_2 to S_1, because of the much larger energy gap between S_1 and S_0.[1]

2) Fluorescence: emission of photons accompanying the $S_1 \rightarrow S_0$ relaxation. Fluorescence emission occurs from S_1 (apart from a few exceptions) and therefore its characteristics (except polarization) do not depend on the excitation wavelength. The fluorescence spectrum is located at higher wavelengths than the absorption spectrum because of the energy loss in the excited state due to vibrational relaxation, Scheme 1.2. In general, the differences between the vibrational levels are similar in the ground and excited states, so that the fluorescence spectrum often resembles the first absorption band ('mirror image' rule). The gap (expressed in wavenumbers) between the maximum of the first absorption band and the maximum of fluorescence is called the Stokes shift. This important parameter can provide information on the excited states. For instance, when the dipole moment of a fluorescent molecule is higher in the excited state than in the ground state the Stokes shift increases with solvent polarity. Excited molecules stay in the S_1 state for a certain time (a few tens of picoseconds to a few hundreds of nanoseconds, depending on the type of molecule and the medium) before emitting a photon or undergoing other deexcitation processes (internal conversion, intersystem crossing). Thus, after excitation of a population of molecules by a very short pulse of light, the fluorescence intensity decreases exponentially with a characteristic time, reflecting the average lifetime of the molecules in the S_1 excited state.[1]

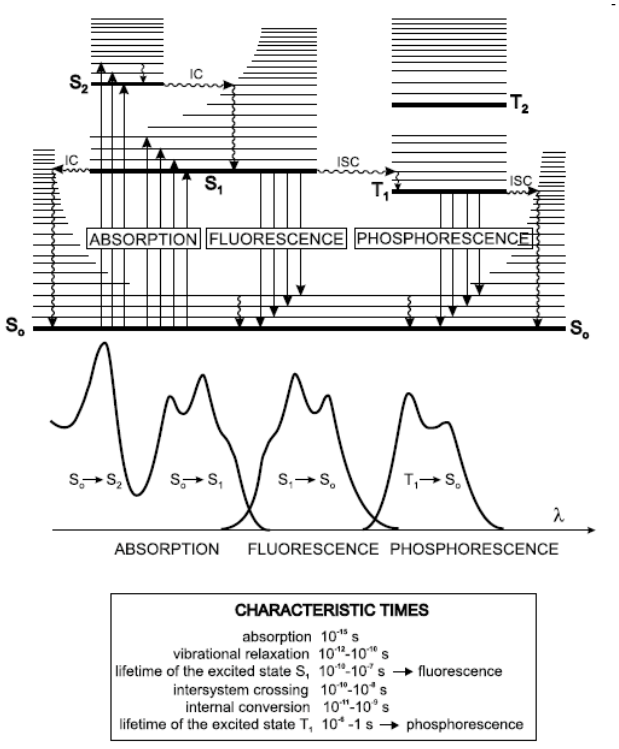

Scheme 1.2 – Perrin–Jablonski diagram and illustration of the relative positions of absorption, fluorescence and phosphorescence spectra.[1]

3) Intersystem crossing (ISC): non-radiative transition between two isoenergetic vibrational levels belonging to electronic states of different multiplicities. For example, an excited molecule in the 0 vibrational level of the S_1 state can move to the isoenergetic vibrational level of the T_n triplet state; then vibrational relaxation brings it into the lowest vibrational level of T_1. Intersystem crossing may be fast enough (10^{-7}–10^{-9} s) to compete with other pathways of de-excitation.[1]

4) Phosphorescence and non radiative deactivation: phosphorescence is the radiative de-excitation of T_1 and in solution at room temperature, non-radiative de-excitation from the triplet state T_1, is predominant over it. In fact, during such a slow process (10^{-6}-1 s), the numerous collisions with solvent molecules (or other molecules, e. g., O_2) favor intersystem crossing and vibrational relaxation in S_0. However, at low temperatures and/or in a rigid medium, phosphorescence can be observed. The phosphorescence spectrum is located at wavelengths higher than the fluorescence spectrum, Scheme 1.2, because the energy of the lowest vibrational level of the triplet state T_1 is lower than that of the singlet state S_1.[1]

Once a molecule is excited and reaches triplet state T_1, it can absorb another photon at a different wavelength because triplet–triplet transitions are spin allowed. These transitions can be observed provided that the population of molecules in the triplet state is large enough, which can be achieved by illumination with an intense pulse of light.[1]

Besides all the previously mentioned processes, excited states can be deactivated by a variety of chemical processes, unimolecular or bimolecular. Excited states are more reactive, as energy rich species, than the ground states which generated them, and they must be considered as completely new chemical species, with completely different reactivity. Excited-state reactions must be fast to compete with the other processes and the key to understanding excited state reactivity is the identification of low energy channels along the excited state surface leading, perhaps *via* some surface crossing, to the potential minima of the ground state products.

1.1.3. Lifetimes, quantum yields and efficiencies

The processes that can take place in a molecule after its excitation are summarized in Scheme 1.3, where k_i is the rate constant for the process *i*. Please note that k_{nr}, the non radiative constant includes k_{isc} and k_{ic} (rate constant for intersystem crossing and internal conversion, respectively).

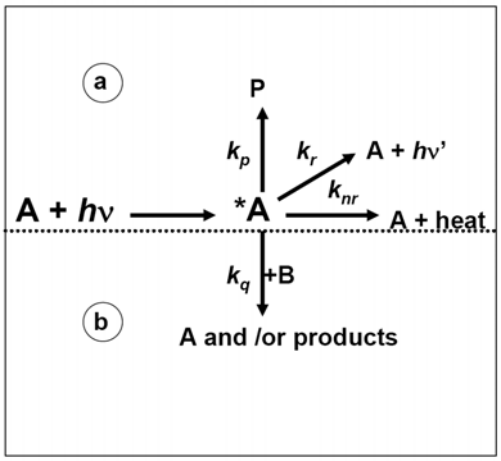

Scheme 1.3 – Unimolecular (a) and bimolecular (b) processes for the deactivation of the excited state. k_r, k_{nr} and k_p are unimolecular radiative constants for radiative decay, radiationless deactivation and chemical reaction, and k_q is a bimolecular (quenching) rate constant.[4]

As in classical kinetics, the disappearance of the excited state molecules, excluding bimolecular processes, can be accounted for by:

$$-\frac{d[^*A]}{dt} = (k_r + k_{nr} + k_p)[^*A] \tag{1.6}$$

Integration of the previous equation makes possible the definition of the lifetime τ of the excited species.

$$\tau_{^*A} = \frac{1}{(k_r + k_{nr} + k_p)} = \frac{1}{\sum_j k_j} \tag{1.7}$$

And for each process efficiency η_i can be defined as:

$$\eta_{i^*A} = \frac{k_i}{\sum_j k_j} = k_i \tau_{^*A} \tag{1.8}$$

Finally, the quantum yield Φ_i of a given process originating an excited state is defined as a ratio between the number of molecules undergoing that process per unit time and the number of photons absorbed per unit time. If the excited state is directly reached by light absorption, the quantum yield coincides with the efficiency of the process:

$$\Phi_i = \eta_{i^*A} \prod_n \eta_n \tag{1.9}$$

where η_n represents the efficiencies of all the processes involved in the population of the excited states.

Kasha's rule for a typical organic molecule, *the emitting level of a given multiplicity is the lowest excited level of that multiplicity*, implies that: 1) the efficiency of internal conversion between higher singlet excited states to S_1 is unity; 2) the lowest singlet excited state usually lives long enough so that ISC, emission and chemical reactions can have appreciable efficiencies; 3) the values of the efficiencies of processes originated by S_1 coincide with the respective quantum yields; 4) the values of the quantum yields of processes from T_1 are products of their efficiencies and efficiency of ISC $S_1 \rightarrow T_1$.[4]

1.1.4. An example of an unimolecular process: *cis-trans* isomerization

One of the processes that deactivate the excited state is *cis-trans* isomerization, and it has been observed for organic compounds such as olefins, azomethines, and azo compounds.[5] We will look into and rationalize the example of the *cis-trans* isomerization of stilbene, which has been thoroughly studied and is a representative example of unimolecular reactions.

A potential-energy diagram for the isomerization of stilbene is represented as a one-dimensional sketch in Scheme 1.4. The reaction coordinate corresponds to torsion of the double bond, involving motion of the phenyl rings.[6] In the ground state a large barrier exists between the *trans* and *cis* forms of stilbene. However, in the excited state of *trans*-stilbene there is a potential minimum and a barrier exists for the twisting motion about the carbon-carbon double bond. On the *cis* side there appears to be little or no barrier to torsional motion. The excited state surface that is sketched arises from a mixing of the first excited state (obtained by a π - π^* transition) of stilbene with one or more higher lying, doubly excited configurations that have a minimum at the 90º twisted form and may be intended only as the adiabatic limit. As a consequence of the barrier in the S_1 state, the quantum yield for the *trans-cis* isomerization of stilbene is temperature dependent; at lower temperatures fluorescence becomes increasingly important as a competing process; and Φ_F becomes nearly unity at temperatures below 100 K.[5]

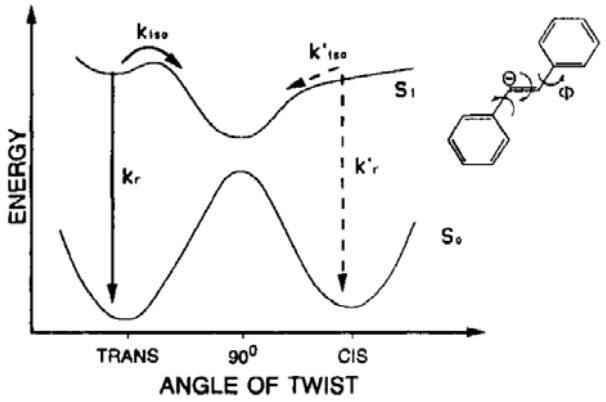

Scheme 1.4 – A schematic representation of the isomerization coordinate is shown for reaction from both the *trans* and *cis* sides. The rate constants k_{iso} and k'_{iso} are for isomerization on the singlet surface and the rate constants k_r and k'_r are radiative constants.[6]

Because of the nature of the higher lying states, the 90º form and the transition state are expected to be polarizable (both biradical and charge-transfer structures have been proposed).[6] After the arrival of the *cis* or *trans*-stilbene to the twisted form (90°), the decay to the ground-state surface is rapid (<1 ps in liquid alkanes). Once on the ground-state surface the product molecule vibrationally decays either to the *trans* or *cis* form. A third reaction channel, believed to be minor, is opened from the *cis* side and produces dihydrophenanthrene.[6]

1.1.5. Bimolecular processes

The most important bimolecular events are energy transfer processes and electron transfer chemical reactions, involving oxidation or reduction of the excited state:

$$^{*}\mathbf{A} + \mathbf{B} \rightarrow \mathbf{A} + {}^{*}\mathbf{B} \qquad \text{energy transfer} \qquad (1.10)$$

$$^{*}\mathbf{A} + \mathbf{B} \rightarrow {}^{+}\mathbf{A} + {}^{-}\mathbf{B} \qquad \text{oxidative electron transfer} \qquad (1.11)$$

$$^{*}\mathbf{A} + \mathbf{B} \rightarrow {}^{-}\mathbf{A} + {}^{+}\mathbf{B} \qquad \text{reductive electron transfer} \qquad (1.12)$$

Bimolecular energy and electron transfer can be interesting because they can be used to quench an excited state, to prevent its luminescence and/or intermolecular reactivity and they can as well be used to sensitize other species, which for instance, do not absorb light.[4] However, it is outside the scope of this thesis to discuss this phenomenon, and many textbooks can be found on the subject.[7]

However, the same kinetic formalism can be used for energy and electron-transfer. For processes requiring diffusion and formation of encounters, the Stern-Volmer model can be used, which assumes statistical mixing of excited state molecule $\mathbf{A}^{*}$ and **Q**, the quencher. $\mathbf{A}^{*}$ can decay by some intramolecular processes and encounter in solution the quencher **Q**. Dividing the lifetime of **A** in the absence of quencher (τ_0), by the lifetime in the presence of the quencher (τ), one obtains the well-known Stern-Volmer equation:

$$\frac{\tau_0}{\tau} = 1 + k_q \tau_0 [Q] \qquad (1.13)$$

Of course that the rate constant of the quenching is controlled by several factors, that are elucidated by a more detailed formalism.[4,7]

1.1.6. Emission and excitation spectra

Emission and excitation spectra are recorded using a spectrofluorometer. The light source is a lamp emitting a constant photon flow, *i.e.* a constant amount of photons per unit time, whatever their energy is.

The fluorescence spectrum or emission spectrum reflects the distribution of the probability of the various transitions from the lowest vibrational level of S_1 to the various vibrational levels of S_0. The emission spectrum is characteristic of a given compound. In practice, the steady-state fluorescence intensity $I_F(\lambda_F)$ measured at wavelength λ_F (selected by a monochromator with a certain wavelength bandpass $\Delta\lambda_F$) is proportional to $F_\lambda(\lambda_F)$ (the fluorescence spectrum) and to the number of photons absorbed at the excitation wavelength λ_E (selected by a monochromator). The proportionality factor depends on several parameters, in particular on the optical configuration for observation (i.e. the solid angle through which the instrument collects fluorescence, which is in fact emitted in all directions) and on the bandwidth of the monochromators. In practice, measurement of the variations in I_F as a function of wavelength λ_F, for a fixed excitation wavelength λ_E, reflects the variations in $F_\lambda(\lambda_F)$ and thus provides the fluorescence spectrum. Because the proportionality factor is generally unknown, the numerical value of the measured intensity I_F has no meaning, and generally speaking, I_F is expressed in arbitrary units (a. u.). The fluorescence intensity is proportional to the concentration only for low absorbances. Deviation from a linear variation increases with increasing absorbance. Moreover, when the concentration of fluorescent compound is high, inner filter effects reduce the fluorescence intensity depending on the observation conditions. In particular, the photons emitted at wavelengths corresponding to the overlap between the absorption and emission spectra can be reabsorbed (radiative transfer). In addition, for mathematical and geometrical reasons, when fluorometry is used for a quantitative evaluation of the concentration of a species, it should be kept in mind that the fluorescence intensity is proportional to the concentration only for diluted solutions.[8]

The variations in fluorescence intensity as a function of the excitation wavelength λ_E for a fixed observation wavelength λ_F represent the excitation spectrum. If it is possible to compensate for the wavelength dependence of the incident light, it depends only on the absorption of light. The corrected excitation spectrum is, thus, identical in shape to the absorption spectrum, provided that there is a single species in the ground state. In contrast, when several species are present, or when a sole species exists in different forms in the ground state (aggregates, complexes, tautomeric forms, etc.), the excitation and absorption spectra are no longer superimposable. Comparison of absorption and emission spectra often provides useful information.[1]

1.1.7. Fluorescence anisotropy

Light is an electromagnetic wave consisting of an electric field *E* and a magnetic field *B* perpendicular both to each other and to the direction of propagation, and oscillating in phase. For natural light, these fields have no preferential orientation, but for linearly polarized light, the electric field oscillates along a given direction. If the incident light is linearly polarized, the probability of excitation of a chromophore is proportional to the square of the scalar product $M_A \cdot E$, i.e. $\cos^2 \theta_A$, θ_A being the angle between the electric vector *E* of the incident light and the absorption transition moment M_A. This probability is maximum when *E* is parallel to M_A of the molecule; it is zero when the electric vector is perpendicular. When a population of fluorophores is illuminated by a linearly polarized incident light, those whose transition moments are oriented in a direction close to that of the electric vector of the incident beam are preferentially excited - *photoselection*. Because the distribution of excited fluorophores is anisotropic, the emitted fluorescence is also anisotropic. Any change in direction of the transition moment during the lifetime of the excited state will cause this anisotropy to decrease, *i.e.* will induce a partial (or total) depolarization of fluorescence. The causes of fluorescence depolarization are: non-parallel absorption and emission transition moments, torsional vibrations, Brownian motion and transfer of the excitation energy to another molecule with different orientation. Fluorescence polarization measurements can thus provide useful information on molecular mobility, size, shape and flexibility of molecules, fluidity of a medium, etc.[1]

In practice, the measurement of fluorescence anisotropy proceeds as illustrated in Scheme 1.5. The sample is excited with vertically polarized light and the electric vector of the excitation light is oriented parallel to the vertical or *z*-axis. The intensity of the emission through a polarizer is then measured. When the emission polarizer is oriented parallel ($\parallel$) to the direction of the polarized excitation, the observed intensity is called $I_\parallel$ and when the polarizer is perpendicular ($\perp$) to the excitation, the intensity is called $I_\perp$. These values are used to calculate the anisotropy *r* as follows:[9]

$$r = \frac{I_{||} - I_{\perp}}{I_{||} + 2I_{\perp}} \tag{1.14}$$

Anisotropy is a dimensionless quantity that is independent of the total intensity of sample, the fluorophore concentration (if there are no artefacts) and is an additive property.

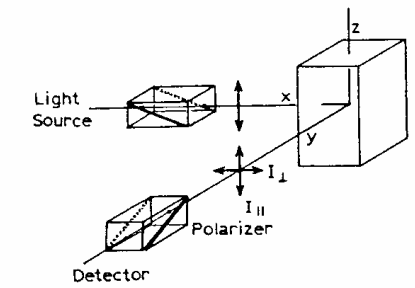

Scheme 1.5 – Schematic diagram for measurement of fluorescence anisotropies.[9]

Considering a single molecule in Scheme 1.6, assuming that the absorption and emission transition moments are parallel - this is nearly true for 1,3,5-hexatriene (DPH, Scheme 1.6) - and that this single molecule is oriented with angles θ relative to the *z*-axis and ϕ relative to the *y*-axis, it is possible to derive an expression for *r*. Of course, in reality the ground-state DPH molecules will be randomly oriented in an isotropic solvent.

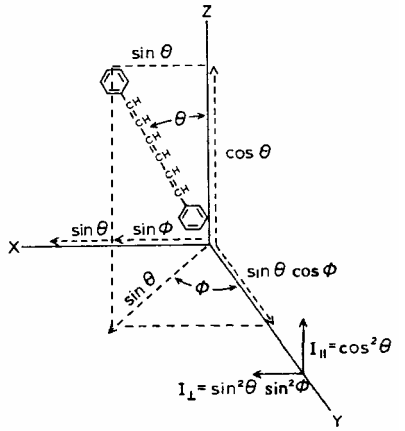

Scheme 1.6 – Emission intensities for a single fluorophore (DPH - 1,3,5-hexatriene) in a coordinate system.[9]

The aim now is to calculate the anisotropy that would be observed for this oriented molecule in the absence of rotational diffusion. The intensity observed through a polarizer is proportional to the square of the projection of the electric field of the radiating dipole onto the transmission axis of the polarizer.[9] These projections are given by:

$$I_{||}(\theta,\phi) = \cos^2\theta \tag{1.15}$$

$$I_{\perp}(\theta,\phi) = \sin^2\theta \sin^2\phi \tag{1.16}$$

In an actual experiment the solution will contain many fluorophores with a random distribution. The anisotropy is calculated by performing the appropriate average based on excitation photoselection and how the selected molecules contribute to the measured intensity. First, consider excitation polarized along the *z*-axis. Such excitation must excite all molecules having an angle ϕ with respect to the *y*-axis with equal probability. That is, the population of excited fluorophores will be symmetrically distributed around the *z*-axis. Any experimentally

accessible population of molecules will be oriented with values of ϕ from 0 to 2π with equal probability. Hence, it is possible to eliminate the ϕ dependence in equation 1.16 and calculate the average value of $\sin^2 \phi$.[9] Then, integration of both equations for the probability of orientation of a molecule relative to the z-axis, and using equation 1.14, one obtains:

$$r = \frac{3\langle \cos^2 \theta \rangle - 1}{2} \tag{1.17}$$

For a single fluorophore oriented along the z-axis, with collinear transitions, $\theta = 0$ and $r = 1.0$. However, it is not possible to obtain a perfectly oriented excited-state population with optical excitation of homogeneous solutions. So, the anisotropies are always less than 1.0. Complete loss of anisotropy is equivalent to $\theta = 54.7°$. This means that the average value of $\cos^2\theta$ is 1/3, where θ is the angular displacement between the excitation and emission moments. But this is only valid for samples that display *z*-axis symmetry, as pointed out previously. Besides, the distribution of molecules that is indeed excited by vertically polarized light, due to photoselection must be considered. Taking into account the maximum photoselection that can be obtained using one photon excitation, it is possible to calculate the maximum anisotropy that is possible to obtain: $r = 0.4$.[9] This is the value which is observed when the absorption and emission dipoles are collinear, and when there are no processes which result in depolarization. This value ($r = 0.4$) is considerably smaller than that possible for a single fluorophore oriented along the z-axis ($r = 1.0$).[9]

It is important to remember that there are other possible origins for polarized light that include reflections and light scattered by the sample. For a dilute scattering solution, the anisotropy is close to 1.0. Scattered light can interfere with anisotropy measurements. If the measured anisotropy for a randomly oriented sample is greater than 0.4, one can confidently infer the presence of scattered light in addition to fluorescence (of course, if the instrument was carefully calibrated).[9]

Few fluorophores display anisotropy right after excitation, fundamental anisotropy r_0, equal to 0.4. For most fluorophores, the r_o values are less than 0.4, and, in general, the anisotropy values depend on the excitation wavelength. This is explained in terms of the transition moments being displaced by an angle β relative to each other. Previously, it was pointed that displacement of the emission dipole by an angle θ from the *z*-axis resulted in a decrease in the anisotropy by a factor of $(3\cos^2\theta - 1)/2$. Similarly, the displacement of the absorption and emission dipoles by an angle β results in a further loss of anisotropy. The observed anisotropy in a vitrified dilute solution is a product of the loss of anisotropy due to photoselection (resulting in a reduction of the anisotropy by a factor of 2/5) and that due to the angular displacement of the dipoles. The fundamental anisotropy of a fluorophore is given by:

$$r_0 = \frac{2}{5}\left(\frac{3\cos^2\beta - 1}{2}\right) \tag{1.18}$$

where β is the angle between the absorption and emission transitions.[9] The term r_0 is used to refer to the anisotropy observed in the absence of other depolarizing processes such as rotational diffusion or energy transfer. The fundamental anisotropy value is zero when β = 54.7°. When β exceeds 54.7°, the anisotropy becomes negative. The maximum negative value (-0.20) is found for β = 90°.

Rotational diffusion of fluorophores is a dominant cause of fluorescence depolarization. This mode of depolarization is described in the simplest case for spherical rotors by the Perrin equation, for a spherical rotor:

$$\frac{r_0}{r_{ss}} = 1 + \frac{\tau}{\phi_R} = 1 + 6D\tau \tag{1.19}$$

where τ is the fluorescence lifetime, r_{ss} is the experimental steady state fluorescence anisotropy, ϕ_R is the rotational correlation time, and D is the rotational diffusion coefficient. If the correlation time is much larger than the lifetime ($\phi_R >> \tau$), then the measured anisotropy (r_{ss}) is equal to the fundamental anisotropy (r_0). If the correlation time is much shorter than the lifetime ($\phi_R >> \tau$), the anisotropy is zero. The rotational correlation time is:

$$\phi_R = \frac{1}{6D} = \frac{\eta V N_A}{RT} \tag{1.20}$$

where η is the viscosity, V is the volume of the rotating unit and N_A is Avogadro's constant. A straightforward derivation of equation 1.19 is obtained on the basis that following a δ-pulse excitation, the time-resolved decay of anisotropy r(t) for a spherical molecule is:

$$r(t) = r_0 e^{\frac{-t}{\phi_R}} = r_0 e^{-6Dt} \tag{1.21}$$

Only spherical molecules display single-exponential anisotropy decay. More complex expressions are predicted for non-symmetric species or molecules. The steady-state anisotropy can be calculated from an average of the anisotropy decay over the intensity decay, and for a single exponential, one obtains the Perrin equation. Using these relations, it is possible to calculate the anisotropy expected for fluorophores in solvents or for labelled macromolecules, assuming that the molecules are spherical.[9]

1.2. Flavylium ions

This aim of this subsection is to introduce flavylium salts, briefly starting by a historical background and proceeding with thermodynamics, kinetics, photochemistry and some reported applications of these multistate molecules.

1.2.1. Structure of flavylium salts and historical background

Flavylium ions are constituted by a basic carbon skeleton of 2-phenyl-1-benzopyrylium, Scheme 1.7. The family of compounds exhibiting this basic structure comprises also anthocyanidins, anthocyanins and deoxyanthocyanins that generically belong to the flavonoid class of natural compounds. They are biosynthesized through a combination of the shikimate pathway and the acetate pathway[10], whose crucial enzyme is *chalcone synthase*.[11]

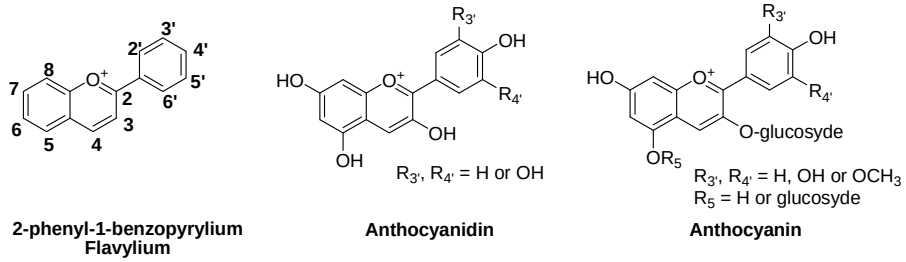

Scheme 1.7 – Structure of flavylium ions, anthocyanidins and anthocyanins.

In anthocyanidins hydroxyl groups are always present in positions 3, 5, 7 and 4', a direct consequence of the biosynthetic pathway[10] and due to their instability are seldom found in plant tissues in the free form.[12] On the contrary, the so-called deoxyanthocyanins corresponding to anthocyanidins lacking the hydroxyl in position 3, are quite stable in solution, and have been isolated from mosses and ferns.[12] Anthocyanins, the ubiquitous colorants responsible for most of the colors, from red to blue, exhibited by flowers, fruits and leaves are 2-phenyl-1-benzopyrylium derivatives characterized by the existence of an *O*-glycoside in position 3 (monoglycoside) and sometimes also in position 5 (diglycosides) or less frequently in position 7.[13]

It was not until the first decade of the last century that Richard Willstätter[14,15] was able to elucidate the structure of anthocyanidins and realize that these are the colorants responsible for the most of the red and blue hues in flowers, fruits, roots, barks and leaves. Finally, in the twenties, Robert Robinson[16] was able to synthesize a several anthocyanins.[17]

The interest in the chemistry of anthocyanins is historically connected to the need of understanding their role in photobiology and to their usefulness as food colorants. Indeed, anthocyanins have been investigated for long as natural food colorants,[18] after recognition of undesired physiological effects of easily synthesized azo dyes. Synthetic flavylium salts are a versatile family of compounds, possessing the same basic structure and identical network of

chemical reactions in aqueous solutions of anthocyanins, and the chemical history of both is intertwined. Indeed, synthetic flavylium salts can be used as models for understanding the behavior of the natural occurring counterparts.

Recently, the conventional frontiers between natural and synthetic flavylium compounds became quite flimsy with the isolation of the compounds 7,4'-dihydroxyflavylium and 7,4'-dihydroxy-5-methoxyflavylium (dracoflavylium)[19] of a natural deep red resin named Dragon's blood, obtained from *Dracaena draco* and *Dracaena cinnabaris*.

1.2.2. Network of reactions

In aqueous solutions, flavylium salts exhibit a complex network of reactions, depicted in Scheme 1.8, for the particular case of 7,4'-dihydroxyflavylium (**DHF**). The equilibrium species at sufficiently acidic pH values is the flavylium cation, $\mathbf{AH^+}$. When the pH is increased two reactions take place: i) proton transfer to form the quinoidal base, **A** and ii) hydration, through position 2, to afford the hemiketal **B**. The proton transfer is faster than the hydration but in many cases the other basic species are more stable than **A** at the equilibrium, which means that **A**, formed as a kinetic product during the first stages of the equilibration processes, latter disappears totally or partially to give the equilibrium distribution of species. The *cis*-chalcone (**Cc**) is formed from **B** by a tautomeric process and the *trans*-chalcone (**Ct**) results from the isomerization of the former species. In basic media, ionized species can be formed, the ionized quinoidal base $\mathbf{A^-}$ and anionic **Ct** species ($\mathbf{Ct^{n-}}$) or even **Cc** ($\mathbf{Cc^{n-}}$) species.

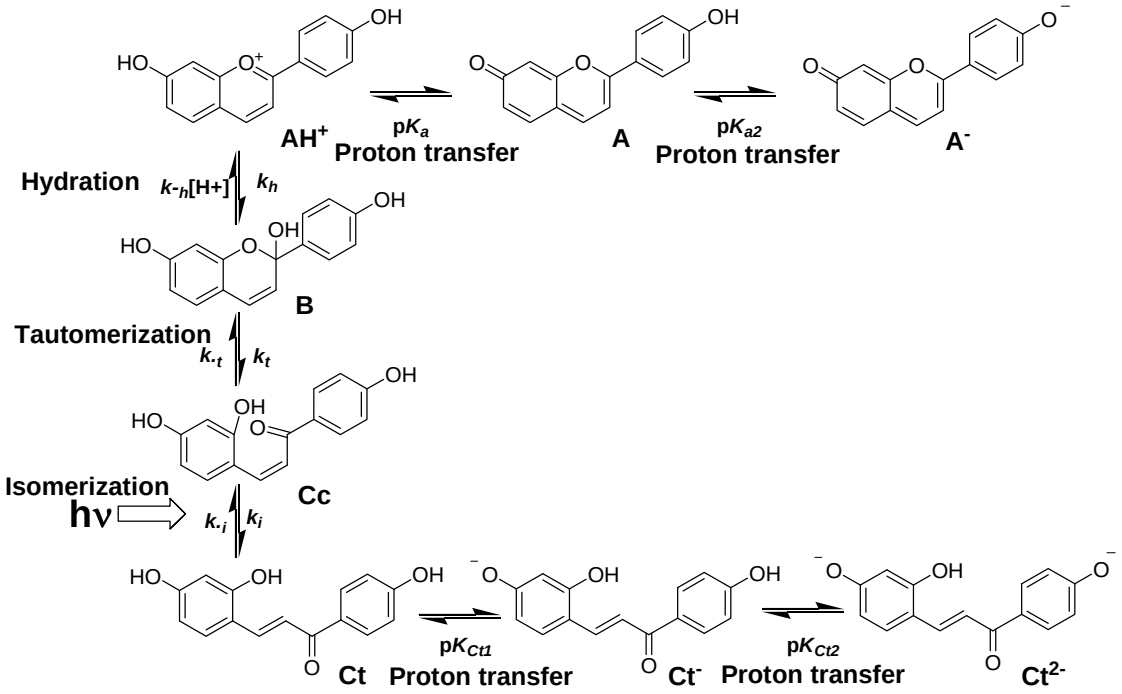

Scheme 1.8 – Network of reactions of **DHF**.

It is worth noting that the colored species are **AH**$^+$ and **A**, all the other species being uncolored or pale yellow (until pH values close to neutral), and that the photochemistry of flavylium compounds arises from the light induced *trans-cis* isomerization.

The investigation of this network started when researchers found out that anthocyanins are notoriously unstable under neutral and basic conditions. These effects with increasing pH were initially investigated by Jurd, Timberlake and Bridle and Harper and Chandler.[12]

In the beginning of the sixties, Jurd was the first author to introduce the structures of both *cis* and *trans*-chalcones.[20,21] Moreover, it was Jurd who proposed the simplistic isomerization of the *trans*-chalcone, to form the *cis*-analogue followed by cyclization to give the flavylium ion. Please note that the mole fraction distribution of the *trans*-chalcone at the equilibrium at room temperature is very small when anthocyanins are in solution, and so in the same period and even later in the literature the authors studying anthocyanins represent generically the chalcones (the notation **C** is frequently used) – in anthocyanins chalcones are present at the equilibrium only in minor amounts.[22] On the other hand, the effect of light in the network was reported by Timberlake and Bridle in 1966, but no explanation was proposed.[23]

However, the sequence of the chemical reactions involved in the network was only firmly established by Brouillard and co-workers, in the late seventies for anthocyanins.[24,25,26,27] In particular, a crucial point of the kinetic process was elucidated by these researchers: at moderately acidic pH values **B** is formed from hydration of **AH**$^+$ and not from **A**[24,25] (only at basic pH values where $^-$OH can attack the quinoidal base directly).[29] As pointed out before, less importance to the formation of the *trans*-chalcone was given because this species is present at minor amounts.

The later work of McClelland carried out with synthetic flavylium salts, possessing *trans*-chalcone as the major species at moderately acidic pH values is already a clear outlook of the network and its kinetics.[28,29] Moreover, this author discussed the hydration reaction, pointing out that it can occur also in position 4, leading to the formation of **B$_4$**. However, the product formed disappears quickly, it is a kinetic product only detected by stopped-flow techniques, to form the thermodynamically stable **B** form that can evolve to **Cc**.[28] In the case of 4'-hydroxyflavylium this species was not taken into account by the same author[29] and it can generally be excluded from the discussion, since in the equilibrium it is present in negligible amounts.

Only in 1994, the complete elucidation of the photochemistry of the flavylium network was reported for the compound 7,4'-dihydroxyflavylium.[30]

1.2.3. Thermodynamics of the network of reactions

The complex network of flavylium compounds in water, from acidic to neutral pH values, is accounted for by equations 1.22 - 1.25:[31]

$\mathbf{AH}^+ + H_2O \rightleftharpoons \mathbf{A} + H_3O^+$	K_a	Proton transfer	(1.22)
$\mathbf{AH}^+ + H_2O \rightleftharpoons \mathbf{B} + H_3O^+$	K_h	Hydration	(1.23)
$\mathbf{B} \rightleftharpoons \mathbf{Cc}$	K_t	Tautomerization	(1.24)
$\mathbf{Cc} \rightleftharpoons \mathbf{Ct}$	K_i	Isomerization	(1.25)

Equations 1.22 - 1.25 can be substituted by a single acid-base equilibrium, with an apparent acidity constant K'_a:

$$\mathbf{AH}^+ + H_2O \rightleftharpoons \mathbf{CB} + H_3O^+ \quad K'_a = \frac{[CB][H_3O^+]}{[AH^+]} \qquad (1.26)$$

$$K'_a = K_a + K_h + K_h K_t + K_h K_t K_i \qquad [CB]=[Ct]+[Cc]+[B]+[A] \qquad (1.27)$$

The mole fraction distribution of the different species is calculated as follows:

$$\chi_{AH^+} = \frac{[H^+]}{[H^+] + K'_a}; \qquad (1.28)$$

$$\chi_A = \frac{K_a}{[H^+] + K'_a}; \qquad (1.29)$$

$$\chi_B = \frac{K_h}{[H^+] + K'_a}; \qquad (1.30)$$

$$\chi_{Cc} = \frac{K_h K_t}{[H^+] + K'_a}; \qquad (1.31)$$

$$\chi_{Ct} = \frac{K_h K_t K_i}{[H^+] + K'_a} \qquad (1.32)$$

Nowadays, a routine procedure involving various experimental techniques, such as pH jumps followed by UV-Vis spectroscopy, NMR spectroscopy, flash photolysis and stopped flow measurements, that allows the determination of all the equilibrium constants (in some cases) has been firmly established.[31,32,33]

A convenient way to represent the flavylium network is the use of an energy level diagram where Gibbs free energy, ΔG^o, of the different equilibria is represented at different pH values, Scheme 1.9 A.[31] At low pH values $\mathbf{AH}^+$ is the most stable species. As pH increases the components of the conjugated bases become the more stable species, the respective equilibrium concentrations depending on the relative energy level. In alternative, the network can be described through the mole fraction distribution in the equilibrium of the several species by means of equations 1.28-1.32, Scheme 1.9 B.

[a] From now on, and for the sake of simplicity, the notation $[H^+]$ will be often used.

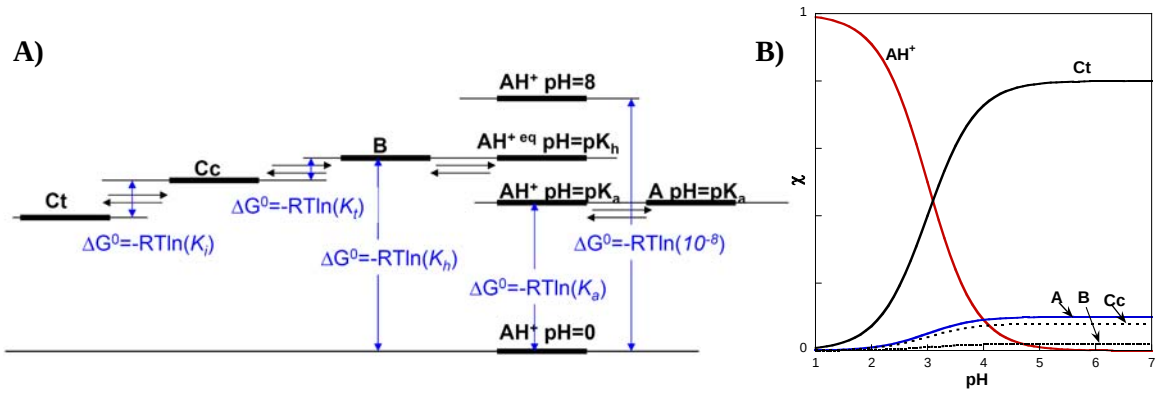

Scheme 1.9 – A) Construction of energy level diagrams. B) Example of mole fraction distribution at the equilibrium.

A pseudo-equilibrium can be assumed when the *cis-trans* isomerization barrier is high enough so that isomerization can be considered to take place much slower, in a second time scale, allowing to consider that **AH**$^+$, **A**, **B** and **Cc** are equilibrated before significant appearance of **Ct**. When this is the case, a pH jump from **AH**$^+$ to more basic pH values is performed and, for instance, after one hour the UV-Vis measurement is performed and **Ct** is not yet detected. The formalism of the pseudo-equilibrium is accounted for by equations 1.33-1.35:

AH$^+$ + H_2O ⇌ **A** + H_3O^+	K_a	Proton transfer	(1.33)
AH$^+$ + $2H_2O$ ⇌ **B** + H_3O^+	K_h	Hydration	(1.34)
B ⇌ **Cc**	K_t	Tautomerization	(1.35)

In a similar way to the previous treatment, equations 1.33 - 1.35 can be substituted by a single acid-base equilibrium, in which $K^{\wedge}_a$ is the pseudo-equilibrium contant:

AH$^+$ + H_2O ⇌ **CB**$^{\wedge}$ + H_3O^+ $\qquad K^{\wedge}_a = \dfrac{[CB^{\wedge}][H^+]}{[AH^+]}$ (1.36)

$K^{\wedge}_a = K_a + K_h + K_h K_t$ $\qquad$ [CB$^{\wedge}$]=[Cc]+[B]+[A] (1.37)

The mole fraction distribution of the different species is calculated from equations 1.38 - 1.41:

$$\chi^{\wedge}_{AH^+} = \frac{[H^+]}{[H^+]+K^{\wedge}_a}; \tag{1.38}$$

$$\chi^{\wedge}_{A} = \frac{K_a}{[H^+]+K^{\wedge}_a}; \tag{1.39}$$

$$\chi^{\wedge}_{B} = \frac{K_h}{[H^+]+K^{\wedge}_a}; \tag{1.40}$$

$$\chi^{\wedge}_{Cc} = \frac{K_h K_t}{[H^+]+K^{\wedge}_a} \tag{1.41}$$

With this treatment for the cases where a pseudo-equilibrium can be defined, identical diagrams to the ones presented in Scheme 1.9 A and B can be easily obtained.

1.2.4 Kinetics of the network of reactions

The chemical processes taking place in Scheme 1.8 can be divided into four different scales of time: i) microseconds for proton transfer [24,25,28] ii) seconds to minutes in the case of the hydration,[24,25,27,28,29] iii) sub-seconds for tautomerization (ring opening and closing),[28,29] iv) between seconds and days for the *cis-trans* isomerization.[28,29] Using the appropriate technique it is possible in most cases to separate if not all, at least three of the four kinetic processes and measure the respective rate constants. The overall kinetic process is very dependent on the magnitude of the *cis-trans* isomerization barrier. If the barrier is high, this kinetic process is the slowest one, as pointed out previously, occurring between hundreds of minutes to days and can be separated from the other processes.

The proton transfer reaction is very fast and the respective kinetics is available, for example, with temperature jump techniques.[24,25, 28]As shown in literature, the system will approach the first (pseudo)equilibrium exponentially with a rate constant k_1 equal to the sum of the forward and backward reactions, $k_1 = k_a + k_{-a}[H^+]$.[34]

To access the other kinetics of the system pH jumps are carried out. For example, starting from $\mathbf{AH^+}$ at very acidic pH values and jumping to moderately acidic, leads to the immediate formation of the quinoidal base **A**, as a kinetic product (not possible to follow by stopped flow techniques). However, the further evolution of the system can be monitored by a common spectrophotometer, and if it is very fast by stopped flow analysis. This process occurs by the hydration reaction of $\mathbf{AH^+}$ to give **B**. The kinetic product **A** disappears with the same rate $\mathbf{AH^+}$, because this equilibrium is much faster than the other, meaning the two species behave like a single species. The tautomerization of **B** leading to **Cc** is now the following process. The rate determining step of this process is usually the hydration and by consequence the system will approach the second equilibrium (pseudo-equilibrium) exponentially with a rate constant k_2 given by:

$$k_2 = \frac{[H^+]}{[H^+] + K_a} k_h + \frac{k_{-h}}{(1 + K_t)} [H^+] \tag{1.42}$$

Finally the rate of the slowest isomerization leading to the final equilibrium is given by k_3:

$$k_3 = \frac{K_h K_t}{[H^+] + K^\wedge_a} k_i + k_{-i} \tag{1.43}^{34}$$

More information about the kinetics of the system can be reached if *reverse pH jumps* are performed, i. e., a solution is allowed to reach the pseudo-equilibrium, before interference of the *trans*-chalcone, and then reacidified. Using stopped flow techniques it is possible to follow this process. As the dehydration reaction depends on the proton concentrations and can be made faster by increasing $[H^+]$ it is possible to observe a bi-exponential formation of flavylium cation: the first kinetics due to the dehydration, and the second one to the tautomerization, *i.e.* (formation of $\mathbf{AH^+}$ from **Cc** through **B**). Indeed, stopped flow measurements are a very powerful method to access the intricate network of reactions of flavylium cations in aqueous solution, particularly to determine K_t.[35,36,37,38]

In the opposite case, if the barrier is small, *cis-trans* isomerization can compete with the hydration-dehydration and the overall kinetic process is more complex. In the case of the flavylium compounds bearing a 7-hydroxy substituent, the system can be described as in equation 1.44 where the hydration and the *cis-trans* isomerization are the rate controlling steps. In other words, $\mathbf{AH^+}$ and **A** can be considered in fast equilibrium behaving as a single species, the same assumption can be made for **B** and **Cc**.

$$\mathrm{A} \underset{}{\overset{K_a}{\rightleftharpoons}} \mathrm{AH^+} \underset{k_{-h}[H^+]}{\overset{k_h}{\rightleftharpoons}} \mathrm{B} \overset{K_t}{\rightleftharpoons} \mathrm{Cc} \underset{k_{-i}}{\overset{k_i}{\rightleftharpoons}} \mathrm{Ct} \tag{1.44}$$

The steady state hypothesis can be applied to the species **B** and **Cc** leading to equation 1.45 where the observed rate constant presents a bell shape curve as a function of pH, in which k_{-i} is a limit for low pH and zero an upper limit for high pH, Figure 1.1 (see Supplementary Material, section 9.1.1).[39,40]

$$k_{obs} = \frac{\dfrac{[H^+]}{[H^+]+K_a} k_i K_t K_h + k_{-i}[H^+]}{[H^+]+\dfrac{k_i K_t}{k_{-h}}} \tag{1.45}$$

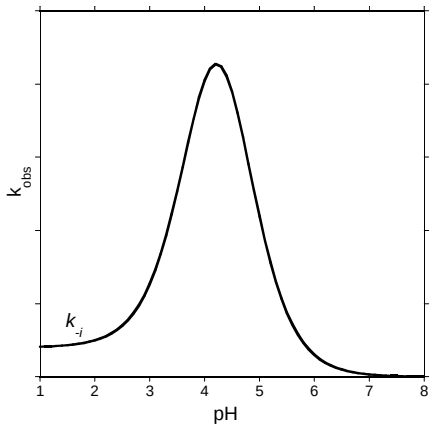

Figure 1.1 – Global rate constant as a function of pH, for the cases where there is no thermal barrier from *cis-trans* isomerisation.

1.2.5. Flash photolysis and continuous irradiation

The use of flash photolysis to study the network of flavylium compounds was introduced by Pina and Maestri in 1997.[40] In most of the cases, the network relevant processes followed by flash photolysis are in the timescale of seconds and an easy experimental set up, using a common spectrophotometer can be used.[41] Immediately after the flash the bleaching of the **Ct** absorption is observed indicating that this species is consumed to give **Cc**, which generally possesses a lower molar absorption coefficient at this wavelength. In a compound, for instance 2'-methoxyflavylium, that has a high thermal barrier, **Ct** does not recover in the time scale of seconds and $\mathbf{AH}^+$ is formed at low pH values. The increase in absorption of the flavylium species follows a first order kinetic process, the respective rate constants showing a pH dependence which is coincident, within experimental error, with the ring closure constants taken from the reversed pH jump experiments, Figure 1.2.[38]

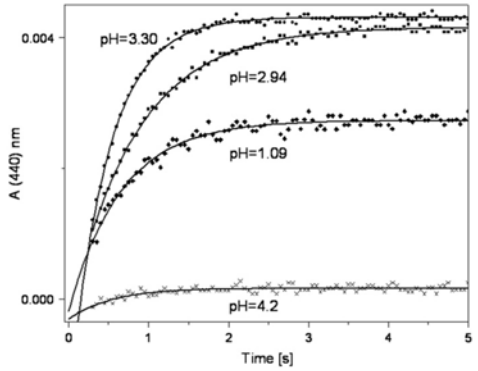

Figure 1.2 – Transient absorption traces obtained by flash photolysis of the compound 2'-methoxyflavylium at 440 nm ($\mathbf{AH}^+$) at indicated pH values.[38]

Two processes exhibiting the same lifetime are observed at different wavelengths, when there is no barrier for *cis-trans* isomerization: i) recovery of **Ct** absorption and ii) formation of $\mathbf{AH}^+$. As the pH increases the amount of flavylium cation formed decreases with concomitant increasing of **Ct** recovery. The global kinetics is compatible with equation 1.46, in which the first term accounts for the recovery of **Ct** and the second term for the formation of $\mathbf{AH}^+$, once again assuming **B** and **Cc** in fast equilibrium.

$$k_{flash} = k_i \frac{K_t}{1+K_t} + k_{-h} \frac{\left[H^+\right]}{1+K_t} \tag{1.46}$$

Equation 1.46 presupposes that both hydration and *cis-trans* isomerization are the rate determining steps and in this case a linear relation of the rate constant as a function of the proton concentration should be observed.

The results of continuous irradiation of an equilibrated **Ct** solution are strongly dependent of the pH, as can be seen in Figure 1.3, for the unsubstituted flavylium ion, a compound with a high barrier.[42] At low pH values the only photoproduct is $\mathbf{AH}^+$, while at pH around 5 only **Cc** is formed. Moreover, if **Cc** absorbs at the wavelength of irradiation, at a certain point the back photoisomerization starts to take place.

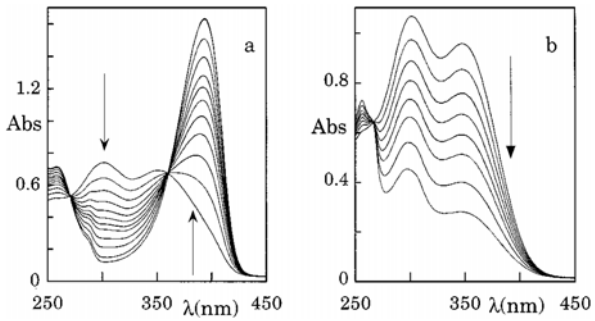

Figure 1.3 – Spectral variations observed upon continuous irradiation (313 nm) of dark equilibrated aqueous solutions of the **Ct** of unsubstituted flavylium as a function of time (initial time increments = 30 s); a) pH = 2.0; b) pH =5.2.[42]

From the initial irradiation points, as the variation in absorption of the photoproduct versus time of irradiation is still linear, it is possible to calculate the isomerisation quantum yield, according to equation 1.47:

$$\Phi = \frac{V_{sol}\dfrac{\Delta A_{\lambda\,obs}}{b\Delta\varepsilon_{\lambda\,obs}}}{\Delta t I_0 (1-10^{-A_{\lambda irr}})} \tag{1.47}$$

in which, V_{sol} is the volume of the solution in L, Δt is the time interval, b is the optical path, λ_{obs} refers to the observation wavelength and λ_{irr} to the irradiation wavelength. Please note that the equation in this form assumes that the photoproduct is not absorbing light at the wavelength of irradiation, and the reagent does not absorb light where the photoproduct is being measured. Finally, I_0 is the light emitted by the source and must be previously determined using an actinometer,[43] like ferrioxalate.[44]

The quantum yield of formation of $\mathbf{AH}^+$ is pH dependent, and in the case of a low thermal barrier it can be given by equation 1.48:

$$\Phi = \Phi_{Ct\rightarrow Cc}\frac{k_{-h}[H^+]}{k_{-h}[H^+]+k_i K_t} = \Phi_{Ct\rightarrow Cc}\frac{[H^+]}{[H^+]+\dfrac{k_i K_t}{k_{-h}}} \tag{1.48}$$

in which, the numerator accounts for the formation of **AH**$^+$ and the denominator is simply a sum of the two processes. That is, the observed quantum yield is given by the product of the intrinsic quantum yield of the reaction by the efficiency of formation of **AH**$^+$.

1.2.6. Photostationary state

Recently it was shown that the photostationary state (PSS) of the flavylium system can be treated with the same expressions used for the equilibrium in the dark, set of equations 1.28-1.32, provided that the isomerization equilibrium constant K_i is substituted by K_i^{PSS}: [45]

$$K_i^{PSS} = \frac{k_i^{photo} + k_i}{k_{-i}^{photo} + k_{-i}} \tag{1.49}$$

where

$$k_i^{photo} = \frac{\Phi_{Cc\rightarrow Ct} I_0 (1-10^{-A_{\lambda_{irr}}}) b\varepsilon_{Cc}}{v_{irr} A_{\lambda_{irr}}}; \tag{1.50}$$

$$k_{-i}^{photo} = \frac{\Phi_{Ct\rightarrow Cc} I_0 (1-10^{-A_{\lambda_{irr}}}) b\varepsilon_{Ct}}{v_{irr} A_{\lambda_{irr}}} \tag{1.51}$$

being ν_{irr} the frequency of irradiation and the other notations have been defined previously.

The photostationary state can be visualized through the energy level diagram shown in Scheme 1.10. A solution of the compound at higher pH values is in this example mainly constituted by **Ct**. However under light **AH**$^+$ and **A** (depending on pH) become more stable and thus they appear as photochemical products. In the dark, the system reverts back to the initial positions the respective rate constant depending on the *cis-trans* isomerization barrier.

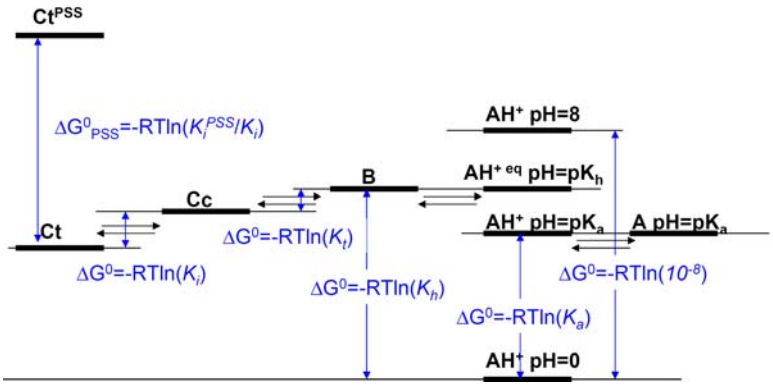

Scheme 1.10 – Construction of energy level diagrams, representing also photostationary state.[45]

This theoretical demonstration was illustrated practically for 7,4'-dihydoxyflavylium, where the concentration of **B** and **Cc** can be neglected and the mole fraction distribution of the species $\mathbf{AH^+}$, **A** and **Ct** at the photostationary state was obtained from decomposition of the spectra in the photostationary state (using the absorption spectrum of the pure species). These experimental data could be fitted and allowed the calculation of the ratio K_i^{PSS}/K_i, and by consequence the energy level of $\mathbf{Ct^{PSS}}$ can be positioned. Considering that the amount of **Cc** at the photostationary state is small in accordance with the spectral variations, an approximation can be done that allows calculating the quantum yield for *trans-cis* isomerisation. The value obtained was demonstrated to be in reasonable agreement with the one obtained through the use of equation 1.48. This recently developed method presents advantages in some cases, namely because experimental errors of Φ can be rather high, due to the **Cc→Ct** thermal isomerization reaction, giving rise to a large uncertainty in the slope of the actinometric measurement, and when the plateau for very acidic pH values is not clearly attained experimentally.[45]

1.2.7. Synthesis

It is outside the scope of this thesis the presentation of an extensive list of synthetic methods leading to flavylium salts,[12] only the most useful, easy to perform and versatile methods will be referred. Some described syntheses involve the preparation of flavonoid precursors with the appropriate carbon skeleton, like 2-hydroxychalcones and flavanones, which seldom are easily accessed, and imply the use of reduction/oxidation steps often with low yields.[12]

The first synthesis of flavylium salts reported in literature, by Bülow and Wagner in 1901 is based on the condensation of β-diketones and resorcinols, Figure 1.4.[46,47] This synthesis is still widely used today, because of its simplicity and high yields, when 4-substituted flavylium salts are needed.

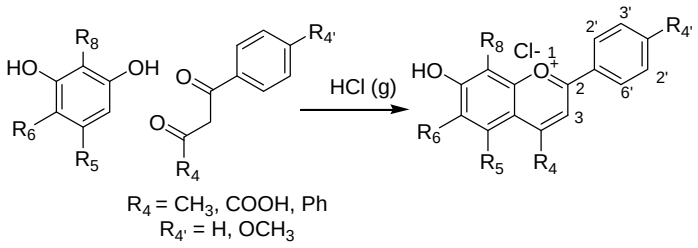

Figure 1.4 – Generic synthesis of flavylium salts based on the condensation of β-diketones and resorcinols. R_x, otherwise indicated can represent OH or alkyl chains. In the case where R_4 is a phenyl ring, $R_{4'}$ must be H, otherwise a mixture of products will be obtained.[48]

Later on, Robinson and co-workers developed a significant work on the synthesis of flavylium salts,[17,49,50] namely a process that involves the condensation of

2-hydroxybenzaldehydes and acetophenones[51] and it is the most widely used method nowadays, Figure 1.5.

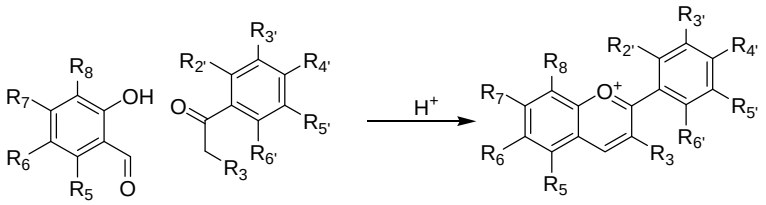

Figure 1.5 – Generic synthesis of flavylium salts based on the condensation of 2-hydroxybenzaldehydes and acetophenones. R_x can represent OH, OCH_3, tertiary amines, alkyl groups (saturated or not), halogens, COOH or NO_2.

Johnson and co-workers also reported a useful synthesis for flavylium salts, based on the condensation of aryl ethynyl ketone and a phenolic derivate, Figure 1.6.[52,53] Although this type of synthetic approach requires always the synthesis of the aryl ethynyl ketone, it is particularly useful when the salicylaldehyde is a benzene-1,3,5-triol (phloroglucinol) derivative, that frequently causes some troubles in Robinson's method.[54] Recently this method, inclusively the synthesis of non commercial reagents, was optimized by Chassaing and his team[54] that showed that it can be used with excellent yields in a series of derivatives and also provided some insight into the mechanism of the reaction. This method can not be used with simple phenol, only resorcinols and phloroglucinols.

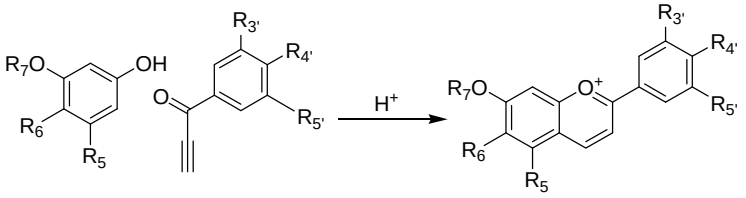

Figure 1.6 – Generic synthesis of flavylium salts based on the condensation of phenols and aryl ethynyl ketones. R_5,R_6= H,OH; R_7=H,CH_3; $R_{3'}$,$R_{4'}$,$R_{5'}$= H, OH or OCH_3.

From this pioneer works on, many flavylium synthesis have been published. However, most of them report only new patterns of substitution in the usual reagents or optimization of solvents and/or acid used. A work that deserves some attention was developed by Katritzky and his co-workers,[55] in which aqueous HBF_4 and acetic anhydride are used instead of the classical gaseous HCl. With this method it is particularly straightforward to obtain flavylium salts.

In Table 1.1, a list of flavylium ions that have been reported in the literature to work as multistate/multifunctional molecular level systems is presented. This topic will be described in the next subsection.

Table 1.1 – Flavylium ions used in multistate/multifunctional systems.

Flavylium	Ref.	Flavylium	Ref.
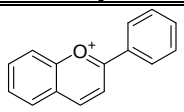	42	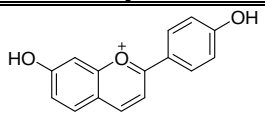	56,57
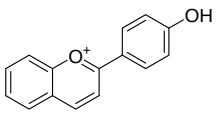	58,59,60	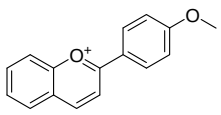	61
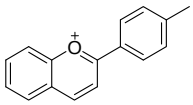	62	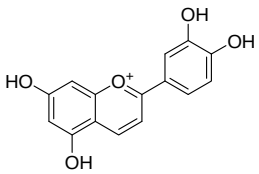	63
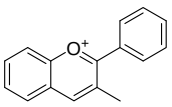	64	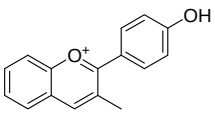	64
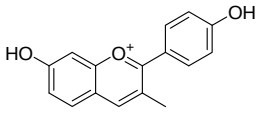	64	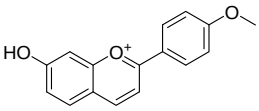	65
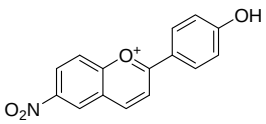	66	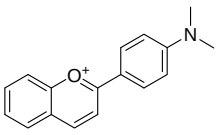	33
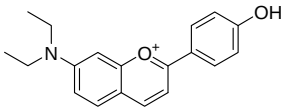	67,68	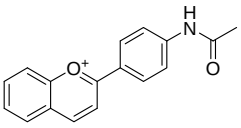	69
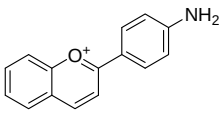	69	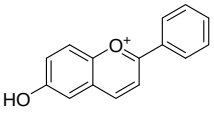	70

Besides isolating the flavylium cation, it is frequently also useful to isolate the *trans*-chalcone. It can be done from the flavylium salt, dissolving the previously isolated species in very basic media so that $\mathbf{Ct}^{n-}$ is formed (the reaction time depending critically of the substituents of the flavylium ion) and then neutralizing carefully the solution[71] or, using a reaction scheme similar to what is presented in Figure 1.5, but using very basic media and neutralizing afterwards.[72]

1.2.8. Multistate/Multifunctional molecular-level systems based on photochromic flavylium compounds

As previously pointed out, the interest in the study of flavylium is closely connected to the use of anthocyanins as food colorants. Indeed, anthocyanins are of the most used vegetable colorants in the food industry.[73] Another significant property of anthocyanins is their antioxidant activity, which plays a vital role in the prevention of neuronal and cardiovascular illnesses, cancer and diabetes, among others.[74]

However, in the last 12 years our group has been exploiting the possibility of using photochromic flavylium ions as the basis for molecular based optical memory devices. In this part a brief summary of this interesting application is outlined.

A photon is simultaneously a quantum of energy and a bit of information. Energy conversion exploits the first property while the second is related to the construction of molecular-level switching devices capable of generate, convert, store and detect signals, a subject entitled as *semiochemistry* by Lehn.[75] These devices imply the application of photochromic molecules, molecules that can be reversibly interconverted between two forms with different colors, with at least one of the reactions being induced by light excitation.[76] The first scientist who carried out systematic investigations on photochromic compounds as computer memory elements was Hirshberg.[77] In the following years, there has been a strong development of research on photochromic molecular memories, with a great number of patents granted, particularly in Japan.[76] Currently, much interest is devoted to the possibility of using photochromic compounds for information processing at the molecular level.

In photochromic systems the interconverting species are isomers, because the photoreaction simply causes rearrangement of the electronic and nuclear structure of the molecule - light excitation causes switching from a stable isomer **X** to a higher-energy isomer **Y** which is expected to reconvert to **X** on overcoming a more or less high energy barrier, being this back reaction fast or slow. Sometimes the photoproduct might be kinetically inert and the process can be reverted only by use of a second light stimulus.[76]

The simplest photochromic compounds are bistable species that can be interconverted between two forms (**X** and **Y**) exhibiting different colors. Most photochromic compounds change their color by photoexcitation and revert to the initial state when kept in the dark (Scheme 1.11 a). Compounds exhibiting this behavior are useless for information storage (or switching purposes) since the written information (switching state) is spontaneously erased (back converted) after a relatively short time.[76]

Other photochromic compounds do not return to the initial state thermally, but can undergo reversible photoisomerization (Scheme 1.11 b). Such compounds can be used for optoelectronic devices. However, they present a severe problem: the light used for reading the written data (detecting the switching state) causes the back-conversion of the sampled

molecules and therefore the gradual loss of information (state definition). Several attempts have been made to overcome this difficulty, including the use of photochemically inactive infrared light to read the status of the system.[76] A general approach to avoid destructive reading is to combine two reversible processes that can be addressed by means of two different stimuli (dual-mode systems). In such systems (Scheme 1.11 c), light is used to convert **X** to **Y** (*write*); a second stimulus (e.g. proton) is then used to transform **Y** (which would be reconverted back to **X** by a direct photon-reading process) into **Z**, another stable state of the system (*lock*) that can be optically detected without being destroyed (*read*). By use of this process the change caused by the writing photon is safeguarded. When the written information must be erased **Z** is reconverted back to **Y** (*unlock*) by an opposite stimulus (e.g. base) and **Y** is then reconverted back to **X** (*erase*). Such a *write-lock-read-unlock-erase* cycle can constitute the basis for optical memory systems with multiple storage and nondestructive readout capacity. This concept of dual-mode stimulation can be taken further and systems capable of existing in several forms (multistate) that can be interconverted by different external stimuli (multifunctional) can be conceived.[76]

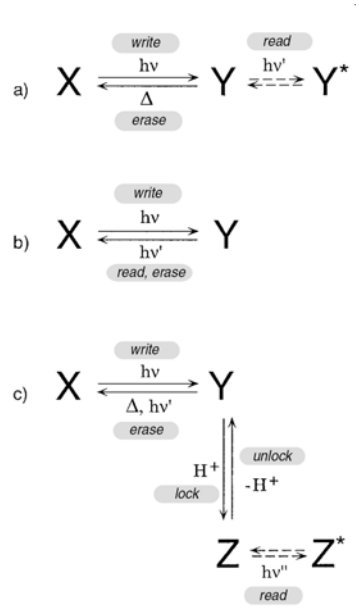

Scheme 1.11 – Schematic representation of the behavior of three types of photochromic systems. a) The photochemical reaction of the form **X** reverts by thermal means in the dark. b) The photochemical reaction of the form **X** reverts only through light excitation of the form **Y**. c) The form **Y** which reverts to **X** through light excitation, can be transformed by means of a second stimulus (such as an acid/base reaction) into another form **Z**, which is stable toward light excitation and, when necessary, can be reconverted to **Y**.[76]

Focusing on the photochromism of flavylium compounds, the selection of the pH to obtain the best performance of a photochromic system is a balance between the need of having the highest possible proton concentration to force the system to form $\mathbf{AH}^+$ and the mole fraction of $\mathbf{AH}^+$ present at the equilibrium. Indeed, if the proton concentration is too high, $\mathbf{AH}^+$ is already present in significant amounts in the equilibrium and the dark state is no longer colorless. In Figure 1.7, the mole fractions of species present at the equilibrium and in the photostationary

state are plotted versus pH. In the case of compounds without hydroxyl substituents the *auto-lock* pH should be the one marked with the arrow in Figure 1.7: it decreases the amount of $\mathbf{AH}^+$ in the dark state, and maximizes the colored $\mathbf{AH}^+$ species after irradiation.

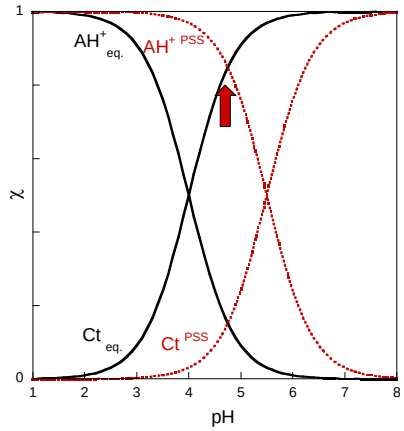

Figure 1.7 – Mole fraction of the species present at the equilibrium and in the photostationary state. Arrows mark the *lock* pH. Example of a compound without hydroxyl groups.

Of course that the just described photochromism is useless for storage purposes, because the photoproduced $\mathbf{AH}^+$ will revert to **Ct**, which is the thermodynamically stable species, even if the process is slow, as in the case of flavylium ions with high thermal barrier for isomerization. The key step to produce a model for a permanent optical memory is the introduction of a second input, addition of protons immediately after the light input, *i.e. write* followed by *lock*.[61] The existence of a thermal *cis-trans* isomerization barrier is a necessary requirement, to avoid the back reaction of **Cc** to **Ct** between the two inputs.

The 4'-methoxyflavylium[61] compound can operate through the *write-lock-read-unlock-erase* cycle illustrated in Scheme 1.11 c and therefore it can be taken as a basis for optical memory systems presenting multiple storage abilities. The behavior of the 4'-methoxyflavilium ion can be described making reference to Scheme 1.12 (which refers to a solution at pH = 3.0), where **Ct**, **Cc**, and $\mathbf{AH}^+$ play the role of the generic species **X**, **Y**, and **Z** of Scheme 1.5 c:

1) the stable form **Ct** can be photochemically converted by irradiation with 365 nm light (*write*) into a form **Cc** that can be reconverted back either thermally or on optical reading;

2) by a second stimulus, addition of acid, **Cc** can be converted into a kinetically inert form $\mathbf{AH}^+$(*lock*). The acid can also be present from the beginning without perturbing the behavior of the system (*autolocking*).

3) the $\mathbf{AH}^+$ species exhibits a spectrum clearly distinct from that of **Ct** and is photochemically inactive, so that it can be optically detected (*read*) without being erased;

4) by addition of base, $\mathbf{AH}^+$ can be reconverted into **Cc** (*unlock*);

5) **Cc** can be thermally or photochemically reconverted into the initial **Ct**, form (*erase*).

It should be noted that the locking time of the written information bit is not indefinite (at 25 °C and pH=3.0, the half-life of the back reaction from $\mathbf{AH}^+$ to **Ct** is *ca.* 8 days).

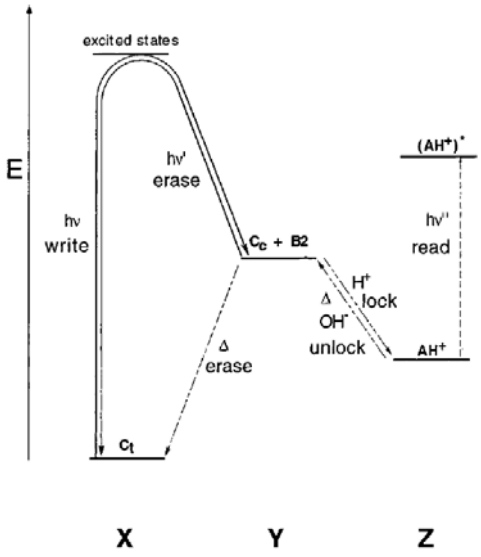

Scheme 1.12 – Schematic energy level diagram for the species involved in the *write-lock-read-unlock-erase* system of 4'-methoxyflavilium, pH = 3.

A cycle equal to that just described can be designed with 4'-hydroxyflavylium[59] and 4'-methylflavylium ion.[62] Among the 4'-substituted flavylium ions, this last compound exhibits the lowest energy barrier for the *cis–trans* isomerisation reaction. Lowering the activation energy of the *cis–trans* isomerisation reaction favors auto-erasing, discouraging its use for an optical memory system.[62] The 4'-hydroxy-3-methylflavylium compound can also be used to operate a *write-lock-read-unlock-erase* cycle.[64]

Due to its high isomerization barrier, also 4'-hydroxy-6-nitroflavylium can be efficiently used in *write-lock-read-unlock-erase* cycles.[66] This compound performs like an optical memory by means of a slightly different cyclic process that involves the following steps: *write/lock-read-unlock-enable/erase-erase*, in which the information is enabled-erased by a second light stimulus.[66]

The 3',4'-(methylenedioxy)flavylium compound, offers the possibility of conceiving two coupled photochromic systems, Scheme 1.13.[35] In the pH range 1 to 6, a cycle capable of *write–read–erase* can be designed. The starting point is the metastable **Ct** species at pH 1.0: **1**) using near-UV light, **Ct** is converted into $\mathbf{AH}^+$ (*write* and *auto-lock*); **2**) once again $\mathbf{AH}^+$ can be easily *readout*. **3**) The system can be *erased* by a pH jump to pH 6.0 in order produce **Cc** (in equilibrium with **B**), which is thermally reconverted into **Ct**. **4**) To prepare the system for a new cycle (*enable*), a second pH jump to 1 should be performed.

The other photochromic system is even more interesting because there is the possibility of two consecutive writing steps.[35] **1**) Starting for example with $\mathbf{Cc}^-$ at pH 11, the first *write* step consists of the irradiation of this species that totally converts into $\mathbf{Ct}^-$; **2**) $\mathbf{Ct}^-$ can be examined by UV-Vis absorption spectroscopy (*read*). **3**) The system can be *erased* through a pH jump to 1 leading to the metastable **Ct** species. **4**) At this point a second *writing* step (the same as the

previous cycle) is possible, converting the system into **AH**$^+$. This last reaction can also be carried out thermally. **5)** Finally, the system should be submitted to a second pH jump to the starting pH value, so that **Cc**$^-$ species is recovered.

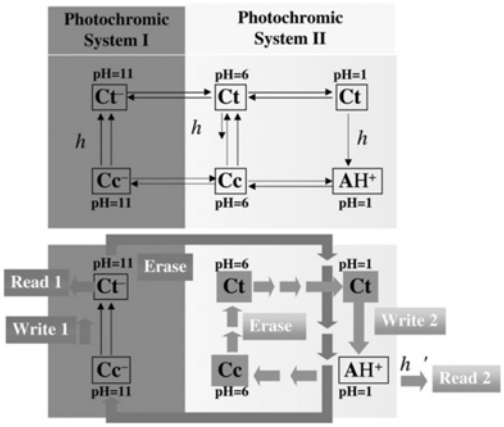

Scheme 1.13 – The network of thermal and photochemical reactions of the compound 3',4'-(methylenedioxy)flavylium allows two *write–read–erase* cycles to be defined.[35]

For the 4'-dimethylamino compound, it is also possible to perform a *write-lock-read-unlock-erase* cycle, operating however in a slightly different way, starting from a **Ct** protonated species (at the amino group), Scheme 1.14.[33]

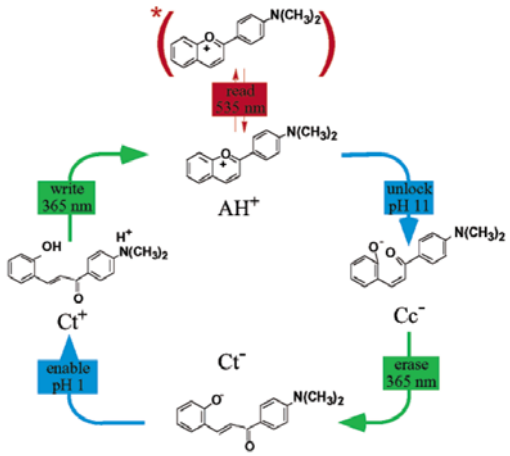

Scheme 1.14 – Example of *the write-lock-read-unlock-erase* cycle based on the 4'-*N*,*N*-dimethylaminoflavylium compound.[33]

A generally overlooked difficulty with photochromic systems is that the starting form is the photoreactive one, so that it cannot be read by absorption spectroscopy without writing.[76] With the 4'-hydroxyflavylium ion it was demonstrated that this difficulty can be overcome starting from **AH**$^+$, which is the thermodynamically stable form at pH = 1. Since **AH**$^+$ is not photosensitive, it can be *read* by light excitation (i. e., by recording its absorption spectrum) without *writing*. Then it can be *unlocked* by a pH jump to 12, which yields the metastable **Cc**$^{2-}$ form. At this stage, one can *write* the optical information obtaining the stable (*locked*) **Ct**$^{2-}$ form that can then be *read*. When necessary, the information stored into **Ct**^{2}- can be *unlocked* by a

pH jump yielding **Ct** and can then be erased by light excitation. The same optimized performance can be obtained starting from $\mathbf{Ct}^{2-}$.

The human brain contains shallow and deep memory forms. The network of processes interconverting the various species 4'-hydroxyflavylium allows the presence of different levels of memory. Once the permanent (deep) $\mathbf{AH}^{+}$ form of memory has been obtained (Scheme 1.15), a jump to pH 12 leads to the formation of a temporary (shallow) memory state, $\mathbf{Cc}^{2-}$, whose spontaneous slow *erasure* to give the deep $\mathbf{Ct}^{2-}$ memory can be accelerated by light. Reset can then be accomplished by a back pH jump to pH 4.[59]

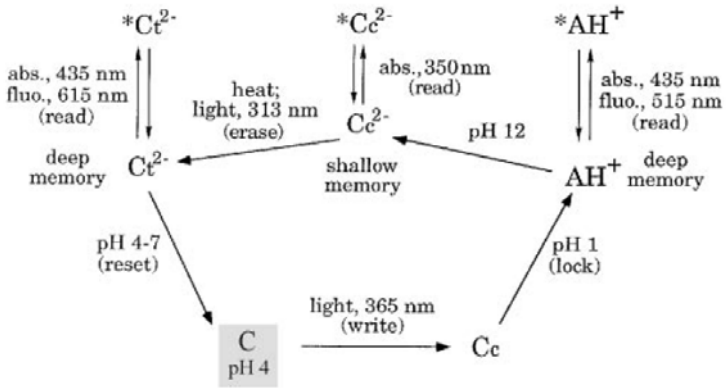

Scheme 1.15 – A *write-lock-read –unlock-erase cycle* with two memory levels. [59]

In the case of the unsubstituted flavylium cation,[42] besides a cycle starting from **Ct**, a cycle based on the anionic species can also be performed, Scheme 1.16. This second cycle starts at pH = 11 with the $\mathbf{Ct}^{-}$ form that is not photosensitive. Then, two different paths can be followed: one begins with a pH jump to pH = 6 which leads to **Ct**; the other starts with a pH jump from 11 to 0, leading to **Ct** that can be photochemically *written* (and *autolocked* because of the low pH) to $\mathbf{AH}^{+}$. When necessary, $\mathbf{AH}^{+}$ can be unlocked by a pH jump to 11 and thermally erased to give back $\mathbf{Ct}^{-}$. Once again in this cycle reading can be performed in both the initial $\mathbf{Ct}^{-}$ (*non-written*) and final $\mathbf{AH}^{+}$ (*written*) states without *writing* or *erasing*. However, auto-unlocking cannot occur and two pH changes per cycle are needed, increasing significantly the overall mass of the system.[42]

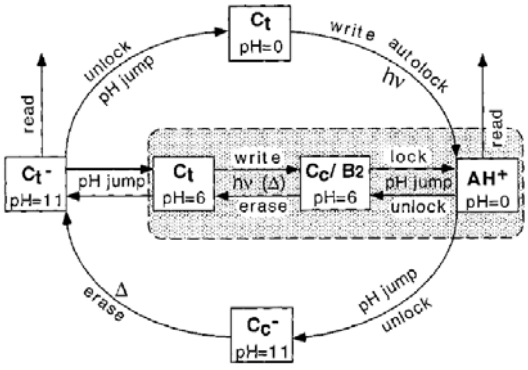

Scheme 1.16 – *Write-read-lock-erase* cycles for the unsubstituted flavylium compound.

The pH driven cycle of compound 7-(*N,N*-diethylamino)-4'-hydroxyflavylium[67] constitutes an example of unidirectional pH cycle because the reverse reaction follows a different pathway from the forward reaction.

Simple (bistable) photochromic systems perform YES/NO logic operations. Multistate/multifunctional molecular-level systems can be taken as bases for more complex logic operations. Chemical systems capable to perform AND, OR, XOR, and XNOR[78] logic operations and integration of logic functions and sequential operation of gates at the molecular-scale have been reported.[76] With the 4'-hydroxyflavylium compound, light excitation and pH jumps can be taken as inputs and absorbance or fluorescence as outputs. Starting from the non-emitting **Ct** species and taking the emission of $\mathbf{AH^+}$ at 515 nm as output signal, jump to pH = 1 alone or light excitation alone are not able to generate the output, whereas when these two inputs are applied in series, the output is obtained (AND logic function, Table 1.2).

Table 1.2 –Truth Table for the AND logic behavior of the 4'-hydroxyflavylium compound starting from Ct at pH = 5.5.[76]

Input 1[a]	Input 2 [b]	Output [c]
0	0	0
1	0	0
0	1	0
1	1	1

[a] pH jump to pH = 1, [b] light excitation at 365 m, [c] absorbance or emission at 515 nm of the $\mathbf{AH^+}$ species.

An interesting system, based on the 4'-methoxyflavylium ion, capable of behaving according to an XOR (eXclusive OR) logic has been reported.[79] The system consists of an aqueous solution containing the **Ct** form of the 4'-methoxyflavylium ion and the $[Co(CN)_6]^{3-}$ complex ion. Excitation by 365 nm light of **Ct**, which is the thermodynamically stable form of the flavylium species in the pH range 3-7, causes the *trans-cis* photoisomerization reaction ($\Phi = 0.04$). If the solution is sufficiently acid (pH < 4), the **Cc** isomer is rapidly protonated with conversion to the 4'-methoxyflavylium ion $\mathbf{AH^+}$, which is kinetically stable under such pH conditions and exhibits an intense absorption band with maximum at 434 nm. At higher pH values, however, protonation does not occur and the **Cc** photoproduct is back converted to **Ct**. As far as $[Co(CN)_6]^{3-}$ is concerned, excitation by 254 or 365 nm light in acid or neutral aqueous solution causes the dissociation of a CN^- ligand from the metal coordination sphere (quantum yield = 0.31), with a consequent increase in pH.[79]

When an acid solution (pH = 3.6) containing 2.5×10^{-5} M **Ct** and 2.0×10^{-2} M $[Co(CN)_6]^{3-}$ is irradiated at 365 nm, most of the incident light is absorbed by **Ct**, which undergoes photoisomerization to **Cc**. Since the pH of the solution is sufficiently acid, **Cc** is rapidly protonated, with the consequent appearance of the absorption band with maximum at 434 nm characteristic of the $\mathbf{AH^+}$ species. On continuing irradiation, it can be observed that the absorption band increase in intensity, reach a maximum value, and then decrease up to complete disappearance. In summary, $\mathbf{AH^+}$ first appears and then disappears with increasing

irradiation time. The reason for this behavior under continuous light excitation is that as **Ct** is consumed with formation of $\mathbf{AH^+}$**,** an increasing fraction of the incident light is absorbed by $[Co(CN)_6]^{3-}$, which undergoes dissociation, causing an increase in the pH of the solution. This not only prevents further formation of $\mathbf{AH^+}$, which would imply protonation of the **Cc** molecules that continue to be formed by light excitation of **Ct**, but also causes the back reaction to **Cc** (and then to **Ct**) of the previously formed $\mathbf{AH^+}$ molecules. Clearly, the examined solution performs like a threshold device as far as the input (light) / output (spectroscopic properties of $\mathbf{AH^+}$) relationship is concerned. Instead of a continuous light source, pulse flash irradiation can be used. Under the input of only one flash, a strong change in absorbance at 434 nm is observed, due to the formation of $\mathbf{AH^+}$. After 2 flashes, however, the change in absorbance practically disappears. In other words, an output (434 nm absorption) can be obtained only when *either* input 1 (flash I) *or* input 2 (flash II) are used, whereas there is no output under the action of *none* or *both* inputs. This shows (Table 1.3) that the above described system behaves according to an XOR (eXclusive OR) logic, under control of an intrinsic threshold mechanism. It is noteworthy that the input and output signals have the same nature (light).[79]

Table 1.3 – Truth Table for the XOR (eXclusive OR) logic behavior of the 4'-methoxyflavylium $[Co(CN)_6]^{3-}$ system starting from pH = 3.6.[79]

Input 1[a]	Input 2 [a]	Output [b]
0	0	0
1	0	1
0	1	1
1	1	0

[a] the two inputs are identical and consist of the amount of photons necessary to achieve the maximum response, [b] variation of absorbance at 434 nm or emission at 515 nm of the $\mathbf{AH^+}$ species.

Several new multistate systems can be designed, and new routes can be envisaged with known systems, for instance, it was already shown that for the unsubstituted flavylium cation different paths can be followed to obtain the same result and for the 4'-hydroxyflavylium compound the network of processes is even more intricate and several species are interconnected by multiple reaction patterns - in order to go from $\mathbf{AH^+}$ to **Ct** three different routes can be chosen.[59] However, what is desirable is to aim at higher levels of operation, for instance, through the assembly of several multistate systems together, each system operating by its own kinetic and thermodynamic rules. A new level of complexity could indeed be introduced by connecting two multistate networks based on 4'-acetamidoflavylium and 4'-aminoflavylium, possessing six- and sevenfold multistates, respectively, and that can be reversibly interchanged by inputs of light, pH jumps and heat. The two networks are connected irreversibly, the 4'-acetamidoflavylium being transformable into the 4'-aminoflavylium by means of a heat input in extremely acidic solutions, Scheme 1.17.[69]

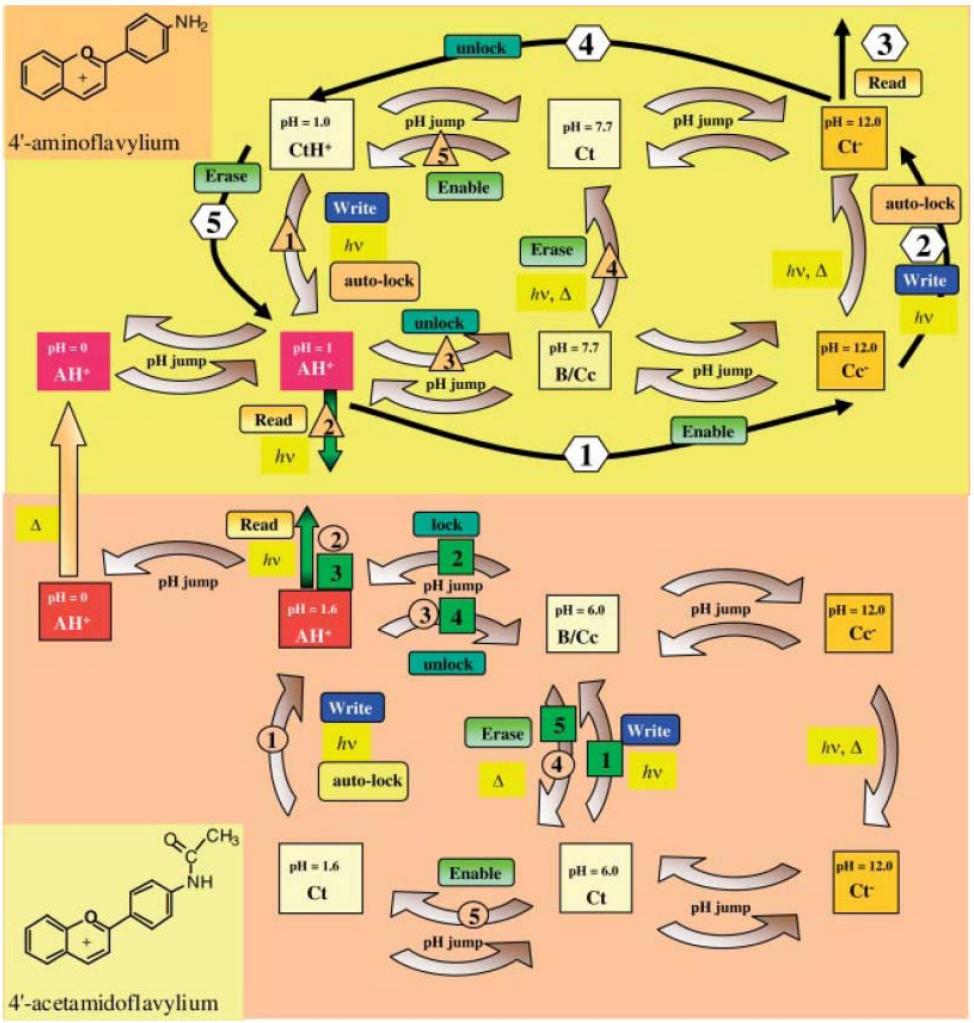

Scheme 1.17 –Thermal, pH-induced and light-induced interconverting pathways between all possible forms in 4'-acetamidoflavylium (bottom) and 4'-aminoflavylium (top) systems, allowing several *write-lock-read-unlock-erase* cycles involving different species.[69]

In the case of 4'-acetamidoflavylium (Scheme 1.17, bottom, numbers inside squares), one possible cycle starts with the **Ct** species in the equilibrium at pH = 6.0: **1**) the photochemical *write* step gives a mixture of **B**/**Cc** (the system has the drawback of not being completely converted into **B**/**Cc** state); **2**) the *lock* step results from the pH jump 6 to 1.6, forming $\mathbf{AH^+}$, which is stable and can be *read*; **3**) the *unlock* step corresponds to the pH jump from 1.6 to 6 to give **B**/**Cc**; **4**) the *erasing* can be achieved by an heat input. For this flavylium, yet another cycle can be conceived, by starting with metastable **Ct** species at acidic pH (Scheme 1.17, bottom, numbers inside circles).

In the case of the compound 4'-aminoflavylium (Scheme 1.17, top), cycles starting from the **Ct** or the $\mathbf{Ct^-}$ species are not feasible as they are not photoactive. However, it is possible to start with the $\mathbf{CtH^+}$ species available in pseudoequilibrium at pH 1 as a metastable species (Scheme 1.17, top, numbers inside triangles). Because of the low pH value of the system, the *autolock* step is spontaneous upon irradiation: **1**) the *cis*-chalcone evolving to **B** (both possibly protonated) and finally to $\mathbf{AH^+}$ which can be *rea*d (**2**). The *unlock* step (**3**), giving **Cc** (in this compound **B** is residual) is made by a pH jump 1 - 7. The *erasing* (**4**) can be done by a heat

input or, better, by using light to allow the formation of **Ct**. At this pH value this compound is thermodynamically stable and photoinactive and the system can be stored. To allow the next cycle, it is necessary to use the *enable* step (**5**) through a pH jump from 7 to 1. Other cycles involving the basic species of the 4'-aminoflavylium can be conceived, passing through the ionized *cis* and *trans*-chalcones (see, *e. g*., Scheme 1.17, top, numbers inside hexagons).

While each memory cycle operates over states of a given flavylium system, the upper level of information would operate over memory cycles within a system and over crossing from one system to another. The sequence of instructions necessary to carry out an optical memory cycle may be defined as its algorithm. On this basis, the *write-lock-read-unlock-erase* cycle starting with the **Ct** species of 4'-acetamidoflavylium at pH = 6.0 (Scheme 1.17, bottom, numbers in squares) is described by an algorithm consisting of the following sequence of instructions: **1**) irradiation at 365 nm, **2**) pH jump from 6.0 to 1.0, **3**) measurement of the absorption at 438 nm ($\mathbf{AH}^+$ absorption), **4**) pH jump 1.0 to 6.0, and **5**) thermal input. Indeed, each memory cycle operates according to a defined and unique algorithm. Moreover, it is possible to change from the 4'-acetamidoflavylium network to the 4'-aminoflavylium one by another algorithm containing two instructions: **1**) pH jump to pH = 0 (or even pH = 1.0), or **2**) thermal input.

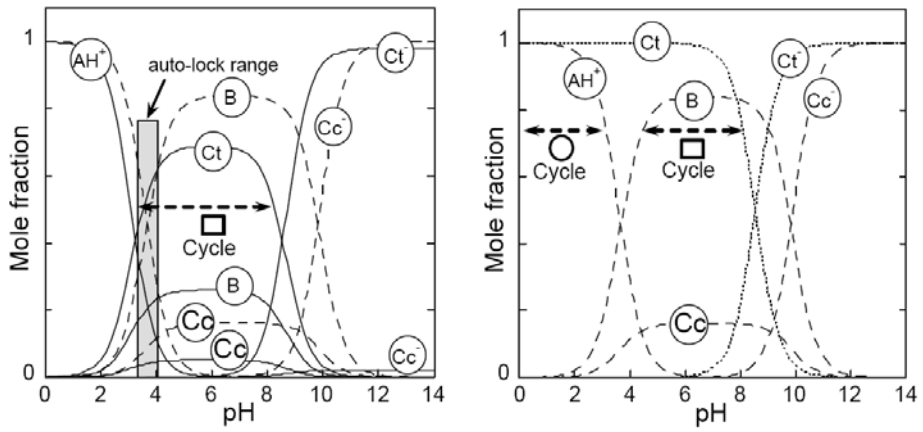

Figure 1.8 –Mole fraction distribution of 4'-acetamidoflavylium: a) solid line -thermodynamic equilibrium, dashed line - pseudo-equilibrium $\mathbf{AH}^+/\mathbf{B}/\mathbf{Cc}/\mathbf{Cc}^-$; b) traced line - pseudo-equilibrium $\mathbf{AH}^+/\mathbf{B}/\mathbf{Cc}/\mathbf{Cc}^-$, dotted line - pseudo-equilibrium $\mathbf{Ct}/\mathbf{Ct}^-$.

A careful analysis of the mole fraction distribution of species in Figure 1.8 at the pseudo and at the final equilibrium for each flavylium system provides a useful aid for building up flow diagrams to allow operation over memory cycles and system crossing. Overlapping the information on Scheme 1.17 with the 4'-acetamidoflavylium distribution of species in Figure 1.18 defines an operational pH range for each memory cycle. A similar exercise can be done for the 4'-aminoflavylium. With this information, a flow diagram such as the one shown in Scheme 1.18 can be constructed. As an example, if the $\mathbf{Ct}^-$ species of 4'-acetamidoflavylium is regarded as the starting point of the upper level cycle, the first step would consist of a pH input to acid. If

pH > 8, the **Ct**$^{-}$ form remains unchanged and a further pH input is necessary (return). At 4.5 < pH < 8, the squares cycle can operate, while for pH < 4.5 the *autolock* pH cycle (circles cycle) is available. After operation of the squares cycle, the system is in the **Ct** multistate, and other inputs of pH can be made (return). On the other hand, after operation of the circles cycle, a heat input permits passage to the 4'-aminoflavylium network. At this point, a new pH input is needed to continue: **1**) if pH < 7 the hexagons cycle can be performed, and **2**) if pH > 7, the system is in its pseudoequilibrium and a heat input is necessary to produce the *trans*-chalcone species. The next step is a further pH input: **1**) if pH > 2, it is necessary to return in order to continue, and **2**) if pH < 2, the triangles cycle can operate, and finally stop.[69]

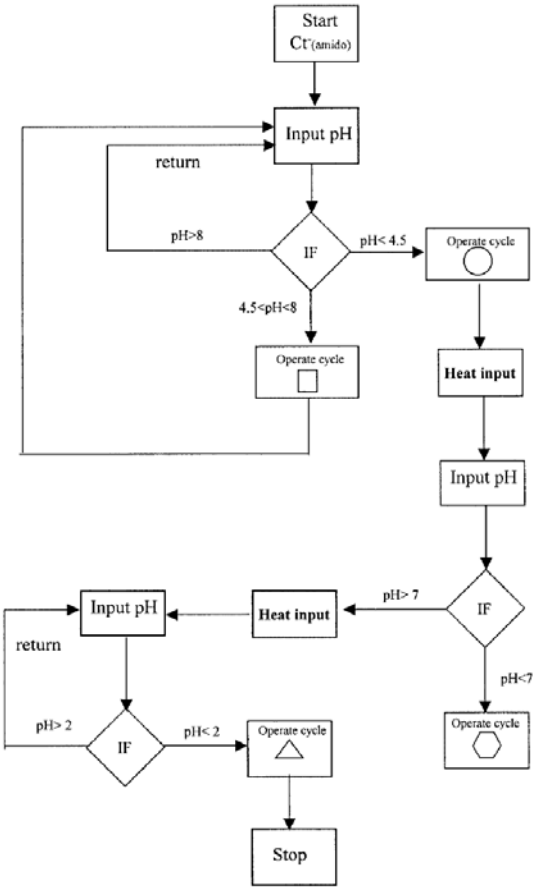

Scheme 1.18 – Example of a flow diagram over memory cycles, defining a sequence of algorithms to be operated in both 4'-acetamidoflavylium and 4'-aminoflavylium chemical networks.

Recently, the synthesis of flavylium ions with new functionalities is opening a new field. The substitution of the flavylium compound in position 6 by a hydroxyl group can be compared with the same substitution in position 4' in terms of the existence of a kinetic barrier for the *cis–trans* isomerization.[70] In the case of the 6-hydroxyflavylium, the quinone/hydroquinone character of the respective chalcones (see Scheme 1.19) allows to obtain quasi-reversible cyclic voltammetry waves. It is well known that flavylium salts and anthocyanins, can be involved in several electrochemical processes, but no reversible electrochemistry was previously reported on flavylium species, not even on flavylium derived chalcones. This compound serves to illustrate for the first time in the flavylium network of

chemical reactions the possibility of using electrochemistry as a new input to reach other states of the network and to achieve even upper level cycles.

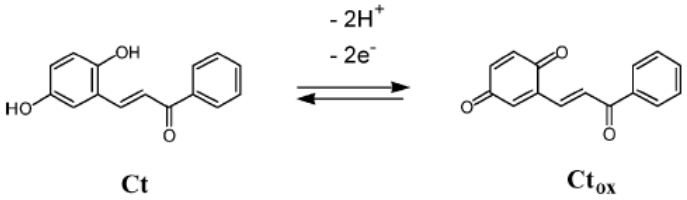

Scheme 1.19 – An electric pulse operating on the **Ct** of 6-hydroxyflavylium.

As discussed above the existence of a *cis–trans* thermal barrier that prevents the back reaction for the operation of an optical memory is required, otherwise the written information is spontaneously *erased* before it can be *read*. The kinetic barrier for *cis–trans* isomerisation is much higher in ionic liquids, which can be explained by a more rigid and stable distribution of **Ct** in the ionic liquid that needs to be disrupted during the thermal isomerization owing to the formation of less-planar intermediates, as well as by the large viscosity of the ionic liquid.[57] This desired property allows operating a *write–read–erase* cycle, for a compound that *per se*, cannot be used as a memory due to the lack of thermal barrier, such as 7,4'-dihydroxyflavylium, Scheme 1.20.

Scheme 1.20 –a) 1-*n*-Butyl-3-methylimidazolium hexafluorophosphate,[bmim][PF_6] (lower phase), **DHF** in 0.01M HCl, $\mathbf{AH^+}$ species (upper phase); b) after moderate shaking, **A** species (lower phase); c) after vigorous shaking, $\mathbf{AH^+}$ species (lower phase); d) after making the aqueous phase alkaline (pH 12) with minimum shaking, $\mathbf{A^-}$ (lower phase), $\mathbf{Ct^{2-}}$ (upper phase); e) after moderate shaking; f) after vigorous shaking, $\mathbf{Ct^{2-}}$ species (upper phase); g) after reacidification of the aqueous phase and vigorous shaking, **Ct** species (lower phase); h) after irradiation of the ionic-liquid phase at 366 nm, $\mathbf{AH^+}$ species.[57]

A very similar cycle was reported using the 4'-hydroxyflavylium compound.[60] Moreover, 7-(*N*,*N*-diethylamino)-4'-hydroxyflavylium exhibits photochromism when used in a water–ionic liquid ([bmim][PF_6]) biphasic systems.[68]

In order to achieve progress towards real practical applications, encapsulation of synthetic flavylium salts in water-permeable crosslinked poly(2-hydroxyethyl methacrylate) (PHEMA) polymer matrices was carried out and a solid multistate/multifunctional system was obtained upon application of light and pH stimuli, Scheme 1.21.[56] This system represents a step towards real applications, but it does present some drawbacks, such as the existence of some leaching during the immersion in acidic and basic solutions (that are used to operate the cycles)

from the more accessible sites. This leaching is reduced in the next cycles probably occurring in more inaccessible sites.[56]

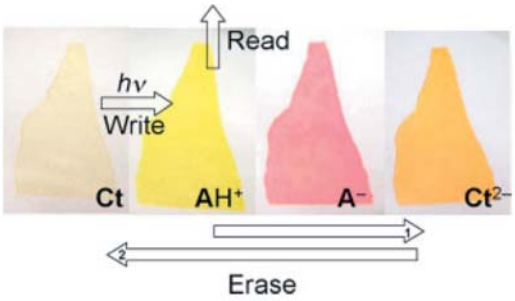

Scheme 1.21 –A cycle to *write-red-erase* in solid state: **DHF** in PHEMA. The first step (*write*) consists in the irradiation of the film containing **Ct** form in acidic media (metastable). The read step can de achieved using a wavelength at which **Ct** species does not absorb, for example 470 nm. To erase the system, a sequence of two pH jumps are necessary: the first one to basic medium produces $\mathbf{Ct}^{2-}$ species; the second one, back to acidic medium, restores the original **Ct** species.[56]

Pursuing the same aim of trying to achieve solid state systems based on flavylium ions,[80] some photochromic systems in solid hydrogel matrices have been reported, for instance, agar-gel and sol-gel matrices. It was possible to conclude that in the sol-gel matrix the coloration/decoloration could be repeated over 50 cycles without significant fatigue. In a silica sol-gel matrix, a fairly good reversibility was obtained up to *ca*. 30 cycles; in the later cycles, extensive degradations took place. This promising results could however be obtained only with specific derivatives of flavylium ions, 4'-(*N,N*-dimethylamino)-flavylium in the case of agar-gel and 4'-(*N*-octylamino)-flavylium in the case of sol-gel matrix.[80]

In conclusion, synthetic flavylium compounds can exist in several forms (*multistate*) that can be interconverted by more than one type of external stimuli (*multifunctional*). The intricate network of their reactions, when examined from the view points of "molecular-level device" and "molecular level logic function", reveals that these systems exhibit very interesting properties even capable of capable mimicking biological systems.[69,79]

1.3. Scope of the present thesis

This thesis intends to provide a deeper understanding of the photochromism associated with the networks of flavylium ions and to explore new media, such as micelles and gels.

In the second chapter, efficient photochromic systems based on the use of positively charged micelles are studied. In the third chapter, it is intended to extend this efficient photochromism to a class of synthetic 2-styryl-1-benzopyrylium salts, which exhibit longer wavelengths of absorption. In a fourth chapter, the use of Pluronic gels and micelles is explored as well as the mechanism of the efficient photochromism observed in these media. Finally, encapsulated flavylium salts are studied. In the fifth chapter, the incorporation inside molecular clips and the problematic of color preservation are explored. In the last chapter, the first steps

towards the encapsulation of flavylium salts inside zeolite L are outlined, and the possibility of performing isomerization inside these nanocontainers is attested.

1.4. References

[1] B. Valeur, *Molecular Fluorescence: Principles and Applications*, Wiley VCH, Weinheim, Germany, **2001**, Chapter 2,3 and 5, 20-71 and 125-154.
[2] P. Atkins, J. de Paula, *Physical Chemistry*, 7th ed, Oxford University Press, Oxford, USA, **2002**.
[3] A. Rauk, *Orbital Interaction Theory of Organic Chemistry*, 2nd edition, John Wiley & Sons, New York, USA, **2001**, Chapter 15, 209-217.
[4] V. Balzani, F. Scandola, *Supramolecular Photochemistry*, Ellis Horwood Limited, Chichester, England, **1991**, Chapter 2, 25-50.
[5] M. Klessinger, J. Michl, *Excited States and Photochemistry of Organic Molecules*, VCH, Weinheim, Germany, **1995**, Chapter 7, 361-490 and references therein.
[6] D. H. Waldeck, *Chem. Rev.* **1991**, 91, 415-436.
[7] N. J. Turro, *Modern Molecular Photochemistry*, University Science Books, California, USA, **1991**.
[8] A. Credi, L. Prodi, *Spectrochimica Acta Part A* **1998**,54, 159-170.
[9] J. R. Lakowicz, *Principles of Fluorescence Spectroscopy*, 3rd ed, Springer, Maryland, USA, **2006**, Chapter 10, 353-370.
[10] P. Dewick, *Medicinal Natural Products, A Biosynthetic Approach*, Wiley VCH, **2002**, New York, USA, Chapter 4, 121-166.
[11] K. Springob, J.-I. Nakajima, M. Yamazaki, K. Saito, *Nat. Prod. Rep.* **2003**, 20, 288-303.
[12] G. A. Iacobucci, J. G. Sweeney, *Tetrahedron* **1983**, 39, 3005-3038 and references therein.
[13] ed. J. B. Harborne, *The Flavonoids*, Chapman and Hall, New York, **1982**.
[14] R. Willsttäter, *On plant pigments*, Nobel Lecture **1915**.
[15] R. Willsttäter, A.E. Everest, *Justus Liebigs Ann. Chem.* **1913**, 401, 189-232; b) R. Willsttäter, H. Mallinson, *Justus Liebigs Ann. Chem.* **1915**, 408, 15-41; c) R. Willsttäter, H. Mallinson, *Justus Liebigs Ann. Chem* **1915**, 408, 147-162.
[16] R. Robinson, *Some polycyclic natural products*, Nobel Lecture, **1947**.
[17] a) A. Robertson, R. Robinson, *J. Chem. Soc* **1927**, 242-247; b) A. Robertson, R. Robinson, *J. Chem. Soc* **1927**, 1710-1717 and the other papers on the series *Experiments on the Synthesis of Anthocyanins*.
[18] ed. P. Markakis, *Anthocyanins as Food Colors – A Series of Monographs*, Academic Press, New York, USA, **1982**.
[19] M. J. Melo, M. Sousa, A. J. Parola, J. Seixas de Melo, F. Catarino, J. Marcalo, F. Pina, *Chem. Eur. J.* **2007**, 13, 1417-1422.
[20] L. Jurd, *J. Org. Chem.*, **1963**, 28, 987-991.
[21] L. Jurd, T. A. Geissman, *J. Org. Chem.* **1963**, 28, 2394-2397.
[22] L. Jurd, Tetrahedron **1969**, 25, 2367-2380.
[23] C. F. Timberlake, P.Bridle, *Nature* **1966**, 8, 158-159.
[24] R. Brouillard, B. Delaporte, *J. Am. Chem. Soc.* **1977**, 99, 8461-8468.
[25] R. Brouillard, J.-E. Dubois, *J. Am. Chem. Soc.* **1977**, 99, 1359-1364.
[26] R. Brouillard, B. Delaporte, J.-E. Dubois, *J. Am. Chem. Soc.* **1978**, 100, 6202-6205.
[27] R. Brouillard, G. A. Iacobucci, J. G. Sweeny, *J. Am. Chem. Soc.* **1982**, 104, 7585-7590.
[28] R. A. McClelland, S. Gedge, *J. Am. Chem. Soc*. **1980**, 102, 5838-5848.
[29] R. A. McClelland, G. H. McGall, *J. Org. Chem.* **1982**, 47, 3730-3736.
[30] P. Figueiredo, J. C. Lima, H. Santos, M.-C. Wigand, R. Brouillard, A. L. Maçanita, F. Pina, *J. Am. Chem. Soc* **1994**, 116, 1249-1254.
[31] F. Pina, M. Maestri, V. Balzani, *in Handbook of Photochemistry and Photobiology*, American Scientific Publishers, Stevenson Ranch, CA, USA, **2003**, Chapter 9, vol. 3, 411-449.
[32] F. Pina, M. Maestri, V. Balzani, *Chem. Commun.* **1999**, 107-114.
[33] A. Roque, C. Lodeiro, F. Pina, M. Maestri, S. Dumas, P. Passaniti, V. Balzani, *J. Am. Chem. Soc.* **2003**, 125, 987-994.
[34] F. Pina, *J. Chem. Soc. Faraday Trans.* **1998**, 94, 2109-2116.
[35] D. Fernandez, F. Folgosa, A. J. Parola, F. Pina, *New J. Chem*. **2004**, 28, 1221-1226.
[36] C. A. T. Laia, A. J. Parola, F. Folgosa, F. Pina, *Org. Biomol. Chem.* **2007**, 5, 69-77.
[37] V. Petrov, R. Gomes, A. J. Parola, A. Jesus, C. A. T. Laia , F. Pina, *Tetrahedron* **2008**, 64, 714-720.
[38] V. Petrov, R. Gomes, A. J. Parola, F. Pina*, Dyes and Pigments* **2009***,* 80, 149-155.
[39] F. Pina, M. J. Melo, A. J. Parola, M. Maestri, V. Balzani, *Chem. Eur. J.* **1998**, 4, 2001-2007.
[40] F. Pina, M. J. Melo, R. Ballardini, L. Flamigni, M. Maestri, *New. J. Chem.* **1997***,* 21, 969-976.
[41] M. Maestri, R. Ballardini, F. Pina, M. J. Melo, *J. Chem. Educ.* **1997**, 74, 1314-1316.

[42] F. Pina, M. J. Melo, M. Maestri, P. Passaniti, N. Camaioni, V. Balzani, *Eur. J. Org. Chem.* **1999**, 3199-3207.
[43] M. Montalti, A. Credi, L. Prodi, M. T. Gandolfi, *Handbook of Photochemistry*, CRC Press, Boca Raton, FL, **2006**, 3rd ed, Chapter 12, 601-616.
[44] C. G. Hatchard, C. A. Parker, *Proc. R. Soc. (London), Ser. A* **1956**, 235, 518-536.
[45] F. Pina, R. Gomes, C. A. T. Laia, *On the Photostationary State of the Flavylium Network of Chemical Reactions*, unpublished work.
[46] C. Bülow, H. Wagner, *Ber. Dtsch. Chem. Ges.* **1901**, 34, 1782-1804.
[47] C. Bülow, H. Wagner, *Ber. Dtsch. Chem. Ges.* **1903**, 36, 1941-1953.
[48] R. Robinson, H. Wagner, *J. Chem. Soc.* **1934**, 1435-1440.
[49] R. Robinson, D. D. Pratt, *J. Chem. Soc., Trans.* **1922**, 121, 1577-1585.
[50] R. Robinson, A. Robertson, *J. Chem. Soc.* **1926**, 1713-1720.
[51] W. H. Perkin, R. Robinson, M. R. Tuner, *J. Chem. Soc., Trans.* **1908**, 93, 1085-1115.
[52] A. W. Johnson, R. R. Melhuish, *J. Chem. Soc.* **1947**, 346-350.
[53] J. W. Gramshaw, A. W. Johnson, T. J. King, *J. Chem. Soc.* **1958**, 4040-4049.
[54] S. Chassaing, M. Kueny-Stotz, G. Isorez, R. Brouillard, *Eur. J. Org. Chem.* **2007**, 2438-2448.
[55] A. R. Katritzky, P. Czerney, J. R. Levell, W. H. Du, *Eur. J. Org. Chem.* **1998**, 2623-2629.
[56] F. Galindo, J. C. Lima, S. V. Luis, A. J. Parola, F. Pina, *Adv. Funct. Mat.* **2005**, 15, 541-545.
[57] F. Pina, J. C. Lima, A. J. Parola, C. A. M. Afonso, *Angew. Chem. Int. Ed.* **2004**, 43, 1525-1527.
[58] A. Roque, F. Pina, S. Alves, R. Ballardini, M. Maestri, V. Balzani, *J. Mat. Chem.* **1999**, 9, 2265-2269.
[59] F. Pina, A. Roque, M. J. Melo, I. Maestri, L. Belladelli, V. Balzani, *Chem. Eur. J.* **1998**, 4, 1184-1191.
[60] D. Fernandez, A. J. Parola, L. C. Branco, C. A. M. Afonso, F. Pina, *J. Photochem. Photobiol. A: Chemistry* **2004**, 168, 185-189.
[61] F. Pina, M. J. Melo, M. Maestri, R. Ballardini,V. Balzani, *J. Am. Chem. Soc* **1997**, 119*,* 5556-556.
[62] M. Maestri, F. Pina, A. Roque, P. Passaniti, *J. Photochem. Photobiol. A* **2000**, 137, 21-28.
[63] M. J. Melo, S. Moura, M. Maestri, F. Pina, *J. Mol. Struct.* **2002**, 612, 245-253.
[64] A. Roque, C. Lodeiro, F. Pina, M. Maestri, R. Ballardini, V. Balzani, *Eur. J. Org. Chem.* **2002**, 16, 2669-2709.
[65] M. C. Moncada, F. Pina, A. Roque, A. J. Parola, M. Maestri, V. Balzani, *Eur. J. Org. Chem.* **2004**, 304-312.
[66] M. C. Moncada, A. J. Parola, C. Lodeiro, F. Pina, M. Maestri, V. Balzani, *Chem. Eur. J.* **2004**, *10*, 1519-1526.
[67] M. C. Moncada, D. Fernandez, J. C. Lima, A. J. Parola, C. Lodeiro, F. Folgosa, M. J. Melo, F. Pina, *Org. Biomol. Chem.* **2004**, 2, 2802-2808.
[68] F. Pina, A. J. Parola, M. J. Melo, C. A. T. Laia, C. A. M. Afonso, *Chem. Commun.* **2007**, 1608-1610.
[69] L. Giestas, F. Folgosa, J. C. Lima, A. J. Parola, F. Pina, *Eur. J. Org. Chem.* **2005**, 4187-4200.
[70] A. Jimenez, C. Pinheiro, A. J. Parola, M. Maestri, Fernando Pina, *Photochem. Photobiol. Sci.* **2007**, 6, 372-380.
[71] A. Roque, J. C. Lima, A. J. Parola, F. Pina, *Photochem. Photobiol. Sci.* **2007**, 6, 381-385.
[72] R. Robinson, H.G. Crabtree, C.K. Das, W. Lawson, R.W. Lunt, P.H. Roberts and P.N. Williams, *J. Chem. Soc*. **1924**, 207-214.
[73] International Food Information Council (IFIC) and Foundation US Food and Drug Administration (FDA), **2004**, *Food ingredients and colors*, Washington, DC, IFIC Foundation.
[74] C.-Ovando, M. L. P.-Hernández, M. E. P.-Hernández, J. A. Rodríguez, C. A. G.-Vidal, *Food Chemistry*, **2009**, 113, 859-871.
[75] J.-M. Lehn, *Supramolecular Chemistry: Concepts and Perspectives*, VCH, Weinheim, Germany, **1995**.
[76] F. Pina, M. Maestri, V. Balzani, *in Molecular Switches*, ed. B. L. Feringa, Wiley-VCH, Weinheim, Germany, **2001**, Chapter 10, 309-337 and references therein.
[77] a) Y. Hirshberg, *J. Am. Chem. Soc.* **1956**, 78, 2304-2312; b) Y. Hirshberg, *New Scientist*, **1960**, 7, 1243.
[78] A. P. de Silva, N. D. McClenaghan, C. P. McCoy., *in Molecular Switches*, ed. B. L. Feringa, Wiley-VCH, Weinheim, Germany, **2001**, Chapter 11, 339-361.
[79] F. Pina, M. J. Melo, M. Maestri, P. Passaniti, V. Balzani, *J. Am. Chem. Soc.* **2000**, 122, 4496-4498.
[80] R. Matsushima, K. Kato, S. Ishigai, *Bull. Chem. Soc. Jpn.* **2002**, 75, 2079-2080.

2. Efficient photochromism from the network of chemical reactions of flavylium ions in CTAB micelles

In this chapter, efficient photochromism from the 7,4'-dihydroxyflavylium (**DHF**) and 7-(*N*,*N*-diethylamino)-4'-hydroxyflavylium (**DEF**) networks are reported in the presence of CTAB micelles, contrary to what is observed in water. The thermodynamics, kinetics and photochemistry of these new systems are characterized.

2.1 Introduction

Photochromism, a term coined by Hirshberg in 1950, is defined as a reversible transformation of chemical species, between two states having observable light absorptions in different regions, induced in one or both directions by electromagnetic radiation:[1]

$$A(\lambda_1) \underset{h\nu_2,\,\Delta}{\overset{h\nu_1}{\rightleftharpoons}} B(\lambda_1) \qquad (2.1)$$

The first examples of photochromism were reported in the end of the nineteenth century in inorganic, organometallic and organic substances. The study of organic photochromism began to increase pronouncedly around 1940, aiming various practical applications that will be briefly summarized.[1]

The most common photochromic systems are unimolecular reactions, driven mostly by UV light (300 to 400 nm) but also by visible light (400 to 700 nm). The reversibility is a main criterion for photochromism and it can be achieved either predominantly thermally or photochemically. For the first type of systems, the thermally driven back reaction can be accompanied by one that is photochemically driven, but the thermal process dominates. The medium can influence or even control the kinetics of this back reaction.[1]

Applications of photochromism are of two generic types:

1) Applications that take profit of the color change itself like: variable transmission optical material such as the photochromic ophthalmic lenses[2] or camera filters, fluid flow visualization,[3] optical information storage,[4,5,6] novelty items (toys, T-shirts, etc.), authentication systems (security printing inks), cosmetics, etc.

2) Applications dependent upon changes in the physical or chemical properties that occur along with photoisomerization, such as changes in refractive index, dielectric constant, conductivity, oxidation/reduction potential, geometrical structure, solubility and viscosity.[1,6] These type of applications include optoelectronic systems (semi-conductors modulated by photochromic pigments), reversible holographic systems, optical switches,[4,5,6] photochemically switchable enzymatic systems, nonlinear optical devices, etc.[1]

Some of these applications have already been commercialized such as polymer-based photochromic eyewear, novelty items and security printing inks. Table 2.1 lists the most common photochromic families of compounds.

Table 2.1 – Frequent photochromic compounds.

Exemplified Photochromic Structure	Description and uses
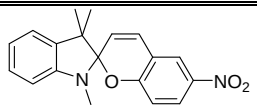	**Spiropyrans**: one of the most widely studied families of photochromic compounds.[1]
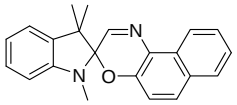	**Spirooxazines**: present excellent photochromic properties and resistance to fatigue, which has resulted on their application in ophthalmic lenses.[1,2]
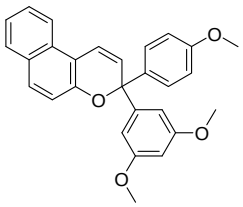	**Benzo and naphtopyrans or chromenes**: thermoreversible photochromic compounds that also found application on ophthalmic lenses. The color of the opened form can be tuned over a wide range of the visible spectrum.[1]
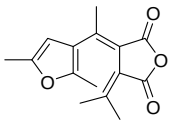	**Fulgides**: this class of photochromic compounds presents no thermal back reaction and because of the stability of the colored form fulgides have potential application in the field of optical storage and security printing.[1]
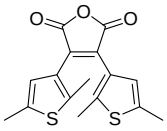	**Diarylethenes with heteroaryl groups**: also present photochromic behavior in which the colored form is thermally stable and targeted to use as information storage.[1,4]
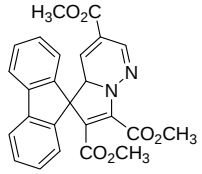	**Dihydroindolizines and related systems**: thermoreversible photochromic systems based on 1,5-electrocyclization reactions.[1]
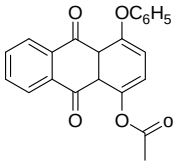	**Quinones**: the mechanism of the photochromism of certain quinones involves proton or group transfer. Their potential applications are focused on recording and multiplication of images, optical memories, etc.[1]
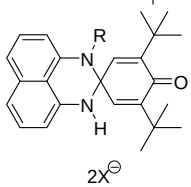	**Perimidinespirocyclohexadienones**: this series of photochromic or thermochromic systems is based on proton transfer and involves valence and prototropic tautomeric intramolecular reactions.[1]
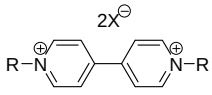	**Viologens**: the photochromism of viologens operates through electron transfer in polymer matrixes or with counter anions possessing long alkyl chains, for example. These systems have the possibility of conceiving erasable photo-electrochromic devices.[1]

The establishment of flavylium compounds as potentially useful organic photochromic is quite recent comparatively to other compounds.[5] The photochromism based on flavylium networks, see Scheme 1.8, arises from the photoinduced *trans–cis* isomerization reaction that produces the **Cc** species upon **Ct** irradiation. In order to obtain efficient photochromic systems,

the essentially colorless **Cc** species should spontaneously give rise to **A** or $\mathbf{AH^+}$, the colored species. The advantages of using flavylium salts include the possibility of tuning the color of the photoproduct from pale yellow to blue (as will be seen in chapter 3) by the introduction of functional groups in specific positions, such as hydroxy, methoxy or amines. Besides, they have the same basic structure of natural occurring anthocyanins, which is expected to be related to a lower toxicity than some of the presented structures in Table 2.1.

According to previous research carried out on the photochromic properties of the synthetic flavylium network of chemical reactions, two different types of photochromic systems can be distinguished, depending on the existence or not of a thermal barrier for *trans–cis* isomerization.[5,7] In the first case, as for example in the 4'-methoxyflavylium compound, the *trans*-chalcone can be obtained at acidic pH values in a metastable state (from protonation of ionized *trans*-chalcones easily formed at high pH values), and by consequence the primary photochemical product, **Cc**, is spontaneously transformed into $\mathbf{AH^+}$, which is the thermodynamic stable species in acidic media, Scheme 2.1 A. This system leads to a good color contrast and is particularly useful for optical memories because the photochemical product is the stable one. However, it has one major drawback: deleting the information in order to enable the system to be reused implies two pH jumps (basification to produce ionized *trans*-chalcones and further acidification) thus increasing the overall mass of the system. On the other hand, at higher (neutral) pH values the primary photochemical product **Cc** rapidly equilibrates with **B** in the subsecond timescale, but does not give $\mathbf{AH^+}$. The species **Ct**, **Cc** and **B** are all colorless (or pale yellow), and thus the color contrast is poor. In this case, the photochemical product is the unstable one, but due to the barrier reverts slowly to the thermodynamic stable species **Ct**, Scheme 2.1 B. This can constitute an advantage for some applications, but the larger drawback of this system is its small color contrast. Moreover, generally the **Cc** species leads also to **Ct** upon irradiation and a stationary state is obtained decreasing the efficiency of the photochromism.

In the absence of thermal barrier, it is not possible to have **Ct** at more acidic pH values, Scheme 2.1 C, thus no photochromism can be observed. At less acidic pH values, such as pH = 6, **Ct** is the main thermodynamic product; its irradiation produces **Cc**, but due to the lack of barrier, **Cc** is rapidly converted into **Ct**, Scheme 2.1 D. Only at intermediate pH values for example pH = 3 an increasing of color can be observed upon irradiation of **Ct**, because the reaction of **Cc** to give $\mathbf{AH^+}$ through **B** can compete with the back reaction to give **Ct**. The drawback of this system is that at pH = 3 there is a significant amount of $\mathbf{AH^+}$ at the equilibrium and so the contrast between the irradiated and non-irradiated solution is small, reducing the performance of the photochromic system (see Figure 1.7)

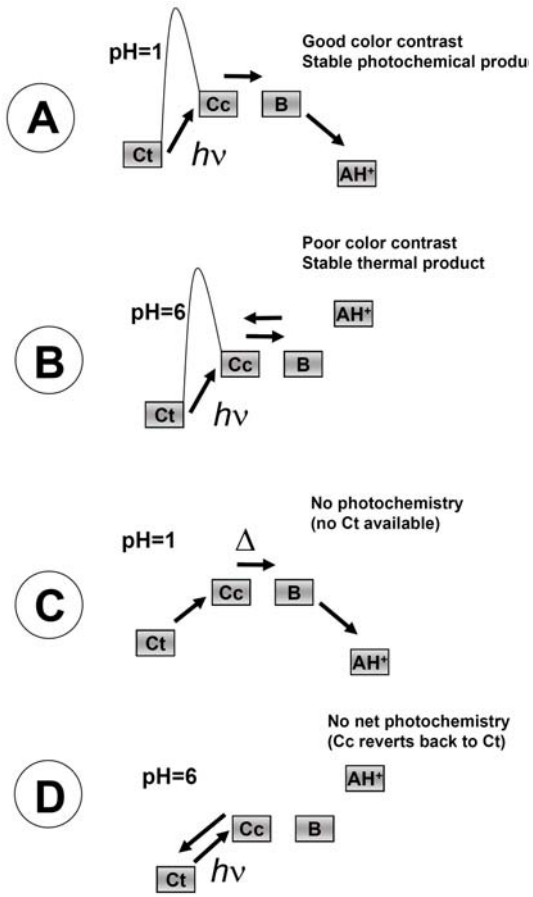

Scheme 2.1 – Photochromism in flavylium networks: A) and B) High thermal barrier compound at acidic and neutral pH values, respectively; C) and D) Low thermal barrier compound at acidic and neutral pH values, respectively.

In this chapter, a novel and general strategy to optimize the photochromic response of the network of species originated by flavylium compounds in aqueous solutions is described. The interaction of the flavylium network with micelles is known to stabilize some species (states) through specific interactions, allowing modulation of the network.[8,9,10] However, up to now, no systematic exploitation of these effects on the photochromic properties of flavylium compounds has been reported. This study takes profit from the strong associative interaction of the neutral *trans*-chalcone species with cetyltrimethylammonium bromide (CTAB) micelles and the repulsive interaction of flavylium cations with the positively charged surface of the micelle. CTAB micelles exhibit a CMC (Critical Micelle Concentration) of 0.8 M and an aggregation number of 55 at 30 ºC.[11]

2.2 7,4'-Dihydroxyflavylium (DHF)

In the case of the compound 7,4'-dihydroxyflavylium (**DHF**), the *trans–cis* thermal barrier is low (65 kJ.mol^{-1})[7] and its network follows the cases C and D in Scheme 2.1. This behavior can be changed by incorporating the flavylium salt in more organized media, such as ionic liquids[12] and hydrogel polymers.[13] The apparent thermal barrier is increased in these cases, but the systems still show drawbacks due to the fact that contact with basic and acidic

solutions is still needed to operate the photochromism. The CTAB micelles do not introduce significant changes in the *cis–trans* isomerization barrier, but differently from water an efficient photochromism with a good color contrast can be achieved with no need of changing the pH.

2.2.1 The reaction network in water

In water, the network of chemical reactions exhibited by 7,4'-dihydroxyflavylium (**DHF**) is described in Scheme 1.8 (where ionized **Cc** species are omitted) and the system can be, as mentioned in the introduction, treated by equations 1.22-1.32. In this case, in water the equilibrium concentrations of **B** and **Cc** can be neglected (but not their role in the kinetics). It was shown previously[14] that pK'_a = 3.1, pK_a = 4.0 and $K_hK_tK_i = 6.9\times10^{-4}$ M and the molar fractions of the species present in the equilibrium can be plotted as shown in Figure 2.1 A. A steady state approach can be considered for the intermediate species, as explained previously in the introduction, that is **Cc** and **B** are in fast equilibrium. As was also already demonstrated, the observed rate constant of the conversion of $\mathbf{AH^+}$ into **Ct** and *vice versa* is given by equation 1.45 (Supplementary Material section 9.1.1). Analysis of previous data from pH jumps[15] leads to the following kinetic rate constants: k_h = 0.02 s^{-1}, $k_iK_t/k_{-h} = 2.1\times10^{-5}$ M, $k_{-i} = 1.8\times10^{-4}$ s^{-1}, and a bell shaped curve that is plotted in Figure 2.1 B.

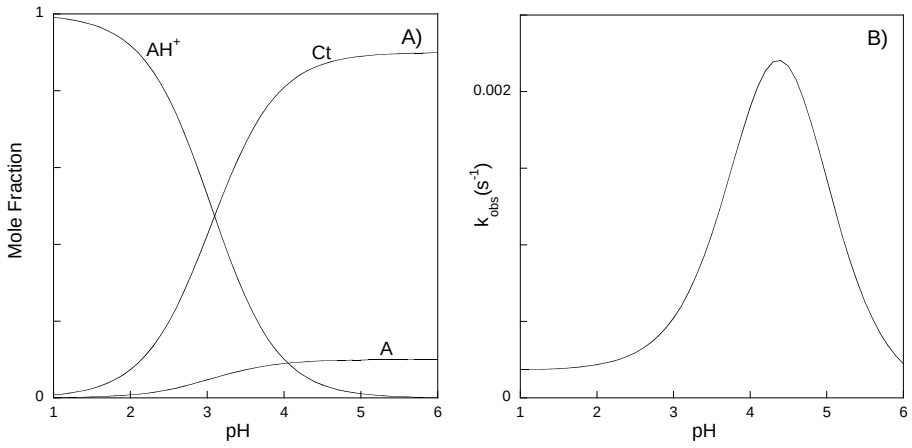

Figure 2.1 – A) Mole fraction distribution of **DHF** at the thermodynamic equilibrium; B) Rates of conversion between **Ct** and $\mathbf{AH^+}$ as a function of pH.

The bell shaped curve in Figure 2.1 B results from the fact that at pH values higher than 4 the amount of $\mathbf{AH^+}$ decreases with increasing pH (see the first term of equation 1.45, where $\{[H^+]/([H^+] + K_a)\}$ corresponds to the mole fraction of $\mathbf{AH^+}$); at pH values lower than 4, the equation tends to k_{-i} which is a small value, as was commented previously. Moreover, the contribution for the observed rate constant is mainly from the first term of equation 1.45, which corresponds to **Ct** formation from $\mathbf{AH^+}$, while the reverse reaction (second term) has a minor contribution.

2.2.2 Addition of CTAB micelles

When the network of chemical reactions is studied in the presence of CTAB micelles, the thermodynamic equilibrium is dramatically shifted, as can be confirmed by Figure 2.2. The pH domain of the flavylium cation is reduced to very acidic media, and **Ct** becomes stable even at low pH values (Figure 2.2 A). This behavior shows that the **Ct** species are bound to the micelle, which has a strong stabilizing effect on such species. Whether it is an effective entrance inside the micelle (into the hydrophobic domain) or a strong electrostatic interaction with the positively charged surface is not possible to unravel (with the experimental techniques used), but nevertheless **Ct** can only exist at such pH if it is located at the micellar phase.

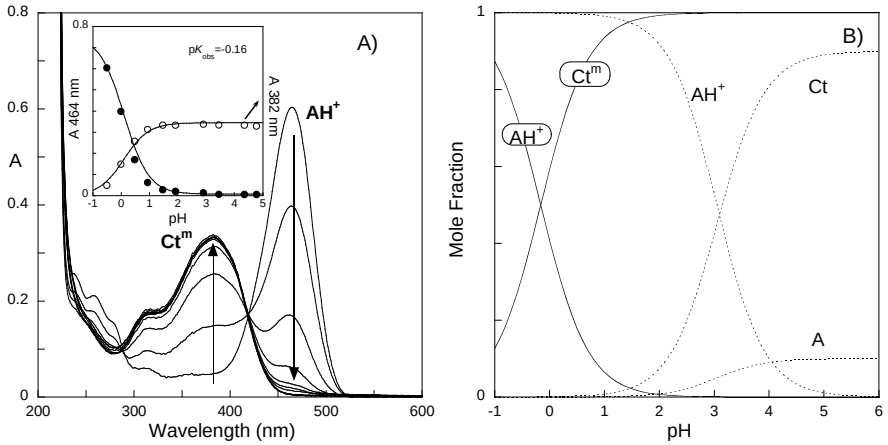

Figure 2.2 – A) Spectral variations at the equilibrium of **DHF** in the presence of CTAB micelles ([**DHF**] = 1.46×10^{-5} M, [CTAB] =1.8×10^{-2} M, arrows indicate increasing pH). B) Mole fraction distribution of the species in the presence of CTAB micelles (full line), and in water (pointed line) for comparison purposes.

As can be seen in Figure 2.2 B, even at pH = 1 the main species is the **Ct**-CTAB adduct (**Ct^{m}**), while in water **AH^{+}** predominates at this pH. This means that if a perturbation is introduced by the addition of CTAB micelles to an aqueous solution of **AH^{+}**, the system should evolve to **Ct^{m}**, Figure 2.3. The experimental results reported in Figures 2.2 and 2.3 can be accounted for by the generic kinetic Scheme 2.2, where all species are considered to have a partition coefficient with the CTAB micelle pseudophase.

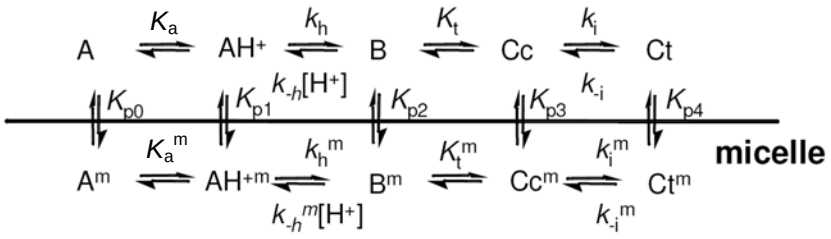

Scheme 2.2 – General scheme in the presence of CTAB micelles.

The mole fraction of **AH^{+}** and **Ct^{m}** can be calculated through the following equations (Supplementary Material 9.2.1):

$$\chi_{AH^+} = \frac{[H^+]}{[H^+] + K'^{\,m}_{a}} \tag{2.2}$$

$$\chi_{Ct^m} = \frac{K'^{\,m}_{a}}{[H^+] + K'^{\,m}_{a}} \tag{2.3}$$

where:

$$K'^{\,m}_{a} = K'_{a} + K_{p0}K_a + K_{p2}K_h + K_{p3}K_tK_h + K_{p4}K_iK_tK_h \tag{2.4}$$

The determined value for $K'^{\,m}_{a}$ is $10^{0.16}$, as can be seen in Figure 2.2 A. According to the data reported in Figures 2.2 and 2.3 there is experimental evidence for considering that $\mathbf{AH^+}$ in the bulk and $\mathbf{Ct^m}$ are the only detectable species at the equilibrium, based on the fact that only the absorption spectra of the species $\mathbf{AH^+}$ and **Ct** are observed, with an isosbestic point (Figure 2.2 A). On this basis, the following approximation can be done:

$$K'^{\,m}_{a} = K_{p4}K_iK_tK_h = 10^{0.16} \tag{2.5}$$

From the values of $K'^{\,m}_{a}$ and $K_hK_tK_i$ mentioned above a value of $K_{p4} = (2.1 \pm 0.3) \times 10^3$ is obtained. This high partition coefficient reflects the fact that practically all **Ct** formed in the bulk water goes inside the micelle, showing its strong thermodynamic stability in this phase.

Concerning the kinetics of **Ct** formation, it should be taken into account that its formation is faster in the presence of CTAB micelles when compared with water (Figure 2.3 B). This suggests that the formation of **Ct** at the aqueous side followed by a fast entrance to the micelle is not the only pathway used by the system; otherwise, the rate would be the same or smaller than that detected in water for pH > 3, with a bell-shaped curve as well. Consequently, **B** and **Cc** species enter the micelle as well, explaining the faster rate for **Ct** formation when compared to water. In order to explain the kinetic rates in the presence of CTAB, some simplifications in Scheme 2.2 can be made, namely a steady state involving the species **B**, **Cc**, $\mathbf{B^m}$ and $\mathbf{Cc^m}$ in fast equilibrium. This assumption is supported by the fact that the rates of ring opening and closure are in the sub-second time scale, faster than any other kinetic processes taking place in this system, and also the solubilization inside the micelles occurs on a much shorter timescale.

The mole fraction of the steady state species in fast equilibrium can be calculated as shown in Supplementary Material (section 9.2.2), using the same approach that was used before for water networks. Then, the rate observed for the thermal process of **Ct** formation can be evaluated by equation 2.6 (Supplementary Material, section 9.2.2):

$$k_{obs} = \frac{\dfrac{[H^+]}{[H^+]+K_a}\dfrac{k_h K_t\left(k_i + k_i{}^m K_{p3}\right)}{\left(k_{-h} + k_{-h}{}^m K_{p2}\right)} + [H^+]k_{-i}{}^m}{[H^+]+\dfrac{(k_i + k_i{}^m K_{p3})K_t}{\left(k_{-h} + k_{-h}{}^m K_{p2}\right)}} \tag{2.6}$$

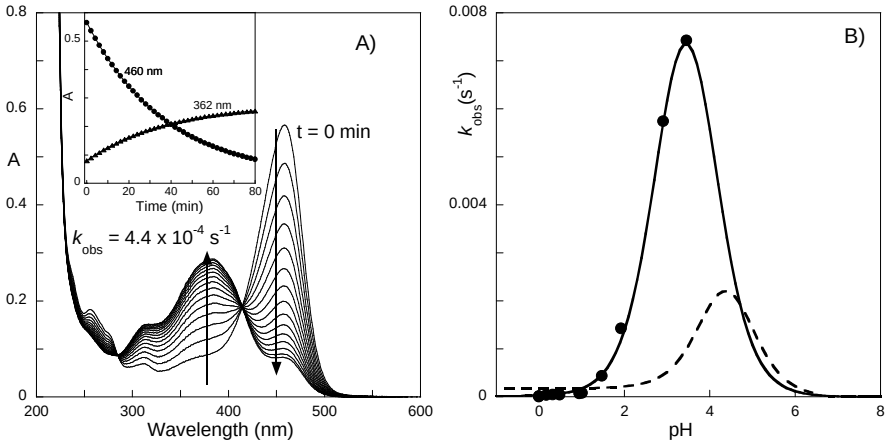

Figure 2.3 – A) Spectral modifications that occur in a solution of [**DHF**] = 1.46×10^{-5} M at pH = 1.47 upon addition of [CTAB] = 1.8×10^{-2} M at 22 ºC, insert shows the decay at two wavelengths with the first order kinetics. B) Rate constants as a function of pH(●), fitting was achieved with eq. 2.6 (full line); bell shaped curve obtained in water (dashed line).

The fitting of the experimental rates for **Ct** formation by means of equation 2.6 is shown in Figure 2.3 B. The following parameters were obtained:

$$\frac{K_t\left(k_i + k_i{}^m K_{p3}\right)}{\left(k_{-h} + k_{-h}{}^m K_{p2}\right)} = 1.5\times10^{-3}\, s^{-1} \tag{2.7}$$

$$k_{-i}{}^m = 2\times10^{-5}\, s^{-1} \tag{2.8}$$

Unfortunately, rate constants for pH values above 3.5 were not determined. The reason is that in these experiments CTAB is added to equilibrated aqueous solutions of $\mathbf{AH}^+$ and, above pH = 3.5 almost all $\mathbf{AH}^+$ is converted to **Ct** and it is also not possible to obtain $\mathbf{AH}^+$ photochemically. Therefore no significant signal could be obtained to confirm the expected bell shape curvature. However, it would have been possible to obtain these kinetic constants using a different experimental approach.

2.2.3 How CTAB micelles improve the photochromism

Figure 2.4 shows the appearance of color upon irradiation of **DHF** in the presence of CTAB micelles. The photochemical process is exactly the reverse of the thermal conversion of $\mathbf{AH}^+$ into **Ct**. That is, upon irradiation of $\mathbf{Ct}^\mathbf{m}$, flavylium species is produced in the bulk. In

order to get more insight into the process, flash photolysis experiments were carried out. The spectral variations confirm that **AH**$^+$ in bulk water is formed at the expenses of **Ct**$^{\mathbf{m}}$.

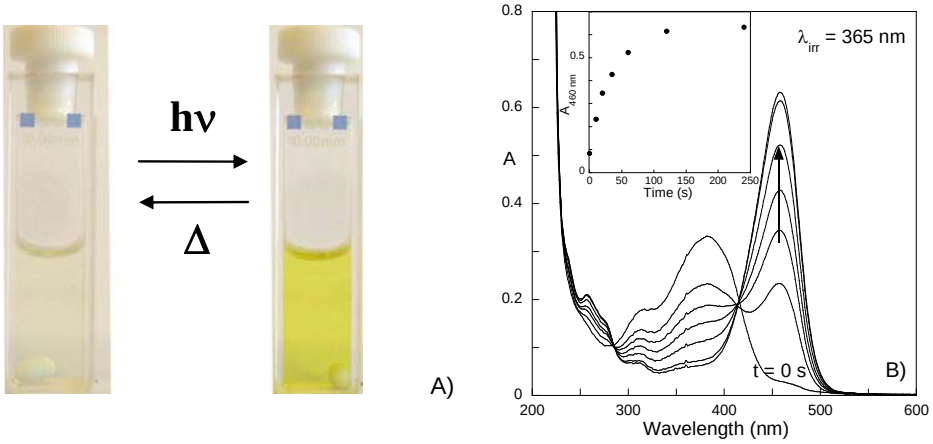

Figure 2.4 – A) Pictures of the cuvette in the beginning and in the end of irradiation shown in B (the lifetime of the colored species is 38 min). B) Spectral modifications that occur in a solution of the flavylium cation [**DHF**] = 1.46×10^{-5} M at pH= 1.47 and [CTAB] = 1.8×10^{-2} M, after irradiation at 365 nm: 0, 10, 20, 35, 60, 120 and 240 s ($I_0 = 6.05\times10^{-7}$ einstein.min^{-1}).

As shown in the inset of Figure 2.5 A, immediately after the flash a bleaching coincident with the λ_{max} of **Ct** is observed, followed by partial recovery of the **Ct** absorbance at 385 nm. It is worth of note that no total recovery of **Ct** is observed. A parallel process takes place at 460 nm (**AH**$^+$ absorption) and both processes have the same rate constant. The fraction of **Ct** not recovered at 385 nm corresponds to the fraction of **Ct** converted into **AH**$^+$. This behavior is qualitatively similar to that observed in the absence of micelles.[15,16]

In order to quantify the traces obtained in the flash photolysis measurements Scheme 2.2 should be used. Two pathways can be considered: i) **AH**$^+$ is formed from **Cc** and/or **B** in the bulk, or ii) inside the micelle followed by its ejection to the bulk solution due to the electrostatic repulsion from the micelle surface. The first pathway would also imply a small partition constant for **Cc** and/or **B**, which is not predicted because the solubility of these neutral species are expected to be higher in the micelle than in bulk water, taking into account that **Ct** exhibits a high partition constant. The exit of neutral species would, nevertheless, occur during the flash photolysis experiment - assuming a very fast partition due to diffusional entrance of **Cc** into the micellar phase and considering K_{p3}~K_{p4}, allows estimating an exit time for **Cc** of *ca.* 1 ms (k_{in}~ k_{diff} × [micelle] = 10^{10} × 3 × 10^{-4} = 3 × 10^6 s^{-1}; $k_{out} = k_{in}/K_{p3}$ ~ 1500 s^{-1}). On the other hand, assuming the second pathway, equation 2.9 can be deduced, assuming negligible mole fractions of **B** and **Cc** in the bulk:

$$k_{flash} = k_i^{\,m} \frac{K_t^{\,m}}{1+K_t^{\,m}} + k_{-h}^{\,m} \frac{\left[H^+\right]}{1+K_t^{\,m}} \qquad (2.9)$$

A reasonable fitting of the experimental data can be obtained, as shown in Figure 2.5 A. The fitting allows also calculation of the following values:

$$k_i^{\,m}\frac{K_t^{\,m}}{1+K_t^{\,m}} = 0.07\ s^{-1} \tag{2.10}$$

$$\frac{k_{-h}^{\,m}}{1+K_t^{\,m}} = 1.52\ M^{-1}s^{-1} \tag{2.11}$$

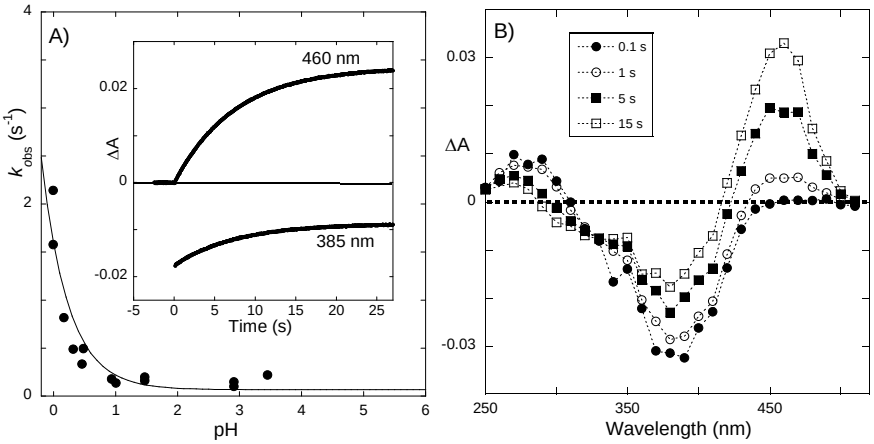

Figure 2.5 – A) Flash photolysis rate constants as a function of pH and fitting achieved with eq. 2.9, inset – representative traces of the flash photolysis experiments obtained at pH = 1.47. B) Time resolved spectra at 0.1, 1, 5 and 15 s at pH = 1.54.

The values found (equations 2.10 and 2.11) are very different from what is found in water (see chapter 5, Figure 5.18), pointing to a much slower dehydration rate in the presence of CTAB micelles (if K_t is assumed not to vary significantly).

The pH dependence of quantum yield for $\mathbf{AH}^+$ formation is reported in Figure 2.6. Considering the same pathway as before, it is possible to deduce equation 2.12 that fits reasonably the experimental data with only one adjustable parameter, the quantum yield of formation of Cc^m from Ct^m ($\Phi_{Ct^m \rightarrow Cc^m}$). It is therefore possible to determine the $\Phi_{Ct^m \rightarrow Cc^m}$ = 0.4. The quantum yields are higher than in water.[17]

$$\Phi = \Phi_{Ct^m - Cc^m}\frac{[H^+]}{[H^+]+\dfrac{k_i^{\,m}K_t^{\,m}}{k_{-h}^{\,m}}} = 0.4\frac{[H^+]}{[H^+]+\dfrac{0.07}{1.52}} \tag{2.12}$$

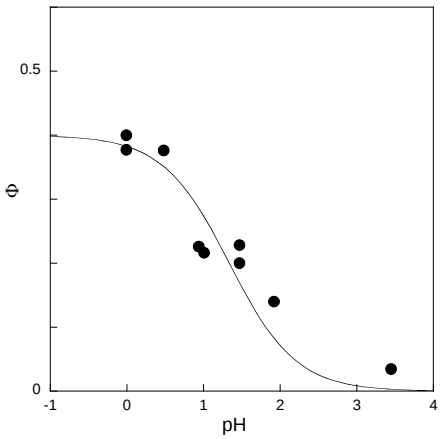

Figure 2.6 –Quantum yields versus pH: ● - experimental data, line - fitting achieved with eq. 2.12.

The coherence of the model was confirmed taking into account that the reported values of the constants fit simultaneously the flash photolysis and quantum yield data. Nevertheless, the first mentioned pathway should not be completely put aside, since it can contribute to the $\mathbf{AH}^+$ formation due to the fact that both **Cc** and **B** are expected to be in fast partition the micellar phase and the bulk. The system exhibits a relatively high fatigue resistance as can be seen in Figure 2.7. When compared with the system without CTAB,[17] the photodegradation is reduced, and therefore the micelles have a stabilizing effect.

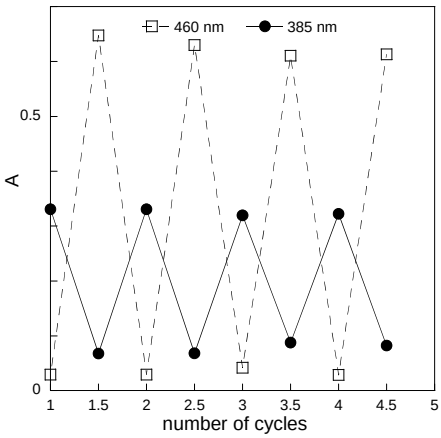

Figure 2.7 – Cycling in a solution of the flavylium cation [**DHF**] = 1.46×10^{-5} M at pH = 1.47 and [CTAB] = 1.8×10^{-2} M. The initial point of a cycle corresponds to absorbance in the beginning of the irradiation and the end point is the absorbance when irradiation is completed. The system takes approximately 2 h to fully recover.

2.3 7-(*N,N*-Diethylamino)-4'-hydroxyflavylium (DEF)

In this subsection another case study, 7-(*N,N*-diethylamino)-4'-hydroxyflavylium (**DEF**) will be extensively discussed to illustrate how the exploitation of CTAB micelles is a general strategy to obtain efficient photochromism from these networks.

2.3.1 The reaction network in water

The network of chemical reactions originated by **DEF** is shown in Scheme 2.3. This aminoflavylium cation follows the same set of chemical reactions, as presented before in Scheme 1.8 ($\mathbf{Ct^{2-}}$ is not shown in Scheme 2.3). However, in very acidic media amino flavylium ions give rise to protonated species on the amino group, from $\mathbf{AH_2^{2+}}$ to $\mathbf{CtH^{+}}$. The network of reactions of the present compound was previously studied,[18] and the *trans*-chalcones do not exhibit measurable photochemistry in water, only in highly viscous borax-glycerol medium,[19] organic solvents,[20] or ionic liquids[21] photochemistry was reported. Microheterogeneous aqueous environments such as micellar solutions, however, have not been explored, despite their promising properties in terms of microviscosity or local polarity within the micelles. Indeed, in CTAB micelles this picture is changed, as will be seen below.

The lack of significant photochemistry in chalcones possessing an amino group was previously reported and attributed to the formation of a highly polar state on the S_1 hypersurface, presumably a twisted intramolecular charge transfer state (TICT)[19] or another ICT mechanism, and will be discussed in detail for another case study in chapter 4. Such a mechanism implies the presence of an extra reaction coordinate at the chalcone singlet excited state, which would quench the *trans-cis* photoisomerization reaction (as well as its fluorescence) giving rise to very low photoisomerization quantum yields.

At the equilibrium, in acidic to slightly basic media, Figure 2.8 A, the system can be as well described as a single equilibrium, because the flavylium cation $\mathbf{AH^{+}}$ and the *trans*-chalcone **Ct** behave as a single acid base reaction, being $pK'_a = 5.9$.[18] In other words, the amount of **B** and **Cc** can be neglected at the equilibrium, although these species control the kinetic processes. The system was fully characterized thermodynamically in previous work, with $pK_a = 6.6$ and $pK_{Ct+} = 4.5$.[18]

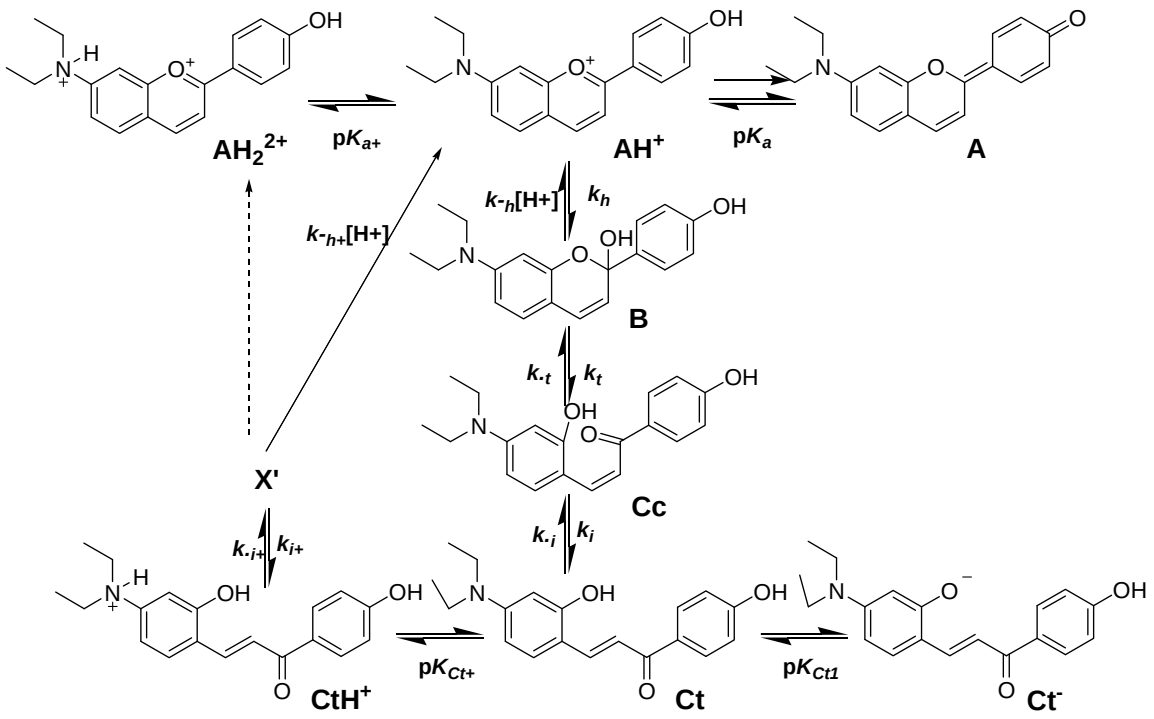

Scheme 2.3 – Reaction network for **DEF**.

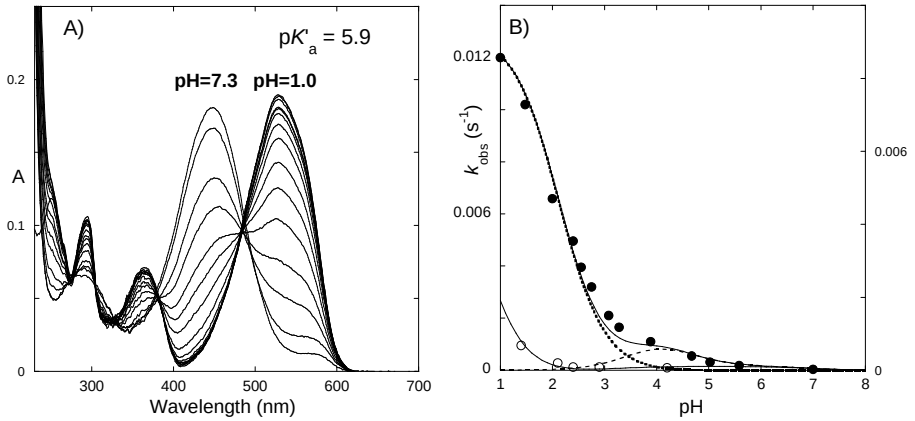

Figure 2.8 –Thermodynamic A) and kinetics B) of **DEF**, [**DEF**] = 6.7×10^{-6} M. A) pH dependent absorption spectra at room temperature after 1 day in the dark. B) ● – reaction rate of $\mathbf{AH^+}$/**A** formation from chalcones as a function of pH upon pH jumps; fitting was achieved by means of eq. 2.14 ○ – experimental rates in the presence of CTAB micelles.

As also reported in previous work, the flavylium $\mathbf{AH^+}$, and the chalcones can be interconverted through pH changes, the respective rates being shown in Figure 2.8 B.[18] The observed rate constants can be accounted for by considering a sum of two components, one involving the species $\mathbf{AH^+}$/**Ct**, as usual, (traced line in Figure 2.8 B) and the other, the species $\mathbf{AH^+}$/$\mathbf{Ct^+}$ (pointed line in Figure 2.8 B), equation 2.13, in which **X'** is composed by **B** and **Cc** species in their protonated (and/or unprotonated forms).[18] This second rate constant is derived in a similar way to what was done in equation 1.45, except that k_{h+} can be ignored, because there is no reversibility from $\mathbf{AH^+}$ (section 9.1.1, Supplementary Material).[18]

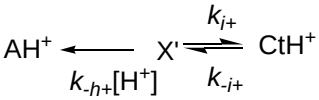

(2.13)

$$k_{obs} = \frac{\frac{[H^+]}{[H^+]+K_a} k_i K_t K_h + k_{-i}[H^+]}{[H^+]+\frac{k_i K_t}{k_{-h}}} + \frac{\frac{[H^+]}{[H^+]+K_{Ct+}} k_{-i+}[H^+]}{[H^+]+\frac{k_{i+} K_t'}{k_{-h+}}} \quad (2.14)$$

The kinetic treatment of this system has permitted to calculate the rate constants in equation 2.14: $k_h = 1.5\times10^{-4}$ s^{-1}, $k_iK_t/k_{-h} = 5.0\times10^{-4}$ M, $k_{-i} = 1.0\times10^{-2}$ s^{-1}, $k_{-i+} = 1.3\times10^{-2}$ s^{-1}, $k_{i+}K_{t'}/k_{-h+} = 7.5\times10^{-3}$ M. [18]

2.3.2 Addition of CTAB micelles

This situation is dramatically changed when CTAB micelles (monomer 5×10^{-3} M) are added to aqueous solutions of **DEF**, Figure 2.9. Addition of CTAB micelles to a solution of $\mathbf{Ct^{2-}}$ leads to a red shifted absorption band indicating the existence of an interaction micelle-unprotonated chalcone, Figure 2.9 A. This process occurs during the mixing time as no further spectral changes were observed. This interaction can be accounted for by the electrostatic attraction between CTAB micelles and $\mathbf{Ct^{2-}}$. However, the electrostatic interaction is not the only parameter to take into account, because the neutral chalcone, **Ct**, also leads to spectral variations upon CTAB micelles addition, forming an adduct herein identified as $\mathbf{Ct^m}$, Figure 2.9 B. Even more interesting is the interaction of $\mathbf{CtH^+}$, with CTAB micelles, Figure 2.9 C. The protonated chalcone can be obtained from **Ct** upon a pH jump: while in the absence of CTAB micelles $\mathbf{CtH^+}$ leads to $\mathbf{AH^+}$, in the presence of the micelles leads to the adduct $\mathbf{Ct^m}$. This result shows that the interaction between **Ct** and the micelle is sufficiently strong to displace the equilibrium towards the adduct formation. On the other hand, at very acidic pH values $\mathbf{AH^+}$ is stable even in the presence of micelles, and no spectral variations are detected, indicating the lack of interaction with the micelles, as expected from the electrostatic repulsion.

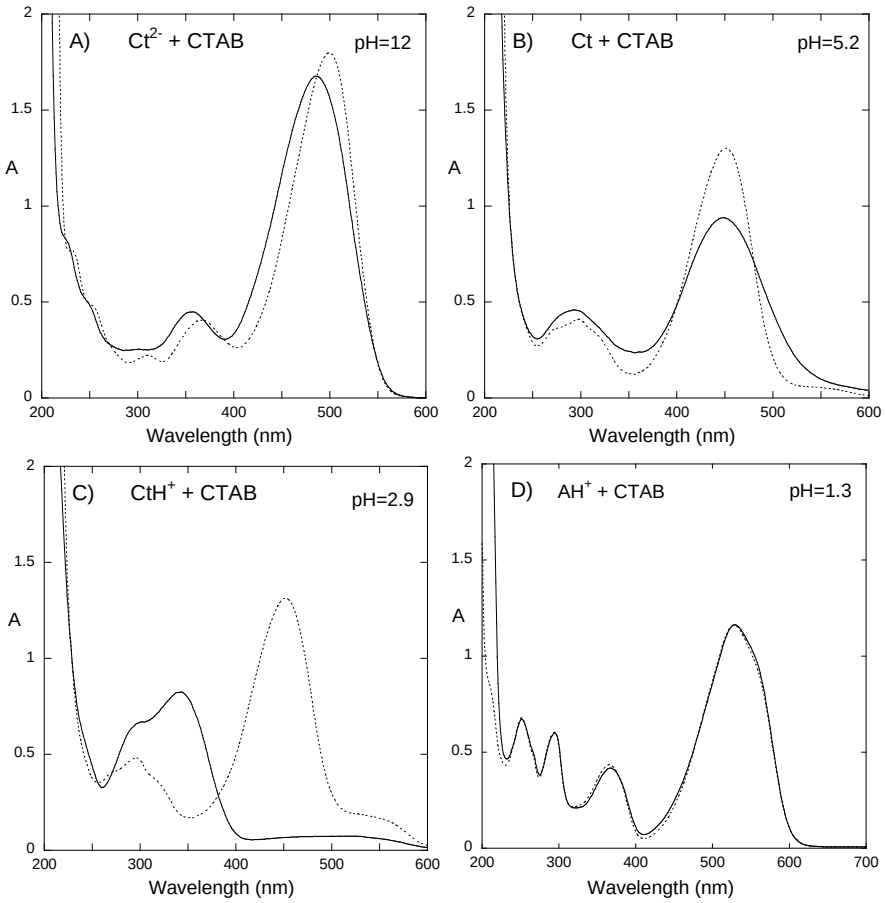

Figure 2.9 – Spectral variations of *trans*-chalcone aqueous solutions at pH 12, $\mathbf{Ct^{2-}}$, A), at pH=5.2, **Ct**, B), at pH = 2.9,$\mathbf{CtH^{+}}$, C) and flavylium cation, $\mathbf{AH^{+}}$, at pH = 1.3, D) of **DEF** (full line). Pointed lines were obtained immediately upon addition of CTAB (pointed lines). [**DEF**] = 3.8×10^{-5} M and [CTAB] = 5×10^{-3} M.

In order to get more information about the **DEF** network in the presence of CTAB micelles in the acidic region, the following experiments were carried out: 1 ml of $\mathbf{Ct^{2-}}$ at pH 12 was added to 2 ml of a solution containing acid and buffer to afford the desired final pH value together with CTAB. This procedure allows instantaneous formation of the transient $\mathbf{CtH^{+}}$. As can be confirmed by Figure 2.10, the protonated chalcone is involved in a partition equilibrium between micelles ($\mathbf{Ct^{m}}$) and bulk water. Taking into account that pK_{Ct+}=4.5,[18] in the pH range of this experiment formation of $\mathbf{CtH^{+}}$ is expected. The partition of $\mathbf{CtH^{+}}$ and **Ct** is finished before the time needed to run a spectrum, *ca.* 30 s. In other words, $\mathbf{CtH^{+}}$ goes very fast inside the micelle to form $\mathbf{Ct^{m}}$ and a pseudo-equilibrium is attained with pK_{obs}=1.1.

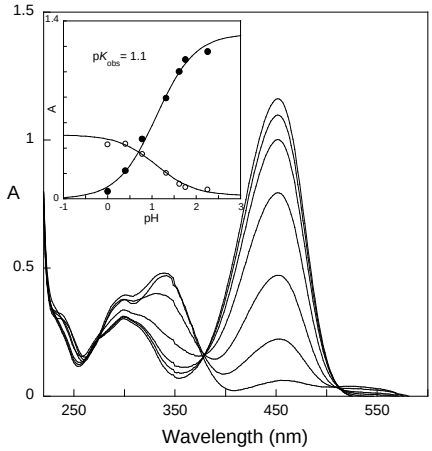

Figure 2.10 – Spectral variations of **DEF** obtained immediately after the following procedure: 1 ml of $\mathbf{Ct}^{2-}$ 1×10^{-4} M at pH 12 was added to 2 ml of a solution containing acid and buffer to give the desired final pH value and CTAB; $[CTAB]_{final} = 5\times10^{-3}$ M; inset – absorption at 450 nm (●) and at 350 nm (○) versus pH, fitting was achieved with pK_{obs}=1.1.

The data reported in Figure 2.10 (pseudo-equilibrium) can be accounted for by the following set of equations and an expression for the molar fractions can be obtained:

$\mathbf{CtH}^+ + H_2O \rightleftharpoons \mathbf{Ct} + H_3O^+$ $\quad K_{Ct+} = 10^{-4.5}$ (2.15)[18]

$\mathbf{Ct} \rightleftharpoons \mathbf{Ct}^{\mathbf{m}}$ $\quad K_{p1}$ Partition of **Ct** (2.16)

$\mathbf{CtH}^+ \rightleftharpoons \mathbf{CtH}^{+\mathbf{m}}$ $\quad K_{p2}$ Partition of $\mathbf{CtH}^+$ (2.17)

$\mathbf{CtH}^{+\mathbf{m}} + H_2O \rightleftharpoons \mathbf{Ct}^{\mathbf{m}} + H_3O^+$ $\quad K_{Ct+}{}^{m} = K_{Ct+}\,K_{p1}/\,K_{p2}$ (2.18)

$$C_0 = [Ct] + [Ct^m] + [CtH^+] + [CtH^{+m}] = [CtH^+]\left(1 + K_{p2} + \frac{K_{Ct+}(1+K_{p1})}{[H^+]}\right) \tag{2.19}$$

$$\chi_{CtH^+} = \frac{[CtH^+]}{C_0} = \frac{\dfrac{[H^+]}{(1+K_{p2})}}{[H^+] + \dfrac{K_{Ct+}(1+K_{p1})}{(1+K_{p2})}} \tag{2.20}$$

So, the inflection point of χ_{CtH+} *versus* pH is equal to $K_{Ct+}(1+K_{p1})/(1+K_{p2}) = 10^{-1.1}$, allowing to calculate:

$$\frac{1+K_{p1}}{1+K_{p2}} = 10^{3.4} \tag{2.21}$$

While Figure 2.10 accounts for a transient situation, the pH dependent spectral variations reported in Figure 2.11 correspond to the equilibrium, where the main species observed are $\mathbf{Ct}^{\mathbf{m}}$ and $\mathbf{AH}^+$.

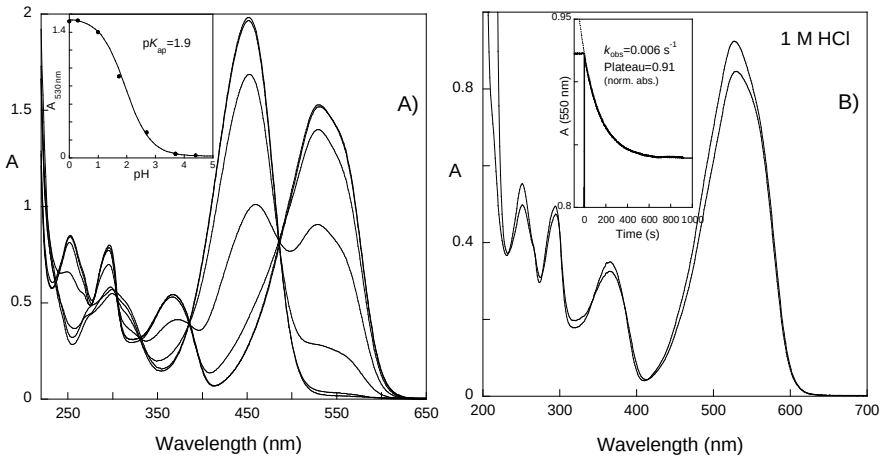

Figure 2.11 – A) pH dependent spectral changes of **DEF** in the presence of CTAB micelles at equilibrium, [**DEF**] = 5×10^{-5} M and [CTAB] = 5×10^{-3} M, inset absorption changes at 530 nm in function of pH and fitting with pK_{obs} = 1.9. B) Effect of the addition of CTAB micelles to a solution of **DEF** (1 M HCl), [**DEF**] = 3×10^{-5} M and [CTAB] 5×10^{-3} M, inset: absorbance changes at 550 nm as a function of time.

The data reported in Figure 2.11 can be accounted for by the following set of equations and, once again, the molar fractions can be defined:

$$\mathbf{AH^+} + H_2O \rightleftharpoons \mathbf{Ct} + H_3O^+ \qquad K'_a = 10^{-5.9} \qquad (2.22)^{18}$$

$$\mathbf{CtH^+} + H_2O \rightleftharpoons \mathbf{Ct} + H_3O^+ \qquad K_{Ct+} = 10^{-4.5} \qquad (2.15)^{18}$$

$$\mathbf{Ct} \rightleftharpoons \mathbf{Ct^m} \qquad K_{p1} \quad \text{Partition of } \mathbf{Ct} \qquad (2.16)$$

$$\mathbf{CtH^+} \rightleftharpoons \mathbf{CtH^{+m}} \qquad K_{p2} \quad \text{Partition of } \mathbf{CtH^+} \qquad (2.17)$$

$$\mathbf{CtH^{+m}} + H_2O \rightleftharpoons \mathbf{Ct^m} + H_3O^+ \qquad K_{Ct+}{}^{m} = K_{Ct+}\,K_{p1}/\,K_{p2} \qquad (2.18)$$

$$C_0 = [AH^+] + [Ct] + [Ct^m] + [CtH^+] + [CtH^{+m}] = [AH^+]\left(1 + \frac{K'_a}{[H^+]} + \frac{K'_a K_{p1}}{[H^+]} + \frac{K'_a}{K_{Ct+}} + \frac{K_{p2}K'_a}{K_{Ct+}}\right) \qquad (2.23)$$

$$\chi_{AH^+} = \frac{[AH^+]}{C_0} = \frac{\dfrac{K_{Ct+}}{K_{Ct+} + K'_a(1+K_{p2})}[H^+]}{[H^+] + \dfrac{K_{Ct+}K_a'(1+K_{p1})}{K_{Ct+} + K'_a(1+K_{p2})}} \qquad (2.24)$$

Besides, the global equilibrium can be accounted for by equation 2.25, being the apparent p$K'_a{}^{m}$ the one shown in Figure 2.11 A:

$$\mathbf{AH^+} + H_2O \rightleftharpoons \mathbf{Ct^m} + H_3O^+ \qquad K'_a{}^{m} = 10^{-1.9} \qquad (2.25)$$

It is worth of note that equation 2.24 predicts the existence of a plateau for high proton concentration. The existence of this plateau was confirmed through the experiment reported in Figure 2.11 B. To an equilibrated solution of $\mathbf{AH^+}$ (1M HCl) the micelle was added and the

absorption spectra monitored as a function of time. The decrease in flavylium concentration even at [HCl] = 1 M is in agreement with the plateau predicted from equation 2.24.

$$\frac{K_{Ct+}}{K_{Ct+} + K_a^{'}(1 + K_{p2})} = 0.91 \tag{2.26}$$

Using equations 2.26, 2.21, 2.22 and 2.18 it is possible to evaluate $K_{p1} = 6280$, $K_{p2} = 1.5$ and $K_{Ct+}{}^{m} = 0.1$. It is, therefore, feasible to determine all the equilibrium constants that define the pH dependent mole fraction distribution of species at equilibrium, Figure 2.12. When the distributions of species in the presence (Figure 2.12 A) and in the absence (Figure 2.12 B) of CTAB are compared, the results show very clearly, similarly to what was seen with 7,4'-dihydroxyflavylium, that the addition of CTAB shifts the **Ct^{m}** domain to more acidic pH values, in this particular case to approximately 4 pH units lower.

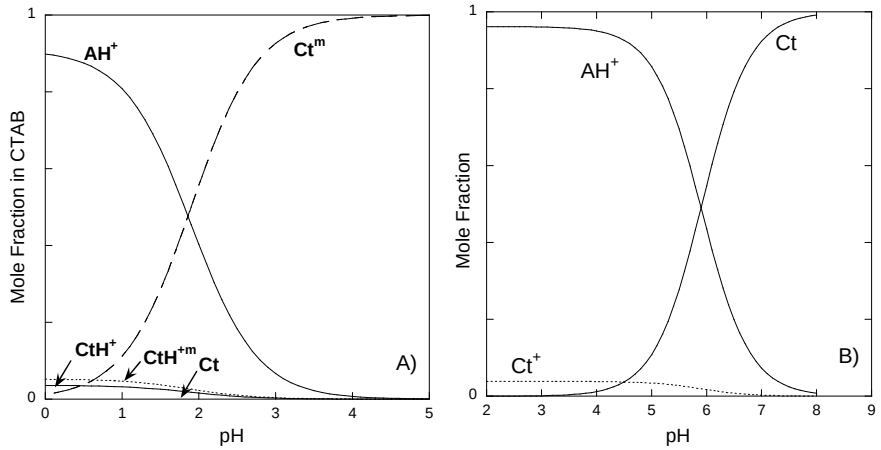

Figure 2.12 –A) Mole fraction distribution of **DEF** in the presence of CTAB micelles at equilibrium. B) In the absence of CTAB for comparison purposes.

2.3.3 Kinetics of the flavylium network in the presence of CTAB micelles

The kinetics of the flavylium disappearance when CTAB is added into the solution was measured at different pH values. The decay of the flavylium cation absorbance follows a first-order kinetic law and is pH dependent, as plotted in Figure 2.13. In order to explain the behavior reported in Figure 2.13, Scheme 2.3 is proposed from which equation 2.27 can be deduced (Supporting Information, 9.3.1):

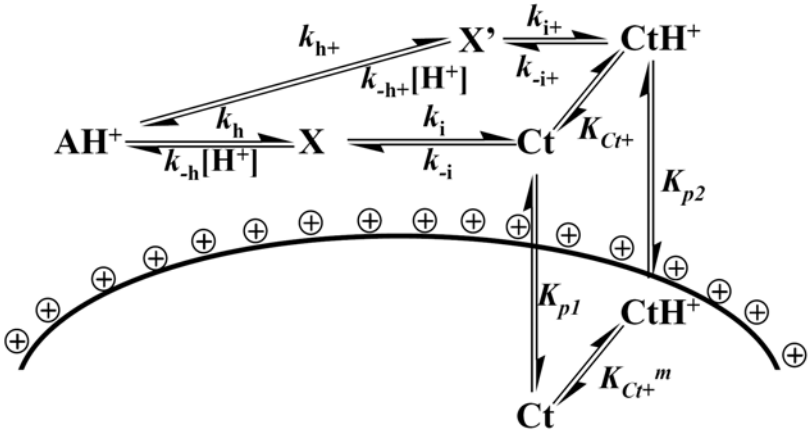

Scheme 2.4 – Species involved in the kinetics of the flavylium thermal formation.

$$k_{obs} = \frac{[H^+]}{[H^+]+K_a}\left(\frac{k_i K_t k_h}{k_{-h}[H^+]+k_i K_T}+\frac{k_{i+}K_{t'}k_{h+}}{k_{-h+}[H^+]+k_{i+}K_{t'}}\right)+\left(\frac{k_{-h+}k_{-i+}\chi_{CtH^+}}{k_{-h+}[H^+]+k_{i+}K_{t'}}\right)[H^+] \qquad (2.27)$$

where χ_{CtH+} is given by equation 2.20 and the other constants have been reported in previous work.[18] The only adjustable parameter is k_{h+}. However, the fitting was achieved with $k_{h+} \sim 0$ s^{-1} (or $< 5\times10^{-5}$ s^{-1}). In equation 2.27, the first term reports the rate of $\mathbf{AH^+}$ entrance from the intermediate X, the second one from the intermediate **X'**, and the last from the back reaction starting from $\mathbf{CtH^+}$. The reverse term from **Ct** was neglected due to its high partition coefficient with the micelle - it is assumed that **Ct** goes instantaneously into the micelle (see Figure 2.12 B) to form $\mathbf{Ct^m}$.

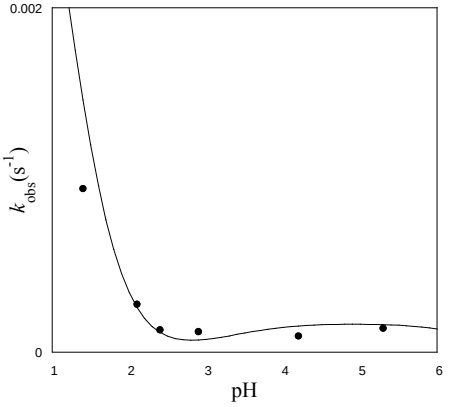

Figure 2.13 – Rate constant for the thermal conversion of $\mathbf{AH^+}$ into $\mathbf{Ct^m}$ *versus* pH at 22 °C. The solid line shows the fit with eq 2.27.

2.3.4 Photochemistry: a gradient of color between yellow and pink-red

The system reported in this work constitutes a beautiful photochromic system, as reported in Figure 2.14. Irradiation of dark equilibrated solutions of **DEF** in the presence of

CTAB micelles leads to the appearance of the characteristic pink-red color of the flavylium cation, Figure 2.14 B. The pH dependent quantum yield of this reaction (λ_{irr} = 436 nm) is relatively low, Φ = 0.001 at pH = 4.25, but the solution becomes strongly pink-red upon a few minutes under direct sunlight. The fast color change upon sunlight exposure results from the relatively good overlap between the absorption spectrum of **Ct$^{(m)}$** and the solar radiation.

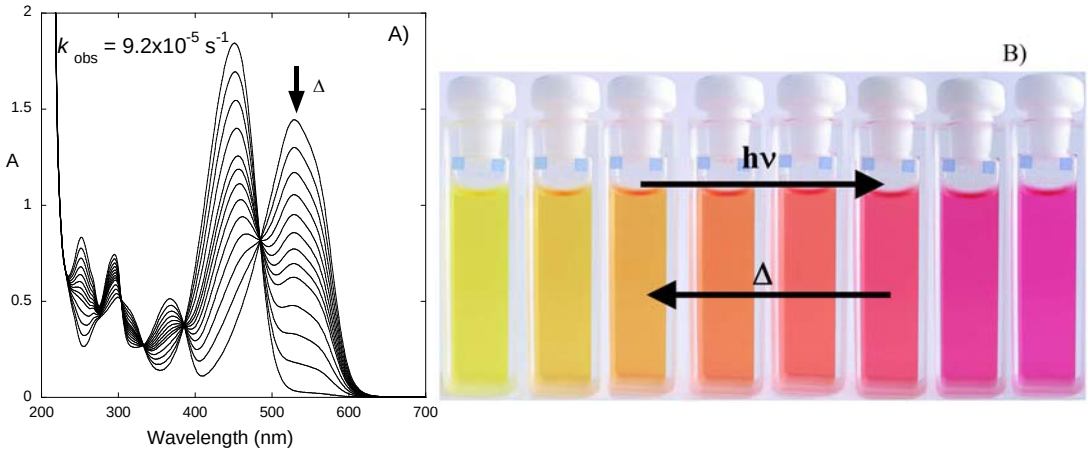

Figure 2.14 –A) Kinetics of the thermal transformation of **AH$^+$** into **Ct**, in the presence of CTAB, at pH = 4.25. B) Irradiation of the previous solution at 436 nm Φ = 0.001 ($I_0 = 2.3\times10^{-7}$ einstein.min^{-1}); at sunlight (bright day) upon 0, 1, 2, 4, 6, 9, 14, 24 min of exposure; [**DEF**] = 5×10^{-5} M and [CTAB] = 5×10^{-3} M.

2.3.5 Flash photolysis and isomerization quantum yields

The photochromism of **Ct^m** implies the existence of an initial *trans-cis* photoisomerization reaction in which **Ct** is converted into **Cc**. Once *cis*-chalcone is formed, it can be converted back into the *trans* isomer or undergo a tautomerization reaction in order to form the hemiketal species **B** and finally the flavylium species **AH$^+$** after dehydration, responsible for the color change. In this case, flash photolysis experiments are able to detect these transient species within the micelle, and some experimental results are presented in Figures 2.15 and 2.16 as transient absorption spectra.

Immediately after the lamp flash, a transient spectra is detected at all pH values, see Figures 2.15 and 2.16, in which strong bleaching is observed within the region where **Ct^m** absorbs, while a transient absorption appears at other wavelengths (290 and 520 nm). At pH = 5.3, the absorption at 520 nm could be either the formation of **AH$^+$** or **Cc**: the **AH$^+$** absorption spectra peaks at about 540 nm, which could originate the peak at 520 nm on the transient absorption, while the **Cc** absorption spectra are unknown for this molecule. This doubt is solved by looking at the final flash photolysis transient absorption spectra after 30 s, before the thermal reaction takes place, when **AH$^+$** is expected to dominate (pH = 2.3), Figure 2.16. Indeed this transient absorption peaks at about 540 nm which is in accordance with **AH$^+$** absorption spectra and is significantly different from the transient spectra obtained immediately after the lamp flash. Therefore, the transient absorption that peaks at 520 nm should be assigned to **Cc**, and thus the initial transient spectra is due to **B** and **Cc** (Figure 2.15 B). Similar *trans*-

chalcones with dialkylamino groups at the same position also show a red shift upon irradiation attributed to the formation of *cis*-chalcones.[20b]

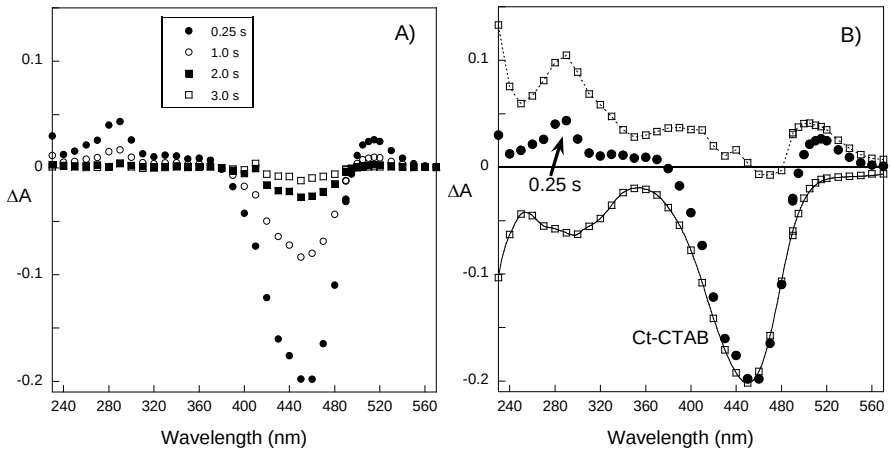

Figure 2.15 – A) Time-resolved absorption spectra at pH = 5.33. B) The points upon 0.25 s after the flash can be fitted as a sum of the absorption spectra of **Ct^{m}**, bleaching, and other species that absorb at 290 and 520 nm.

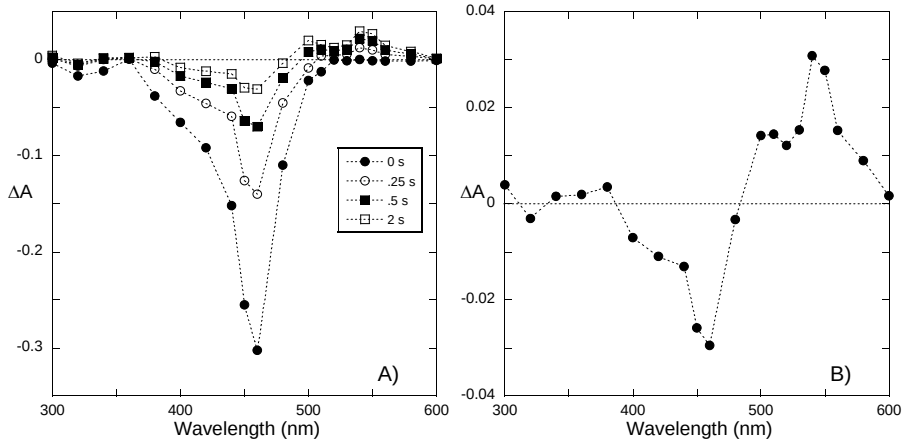

Figure 2.16 – A) Time-resolved absorption spectra at pH = 2.31. B) Detail of the spectrum of the final (30 s) flash photolysis process.

Flash photolysis on CTAB micelles can resolve the presence of **B** and **Cc** species at the micellar phase. As the pH changes within the range 1.5-6, the flash photolysis traces reveal the prompt formation of **Cc** (at higher pH), the formation of **B** from **Cc** (specially evident at pH ~3.3, Figure 2.17) and the formation of **AH**$^{+}$ from **B** (at lower acidic pH). These rich chemical dynamics can be summarized in Scheme 2.5.

This scheme relies on several approximations. At the pH range of interest (1.5-6), the presence of protonated chalcone and hemiketal species is negligible (Figure 2.10), and therefore these species are not considered. However, **AH**$^{+}$ has positive charge and is expected to move into the bulk water giving rise to a metastable **AH**$^{+}$. Because at this pH range the flavylium in water is thermodynamically stable when compared with chalcone species, its conversion to **Ct^{m}** will follow the thermal mechanism described before.

With dependence on pH, the flash photolysis traces could be fitted with either single-exponential or biexponential functions. One of the experimental rate constants, k_{flash}^{I} , changes with pH from about 5 s^{-1} at pH = 1.7 to about 0.4 s^{-1} at pH = 5.85 and is assigned to either the formation of $\mathbf{AH^+}$ at acidic pH or the back isomerization to $\mathbf{Ct^m}$ at less acidic pH. The second experimental rate constant, k_{flash}^{II} , is only evident in a narrow pH range, from 2 to 3.6 (Figures 2.17 and 2.18) and is around 6 s^{-1}. This step is assigned to the $\mathbf{B^m}$ formation from $\mathbf{Cc^m}$.

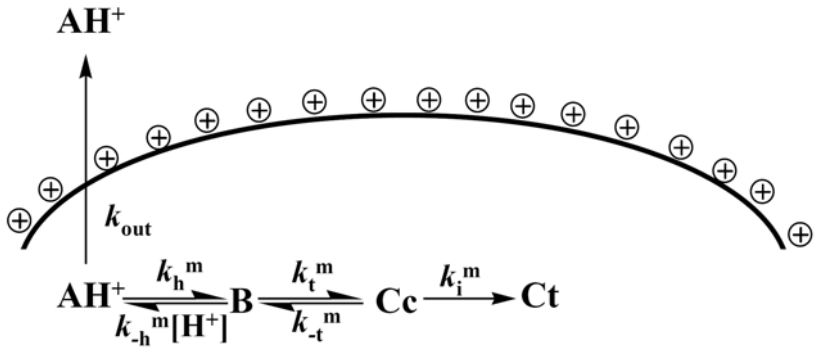

Scheme 2.5 – Species involved in the kinetics of the flavylium photochemical formation.

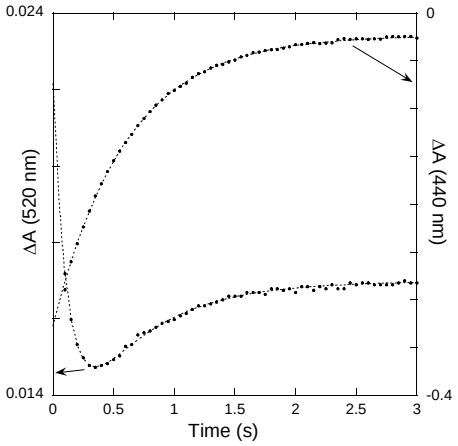

Figure 2.17 –Traces of the **DEF** flash photolysis, [**DEF**] = 5×10^{-5} M and [CTAB] = 5×10^{-3} M at pH = 3.3.

The following expressions could be derived from Scheme 2.5 in order to explain the kinetics (Supporting Information, section 9.3.2):

$$k_{flash}^{\ I} = k_i^{\ m} + \frac{k_{-t}^{\ m}\beta[H^+]}{k_t^{\ m} + \beta[H^+]} \tag{2.28}$$

$$k_{flash}^{\ II} = k_t^{\ m} + k_{-t}^{\ m} \tag{2.29}$$

where

$$\beta = \frac{k_{-h}{}^{m} k_{out}}{k_{h}{}^{m} + k_{out}} \tag{2.30}$$

If $k_{out} >> k_h{}^m$, then $\beta \sim k_{-h}{}^m$, which is a plausible approximation since k_h for flavylium cations bearing amino groups are normally low[22,18,23] and for this particular molecule $k_h = 1.5\times10^{-4}$ s^{-1}.[18]

Unfortunately, this simpler set of equations runs into trouble because they require that certain approximations take place, namely, the tautomerization step must be very fast in order to have a fast equilibrium. Obviously this is not the case and the matrix method must be used in order to obtain the correct analytical solutions of the kinetic scheme (Supporting Information, section 9.3.2). The rate constants are given by:

$$k_{flash}{}^{I} = \frac{(k_t{}^m + \beta[H^+] + k_i{}^m + k_{-t}{}^m) - \sqrt{(k_t{}^m + \beta[H^+] + k_i{}^m + k_{-t}{}^m)^2 - 4k_i{}^m k_t{}^m - 4(k_i{}^m + k_{-t}{}^m)\beta[H^+]}}{2} \tag{2.31}$$

$$k_{flash}{}^{II} = \frac{(k_t{}^m + \beta[H^+] + k_i{}^m + k_{-t}{}^m) + \sqrt{(k_t{}^m + \beta[H^+] + k_i{}^m + k_{-t}{}^m)^2 - 4k_i{}^m k_t{}^m - 4(k_i{}^m + k_{-t}{}^m)\beta[H^+]}}{2} \tag{2.32}$$

From equations 2.31 and 2.32, one can derive:

$$k_{flash}{}^{I} + k_{flash}{}^{II} = k_i{}^m + k_t{}^m + k_{-t}{}^m + \beta[H^+] = a + \beta[H^+] \tag{2.33}$$

And therefore a plot of $k_{flash}{}^{I} + k_{flash}{}^{II}$ *versus* $[H^+]$ should give a straight line with slope β and with intercept *a* equal to $k_i{}^m + k_t{}^m + k_{-t}{}^m$ (Figure 2.19 A). With the solutions obtained from the analysis with equation 2.33, equations 2.31 and 2.32 can be rearranged:

$$k_{flash}{}^{II} - k_{flash}{}^{I} = \sqrt{(a + \beta[H^+])^2 - 4k_i{}^m k_t{}^m - 4(k_i{}^m + k_{-t}{}^m)\beta[H^+]} \tag{2.34}$$

$$\frac{(a + \beta[H^+])^2 - \left(k_{flash}{}^{II} - k_{flash}{}^{I}\right)^2}{4} = k_i{}^m k_t{}^m + (k_i{}^m + k_{-t}{}^m)\beta[H^+] \tag{2.35}$$

Representing the first term in equation 2.35 as a function of $[H^+]$, a straight line is indeed obtained (Figure 2.19 B) and all the kinetic constants can now be evaluated. From these plots, one obtains $k_i{}^m$ =3.5 s^{-1}, $k_t{}^m$ = 2.2 s^{-1}, $k_{-t}{}^m$ = 1.8 s^{-1} and $\beta \sim k_{-h}{}^m$ = 970 M^{-1} s^{-1}.

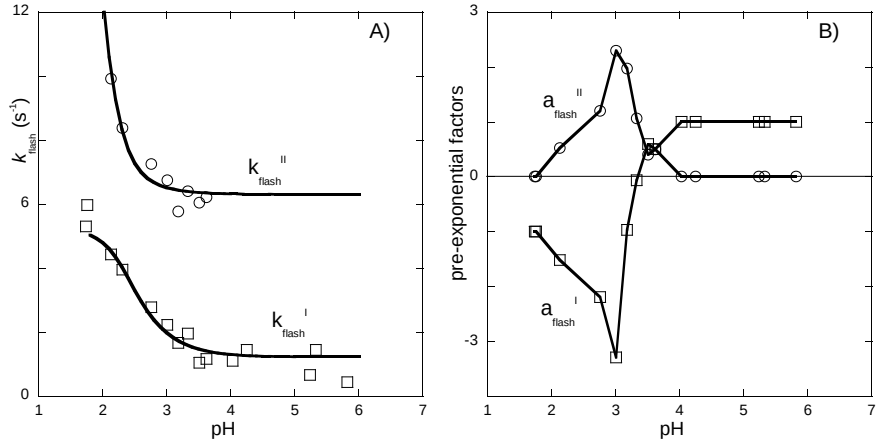

Figure 2.18 – A) Flash photolysis experimental rate constants fitted with eqs. 2.31 and 2.32. B) pre-exponential factors obtained from the analysis of the kinetic traces with biexponential functions, the lines are only guidelines.

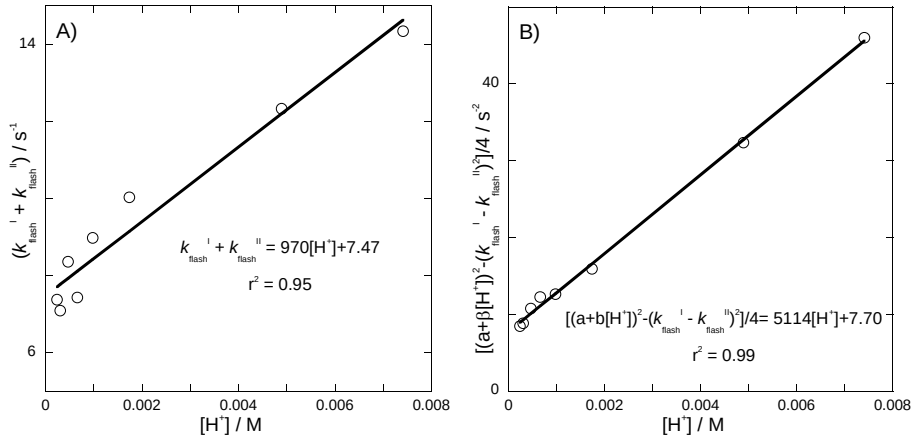

Figure 2.19 – A) Plot for the determination of the kinetic rate constants using eq. 2.33. B) Plot for the determination of the kinetic rate constants using 2.35.

An expression for the quantum yield of $\mathbf{AH}^+$ formation can also be deduced and compared with experimental results. According to Scheme 2.5 (section 9.3.3, Supplementary Material):

$$\Phi = \Phi_{Ct^m \rightarrow Cc^m} \frac{\beta[H^+] k_{-t}{}^m}{\beta[H^+](k_{-t}{}^m + k_i{}^m) + k_t{}^m k_i{}^m} \tag{2.36}$$

the quantum yield should increase as pH decreases. The only fitting parameter in equation 2.36 is $\Phi_{Ctm \rightarrow Ccm}$, which is the photoisomerization quantum yield of **Ct** in the micelle, and the fit is presented in Figure 2.20 with $\Phi_{Ctm \rightarrow Ccm} = 0.03$.

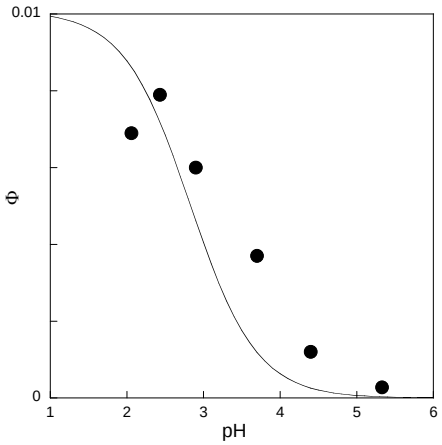

Figure 2.20 – pH dependence of the flavylium quantum yield formation upon irradiation at 436 nm fitted with eq 2.36.

Figure 2.21 summarizes the results obtained for the **DEF** network in water and CTAB micelles. The photochemistry when CTAB is added is, once again, explained by unbalanced pH dependence: within the pH range between 2 and 5, $\mathbf{AH^+}$ in water is more stable than **Ct** but inside the micelles $\mathbf{Ct^m}$ is even more stable than $\mathbf{AH^+}$. Therefore, when $\mathbf{AH^+}$ is photochemically produced inside the micelle, it goes to the bulk water very fast (with a rate constant that was not possible to determine with the present experiments) and afterwards it converts back to $\mathbf{Ct^m}$ only after about 3 h due to a slow hydration step. The pH dependence of the $\mathbf{AH^+}$ thermal conversion to $\mathbf{Ct^m}$ is small, but the photochemical quantum yield changes abruptly from pH = 5 to pH = 2. The best color contrast, however, occurs for pH above 3, because the $\mathbf{AH^+}$ concentration is negligible at thermodynamic equilibrium but still the photochemical quantum yield allows for complete conversion upon irradiation.

Thermodynamics
$pK_{CtH+} = 4.5$
$pK_{CtH+m} = 0.9$
$K_{p1} = 6280$
$K_{p2} = 1.5$

Kinetics
$k_h = 1.5\times10^{-4}$ s^{-1}
$k_{-i} = 1.0\times10^{-2}$ s^{-1}
$k_iK_t/k_{-h} = 5.0\times10^{-4}$ s^{-1}
$k_{i+}K_{t'}/k_{-h+} = 7.5\times10^{-3}$ s^{-1}
$k_{-i+} = 1.3\times10^{-2}$ s^{-1}
$k_{h+} \sim <5\times10^{-5}$ s^{-1}
$k_i^m = 3.5$ s^{-1}
$k_t^m = 2.2$ s^{-1}
$k_{-t}^m = 1.8$ s^{-1}
$\beta \sim k_{-h}^m = 970$ M^{-1} s^{-1}

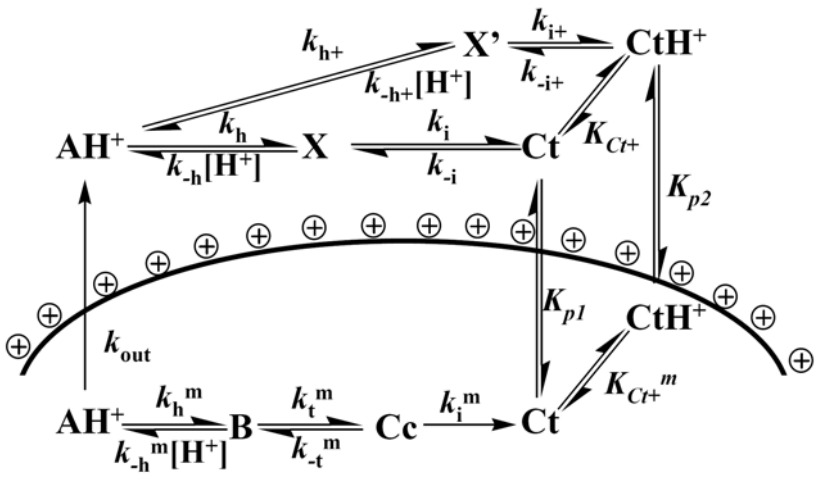

Figure 2.21 –Summary of the results obtained for **DEF** network in water and CTAB micelles.

2.4 Experimental Part

7,4'-Dihydroxyflavylium (**DHF**) perchlorate[17] and 7-(*N,N*-Diethylamino)-4'-hydroxyflavylium (**DEF**) tetrafluoroborate[18] were available from previous studies.

All other chemical used were of analytical grade. Solutions were prepared using Millipore water. The pH of solutions was adjusted by addition of HCl, NaOH, or universal buffer (Theorell and Stenhagen)[24] and was measured using a Radiometer Copenhagen PHM240 pH/ion meter. UV-Vis absorption spectra were recorded using a Varian- Cary 100 Bio spectrophotometer or Shimadzu VC2501-PC.

A concentration of 1.46×10^{-5} M of 7,4'-dihydroxyflavylium (**DHF**) perchlorate flavylium cation and a concentration of 0.018M CTAB were used. Quantum yields were determined by irradiation at 365 nm, using a medium pressure mercury arc lamp, and the excitation bands were isolated with interference filters (Oriel). Actinometry was made using the ferrioxalate system.[25] To monitor the transient species we used a Perkin-Elmer Lambda6 spectrophotometer with a slightly modified sample compartment, with a slit (5 mm wide and 20 mm high) on the external side of the sample holder in order to perform light excitation perpendicular to the analyzing beam; and with the sample compartment shielded with black metal piece. As a pulsed light source a commercially available Philips 38CT camera flash was used, placed in close contact with the slit opened in the sample holder. The excitation was made with the white light of the camera flash and the time-resolution is about 0.1 s at least. Further details are described elsewhere.[16]

For 7-(*N,N*-diethylamino)-4'-hydroxyflavylium (**DEF**) a concentration of 5.0×10^{-5} M and 5.0×10^{-3} M CTAB were used in all kinetic rate measurement, flash photolysis, and quantum yield determination experiments. All experiments were performed as for **DHF**, except that quantum yields were determined by irradiation at 436 nm.

2.5 Conclusions

A general strategy to obtain photochromism from the network of chemical reactions originated by flavylium compounds was achieved. This strategy is particularly useful for flavylium salts bearing amino groups which give rise to a variety of beautiful colors but lack photochemistry in water. Dramatic changes in the properties of the flavylium network can be achieved in heterogeneous media because specific interactions of some of the states with the different chemical environments take place. In particular, charged interfaces can be used to achieve efficient photochromism of flavylium compounds lacking *cis–trans* isomerization thermal barrier and, most importantly, with no need of pH changes for the photochromism to operate, which constitutes an important improvement over previously described systems dependent on pH jumps. Even when the systems are used at the *lock* pH (Figure 1.7), the color

contrast is poorer than when micelles are used and the photodegradation can be more accentuated.

Introduction of CTAB micelles in aqueous solutions of 7-(*N,N*-diethylamino)-4' hydroxyflavylium shifts the equilibrium to lower pH values, stabilizing *trans*-chalcone for pH > 3 and defining a yellow dark state. At such pH values in the bulk, $\mathbf{AH^+}$ is still more stable than **Ct** and is slowly converted into $\mathbf{Ct^m}$. Under thermodynamic equilibrium, irradiation of $\mathbf{Ct^m}$ leads to the production of $\mathbf{AH^+}$, which is quickly ejected to the bulk, that is, the system switches to a pink-red state giving rise to a significant photochromism. Both quantum yield and efficiency of $\mathbf{AH^+}$ formation are increased upon addition of CTAB micelles. The best color contrast is obtained at pH = 4.25 with $\Phi = 0.001$ and a recovery lifetime of approximately 3 h.

Similarly and differently from what is observed in water, efficient photochromism with a strong color contrast has been observed for the multistate compound 7,4'-dihydroxyflavylium in the presence of CTAB micelles. Once again, two states are responsible for the photochromism: *trans*-chalcone (inside the micelle) in the dark, and $\mathbf{AH^+}$ (in bulk water) upon irradiation. The best color contrast is obtained at pH = 1.5, from a solution practically colorless in the dark, to an intense yellow upon irradiation ($\Phi = 0.21$). The system is also thermally reversible with a lifetime of 38 min at room temperature, and exhibits a reasonable stability.

After the development of this work, other photochromic enhanced systems based on flavylium salts in heterogeneous media have been reported, namely taking profit of the negatively charged AOT (Sodium bis(2-ethylhexyl)sulfosuccinate) reverse micelles.[26] These systems present high quantum yields and a wide range of operational pH values.[26]

2.6 References

[1] ed. J. C. Crano, R. J. Guglielmetti, *Organic Photochromic and Thermochromic Compounds*, Vol. 1 *Main Photochromic Families*, Plenum Press, New York, USA, **1999**.
[2] J. C. Crano, T. Flood, D. Knowles, A. Kumar, B. Van Gemert, IUPAC, *Pure and Applied Chemistry* **1996**, 68, 1395-1398.
[3] S. Kurada, G.W. Rankin, K. Sridhar, *Opt. Lasers Eng.* **1994**, 20, 177-194.
[4] M. Irie, IUPAC, *Pure and Applied Chemistry* **1996**, 68, 1367-1371.
[5] ed. B. L. Feringa, Wiley-VCH, Weinheim, Germany, **2001**.
[6] Guest ed. M. Irie, *Photochromism: Memories and Switches, Chem. Rev.* **2000**, 100, 5, 1683-1890.
[7] A. Roque, J. C. Lima, A. J. Parola, F. Pina, *Photochem. Photobiol. Sci.* **2007**, 6, 381-385.
[8] A. Roque, F. Pina, S. Alves, R. Ballardini, M. Maestri, V. Balzani, *J. Mat. Chem.* **1999**, 9, 2265-2269.
[9] F. Pina, M. J. Melo, S. Alves, R. Ballardini, M. Maestri, P. Passaniti, *New J. Chem.* **2001**, 25, 747-752.
[10] M. J. Melo, S. Moura, M. Maestri, F. Pina, *J. Mol. Struct.* **2002**, 612, 245-253.
[11] S. P. Moulik, *Current Science* **1996**, 71, 368-376.
[12] F. Pina, J. C. Lima, A. J. Parola, C. A. M. Afonso, *Angew. Chem. Int. Ed.* **2004**, 43, 1525-1527.
[13] F. Galindo, J. C. Lima, S. V. Luis, A. J. Parola, F. Pina, *Adv. Funct. Mat.* **2005**, 15, 541-545.
[14] F. Pina, L. Benedito, M. J. Melo , A. J. Parola, J. C. Lima, A. L. Maçanita., *Anales de Quimica* **1997,** 93, 111-118.
[15] F. Pina, M. J. Melo, R. Ballardini, L. Flamigni, M. Maestri, *New. J. Chem.* **1997***,* 21, 969-976.
[16] M. Maestri, R. Ballardini, F. Pina, M. J. Melo, *J. Chem. Educ.* **1997**, 74, 1314-1316.
[17] P. Figueiredo, J. C. Lima, H. Santos, M. C. Wigand, R. Brouillard, A. L. Macanita, F. Pina, *J. Am. Chem. Soc.* **1994**, 116, 1249-1254.

[18] M. C. Moncada, D. Fernandez, J. C. Lima, A. J. Parola, C. Lodeiro, F. Folgosa, M. J. Melo, F. Pina, *Org. Biomol. Chem.* **2004**, 2, 2802-2808.
[19] H. Wünscher, G. Haucke, P. Czerney, U. Kurzer, *J. Photochem. Photobiol. A* **2002**, 151, 75-82.
[20] a) R. Matsushima, H. Mizuno, H. Itoh, *J. Photochem. Photobiol. A* **1995**, 89, 251-256; b) . R. Matsushima, S. Fujimoto, K. Tokumura, *Bull. Chem. Soc. Jpn.* **2001**, 74, 827-832.
[21] F. Pina, A. J. Parola, M. J. Melo, C. A. T. Laia, C. A. M. Afonso, *Chem. Commun.* **2007**, 16, 1608-1610.
[22] A. Roque, C. Lodeiro, F. Pina, M. Maestri, S. Dumas, P. Passaniti, V. Balzani, *J. Am. Chem. Soc.* **2003**, 125, 987-994.
[23] C. A. T. Laia, A. J. Parola, F. Folgosa, F. Pina, *Org. Biomol. Chem.*, **2007**, 5, 69-77.
[24] F. W. Küster, A. Thiel*, Tabelle per le Analisi Chimiche e Chimico- Fisiche*, 12th ed.; Hoepli, Milano, Italy, **1982**, 157-160.
[25] C. G. Hatchard, C. A. Parker, *Proc. R. Soc. (London), Ser. A* **1956**, 235, 518-536.
[26] V. Petrov, C. A. T. Laia, F. Pina, *Langmuir* **2009**, 25, 594-601.

3. 2-Styryl-1-benzopyrylium compounds: extending the color palette

In this chapter, the synthesis and characterization of 2-styryl-1-benzopyrylium salts is presented. The photochemistry of these compounds and related flavylium compounds is studied, explaining the poor photochemistry arising from the 2-styryl-1-benzopyrylium network in water.

3.1 Introduction

Anthocyanins have long been used as natural food colorants after recognition of undesired physiological effects of easily synthesized azo dyes.[1] As pointed out in the Introduction, synthetic flavylium salts, possess the same basic structure and identical network of chemical reactions of anthocyanins and are a versatile family of compounds. Their color and physico-chemical properties have been widely studied and are greatly dependent on the nature and position of the functional groups attached to the 2-phenyl-1-benzopyrylium skeleton.[2]

Structurally related to flavylium compounds, and suggested as potential color additives for fruit drinks and juices[3] are 2-styryl-1-benzopyrylium salts that have the same basic skeleton with an extra double bond linking the benzopyrylium and the phenyl systems, see Scheme 3.1. The introduction of this double bond leads to an extended conjugation that might have profound effects in the color and reaction network; particularly, it shifts the absorption maxima to the red, which allows obtaining darker and stronger tonalities.[3,4]

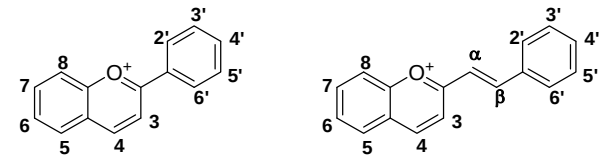

Scheme 3.1 – Structure of 2-styryl-1-benzopyrilium compared with flavylium.

On the other hand, it is documented in the literature, by Amic and co-workers,[4] that the pK'_a of these pyrylium salts increases with the introduction of the double bond in the basic skeleton of anthocyanins (which retards the loss of color to higher pH values), attesting its usefulness as food colorants, as patented by Jurd in 1967.[3] The introduction of this extra double bond also offers the possibility of having an extra isomerization that would increase the number of available states in multistate/multifunctional systems based on 2-styryl-1-benzopyrylium salts. To our knowledge, no extensive study of this kind of compounds is reported in the literature, with the exception of the work by Amic *et al.* on 7-hydroxy-2-(4-methoxystyryl)-1-benzopyrylium.[4]

However, the synthesis of 2-styryl-1-benzopyrylium salts was reported in the literature as early as 1922,[5] and mainly two methods were described: acidification of the corresponding distyryl ketones and condensation of a salicylaldehyde with a styrylmethylketone in acidic media, Figure 3.1. Styrylmethylketones can be synthesized with various functional groups.[6]

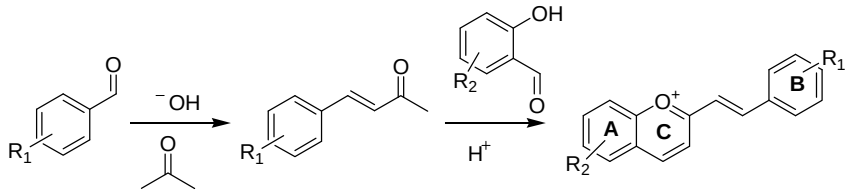

Figure 3.1 – Generic synthesis of 2-styryl-1-benzopyrylium salts based on the condensation of 2-hydroxychalcones and styrylmethylketones.

In this chapter, the syntheses of a series of 2-styryl-1-benzopyrylium salts through acidic condensation is performed, and thermodynamic as well as kinetic studies on three of them are carried out, identifying the nature and pH range of the species involved, as the information available in the literature is quite scarce. This fact prompted the investigation in more detail to understand how the introduction of the double bond affects the kinetics and the thermodynamics of the network of chemical reactions reported in Scheme 1.8 and, particularly, how the photochromic properties of the chalcones derived from 2-styryl-1-benzopyrylium systems compare with those arising from the 2-phenyl analogues. A particular emphasis on the photochromic properties of the chalcones derived from 2-styryl-1-benzopyrylium systems comparing with those arising from the 2-phenyl analogues is given.

3.2 Synthesis and characterization

The synthetic approach, in Figure 3.1, was tested with adequate starting materials and six 2-styryl-1-benzopyrylium salts were obtained with poor to reasonable isolated yields (see sections 3.6.1 and 3.6.2). The yields seem to be better when gaseous HCl is used instead of aqueous HBF_4. In all NMR experiments, performed at pH 1, where the flavylium cation is the thermodynamic stable species, clear evidence was found for the existence of the double bond in *trans* configuration – in all cases, protons β and α show coupling constants between 15 and 16 Hz.[7] All compounds were also identified by Mass Spectrometry (MALDI TOF, FD, EI) and Elemental Analysis.

For compound 7-Hydroxy-2-(4-hydroxystyryl)-1-benzopyrylium chloride, **DHS**, a NMR spectrum was obtained in an equilibrated solution at pH 6. At these pH values, the species equivalent to **Ct** in Scheme 1.8 should be the thermodynamically stable species. Two double bonds could be identified, with a geometry that is clearly *trans* in both cases as evidenced by the presence of two pairs of doublets with scalar coupling constants between 15 and 16 Hz. The same NMR spectrum was obtained upon a pH jump from 1 to 6 and from 12 to 6. On this basis, from now on and for the sake of simplicity, **Ct** will also be the designation of this species in 2-

styryl-1-benzopyrylium salts, knowing that it corresponds to the *trans–trans*-isomer, see Scheme 3.2.

The NMR spectrum was also performed at pH 12, where $\mathbf{Ct^{2-}}$ should be the thermodynamically stable species and, again, the *trans–trans* configuration was found.

In conclusion, as pointed out previously by Amic,[4] it is apparent that the same network of reactions of flavylium salts can be applied to 2-styryl-1-benzopyrylium salts, according to Scheme 3.2.

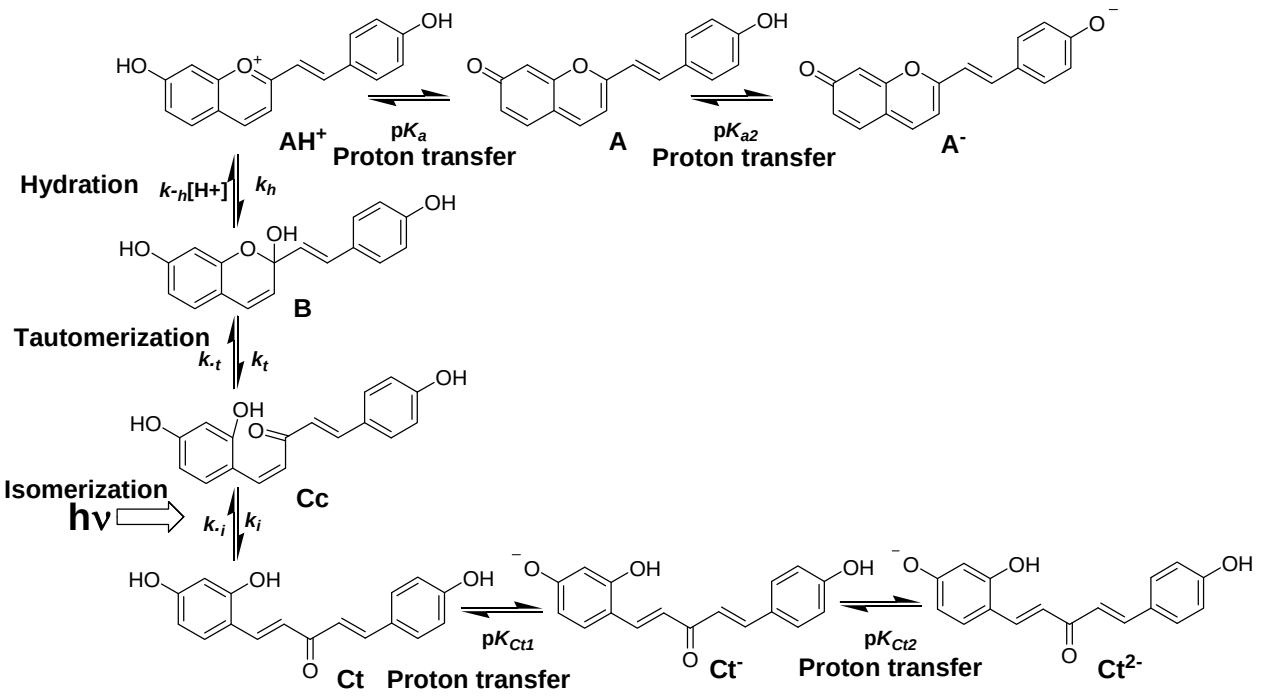

Scheme 3.2 – Network of reactions of 2-styryl-1-benzopyrylium salts in water.

3.3 Networks of 2-styryl-1-benzopyrylium in water

3.3.1 2-Styryl-1-benzopyrylium salts without OH in position 7

Differently from 2-styryl-1-benzopyrylium tetrafluoroborate, 2-(2-hydroxystyryl)-1-benzopyrylium tetrafluoroborate and 2-(4-hydroxystyryl)-1-benzopyrylium tetrafluoroborate, solutions of 7-hydroxy-2-styryl-1-benzopyrylium tetrafluoroborate (**HS**), 7-hydroxy-2-(4-hydroxystyryl)-1-benzopyrylium chloride (**DHS**) and 7-hydroxy-2-(4-dimethylaminophenyl)-1-benzopyrylium chloride (**DAS**) are stable and thermodynamic and kinetic studies could be carried out. We did not succeed to stabilize solutions of 2-styryl-1-benzopyrylium compounds lacking a hydroxyl substituent in position 7. Usually, a precipitate is observed in old aqueous solutions of 2-styryl-1-benzopyrylium tetrafluoroborate and if this precipitate is filtered off, after some days it is reformed. The spectral evolutions do not reach a final state of equilibrium, at least after one month, even in diluted solutions (10^{-7} M) where no precipitate is observed. On the other hand, these compounds are sensitive to light, showing some photodegradation. We

have tried preparing solutions also in water–organic solvent mixtures (alcohols, acetonitrile), in the absence of oxygen, in the dark, in the presence of SDS micelles and with various acid concentrations; in all cases, there is a spectral evolution that could neither be suppressed nor understood. It could be speculated that the predictable presence of a thermal barrier between *trans* and *cis*-chalcones is related with the observed instability of the solutions.[8]

3.3.2 7-Hydroxy-2-styryl-1-benzopyrylium tetrafluoroborate (HS)

In principle, if the insertion of the double bond has no effect, 2-styryl-1-benzopyrylium salts should behave similar to flavylium ions, according to Scheme 3.2.

After verifying the stability of the aqueous mother solution at pH 1, pH jumps were performed to various final pH values by mixing 1 ml of buffer at the desired pH value, 1 ml of 0.1 M base and, finally, 1 ml of the 2.5×10^{-5} M mother solution of the compound under study at pH = 1.0. In Figure 3.2, the $\mathbf{AH^+}$ species of **HS** (λ_{max} = 471 nm, ε_{max} = 32000 $cm^{-1}M^{-1}$) is transformed immediately after the pH jump into a species with absorption maximum at 512 nm, that by analogy with flavylium salts[2] must correspond to the quinoidal base **A** (ε_{max} = 16800 $cm^{-1}\,M^{-1}$), according to equation 1.22. Fitting of the experimental data allows the determination of $pK_a = 3.7 \pm 0.1$. The formation of the quinoidal base **A** upon deprotonation of $\mathbf{AH^+}$ is the fastest process but this species is not the most thermodynamically stable. Most of **A** disappears with time to give mostly **Ct** (and **B** and **Cc**, that however are not detected in the equilibrium), according to equation 1.26. At the final thermodynamic equilibrium, Figure 3.3, the major species **Ct** (λ_{max} = 380 nm) is formed with $pK'_a = 3.1 \pm 0.1$. At pH values in which $\mathbf{AH^+}$ is no longer available, it is possible to define:

$$C_0 = [A] + [B] + [Cc] + [Ct] = [A]\left(1 + \frac{K_h}{K_a} + \frac{K_t K_h}{K_a} + \frac{K_i K_t K_h}{K_a}\right) \tag{3.1}$$

Equation 3.1 can be rearranged to equation 3.2 that allows calculation of the percentage of base **A** present at the final equilibrium. In this case, **A** is present in 24 ± 5%, the major component being **Ct** and the other species are present in non-detectable concentrations.[2]

$$\frac{[A]}{C_0} = \frac{K_a}{K'_a} \tag{3.2}$$

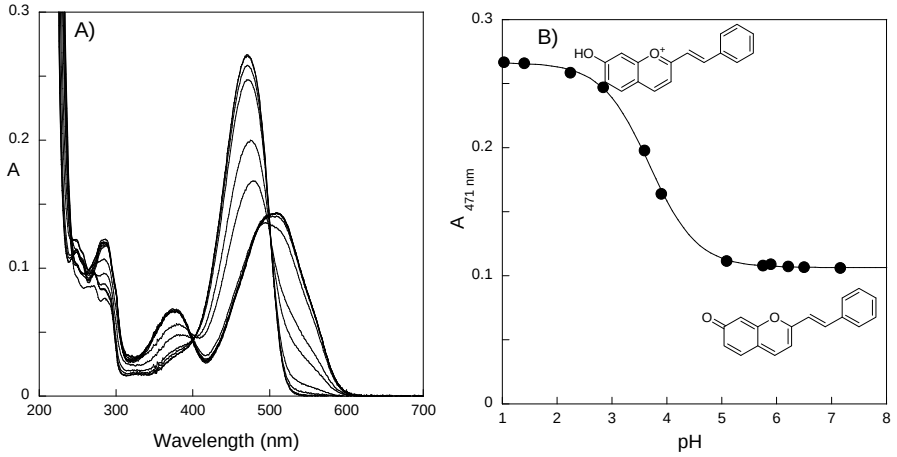

Figure 3.2 – A) Spectra run immediately after a pH jump from a 2.5×10^{-5} M solution at pH = 1 to 1.03, 1.4, 2.24, 2.84, 3.59, 3.9, 5.09, 5.75, 5.89, 6.21, 6.5 and 7.16. B) Changes in absorption at 471 nm, fitted with a $pK_a = 3.7 \pm 0.1$.

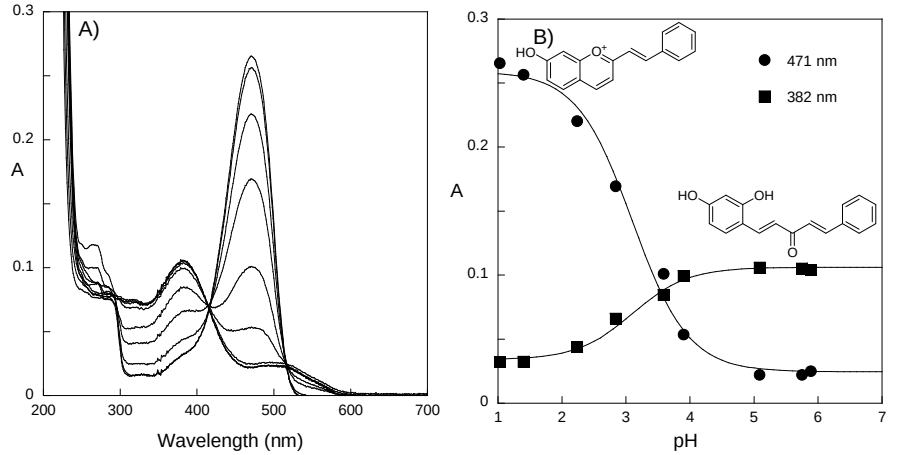

Figure 3.3 – A) Thermal equilibrated solutions in the dark upon a pH jump from 1 to 1.03, 1.4, 2.24 2.84, 3.59, 3.9, 5.09, 5.75 and 5.89. B) Changes in absorption at 471 (●) and 382 nm (■) simultaneously fitted with a $pK'_a = 3.1 \pm 0.1$.

In order to study the kinetic properties of the system, pH jumps from 1 to more basic pH values were performed and followed by UV-Vis absorption spectroscopy. In Figure 3.4, the example of a pH jump to 4.53 is presented. It is possible to distinguish that immediately after adding the base, the quinoidal base, **A**, is formed and then converted into the *trans*-chalcone, **Ct**. It is worth of note that **A** only communicates with the rest of the system through $\mathbf{AH}^+$.[9] It was seen previously that the kinetics of the system is given by equation 1.45 (see Supplementary Material, section 9.1.1).

$$k_{obs} = \frac{\dfrac{\left[H^+\right]}{\left[H^+\right]+K_a} k_i K_t K_h + k_{-i}\left[H^+\right]}{\left[H^+\right]+\dfrac{k_i K_t}{k_{-h}}} \tag{1.45}$$

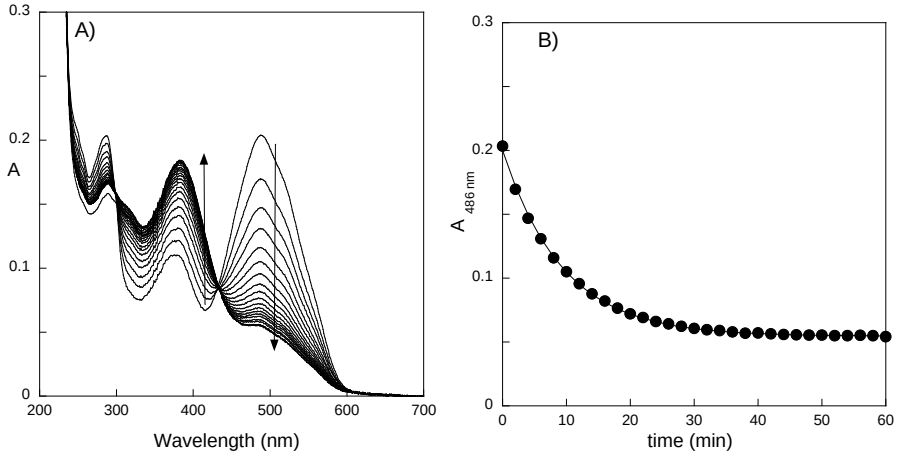

Figure 3.4 – A) Spectral evolution after a pH jump from pH = 1 to 4.53 followed every 2 min. The pH jump was performed as previously mentioned. B) Fitting of the decay of absorption at 486 nm was achieved with $k_{obs} = 1.8 \times 10^{-3}$ s^{-1}.

Figure 3.5 reports the best fitting of the k_{obs} values determined upon pH jumps versus pH, together with the fitting obtained for the constants reported in the literature for 7-hydroxyflavylium (**HF**)[10] for comparison purposes. From Figure 3.5, it is clearly seen that the behavior of **HF** and **HS** is very similar, although the rates observed are *ca* 5-fold higher for the flavylium ion.

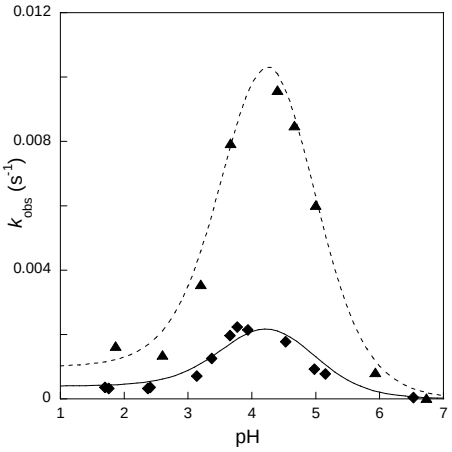

Figure 3.5 – Observed rate constants versus pH for **HS** (this work ♦) and (▲) for HF.[10] Fitting of experimental data with eq. 1.45 was achieved with constants reported in Table 3.2.

Concerning the photochemistry of the system, it was observed that an equilibrated solution at pH = 3.95 essentially suffers no changes when irradiated in a solar lamp for 30 min. At pH = 5.75, there seems to be a degradative photochemical process, because the observed final state does not recover after several days; moreover, when the irradiated solutions are acidified only a very small percentage of flavylium is recovered.

In basic media, ionized *trans*-chalcones can be obtained. Starting from an equilibrated solution at pH = 12 and titrating back to acid, the successive protonations of the $\mathbf{Ct^{n-}}$ species can be achieved. By inspection of Figure 3.6 and the simultaneous fitting of absorptions at 509 nm

(main absorbing species $\mathbf{Ct^{2-}}$) and 382 nm (**Ct**), pK_{Ct1} = 7.7 ± 0.1 and pK_{Ct2} = 9.3 ± 0.1 were obtained.

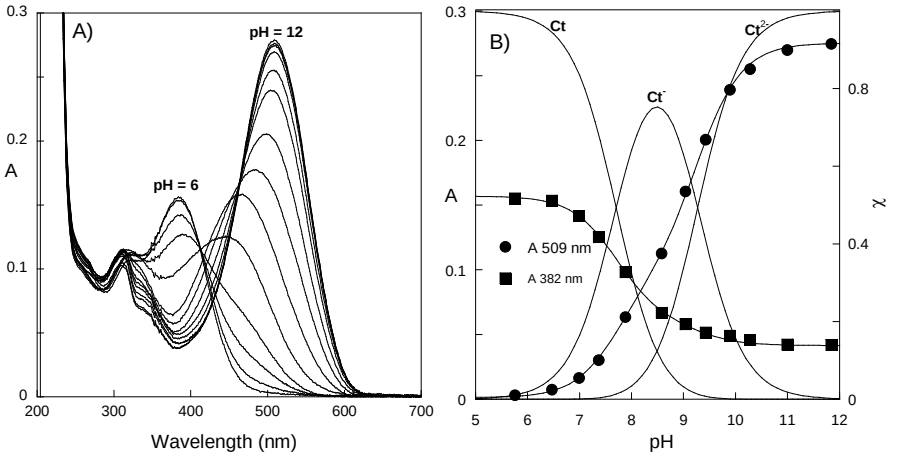

Figure 3.6 –A) Spectrophotometric titration of the trans-chalcones of **HS**; pH values 12.4, 12.19, 11.84, 11.00, 10.28, 9.89, 9.43, 9.04, 8.58, 7.88, 7.37, 6.99, 6.47 and 5.76. B) Changes in absorption at 509 and 382 nm, simultaneously fitted with pK_{Ct1} = 7.7 ± 0.1 and pK_{Ct2} = 9.3 ± 0.1

The results obtained for this compound, as well as for **DHS** and **DAS**, which will be presented in the next subsections, are summarized in Tables 3.1 and 3.2. For purposes of easy comparison, data for the corresponding flavylium compounds are also shown. In conclusion, the absorption maximum of the flavylium ion changes *ca*. 35 nm to higher wavelengths upon introduction of the double bond. On the other hand, the pK'_a value is 0.4 units higher for the styryl derivative, showing that the effective color loss is only slightly shifted to higher pH values. The benzopyrylium core is more stable towards hydration in **HS** than in **HF** as evidenced by k_h (Table 3.2 and Figure 3.5). There is no evidence for the existence of an extra isomerization and the usual reaction network for the flavylium ion could be applied to 7-hydroxy-2-styryl-1-benzopyrylium, with no restrictions. Although the values found for the kinetic constants are always higher for the flavylium compound, it is not yet understood why the styryl derivative presents no photochemistry in water, which is going to be discussed on section 3.5.

Table 3.1 –Thermodynamic constants obtained in aqueous solutions at 298 K for **HF**, **DHF**, **DAF**, **HS** and **DHS** (constants for **DAS** were obtained in 29 % acetonitrile).

	pK'_a	pK_{a+}	pK_a	pK_{a2}	%A	pK_{Ct+}	pK_{Ct1}	pK_{Ct2}	$K_hK_tK_i$ (M)
HS	3.1 ± 0.1	-	3.7 ± 0.1	-	24 ± 5	-	7.7 ± 0.1	9.3 ± 0.1	(6 ± 1) × 10^{-4}
HF[10]	2.7	-	3.6	-	14	-	N/A	N/A	1.71 × 10^{-3}
DHS	3.4 ± 0.1	-	4.1 ± 0.1	8.1 ± 0.1	20 ± 4	-	7.9 ± 0.1	9.4 ± 0.1	(3.2 ± 0.8) × 10^{-4}
DHF[11]	3.1	-	4.0	8.0	13	-	8.1	10.2	6.91 × 10^{-4}
DAS	4.0 ± 0.1	0.7 ± 0.1	5.1 ± 0.1	-	8.0 ± 2	2.9 ± 0.2	8.6 ± 0.1	10.4 ± 0.1	(9 ± 2) × 10^{-5}
DAF[12]	4.4 ± 0.1	-0.2 ± 0.2	5.4 ± 0.2	-	8.0 ± 2	2.3 ± 0.2	8.1 ± 0.1	9.6 ± 0.1	(5 ± 1) × 10^{-5}

Table 3.2 – Kinetic constants obtained in aqueous solutions at 298 K for **HF**, **DHF**, **DAF**, **HS** and **DHS** (constants for **DAS** were obtained in 29 % acetonitrile)

	$K_hK_tk_i$ (M.s^{-1})	K_tk_i/k_{-h}(M)	k_{-i} (s^{-1})	k_h (s^{-1})	k_{-i+} (s^{-1})	$k_{i+}K_{t'}/k_{-h+}$ (M)
HS	$(6 \pm 1) \times 10^{-7}$	$(1.5 \pm 0.3) \times 10^{-5}$	$(4 \pm 1) \times 10^{-4}$	0.04 ± 0.01	-	-
HF[10]	3.1×10^{-6}	1.5×10^{-5}	1.0×10^{-3}	0.21	-	-
DHS	$(2.9 \pm 0.5) \times 10^{-7}$	$(6 \pm 1) \times 10^{-5}$	$(1.5 \pm 0.4) \times 10^{-4}$	$(5 \pm 1) \times 10^{-3}$	-	-
DHF[11]	3.8×10^{-7}	2.1×10^{-5}	1.8×10^{-4}	0.02	-	-
DAS	$(1.0 \pm 0.4) \times 10^{-7}$	$(1.0 \pm 0.4) \times 10^{-3}$	$(1.0 \pm 0.4) \times 10^{-5}$	$(1.0 \pm 0.5) \times 10^{-4}$	$(4.0 \pm 0.8) \times 10^{-3}$	1.0 ± 0.2
DAF[12]	$(1.0 \pm 0.4) \times 10^{-7}$	$(1.0 \pm 0.4) \times 10^{-3}$	$(5 \pm 2) \times 10^{-4}$	$(1.0 \pm 0.5) \times 10^{-4}$	$(5 \pm 1) \times 10^{-3}$	0.25 ± 0.05

3.3.3 7-Hydroxy-2-(4-hydroxystyryl)-1-benzopyrylium chloride (DHS)

In the case of the dihydroxy derivative, essentially the same results described above were found. In Figure 3.7, the titration after immediate pH jumps, leading to the formation of **A** and in this case also $\mathbf{A}^-$, is shown, as well as the situation in equilibrium and the protonation steps for the *trans*-chalcones. The maximum absorption of **DHS** occurs at 510 nm (ε_{max} = 32000 cm^{-1}M^{-1}), which is ~51 nm red shifted when compared with **DHF** (7,4'-dihydroxyflavylium) analogue.[11] Taking into account that the absorption bands should be assigned to π–π* transitions (with charge transfer character), the relatively large red shift observed can, once again, be attributed to the extended conjugation of the π system brought by the introduction of one more conjugated double bond.[13] When a pH jump on the $\mathbf{AH}^+$ species is carried out to moderately acidic and basic pH values the spectra obtained immediately after are those of the quinoidal bases **A** (λ_{max} = 515 nm, ε_{max} = 19500 cm^{-1}M^{-1}) and $\mathbf{A}^-$ (λ_{max} = 505 nm, ε_{max} = 30000 cm^{-1}M^{-1}), also red shifted relatively to the **DHF** corresponding species (495 nm and 535 nm, respectively[11]).

In Figure 3.8, the rate constants of the pH jumps versus pH are shown in comparison with those of **DHF**. As can be seen from Tables 3.1 and 3.2, which summarize the results obtained, the values of pK_a for the conversion of **DHS** into the quinoidal base and ionized quinoidal base are 4.1 ± 0.1 and 8.1 ± 0.1, which compare with 4.0 and 8.0 in the case of the analogue **DHF**. In terms of kinetic data, once more, the rate constants present the same trend but are slightly lower than in the case of **DHF**.

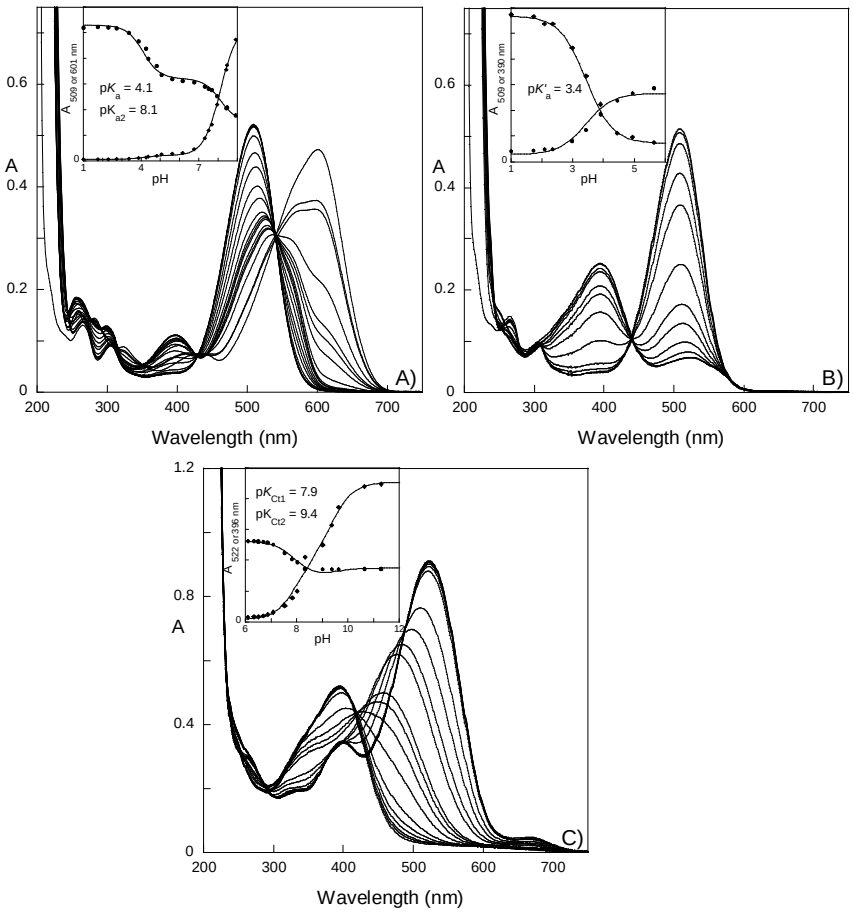

Figure 3.7 – A) Immediate titration upon a pH jump from a stock solution of **DHS** 1.6×10^{-5} M at pH =1.0 to basic pH values, inset, fitting of the absorptions at 509(●) and 601 nm (♦) with pK_a = 4.1 ± 0.1 and pK_{a2} = 8.1 ± 0.1.B) The same as A but upon equilibrium, inset, fitting of the absorptions at 509 (♦) and 390 nm (●) with pK'_a = 3.4 ± 0.1. C) Protonation steps of the *trans*-chalcones, inset, fitting of the absorptions at 396 (●) and 522 nm (♦) with pK_{Ct1} = 7.9 ± 0.1 and pK_{Ct2} = 9.4 ± 0.1.

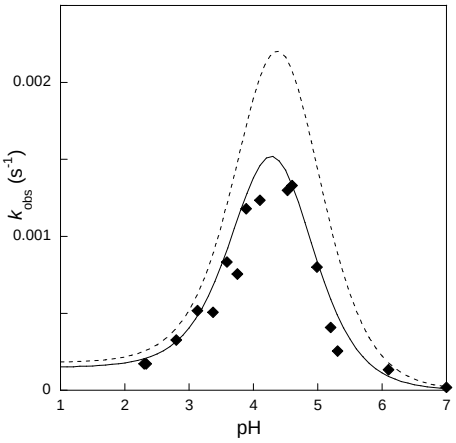

Figure 3.8 – Observed rate constants versus pH for **DHS** (this work ♦) and for **DHF** (traced line).[11] Fitting of experimental data with eq. 1.45 was achieved with constants reported in Table 3.2.

3.3.4 7-Hydroxy-2-(4-dimethylaminostyryl)-1-benzopyrylium chloride (DAS)

In the case of amino substituted flavylium ions, because of the presence of the nitrogen atom that can protonate, two more equilibria must be considered: the formation of $\mathbf{AH_2^{2+}}$ and of $\mathbf{CtH^+}$. In Figure 3.9, the titration obtained upon pH jumps from a mother solution at pH 1 to either lower and higher pH values shows the presence of three species: $\mathbf{AH_2^{2+}}$ (λ_{max} = 464 nm, ε_{max} = 22600 $cm^{-1}\,M^{-1}$, $\mathbf{AH^+}$ (λ_{max} = 639 nm, ε_{max} = 47800 $cm^{-1}\,M^{-1}$), and **A** (λ_{max} = 616 nm, ε_{max} = 28200 $cm^{-1}\,M^{-1}$). In equilibrium, the species present are $\mathbf{AH_2^{2+}}$ (not shown in spectra), $\mathbf{AH^+}$ and **Ct**. Finally, at basic pH values the ionized **Ct** species are once again the thermodynamically stable species. In this case, similarly to what occurs for the flavylium analogues,[14] if an equilibrated solution of $\mathbf{Ct^{2-}}$ is acidified to a relatively acidic pH value, the immediate formation of $\mathbf{CtH^+}$ (spectrum not shown) is observed, which converts to the thermodynamically stable species $\mathbf{AH^+}$. Because the **Ct** of **DAS** is rather insoluble in water, all measurements were carried out in the presence of 29% acetonitrile.

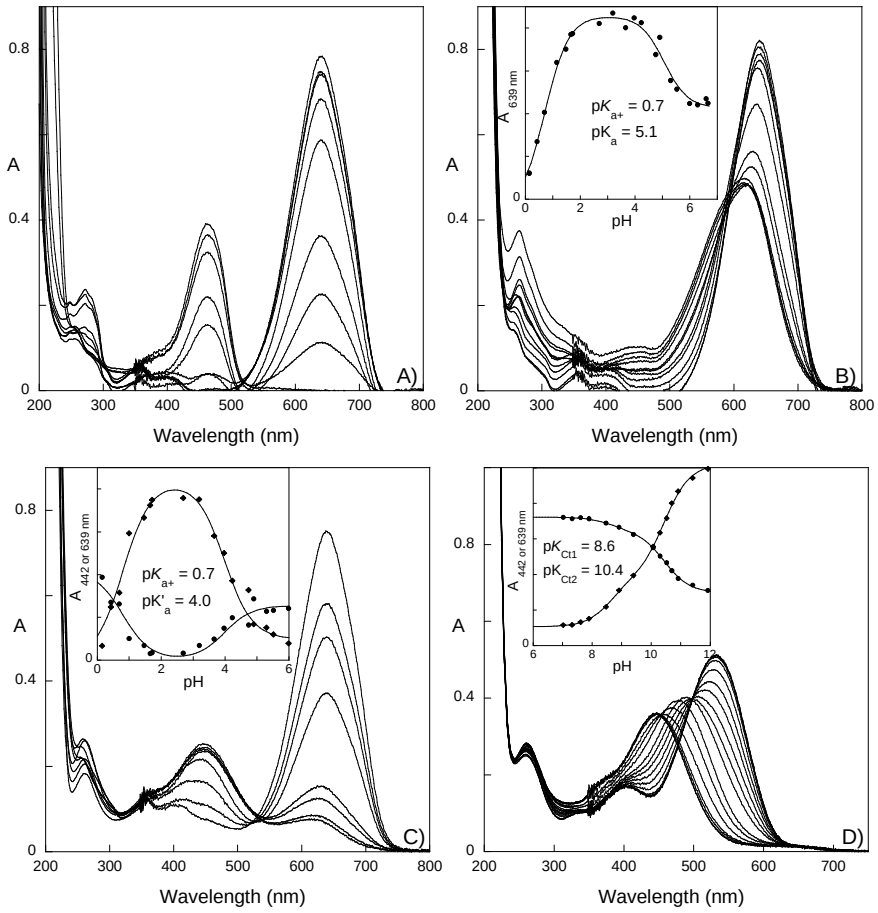

Figure 3.9 – Spectrophotometric titration upon pH jumps from a stock solution of **DAS** at pH = 1.0 to acidic pH values or basic pH values; final [**DAS**] = 1.7×10^{-5} M 1. A) From pH 0 to pH 3. B) From pH 3 to pH 7, inset, fitting of the absorption at 639 nm with pK_{a+} = 0.7 ± 0.1 and pK_a = 5.1 ± 0.1. C) The same as B but upon equilibrium, inset, fitting of the absorptions at 442 (●) and 639 nm (♦) with pK_{a+} = 0.7 ± 0.1 and pK_a = 4.0 ± 0.1 C) Spectrophotometric titration of $\mathbf{Ct^{2-}}$, inset, fitting of the absorptions at 422 (●) and 533 nm (♦) with pK_{Ct1} = 8.6 ± 0.1 and pK_{Ct2} = 10.4 ± 0.1.

To take into account the process in which $\mathbf{AH^+}$ is formed from $\mathbf{CtH^+}$, as explained before, equation 2.14 must be used.[14]

$$k_{obs} = \frac{\frac{[H^+]}{[H^+]+K_a} k_i K_t K_h + k_{-i}[H^+]}{[H^+]+\frac{k_i K_t}{k_{-h}}} + \frac{\frac{[H^+]}{[H^+]+K_{Ct+}} k_{-i+}[H^+]}{[H^+]+\frac{k_{i+} K_t'}{k_{-h+}}} \quad (2.14)$$

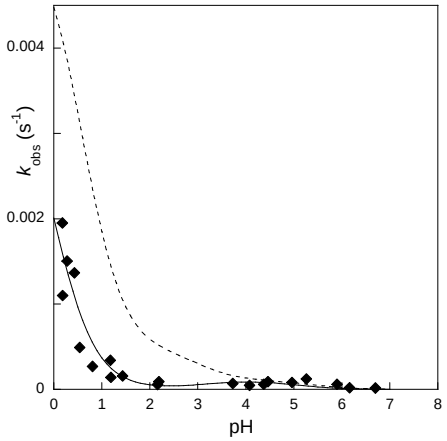

Figure 3.10 – Observed rate constants versus pH for **DAS** (this work ♦) and for **DAF** (traced line).[12] Fitting of experimental data with eq. 2.14 was achieved with constants reported in Table 3.2.

Due to the fact that there are many parameters to be adjusted, there is some uncertainty in the values obtained, particularly $K_h K_t k_i$, $K_t k_i / k_{-h}$, k_{-i} and k_h that are calculated through these adjusted parameters. Nevertheless, as shown in Figure 3.10, once again the rate constants obtained for 2-styryl-1-benzopyrylium are lower than those of its flavylium counterpart; 4'-dimethylamino-7-hydroxyflavylium, **DAF** (see Supplementary Material, section 9.4). The summary of the results obtained for **DAS** in comparison with **DAF** are shown in Tables 3.1 and 3.2. The values of pK'_a obtained for the two compounds are hardly comparable, since acetonitrile is expected to stabilize the neutral form and so lower the pK'_a value. However, the pK_{a+} of the styryl is significantly higher than in the case of the corresponding flavylium (- 0.2 in water), which is comprehensible on the basis of a longer charge separation in the species $\mathbf{AH_2^{2+}}$ of **DAS**, and consequent smaller repulsion between positive charges.

3.3.5 Comments on the water networks

In Table 3.3, the most relevant parameters related to color loss are listed for **HS**, **DHS** and **DAS**. The pK'_a is related to the thermodynamic stability of $\mathbf{AH^+}$ (strongly colored) *versus* **Ct** (colorless or pale yellow) and eventually a low percentage of **A** (colored). The value of k_h accounts for the rate of hydration to form the colorless **B**, initiating the color loss process. Except for **DAS**, the values of pK'_a are slightly higher and the hydration rates are lower for 2-styryl-1-benzopyrylium than for their flavylium analogues. Taking into account that the studies for **DAS** were performed in a mixture containing approximately 30% of acetonitrile (due

to insolubility), which is a more apolar solvent that stabilizes neutral forms such as **Ct**, **B** and **A**, the pK'_a could also be higher for **DAS** in water when compared to that of its flavylium counterpart.

Table 3.3 – pK'_a and k_h (s^{-1}) obtained in aqueous solutions at 298 K for **HF**, **DHF** , **DAF**, **HS** and **DHS** (constants for **DAS** were obtained in 29 % acetonitrile)

	pK'_a	k_h (s^{-1})
HS	3.1 ± 0.1	0.04 ± 0.01
HF[10]	2.7	0.21
DHS	3.4 ± 0.1	$(5 \pm 1) \times 10^{-3}$
DHF[11]	3.1	0.02
DAS	4.0 ± 0.1	$(1.0 \pm 0.5) \times 10^{-4}$
DAF[12]	4.4 ± 0.1	$(1.0 \pm 0.5) \times 10^{-4}$

3.4 Efficient photochromism in the presence of CTAB micelles

No photochemistry or very poor photochemistry was detected in water either for **HS**, **DHS**, contrary to what happens for **HF** and **DHF**. Both **DAS** and **DAF** are, practically speaking, photochemically inert. However, once again efficient photochromic systems could be obtained in CTAB micelles.

Similarly to the behavior of the flavylium analogues, the **Ct** species is stabilized in the presence of CTAB micelles, and by consequence, it is possible to have a solution of **Ct** at pH = 1.4 without $\mathbf{AH^+}$. Irradiation of **DHS** in the presence of CTAB micelles ([CTAB] = 0.2 M) gives rise to the formation of an intense red color, as shown in Figure 3.11. The process occurs with a quantum yield of $\Phi = 0.07$ at $\lambda_{irr} = 436$ nm, and the system reverts back to the initial state with a rate constant of 7.9×10^{-4} s^{-1} at pH = 1.44 and 295 K.

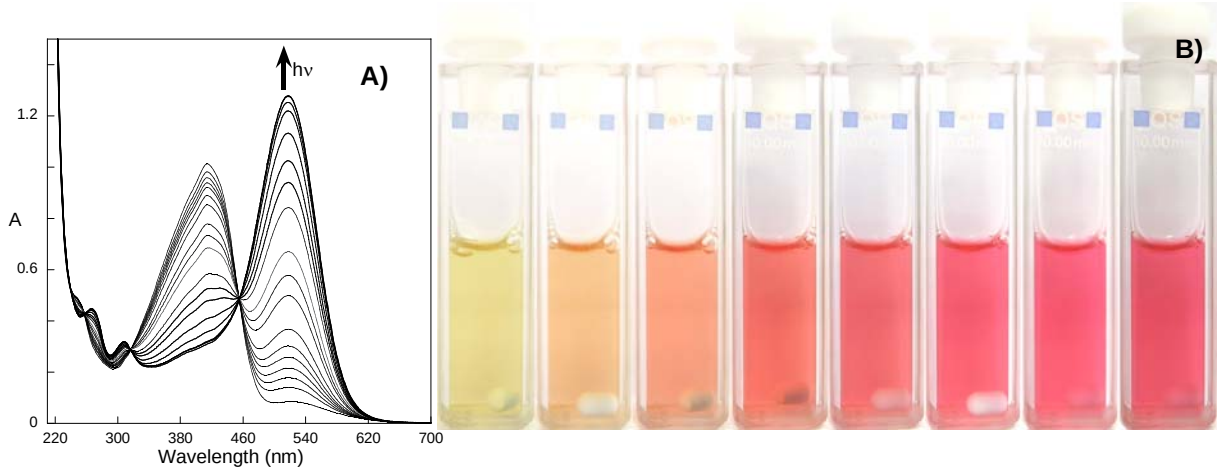

Figure 3.11 –A) Spectral changes occurring upon irradiation of **DHS** (4.95×10^{-5} M) in the presence of CTAB micelles (0.2 M) at pH = 1.44 for the following irradiation times: 0, 0.25, 0.5, 0.75, 1, 1.5, 2, 3, 4, 5, 7, 9, 11, 15, 20, 30, and 40 min ($I_0 = 2.8 \times 10^{-7}$ einstein.min^{-1} at λ_{irr} =436 nm). B) Color of the solutions at 0, 1, 3, 7, 11, 20, 30 and 40 min of irradiation

While **DAF** is pink (λ_{max} = 540 nm in water), **DAS** is blue (λ_{max} = 639 nm in water/acetonitrile 71/29), which allows the exploitation of a strong color contrast upon irradiation, see Figure 3.12. Although the quantum yields are low (Φ = 0.02 at 436 nm, pH = 1.9, 0.2 M CTAB; $I_0 = 2.8 \times 10^{-7}$ einstein.min^{-1}), this is, to our knowledge, the first time in which a photochromic system based on derivatives of natural anthocyanins is reported that shows such a deep change in λ_{max} upon irradiation. Furthermore, the change of color is relatively fast upon direct solar irradiation and it reverts to its initial state in the dark with a rate constant 1.0×10^{-4} s^{-1}.

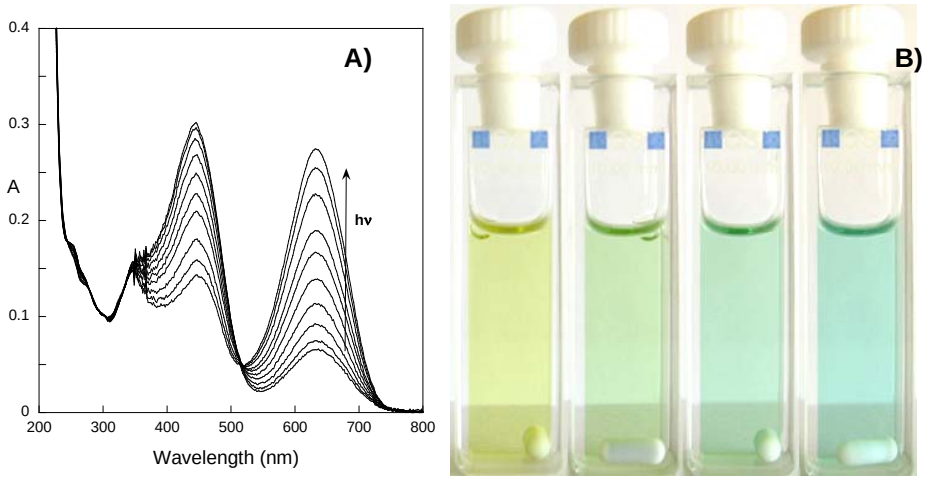

Figure 3.12 –A) Irradiation of an equilibrated solution of **DAS** (**Ct**) at pH 1.9 in 0.2 M CTAB ($I_0 = 2.8 \times 10^{-7}$ einstein.min^{-1} at λ_{irr} =436 nm, Φ = 0.02), t = 0, 1, 3, 6, 10, 15, 20, 30, 40 and 50 min. B) Observed color at irradiation times t = 0, 15, 30 and 50 min.

3.5 Photochemistry of 7-Hydroxy-2-(4-hydroxystyryl)-1-benzopyrylium and related compounds

The very poor of photochemistry in water for **DHS** in contrast to **DHF** was the striking result that prompted into a deeper investigation of the photochemistry of these compounds. The influence of CTAB micelles was also studied. Model chalcone compounds lacking the 2-hydroxyl group had to be synthesized and studied as model compounds. The role of chemical reactions in the triplet excited state was studied by laser flash photolysis in order to investigate the photochemical pathway that leads to the photochromic effect.

3.5.1 Chalcones lacking a hydroxyl group in position 2

In order to clarify the photochemical studies, chalcones **31** and **32** were synthesized, Scheme 3.3. The advantage of these model compounds is the possibility of working at acidic pH values without the formation of the network reported in Scheme 3.1. This strategy was crucial to the comprehension of the transient absorptions of the 2-hydroxychalcone systems, as will be explained below.

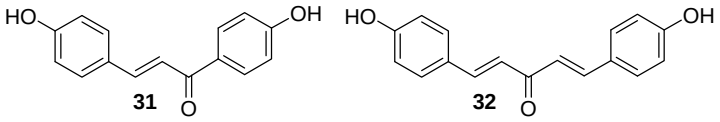

Scheme 3.3 – Structure of model chalcones.

The UV-Vis absorption titration of **31** (Figure 3.13) is compatible with the existence of two acid/base equilibria with pK_a values of 7.9 and 9.0. Identical pK_a values were obtained by means of fluorescence emission titration (Figure 3.14) excluding the existence of ESPT (excited-state proton transfer) in the framework of the Weller theory.[15] However, the much lower emission intensity of the $\mathbf{Ct}^-$ species in comparison with **Ct** and $\mathbf{Ct}^{2-}$, suggests the possibility of a singlet excited-state deactivation channel of this species by formation of a tautomer mediated by water, as shown in Scheme 3.4.

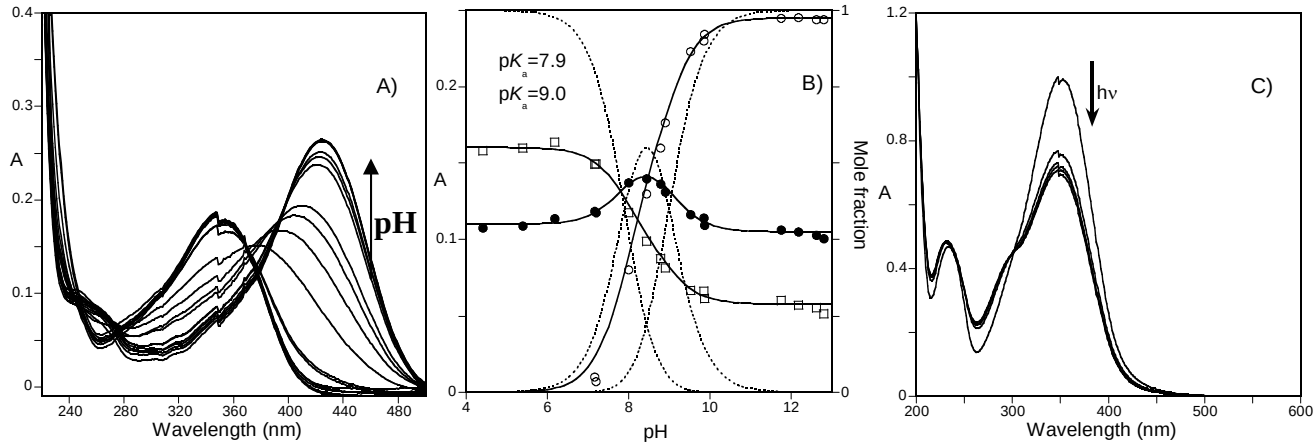

Figure 3.13 – A) Absorption of compound **31** as a function of pH. B) Mole fractions of **Ct**, $\mathbf{Ct}^-$ and $\mathbf{Ct}^{2-}$ as a function of pH and fitting of absorptions with pK_as 7.9 and 9.0. C) Irradiation of the **Ct** species (pH=6.1).

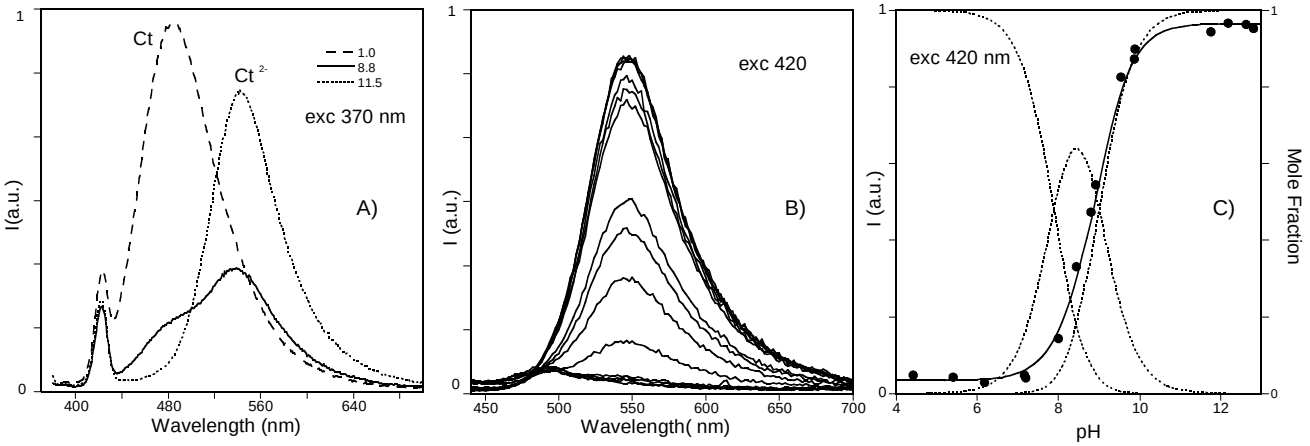

Figure 3.14 – Emission from compound **31** as a function of pH, A) exciting at 370 nm, B) exciting at 420 nm. C) Fitting of the emission at 550 nm as a function of pH, with pK_as 7.9 and 9.0.

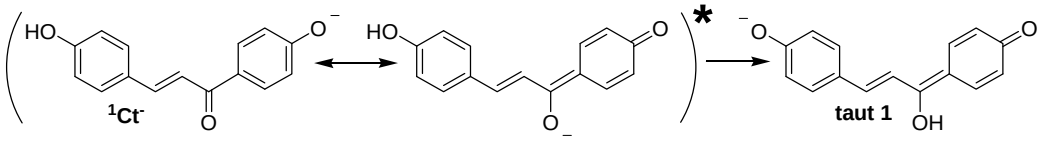

Scheme 3.4 – Tautomerization of **Ct**$^-$.

Irradiation of compound **31** was carried out at pH = 1.2 and 6.1 at the excitation wavelength of 365 nm, and the qualitative behavior is similar at both pH values, Figure 3.13 C. During the first seconds of the reaction, the *trans* species is consumed, and a steady state is reached, by formation of the *cis*-chalcone due to a photoisomerization reaction. The formation of this species was identified by NMR (experiments not shown). However, for longer irradiations times, subsequent spectral variations take place, leading to different species. We did not investigate in detail the second photoproduct.

In Figure 3.15, the results from the nanosecond flash photolysis of the nonionized compound **31** are presented. Immediately after the flash, a bleaching of the **Ct** species can be observed together with the formation of an absorption band extended into the visible. This absorption cannot be attributed to the *cis*-chalcone (**Cc**) because this species does not absorb at these wavelengths, as shown from the irradiation experiments (Figure 3.13 C). An alternative would be the formation of ionized chalcones, **Ct**$^-$ or **Ct**$^{2-}$, by successive deprotonation of the singlet excited state. ESPT was excluded above on the basis of the coincidence of the fluorescence emission titration curves with those obtained from the absorption spectra (Figures 3.13 and 3.14). Moreover, such ionized species do not have absorption features at wavelengths above 480 nm (**Ct**$^{2-}$ peaks at 435 nm and **Ct**$^-$ peaks at around 400 nm, while the transient absorption spectra peaks at around 500 nm). On this basis, the most reliable alternative is the attribution of the transient absorption to the triplet state, in agreement with the transient absorptions reported by Norikane[16] and Givens and Wirz[17] for analogous *p*-hydroxyacetophenones. The decay constants of the transient absorptions are affected by molecular oxygen, as expected for a triplet state, but the effect is not the same through all of the wavelengths because the shapes of the curves in Figure 3.14 A and B, respectively, in the absence and presence of oxygen are not identical, as would be expected for a quenching occurring in a single species, suggesting the existence of two species.

The existence of two different transient absorptions is clearly confirmed from the data at acidic pH values, one experiment that is only possible in chalcones lacking the hydroxyl in position 2. At pH = 1.2, the transient absorption is more intense, and the shape of the curve is compatible with the formation of a single absorption band and single exponential kinetics; Figure 3.15 C (and Figure 3.16). A global analysis of the decays was carried out according to the following expression:

$$\Delta A_\lambda = a_{1\lambda} e^{-t/\tau_1} + a_{2\lambda} e^{-t/\tau_2} + a_{3\lambda} \qquad (3.3)$$

where ΔA_λ refers to the measured change in absorbance at wavelength λ, τ_1 and τ_2 are the lifetimes of the two detected processes, $a_{1\lambda}$ and $a_{2\lambda}$ are the respective amplitudes, and $a_{3\lambda}$ is the residual amplitude after the two processes had finished. At pH = 6.1 (air-equilibrated), the experimental data could be fitted with τ_1 = 0.38 μs (open circles) and τ_2 =1.5 μs (black circles) with components represented in Figure 3.16 A; the same experiment carried out in argon saturated solutions leads to similar spectral variations with lifetimes of τ_1 = 0.35 μs and τ_2 = 6 μs. At pH = 1.2, only one process is observed with a lifetime of 0.74 μs, see Figure 3.16 B.

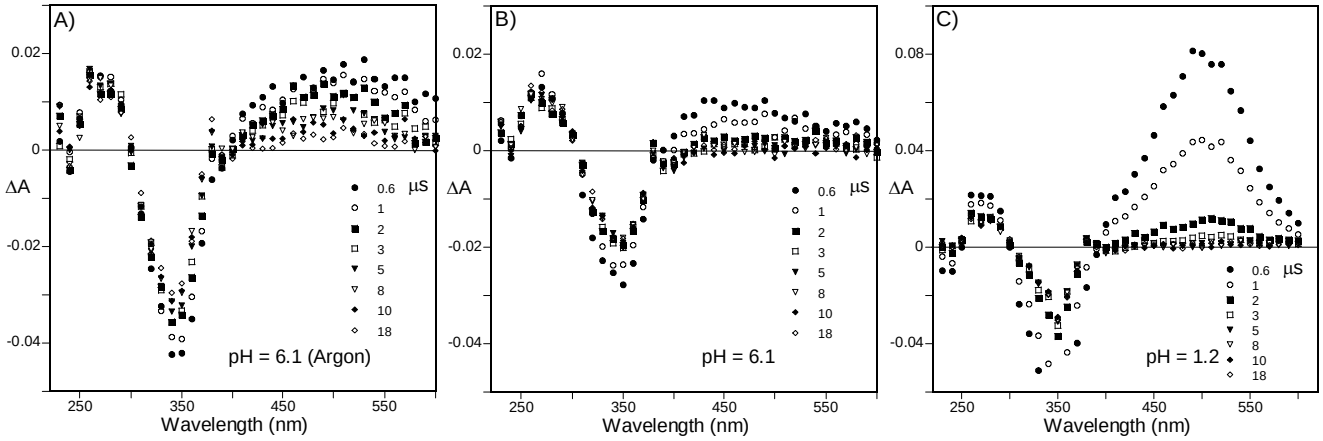

Figure 3.15 – Transient absorption spectra of compound **31** in a mixture of water (90%) and ethanol (10%). Time indicates the delay after the laser pulse. A) pH = 6.1, solution saturated with argon. B) pH = 6.1, air-equilibrated solution. C) pH = 1.2, air-equilibrated solution.

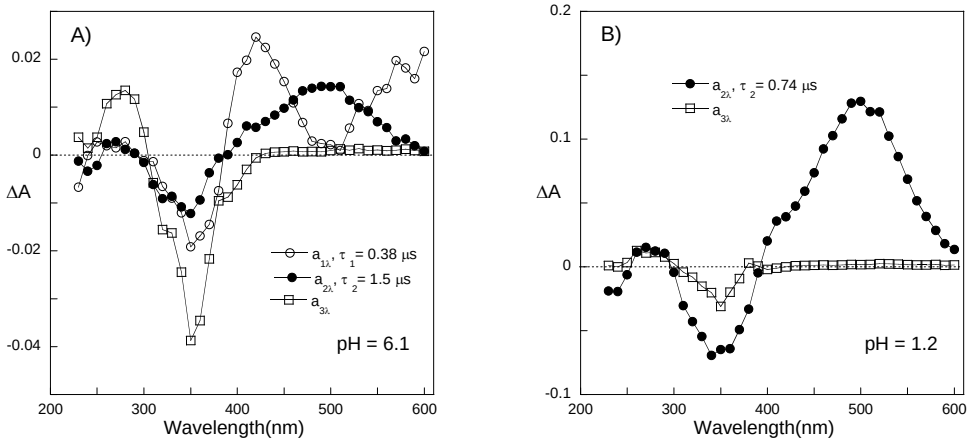

Figure 3.16 –Pre-exponential factors calculated from global analysis of the decays obtained for compound **31** in a mixture of water (90%) and ethanol (10%) at pH = 6.1 A) and 1.2 B) in air-equilibrated solutions (○, $a_{1\lambda}$; ●, $a_{2\lambda}$; □, $a_{3\lambda}$ - corresponding lifetimes according to labels in graphics).

An explanation for this behavior can be found in Scheme 3.5, in partial agreement with previous results reported by Wirz for a related compound (p-hydroxyacetophenone)[17] and by Phillips.[18] Excited-state proton transfer in the triplet state would occur at pH = 6.1, leading to the formation of ionized species ^{3}**Ct**$^-$ in equilibrium with ^{3}**Ct**. As pointed out by Wirz, such process would be fast since the deprotonation rate constant should be greater than 3×10^7 s^{-1} and, therefore, difficult to detect in our laser flash photolysis experimental setup due to

fluorescence interferences. However, it was possible to observe a process with a lifetime of 31 ns that we could tentatively assign to the formation of ^{3}**Ct**$^-$ (not shown).

The pre-exponential factors at pH = 6.1 (open circles for the 0.38 μs process) define a valley at around 500 nm, with a shape roughly symmetric to the absorption of transient corresponding to 1.5 μs process (black circles). This suggests a sequential process where ^{3}**Ct**$^-$ evolves to a tautomeric species (^{3}**Taut$_2$**) responsible for the absorption of the second transient. On the other hand, this last transient is the only transient absorption at pH = 1.2. In this case, the tautomer would be directly formed from ^{3}**Ct** by acidic catalysis, Scheme 3.5. The back processes in the ground state might be too fast to be observed, as pointed out in the literature.[18]

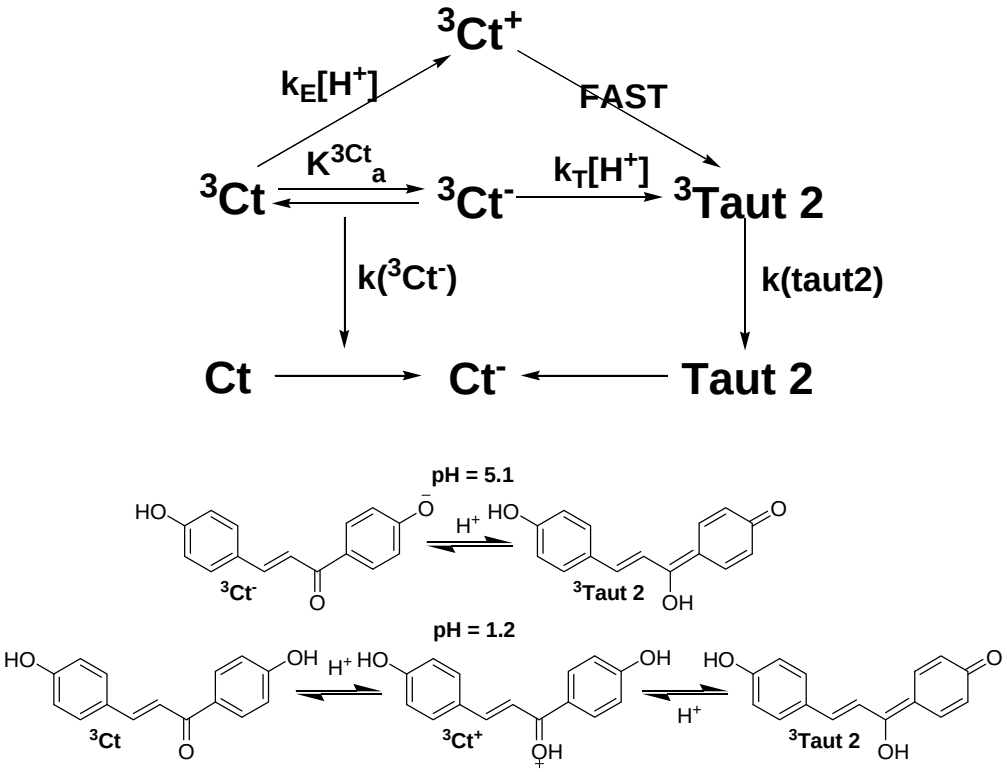

Scheme 3.5 – Excited state deactivations.

Taking the kinetic model of Scheme 3.5, it is possible to obtain the following expressions for the amplitudes of equation 3.3 (Supplementary Material, section 9.5)

$$a_{1\lambda} = \left(\left[{}^3Ct\right] + \left[{}^3Ct^-\right]\right)_{t=0}\left(\Delta\varepsilon_{{}^3Ct\lambda}\frac{\left[H^+\right]}{\left[H^+\right]+K_a^{{}^3Ct}} + \Delta\varepsilon_{{}^3Ct^-\lambda}\frac{K_a^{{}^3Ct}}{\left[H^+\right]+K_a^{{}^3Ct}} - \Delta\varepsilon_{{}^3Taut2\lambda}\alpha\right) \qquad (3.4)$$

$$a_{2\lambda} = \left(\left[{}^3Ct\right] + \left[{}^3Ct^-\right]\right)_{t=0}\Delta\varepsilon_{{}^3Taut2\lambda}\alpha \qquad (3.5)$$

in which $\left(\left[{}^3Ct\right]+\left[{}^3Ct^-\right]\right)_{t=0}$ is the amount of triplet **Ct** species formed from intersystem crossing from the singlet excited state, and:

$$\alpha = \frac{\left[H^+\right]^2 + \frac{k_T K_a^{\,{}^3Ct}}{k_E}\left[H^+\right]}{\left[H^+\right]^2 + \left(\frac{k_T K_a^{\,{}^3Ct}}{k_E} - \frac{k(taut2)}{k_E}\right)\left[H^+\right] + \frac{K_a^{\,{}^3Ct}}{k_E}\left(k\left({}^3Ct^-\right) - k(taut2)\right)} \tag{3.6}$$

The amount of **^{3}Taut2** formed is therefore proportional to the ratio α. Such a ratio would be pH-dependent, increasing with [H$^+$] for high pH but reaching unity for low pH. At very low pH, a sequential step is not required since the reaction proceeds directly from **^{3}Ct** to **^{3}Taut2**. It is worth taking into account that this scheme ignores **^{3}Ct^{2-}**, which might be a too strong assumption for higher pH. The formation of such species could also give rise to **Taut1** via a protonation reaction. However, no strong evidence for the presence of these compounds is available with the current experimental data.

In the case of compound **32**, both absorption and emission are significantly red-shifted in comparison with compound **31**, but in general follow the same trend, Figure 3.17. The pH-dependent absorption and fluorescence emission spectra can be accounted for by considering two acid-base equilibria with pK_as of 8.3 and 8.8. As in the previous compound **31**, the contribution of the **Ct$^-$** form to the emission is smaller than that in the other forms. It is worth noting that in compound **32**, the acidic constants are much closer than those in compound **31**, a behavior explained by the symmetry observed in the former, where the two hydroxyls are identical and more distant from each other.

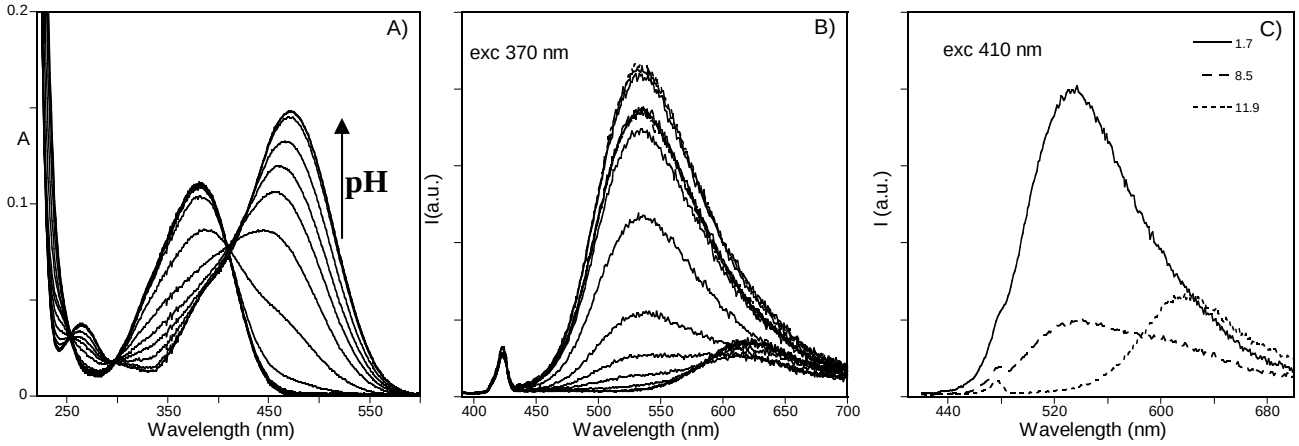

Figure 3.17 – Absorption spectra A), fluorescence emission at λ_{exc} = 370 nm B) and λ_{exc} = 410 nm C) of compound **32** as a function of pH. Global fitting was achieved for pK_a 8.3 and 8.8.

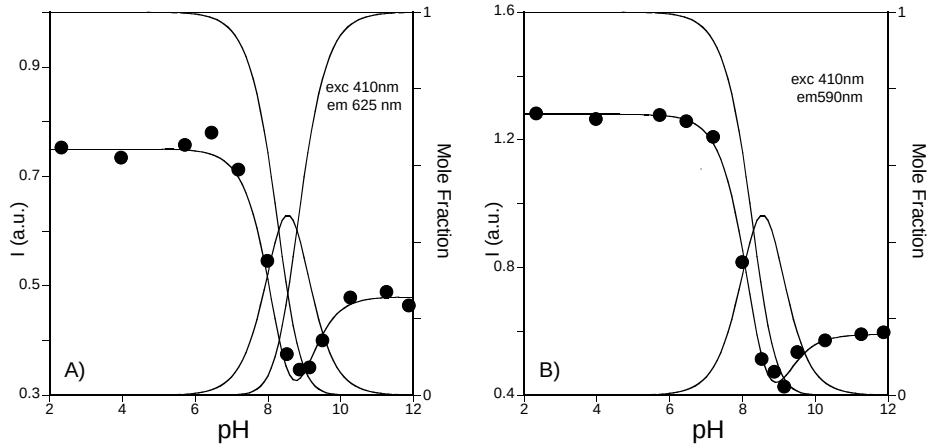

Figure 3.18 – Fitting of the fluorescence emission at λ_{em} = 625 nm A) and λ_{em} = 590 nm B) of compound **32** as a function of pH. Global fitting was achieved for pK_a 8.3 and 8.8.

The transient absorption of compound **32** in Figure 3.19 is also similar to the one reported for compound **31** in Figure 3.15, with τ_1 = 0.37 μs and τ_2 = 1.0 μs at pH = 4.8 and τ = 1.0 μs at pH = 1.2 – Figure 3.19. In Figure 3.20 the comparison between a mono-exponential and a biexponential fitting is made, justifying the use of double exponential fittings at pH = 4.8.

One difference is, however, the lack of significant remaining absorption after the triplet decays (compare Figure 3.15 B with Figure 3.19 A), suggesting that only a small amount of a *cis* species is formed upon light absorption, rendering the quantum yield of the photochemical reaction very low. This is probably the reason why there is no experimental evidence for the formation of a *cis-cis* species since this last species would be a consequence of the isomerization of *trans-cis*, which is lacking. On the other hand, the ratio between the absorption maximum of the triplet divided by the maximum of the bleaching of **Ct** taken immediately after the flash is 0.6 for compound **31** and 1.6 for compound **32**. In other words, the fraction of triplet formation in compound **32** is much higher, but at the same time, the recovery of **Ct** is also much higher, and by consequence the conversion of **Ct** to **Cc** is very small. This result is compatible with an isomerization taking place in the singlet excited state; in the case of compound **32**, the triplet is privileged with a consequent loss in isomerization efficiency. The **Taut2** formation yield appears to be rather independent of the pH, being the same at pH = 4.8 and 1.2. If the α parameter is given by equation 3.6, than such a result means that acidic catalysis for the formation of **Taut2** may be dominating.

In conclusion, compounds **31** and **32** behave similarly as far as absorption and emission are concerned, but photoinduced formation of **Cc** is much more efficient in the former.

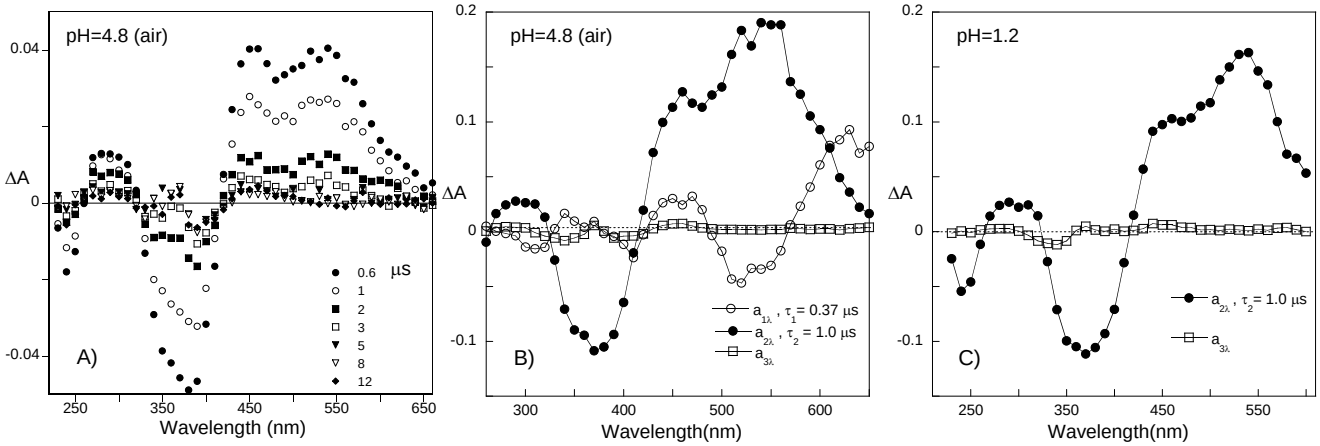

Figure 3.19 – Transient absorption spectra of compound **31** in a mixture of water (90%) and ethanol (10%). Time indicates the delay after the laser pulse. A) pH = 6.1, solution saturated with argon. B) pH = 6.1, air-equilibrated solution. C) pH = 1.2, air-equilibrated solution (○, $a_{1\lambda}$; ●, $a_{2\lambda}$; □, $a_{3\lambda}$ - corresponding lifetimes according to labels in graphics).

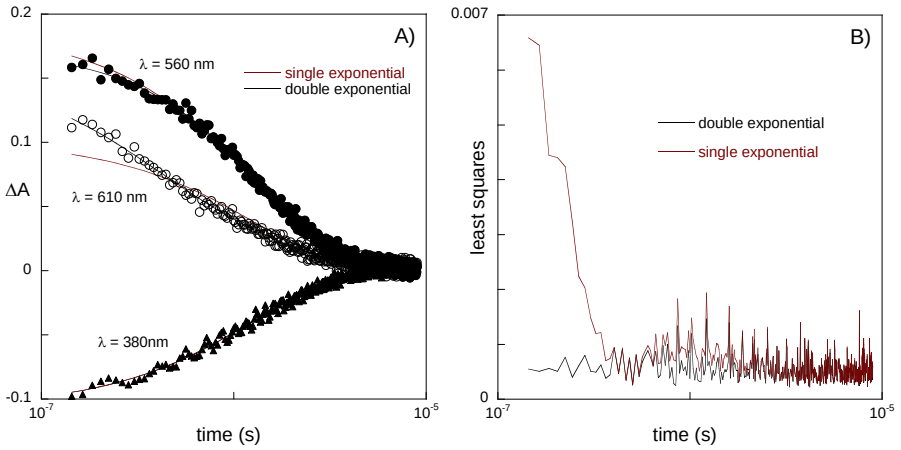

Figure 3.20 – Fitting of laser flash photolysis traces with single and double exponential kinetics with global analysis (sample data: compound **32**, pH = 4.8) at selected wavelengths A). B) Least squares sum as a function of time for the global analysis.

3.5.2 7,4'-Dihydroxyflavylium (DHF)

7,4′-Dihydroxyflavylium (**DHF**) was studied with great detail in previous work.[2,11,24] Here, the absorption and emission titrations of *trans*-chalcones are reported, Figures 3.21 and 3.22, and once again no evidence for ESPT processes are found. The transient absorption spectra of the corresponding neutral chalcone, 2,4,4′-trihydroxychalcone, not yet reported at this time scale, are presented in Figure 3.23. Differently from compounds **31** and **32**, the data could be fitted by a monoexponential with τ = 0.42 µs. It is worth noting that in **DHF**, the intensity of the transient absorptions from the triplets is relatively small. Moreover, there is a significant bleaching at around 365 nm after the triplets decay (10 µs) indicating that **Ct** is efficiently converted into **Cc**, in accordance with the high quantum yield of isomerization presented by this compound.

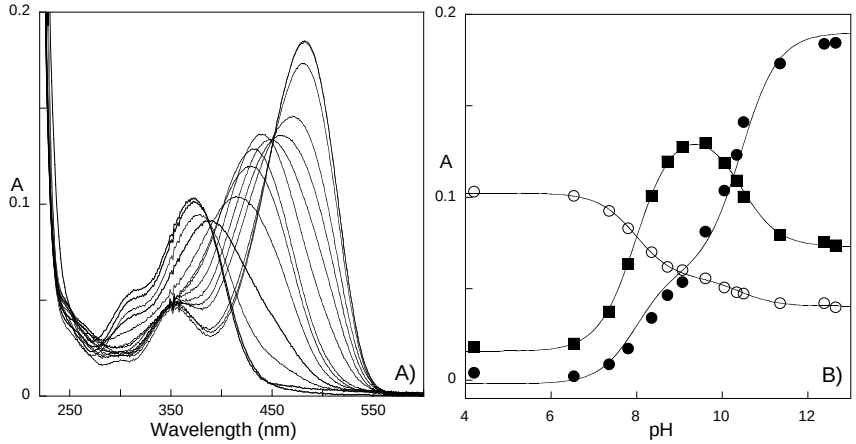

Figure 3.21 – A) Absorption spectra of the chalcones of **DHF**. B) Fitting of the absorptions at (●) 481 nm, (○)370 nm and (■) 427 nm pK_a=8.0 and 10.4

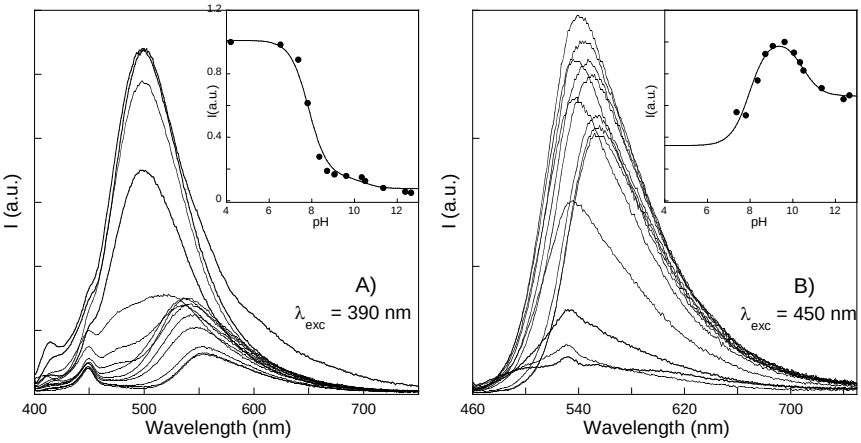

Figure 3.22 – A) Emission spectra of the chalcones of **DHF** at λ_{exc} = 390 nm: inset fitting of the emission at 505 nm (corrected for the absorbed light) for pK_a=7.85 and 10.4. B) Emission spectra of the chalcones of **DHF** at λ_{exc}=450 nm: inset fitting of the emission at 545 nm (corrected for the absorbed light) for pK_a = 8.0 and 10.4.

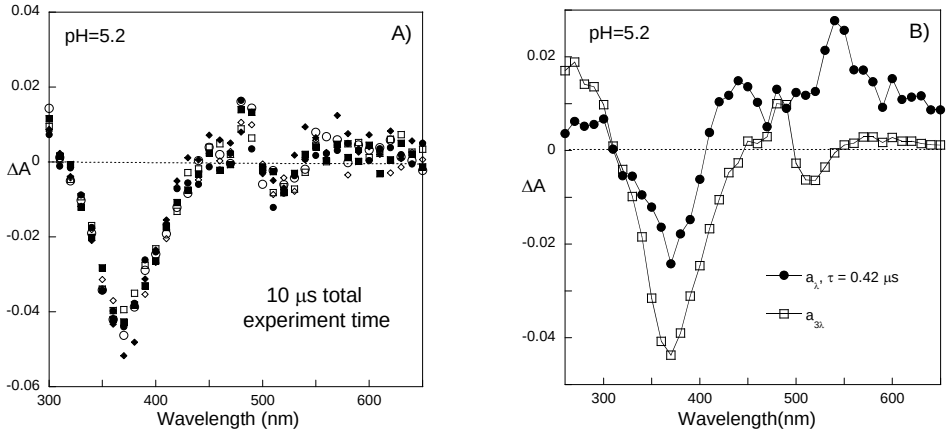

Figure 3.23 –Transient absorption of the chalcone of **DHF** at pH = 5.2 in a mixture of water (90%) and ethanol (10%) in an air-equilibrated solution A). Pre-exponential factors obtained from global analysis of the decays B) (●, a_λ; □, $a_{3\lambda}$ - corresponding lifetimes according to labels in graphics).

3.5.3 7-Hydroxy-2-(4-hydroxystyryl)-1-benzopyrylium (DHS)

The details of kinetic and thermodynamic equilibria for **DHS** were previously presented. The fluorescence emission spectra of the *trans*-chalcones of **DHS** follow the same pattern of the parents lacking the hydroxyl in position 2, Figure 3.24. A mixture of water and ethanol (10 %) was also used to attain sufficient solubility for the laser flash photolysis experiments. The titration curves can be fitted by the same set of pK_a's of the absorption, excluding once more the existence of ESPT from the singlet excited state. Transient absorption spectra are represented in Figure 3.25 and present the same general trend of the chalcones lacking the 2-hydroxyl substituent, and by consequence, they are assigned to ^{3}**Ct**/^{3}**Ct**$^-$ and to the t-t absorption of a tautomer (see Scheme 3.6).

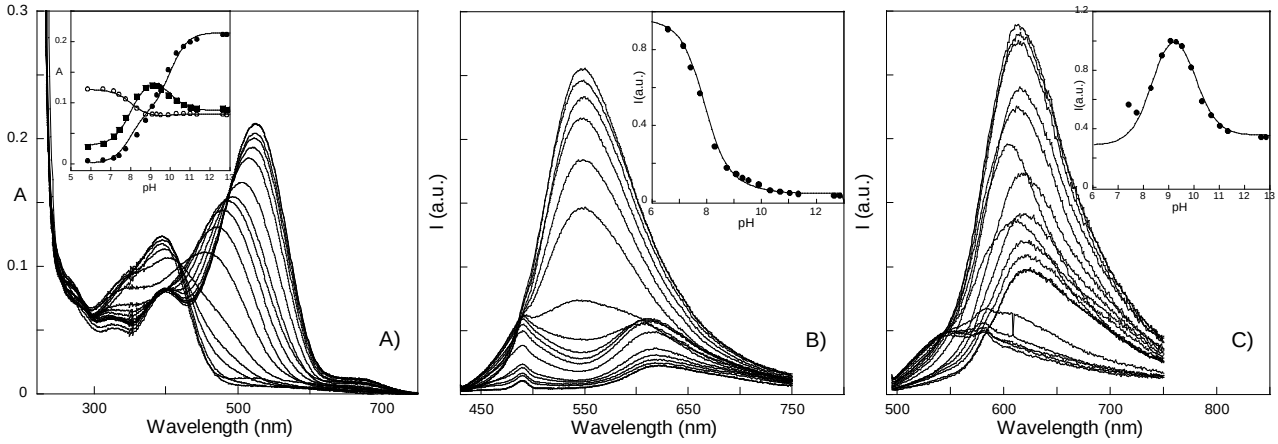

Figure 3.24 – A) Absorption spectral variations upon pH jumps of a solution at pH = 12 (**Ct^{2-} DHS**) to less basic pH values, inset: fittings at (●) 525, (O) 400 and (■) 445 nm, with pK_a's of 8.0 and 10.0 in water (90%) and ethanol (10 %). B) Fluorescence emission titration of the *trans*-chalcones of **DHS** in water (90%) and ethanol (10 %) λ_{exc} = 420 nm; inset: fitting of the emission at λ_{em} =550 nm was achieved with pK_a's of 8.0 and 10.0. B) the same upon λ_{exc} = 485 nm, inset: fitting of the emission at λ_{em} = 620 nm was achieved for pKa's of 8.4 and 10.0.

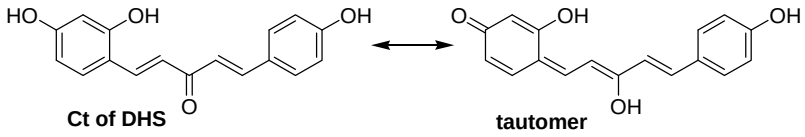

Scheme 3.6 – Tautomer from *trans*-chalcone of **DHS**.

One important point is the great recovery of the absorption at around 390 nm, as observed for compound **32** but not for compound **31**, showing only a very small amount of **Cc** produced upon the flash. The global analysis of the transient absorptions obtained in the absence of oxygen reveals the presence of the two triplets with lifetimes of 3.3 (●) and 0.5 μs (○), while in the presence of oxygen, the data can be fitted with a monoexponential lifetime of 1.0 μs.

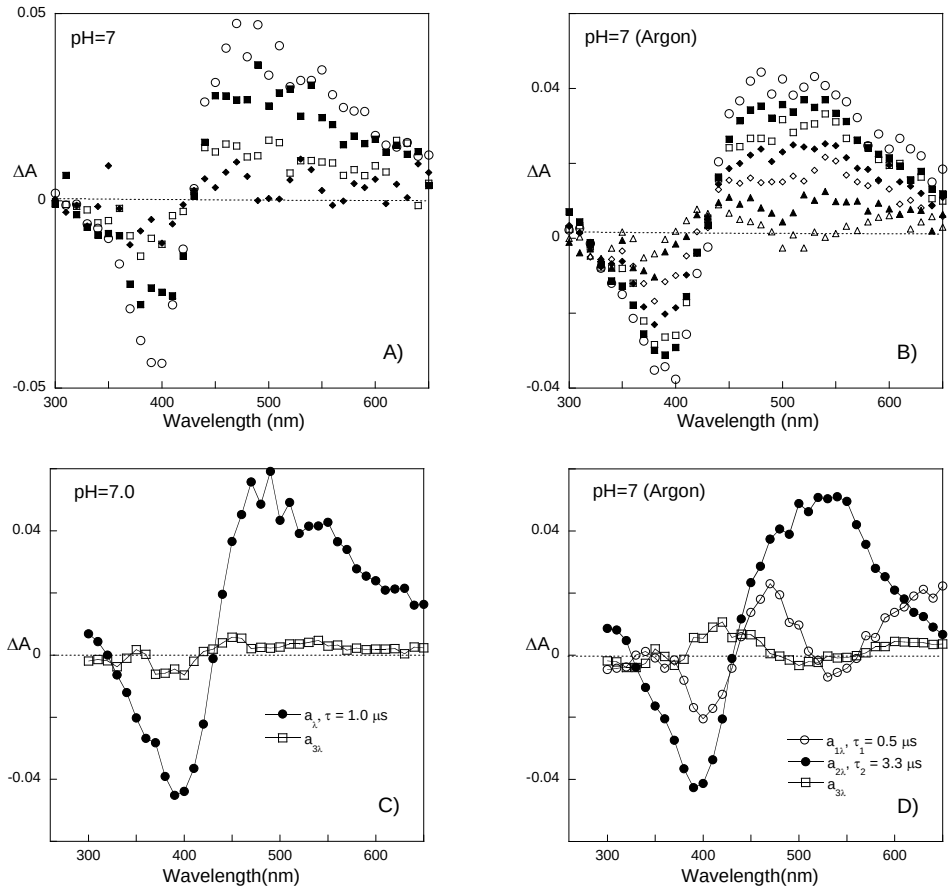

Figure 3.25 –Transient absorption spectra of **DHS** in water (90%) and ethanol (10%) at pH = 7 obtained by nanosecond flash photolysis in air equilibrated solution A) and upon bubbling argon for 20 min B). C) pre-exponential factors obtained from global analysis of the decays in A). D) global analysis of the decays in B) (○, $a_{1\lambda}$; ●, $a_{2\lambda}$; □, $a_{3\lambda}$ - corresponding lifetimes according to labels in graphics).

In order to get more insight on the photochemical behavior, flash photolysis experiments on the time scale of seconds were carried out. The results are presented in Figure 3.26 and confirm the small absorbance variations that take place during the photochemical process. The formation of the *cis*-chalcone from the *trans*-chalcone is much less efficient than that in the case of the **DHF** analogue, and by consequence, the amplitudes of the signals are very low. However, the trend of the changes is similar. As can be seen in Figure 3.26, a bleaching of the absorption of the **Ct** species (396 nm) occurs immediately after the flash, and a partial recovery of **Ct** occurs according to a monoexponential process with lifetime of 2.1 s^{-1} (Figure 3.26 A). When the absorption is followed, at 510 nm (Figure 3.26 B), formation of $\mathbf{A}/\mathbf{AH}^+$ is observed with an identical rate constant.

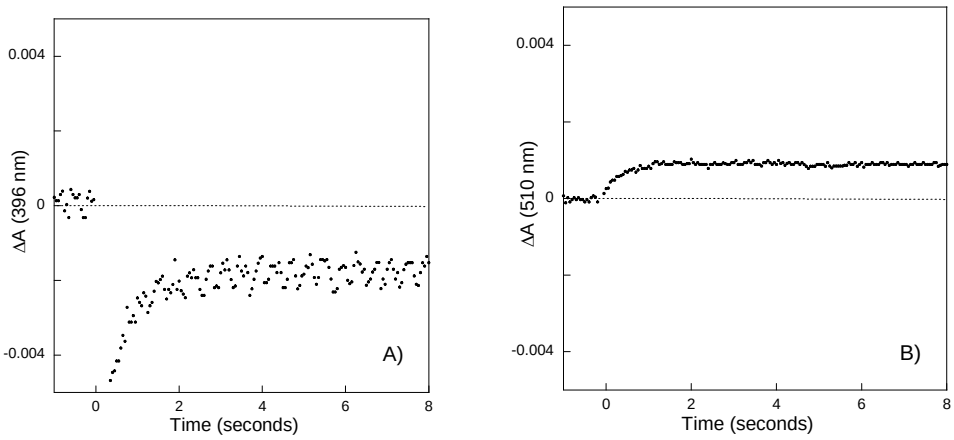

Figure 3.26 – Transient absorption of **DHS** equilibrated solution at pH = 4.9 followed at 396 A) and 510 nm B) in the seconds time scale. The fitting was achieved with $\tau = 2.1\ s^{-1}$.

The results of the flash photolysis experiments on the second time scale can be summarized as follows. The first process immediately after the flash (not available on this time scale) is attributed to the formation of **Cc** at the expenses of **Ct**. Like in the case of the parent **DHF**, **Cc** (and **B**) is not thermodynamically stable, and the second process with a lifetime of $2.1\ s^{-1}$ results from two competitive processes taking place in parallel, one backward corresponding to the recovery of **Ct** and the other forward leading to the colored species **A** (or $\mathbf{AH^+}$ depending on pH). A third process (not shown) is due to the recovery of the **Ct** species from $\mathbf{AH^+}$/**A** and occurs like the kinetics obtained from the pH jump experiments reported in Figure 3.8.

3.5.4 Effects of the addition of CTAB micelles

One important difference between **DHS** and the **DHF** analogue is its much less efficient photochemistry in water. This behavior was already explained on the basis of the transient absorptions experiments shown above.

The lack of efficient photochemistry in water can be overcome by the introduction of CTAB micelles Figure 3.11, as was shown before, similarly to the behavior of the flavylium analogues. Transient absorption spectra on the time scale of seconds of **DHS** in the presence of CTAB micelles was performed, and the results present the same pattern as that in water, but the intensity of the signals is higher, Figure 3.27. More information was obtained by the transient absorption on the time scale of microseconds. It is clear that the triplet state followed at 470 nm decays while the **Ct** is recovered at 396 nm with a lifetime of 1 μs, Figure 3.28. However, no complete recovery of **Ct** was observed, and after the triplet decay, the net result is the formation of **Cc** at the expense of **Ct**, in agreement with the observation of photochromism in the presence of CTAB micelles.

One possible reason for the lack of significant photochemistry in water compared with CTAB micelles could be the deactivation by internal conversion of the singlet state due to the formation of hydrogen bonding in water. In CTAB, the extent of the hydrogen bonding is

reduced, and not only can more isomerization (from the singlet) take place but also more formation of the triplet state occurs.[19]

In addition, and according to the results reported for other 2-phenyl-1-benzopyryliums, it is expected that once $\mathbf{AH^+}$ is formed, it is rapidly ejected to the bulk solution, favoring the forward reaction in competition with the back reaction on the time scale of seconds (see chapter 2).

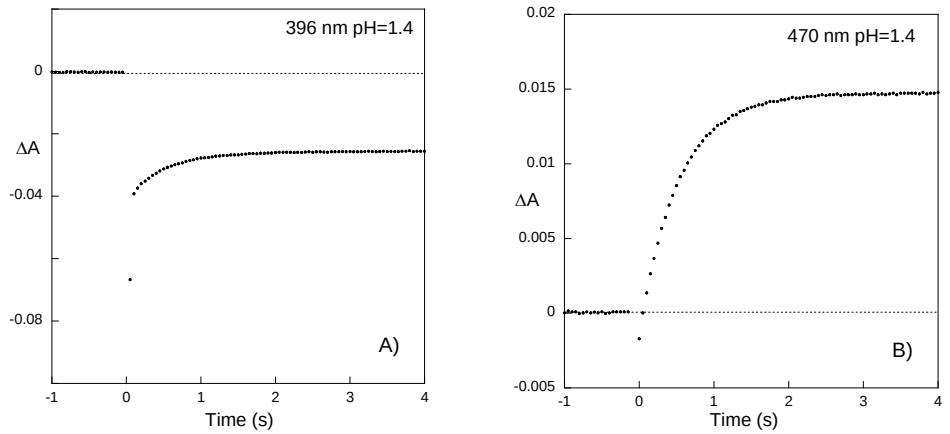

Figure 3.27 –Transient absorptions of **DHS** in the presence of CTAB 0.2 M at pH = 1.4, in the seconds timescale.

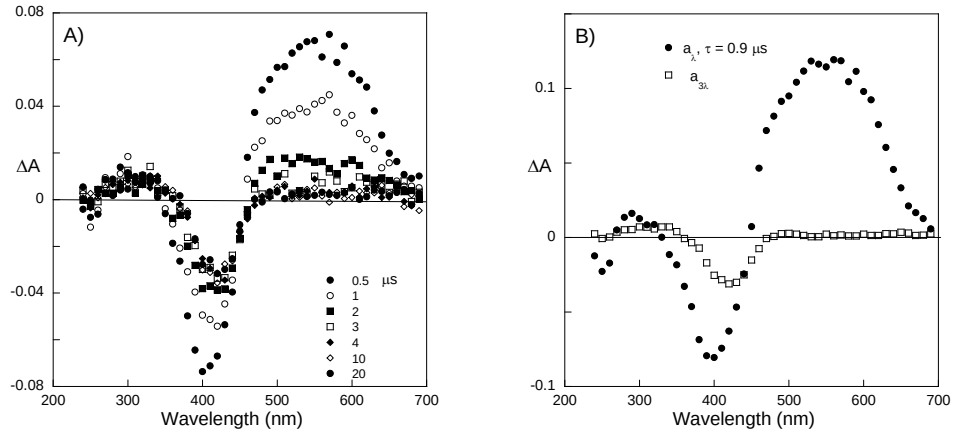

Figure 3.28 – A) Transient absorption spectra obtained by nanosecond flash photolysis in 0.2 M CTAB at pH = 1.44. B) Pre-exponential factors obtained from global analysis of the decays; $\tau = 0.9$ μs (●, a_λ; □, $a_{3\lambda}$).

3.6 Experimental Part

All reagents and solvents used were of analytical grade. NMR spectra were run on a Bruker AMX 400 instrument operating at 400.13 MHz (^{1}H) or 100.62 MHz (^{13}C). Mass spectra were run on Micromass GCT apparatus for EI and FD ionization and on an Applied Biosystems Voyager-DE^{TM} PRO for MALDI. Elemental analyses were obtained on a Thermofinnigan Flash EA 1112 Series instrument.

3.6.1 Synthesis of styrylmethylketones

Styrylmethylketones were prepared according to the method described by Buck and Heilbron.[6]

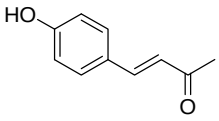

Synthesis of *p*-hydroxystyrylmethylketone: *p*-Hydroxybenzaldehyde (4.00 g, 33 mmol) was dissolved in 15 ml of acetone and the solution treated with 5.3 ml of 50% NaOH (66.3 mmol NaOH). 10 ml of water were then added and the mixture was gently warmed for a few moments and left overnight. By the following day, the whole had solidified to a mass, which was dissolved in water and acidified with HCl 6 M until a yellow oil was observed. In an ice bath, the oil crystallized into a golden-yellow solid (4.55 g, 28 mmol) that was filtered off and dried. **Yield**: 84.0 %. **^{1}H-NMR** ($CDCl_3$, 400.13 MHz) δ (ppm): 7.51–7.45 (3H, m), 6.88 (2H, d, ArH, ^3J = 8.6 Hz), 6.61 (1H, d, ^3J = 16.2 Hz), 6.05 (1H, br s, OH), 2.38 (3H, s).

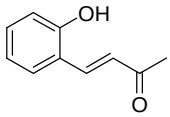

Synthesis of *o*-hydroxystyrylmethylketone: Salicylaldehyde (7.5 ml, 71 mmol) was dissolved in 30 ml of acetone and the solution treated with 10.5 ml of 50% NaOH. 20 ml of water were then added and the mixture was left in an ultrasound cleaner bath for approximately 20 min at 60 ºC. After that, the whole had solidified to a mass that was re-dissolved in water and treated with HCl 6 M. In an ice bath, the oil that had appeared crystallized into a yellow solid that was filtered off and dried. This solid was recrystallized from a solvent mixture ethanol/ water (5.47 g, 34 mmol). **Yield**: 47.5 %. **^{1}H-NMR** ($CDCl_3$, 400.13 MHz) δ (ppm): 7.87 (1H, d, ^3J = 16.4 Hz), 7.66 (1H, br s), 7.47 (1H, dd, ^3J = 7.9 Hz, ^4J = 1.3 Hz), 7.26 (1H, ddd, ^3J = 7.7 Hz, ^4J =1.6 Hz), 7.02 (1H, d, ^3J = 16.4 Hz), 6.93–6.90 (2H, m), 2.43 (3H, s).

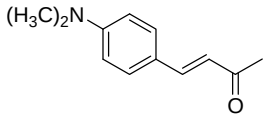

Synthesis of *p*-dimethylaminostyrylmethylketone: p-Dimethylaminobenzaldehyde (10.48 g, 70 mmol) was dissolved in 30 ml of acetone and the solution treated with 10 ml of 50% NaOH. 20 ml of water were then added and the mixture was left heated overnight at approximately 50 ºC. By the following day, the reaction mixture was neutralized with HCl 6 M, and the orange solid that precipitated out was filtered off, washed with diethyl ether and dried (11.62 g, 61 mmol). **Yield**: 87.5 %. **^{1}H-NMR** ($CDCl_3$, 400.13 MHz) δ (ppm): 7.50–7.43 (3H, m), 6.68 (2H, d, ^3J = 8.9 Hz), 6.54 (1H, d, ^3J = 16.1 Hz), 3.03 (6H, s), 2.34 (3H, s).

3.6.2 Synthesis of 2-styryl-1-benzopyrylium salts

These salts were prepared according to a procedure adapted either from Katritzky[20] or Robinson,[21] both frequently used in the synthesis of 2-phenyl-1-benzopyrylium salts.

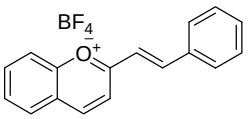

Synthesis of 2-styryl-1-benzopyrylium tetrafluoroborate: Salicylaldehyde (1.0 ml, 9.4 mmol) and benzalacetone (1.36 g, 9.3 mmol) were dissolved in 10 ml of acetic acid and 2 ml of HBF_4.[20] 10 ml of acetic anhydride were then added dropwise and the temperature of the reaction mixture reached 75 ºC. The reaction mixture was stirred overnight. By the following day, 5 ml of ethyl acetate were added and the brown precipitated solid was filtered off, washed with diethyl ether and dried (0.69 g, 2.2 mmol). **Yield**: 23.7 %. **^{1}H-NMR** (D_2O/DCl, pD≈1.0, **AH^+** species, 400.13 MHz) δ (ppm): 8.79 (1H, d, ^3J = 8.6 Hz), 8.18 (1H, d, ^3J = 15.9 Hz), 7.86 (1H, t, ^3J = 7.5 Hz), 7.75–7.81 (3H, m), 7.51 (1H, t, ^3J = 7.5 Hz), 7.47 (2H, br d, ^3J = 7.2 Hz), 7.27 (1H, d, ^3J = 15.9 Hz), 7.06–7.12 (3H, m). **FD MS** m/z (%): 233.096 $[M]^+$ (100), 250.099 $[M+OH]^+$ (45). **EA** calcd for $C_{17}H_{13}BF_4O$: C 63.79, H 4.09; found: C 63.51, H 4.45.

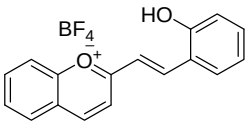

Synthesis of 2-(2-hydroxystyryl)-1-benzopyrylium tetrafluoroborate: Salicylaldehyde (0.42 ml, 3.9 mmol) and *o*-hydroxystyrylmethylketone (0.65 g, 4.0 mmol) were dissolved in 4 ml of acetic acid and 0.8 ml of HBF_4.[20] 4 ml of acetic anhydride were then added dropwise and the temperature of the reaction mixture rose until 68 ºC. The reaction mixture was stirred overnight. By the following day, the precipitated solid was filtered off, washed with water and then carefully with diethyl ether and dried (0.41 g, 1.2 mmol). **Yield**: 30.8 %. **^{1}H-NMR** (D_2O/DCl, pD≈1.0, **AH^+** species, 400.13 MHz) δ (ppm): 8.87 (1H, d, ^3J = 8.8 Hz), 8.27 (1H, d, ^3J = 15.9 Hz), 7.78-7.88 (4H, m), 7.61 (1H, d, ^3J = 7.7 Hz), 7.51 (1H, t, ^3J = 7.5 Hz), 7.26 (1H, d, ^3J = 15.9 Hz), 7.16 (1H, t, ^3J = 7.7 Hz), 7.00 (1H, t, ^3J = 7.5 Hz), 6.83 (1H, d, ^3J = 8.1 Hz). **FD MS** m/z (%): 248.080 $[M-H]^+$ (100). **EA** calcd for $C_{17}H_{13}BF_4O_2$: C 60.75, H 3.90; found: C 60.32, H 3.89.

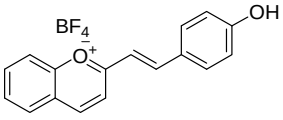

Synthesis of 2-(4-hydroxystyryl)-1-benzopyrylium tetrafluoroborate: Salicylaldehyde (1.0 ml, 9.4 mmol) and *p*-hydroxystyrylmethylketone (1.50 g, 9.3 mmol) were dissolved in 10 ml of acetic acid and 2 ml of HBF_4.[20] 9 ml of acetic anhydride were then added dropwise and the temperature of the reaction mixture rose until 75 ºC. The reaction mixture was stirred overnight. By the following day, the precipitated solid was filtered off, washed with water and then carefully with diethyl ether and dried (0.93 g, 2.8 mmol). **Yield**: 30.1 %. **^{1}H-NMR** (D_2O/DCl, pD≈1.0, **AH^+** species, 400.13 MHz) δ (ppm): 8.61 (1H, d, ^3J = 8.6 Hz), 8.16 (1H, d, ^3J = 15.7 Hz), 7.86 (1H, t, ^3J = 7.8 Hz), 7.78 (1H, d, ^3J = 7.9 Hz), 7.71 (1H, d, ^3J = 8.6 Hz), 7.64 (1H, d, ^3J = 8.9 Hz), 7.53 (1H, t, ^3J = 7.6 Hz), 7.44 (2H, d, ^3J = 8.2 Hz), 7.04 (1H, d, ^3J = 15.7 Hz), 6.49 (2H, d, ^3J = 8.2 Hz). **FD MS** m/z (%): 248.088 $[M- H]^+$ (100). **EA** calcd for $C_{17}H_{13}BF_4O_2 \cdot H_2O$: C 57.66, H 4.27; found: C 57.12, H 4.69.

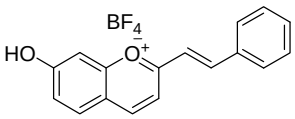

Synthesis of 7-hydroxy-2-styryl-1-benzopyrylium tetrafluoroborate (**HS**): 2,4-Dihydroxybenzaldehyde (1.24 g, 9.0 mmol) and benzalacetone (1.37 g, 9.4 mmol) were dissolved in 10 ml of acetic acid and 2 ml of HBF_4.[20] Acetic anhydride (8.5 ml) was then added dropwise and the temperature of the reaction mixture rose until 85 ºC. The reaction mixture was stirred overnight. By the following day, the precipitated solid was filtered off, washed with water and then carefully with diethyl ether and dried (0.95 g, 2.8 mmol). **Yield**: 31.1 %. **^{1}H-NMR** (D_2O/DCl, pD≈1.0, **AH^+** species, 400.13 MHz) δ (ppm): 8.94 (1H, d, ^{3}J = 8.3 Hz), 8.25 (1H, d, ^{3}J = 16.1 Hz), 8.03 (1H, d, ^{3}J = 8.7 Hz), 7.72–7.78 (3H, m), 7.35–7.49 (6H, m). **MS FD** m/z (%): 248.091 $[M-H]^+$ (100). **EA** calcd for $C_{17}H_{13}BF_4O_2$: C 60.75, H 3.90; found: C 60.61, H 3.88.

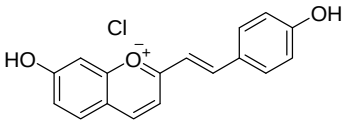

Synthesis of 7-hydroxy-2-(4-hydroxystyryl)-1-benzopyrylium chloride (**DHS**): 2,4-Dihydroxybenzaldehyde (1.40 g, 10 mmol) and *p*-hydroxystyrylmethylketone (1.61 g, 10 mmol) were dissolved in 25 ml of acetic acid. The solution was saturated with dry hydrogen chloride (3 h 30 min).[21] The solution became dark purple and a solid precipitated out. The precipitated solid was filtered off, carefully washed with diethyl ether and dried. The solid was recrystallized by dissolving it in acetonitrile with a few drops of HCl and letting diethyl ether gently diffuse (2.34 g, 7.7 mmol). **Yield**: 78.0 %.**^{1}H-NMR** (D_2O/DCl, pD≈1.0, **AH^+** species, 400.13 MHz) δ (ppm): 8.59 (1H, d, ^{3}J = 8.7 Hz), 8.10 (1H, d, ^{3}J = 16.1 Hz), 7.77 (1H, d, ^{3}J = 8.3 Hz), 7.51 (2H, d, ^{3}J = 8.6 Hz), 7.46 (1H, d, ^{3}J = 8.3 Hz), 7.08-7.14 (2H, m), 7.05 (1H, d, ^{3}J =16.1 Hz), 6.70 (2H, d, ^{3}J = 8.6 Hz). **^{1}H -NMR** (D_2O/CD_3OD, pD = 6.1, **Ct** species, 400.13 MHz) δ (ppm): 7.87 (1H, d, ^{3}J = 15.9 Hz), 7.57 (1H, d, ^{3}J = 15.8 Hz), 7.51 (2H, d, ^{3}J = 8.4 Hz), 7.47 (1H, d, ^{3}J = 8.6 Hz), 7.03 (1H, d, ^{3}J = 15.4 Hz), 6.99 (1H, d, ^{3}J = 15.2 Hz), 6.81 (2H, d, ^{3}J = 8.6 Hz), 6.38 (1H, d, ^{3}J = 8.2 Hz), 6.30 (1H, br s). **^{1}H -NMR** (D_2O/CD_3OD, pD≈12, **Ct^{2-}** species, 400.13 MHz) δ (ppm):8.52 (1H, d, ^{3}J = 15.4 Hz), 7.48 (1H, d, ^{3}J = 15.4 Hz), 7.37 (2H, d, ^{3}J = 8.6 Hz), 7.27 (1H, d, ^{3}J = 8.8 Hz), 7.15 (1H, d, ^{3}J = 15.5 Hz), 6.59 (2H, d, ^{3}J = 8.4 Hz), 6.55 (1H, d, ^{3}J = 15.6 Hz), 5.98 (1H, s), 5.96 (1H, d, ^{3}J = 9.1 Hz). **EI MS** m/z (%): 57.069 (100), 69.069 (55), 83.082 (50), 160.052 (50), 264.080 (30), 265.084 $[M]^+$ (20), 266.092 (25). **EA** calcd for $C_{17}H_{13}O_3Cl\cdot(1/2)H_2O$: C 65.92, H 4.56; found: C 65.71, H 4.88.

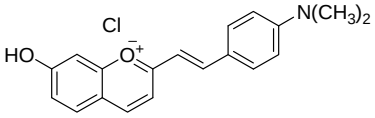

Synthesis of 7-hydroxy-2-(4-dimethylaminophenyl)-1-benzopyrylium chloride (**DAS**): 2,4-Dihydroxybenzaldehyde (0.69 g; 5 mmol) and *p*-dimethylaminostyrylmethylketone (0.94 g; 5 mmol) were dissolved in 10 ml of acetic acid. The solution was saturated with dry hydrogen chloride.[21] The solution became dark green and was left under stirring overnight. A solid was precipitated by the addition of ethyl acetate that was filtered off, carefully washed with diethyl ether and dried. **Yield**: 54.9 %. **^{1}H-NMR** (D_2O/DCl, pD≈1.0, **AH^+** species, 400.13

MHz) δ (ppm): 8.23 (1H, d, ^3J = 8.6 Hz), 7.38 (1H, d, ^3J = 15.9 Hz), 7.26 (1H, d, ^3J = 8.6 Hz), 7.07 (3H, m), 6.86 (2H, d, ^3J = 8.3 Hz), 6.60 (1H, d, ^3J =5.3 Hz), 6.55 (1H, d, ^3J = 5.3 Hz),6.52 (1H, s), 2.66 (6H, s). **MALDI TOF MS** (+): 292.6156 $[M]^+$(100), 293.6040 (65), 291.6009 (20). **EA** calcd for $C_{19}H_{19}Cl_2NO_2 \cdot (3/2)\ H_2O$: C 58.32, H 5.67, N 3.58; found: C 57.98, H 5.53, N 3.65.

3.6.3 Synthesis of model compounds

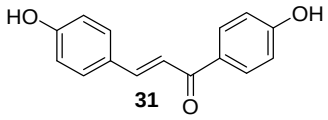

31

Synthesis of (*E*)-1,3-Bis(4-hydroxyphenyl)prop-2-en-1-one (4,4′-Dihydroxychalcone) **31**: *p*-Hydroxybenzaldehyde (2 mmol, 0.244 g) and 4′-hydroxyacetophenone (2.42 mmol, 0.33 g) were dissolved in 5 ml of diethyl ether; 2 ml of ethanol and 2 ml of sulfuric acid were then added. The solution became orange and was left under stirring for 3 h. A dark yellow solid precipitated by the addition of water, which was filtered off, and the solid was carefully washed with water and dried. Purification was made by flash chromatography in diethyl ether/hexane (1:1). A yellow solid was obtained (0.23 g, 0.96 mmol). **Yield**: 46.9 %. **^{1}H-NMR** (CD_3OD, 400.13 MHz) δ (ppm): 7.99 (2H, d, ^3J = 8.6 Hz), 7.70 (1H, d, ^3J = 15.5 Hz), 7.60 (2H, d, ^3J = 8.1 Hz), 7.54 (1H, d, ^3J = 15.2 Hz), 6.88 (2H, d, ^3J = 8.5 Hz), 6.83 (2H, d, ^3J = 8.3 Hz). **^{13}C-NMR** (CD_3OD, 100.62 MHz) δ (ppm): 191.02, 163.64, 161.35, 145.71, 132.17, 131.62, 131.13, 127.83, 119.51, 116.83, 116.32. **MALDI TOF MS** (+): 241.1 $[M+H]^+$ (100%), 242.1 $[M+2H]^+$ (21.5%). **EA** calcd for $C_{15}H_{12}O_3$: C 74.99, H 5.03; found: C 74.67, H 5.30.

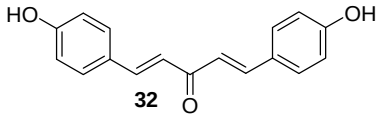

32

Synthesis of (1*E*,4*E*)-1,5-Bis(4-hydroxyphenyl)penta-1,4-dien-3-one **32**: *p*-Hydroxybenzaldehyde (0.32 mmol, 0.039 g) and *p*-hydroxystyrylmethylketone (0.32 mmol, 0.052 g) were dissolved in 2 ml of ethanol; 1 ml of sulfuric acid was then added. The solution became dark red and was left under stirring for 5 h. A dark brown solid was precipitated by the addition of water, which was filtered off, and the solid was carefully washed with water and dried (0.072 g, 0.27 mmol). **Yield**: 84.2 %. **^{1}H-NMR** (CD_3OD, 400.13 MHz) δ (ppm): 7.69 (2H, d, ^3J = 15.7 Hz), 7.55 (4H, d, ^3J = 6.0 Hz), 7.04 (2H, d, ^3J = 15.4 Hz), 6.81 (4H, d, ^3J = 6.3 Hz). **MALDI TOF MS** (+): 267.1 $[M+H]^+$ (100%), 268.1 $[M+2H]^+$ (28.4%). **EA** calcd for $C_{17}H_{14}O_3$: C 76.68, H 5.30; found: C 76.75, H 5.41.

3.6.4 Measurements

Solutions were prepared using Millipore water and acetonitrile or ethanol (when needed and indicated in the text). The pH of solutions was adjusted by addition of HCl, NaOH or universal buffer of Theorell and Stenhagen.[22] and pH was measured in a Radiometer Copenhagen PHM240 pH/ion meter. UV-Vis absorption spectra were recorded in a Varian-Cary

100 Bio spectrophotometer or in a Shimadzu VC2501-PC. Quantum yields were determined by irradiation at 436 nm, using a medium pressure mercury arc lamp and the excitation bands were isolated with interference filters (Oriel). Actinometry was made using the ferrioxalate system.[23] Some irradiations were performed in a 300W solar lamp from OSRAM.

Second and subsecond flash photolysis experiments were performed as previously described.[24] Nanosecond laser flash photolysis experiments were run on a LKS.60 nanosecond laser photolysis spectrometer from Applied Photophysics, exciting at 355 nm. Aqueous solutions of chalcones for these experiments were prepared in the presence of 10 % ethanol to enhance solubility.

3.6.5 Data Analysis

Laser flash photolysis traces at each wavelength were analyzed with a global analysis method. Least squares fittings of the experimental data with single or double exponential kinetics were performed using Solver from MS Excel, by adjusting globally the rate constants to all kinetic traces for each pH and the exponential factors for each kinetic trace at a specific wavelength.

3.7 Conclusions

A series of 2-styryl-1-benzopyrylium salts were synthesized and thoroughly studied in comparison with flavylium analogues. Although the known network of reactions of flavylium salts could be applied and no evidence was found for the isomerization of the second double bond, the absorption maxima are pronouncedly red shifted compared with flavylium analogues (up to 90 nm). 2-Styryl-1-benzopyrylium salts are also more stable towards color loss, which occurs at slightly higher pH values and kinetically more inert towards hydration than their corresponding flavylium ions. Moreover, this family of compounds also allows the design of new photochromic systems, despite the poor photochemistry in water, with significant color changes in the presence of CTAB micelles that stabilize the **Ct**. In particular, a photochromic system switching from yellow to light blue based on derivatives of natural anthocyanins is for the first time documented.

The work presented in this chapter provides evidences for a singlet state isomerization process, achieved by studying chalcones lacking a hydroxyl group in position 2 in water/ethanol mixed solvents, where no *trans-cis* isomerization is found in the triplet state. By analogy with 2-phenyl-1-benzopyrylium, it is expected that micelles other than CTAB or gels would be also good matrices to achieve photochromic systems involving 2-styryl-1-benzopyrylium derivatives.

3.8 References

[1] ed. P. Markakis, *Anthocyanins as food colors – a series of monographs*, Academic Press, New York, USA, **1982**.
[2] F. Pina, M. Maestri, V. Balzani, *in Handbook of Photochemistry and Photobiology*, American Scientific Publishers, Stevenson Ranch, CA, USA, **2003**, Chapter 9, vol. 3, 411-449.
[3] L. Jurd, US Patent 3.301.683, **1967**.
[4] D. Amic, N. Trinajstic, D. Davidovicamic, *J. Chem. Soc. Perkin Trans. 2* **1992**, 11, 1933.
[5] J. S. Buck , I. M. Heilbron, *J. Chem. Soc. Trans* **1922**, 121, 1198-1212.
[6] J. S. Buck , I. M. Heilbron, *J. Chem. Soc. Trans* **1922**, 121, 1095-1101.
[7] R. M. Silverstein, *Spectrometric identification of organic compounds*, John Wiley & Sons, New York, USA, **1997**.
[8] A. Roque, J. C. Lima, A. J. Parola, F. Pina, *Photochem. Photobiol. Sci.* **2007**, *6*, 381-385.
[9] R. Brouillard, J.-E. Dubois, *J. Am. Chem. Soc.* **1977**, 99, 1359-1364.
[10] F. Pina, M. J. Melo, A. J. Parola, M. Maestri, V. Balzani, *Chem. Eur. J.* **1998**, *4*, 2001-2007.
[11] F. Pina, L. Benedito, M. J. Melo, A. J. Parola, J.C. Lima , A. L. Macanita , *Anales de Quimica* **1997**, 93,111-118.
[12] See Supplementary Material, section 9.4.
[13] a) G. Haucke, P. Czerney, C. Igney, *Ber. Bunsenges. Phys. Chem.* **1989**, 93, 805-815; b) G. Haucke, P. Czerney, F. Cebulla, *Ber. Bunsenges. Phys. Chem.* **1992**, 96, 880-886.
[14] M. C. Moncada, D. Fernandez, J. C. Lima, A. J. Parola, C. Lodeiro, F. Folgosa, M. J. Melo, F. Pina, *Org. Biomol. Chem.* **2004**, *2*, 2802-2808
[15] a) A. H. Weller, *Elektrochem*. **1952**, 56, 662–668; b) A. H. Weller, *Prog. React. Kinet.* **1961**, 1, 187-214; c) H. Beens, K. H. Grellmann, M. Gurr, A. H. Weller, *Discuss. Faraday Soc.* **1965**, 93, 183-193.
[16] Y. Norikane, H. Itoh, T. Arai, *J. Phys. Chem A* **2002**, 106, 2766-2776.
[17] P. G. Conrad, R. S. Givens, B. Hellrung, C. S. Rajesh, M. Ramseier, J. Wirz, *J. Am. Chem. Soc.* **2000**, 122, 9346-9347.
[18] P. Zuo, C. Ma, W. M. Kwok, W. S. Chan, D. L. Phillips, *J. Org. Chem.* **2005**, 70, 8661-8675.
[19] A. O. Doroshenko, V. G. Pirvarenko, *J. Photochem. Photobiol. A* **2003**, 156, 55-64.
[20] A. R. Katritzky, P. Czerney, J. R. Levell, W. H. Du, *Eur. J. Org. Chem.* **1998**, 2623-2629.
[21] R. Robinson, D. D. Pratt, *J. Chem. Soc., Trans.* **1922**, *121*, 1577-1585.
[22] F. W. Küster, A. Thiel, *Tabelle per le Analisi Chimiche e Chimico- Fisiche*, 12th ed.; Hoepli, Milano, Italy, **1982**, 157-160.
[23] C. G. Hatchard, C. A. Parker, *Proc. R. Soc. (London), Ser. A* **1956**, 235, 518-536.
[24] a) F. Pina, M. J. Melo, R. Ballardini, L. Flamigni, M. Maestri, *New. J. Chem.* **1997**, *21*, 969-976; b) M. Maestri, R. Ballardini, F. Pina, M. J. Melo, *J. Chem. Educ.* **1997**, *74*, 1314-1316.

4. Photochromism of the flavylium network in Pluronic F127 micelles and gels

The photochromism of the compound 4'-*N,N*-dimethylamino-7-hydroxyflavylium (**DAF**) incorporated in Pluronic F127 micelles and gels was studied in great detail throughout this chapter.

4.1 Introduction

In aqueous solutions, flavylium compounds give rise to a complex network of reactions, whose study is relatively well established in the literature, as previously pointed out in the Introduction, also for amino compounds.[1] 4'-*N,N*-dimethylamino-7-hydroxyflavylium (**DAF**) was used throughout the study carried out in this chapter, and its aqueous network of reactions is schematized in Scheme 4.1 (Supplementary Material, section 9.4)

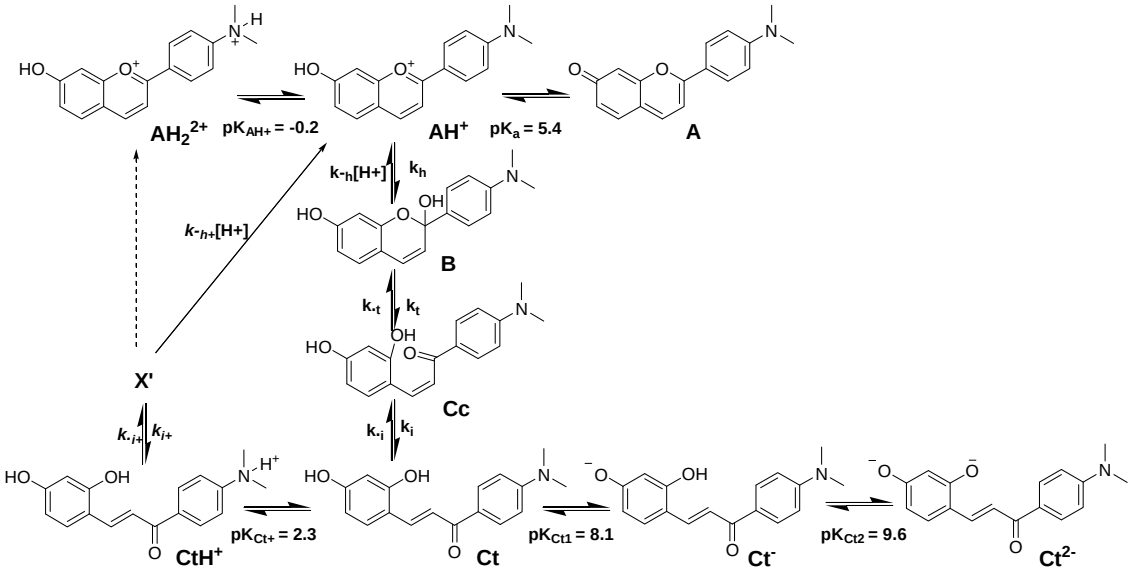

Scheme 4.1 –Network of ground-state reactions of **DAF** in aqueous solutions.

At moderate pH values, from 1 to 6.5, equilibrated solutions behave as a single acid-base equilibrium, equations 1.26 and 1.27, Figure 4.1 A. The conjugated base (**CB**) is mainly constituted by **Ct** 92 % and **A** 8 %, the species **B** and **Cc** appearing in undetectable concentrations. The spectra of the species present in equilibrium are shown in Figure 4.1 B, $\mathbf{AH^+}$ peaks at 535 nm, **A** at *ca* 550 nm and **Ct** has a maximum at 411 nm.

As explained previously, the photochromism of flavylium compounds is a consequence of the photoisomerization of the **Ct** species, which converts to the **Cc** species. **Cc** spontaneously converts into the colored $\mathbf{AH^+}$ or **A** species (through **B**), if the pH is chosen carefully, defining the flavylium network of species as a photochromic system.

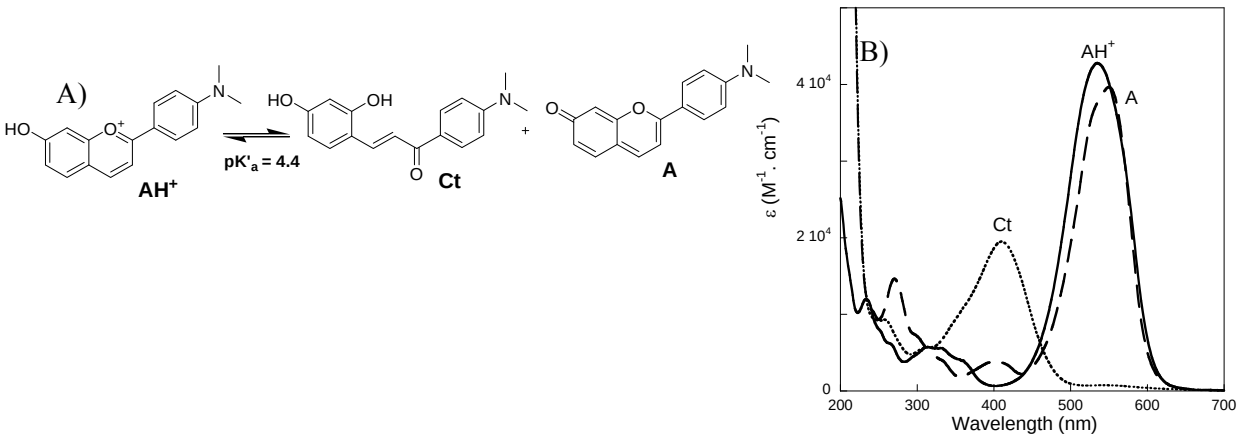

Figure 4.1 – A) pK'_a of **DAF** in aqueous solutions. B) Spectra of the main species present in the equilibrium from pH 1 to 6.5.

Recently it was reported that photochromic micellar systems and gels switching from a variety of colors are obtained by incorporation of flavylium compounds in Pluronic F127,[2] a triblock copolymer (PEO-PPO-PEO) of polyethylene oxide (PEO) and polypropylene oxide (PPO), as shown in Figure 4.2.

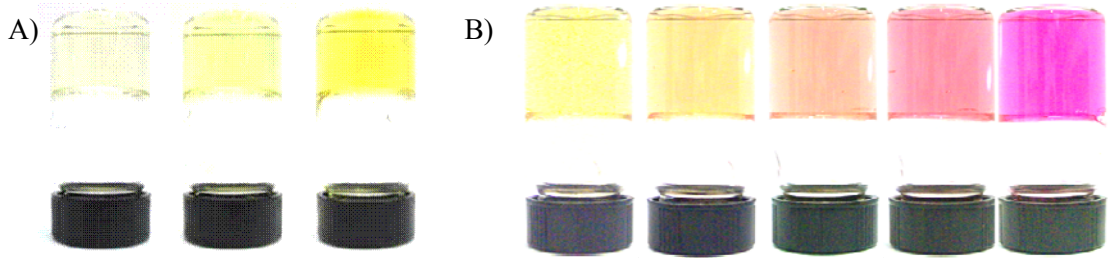

Figure 4.2 – A) 7,4'-Dihydroxyflavylium (**DHF**) in 30 % Pluronic gel at pH = 3, upon sunlight exposure at room temperature (last picture 1 minute). B) 7-*N*,*N*-Diethylamino-4'-hydroxyflavylium (**DEF**) in 30 % Pluronic gel at pH = 4.9, upon sunlight exposure at room temperature (last picture 3.5 minutes).[2]

Pluronic F127 has a nominal molecular weight of 12 500 and a PEO/PPO ratio of 2:1 by weight. Both micelles and gels are formed reversibly only when a critical concentration and temperature is exceeded, and are transparent in the visible region. The reversible thermal behavior of both dilute and concentrated Pluronic F127 solutions has been studied extensively, motivated by the numerous pharmaceutical applications of this family of polymers, and their micellization and gelation properties are well-known.[2,3] The gels formation is associated with "hardsphere crystallization" as the micelles pack - the PEO chains in the micellar mantle interpenetrate extensively in the gel.[3] At even higher temperatures, the gel "dissolves" again.[3] The gels and micelles consist of two domains, an outer aqueous environment hospitable to hydrophilic molecules and a more hydrophobic PPO-rich core region suitable for incorporation of hydrophobic compounds.[2] In the Pluronic gel or micelle, the **Ct** which is more hydrophobic than **AH**$^+$, is stabilized preferentially by the nonionic polymer environment, shifting the equilibrium (equation 1.26) toward the right.[2] In the presence of the polymer the **Ct** spectrum is temperature-dependent and shifts to the blue at higher temperatures, when the micelles are

formed and the absorption band of **AH**$^+$ practically disappears at pH values where it is still the thermodynamically stable species in water. The blue shift is due to the decrease in polarity afforded by the micellar environment.[2] When the **Ct** species in Pluronic F127 micellar solutions or gels is irradiated the colored **AH**$^+$/**A** species forms. The preferential interaction of the **Ct** species with Pluronic F127 is particularly convenient for the enhanced performance of this photochromic system since it favors the spontaneous conversion of **Cc** into **AH**$^+$/**A**, permitting work at lower pH values,[2] similarly to what was explained before for the systems in the presence of CTAB micelles.

In this chapter, the pH and light dependent network of chemical reactions occurring in 4'-(*N,N*-Dimethylamino)-7-hydroxyflavylium (**DAF**) are used as a multiprobe suitable for study the microenvironment of micelles and gels of Pluronic polymer F127. This compound allows to obtain better photochromic systems, in terms of color contrast, than the ones previously reported,[2] because the initial **Ct** state is transparent and a strong red-pink color (**AH**$^+$/**A**) is observed after irradiation. Moreover, we use techniques such as fluorescence, fluorescence anisotropy and time resolved fluorescence and fluorescence anisotropy to gain some insight into the photochromic mechanism. Several experimental evidences for the existence of a non-uniform distribution of molecules in Pluronic micelles or gels, for the fact that only molecules with a certain location respond to the light stimulus and for the presence of a very small barrier in the singlet excited state of **Ct** will be presented.

4.2 General properties of DAF and its photochromism in Pluronic micelles and gels

In this work, the new compound 4'-*N,N'*-dimethylamino-7-hydroxyflavylium (**DAF**) was investigated because it exhibits a good photochromic contrast switching from colorless to intense red-pink, see Figure 4.3. No significant photochemistry was observed in water as reported for other flavylium compounds bearing amino substituents.

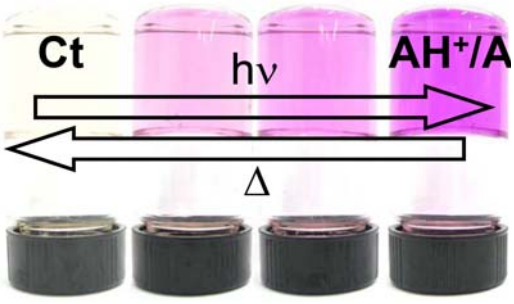

Figure 4.3 – Solar irradiation of a gel (25 % Pluronic F127 at 30 ºC) containing **DAF** at pH = 4.0: 0, 15, 30 and 60 s upon exposure to sunlight. See below for details.

One interesting application of this system, besides its photochromic properties, is the possibility of studying the microenvironment of the micelles and gels taking profit from: i)

changes in the UV-Vis absorption maxima of the different species, ii) shifts occurring in the equilibrium, equation 1.26, due to the preferential stabilization of some species, iii) switching from a neutral probe to a charged one by means of a light stimulus.

In order to explore the changes in the absorption maximum, the absorption spectra of solutions of **DAF** in mixtures water/1,4-dioxane was carried out. The **Ct** absorption maximum is blue shifted by decreasing of water content, *see* Figure 4.4 A. The data reported in Figure 4.4 A was used as a calibration curve to predict the local polarity of the **Ct** species in the presence of various concentrations of Pluronic F127 and has a linear correction with $E_T(30)$ parameter for these mixtures[4] (not shown). For low concentration of the polymer (1.5%) the wavenumber of the absorption maxima was represented as a function of the temperature, Figure 4.4 B, for pH = 2.0 (**AH**$^+$) and pH = 6.0 (**Ct**). Regarding the **Ct** absorption maximum, a plateau is observed at low temperatures lying at 24300 cm^{-1}, suggesting that this species is essentially surrounded by water. On the other hand, at high temperatures a value of 25740 cm^{-1} was registered corresponding to *ca.* 88% of dioxane, a more hydrophobic environment as expected to be found for the distribution of the compound within the micelles. The shifts on the absorption maximum are thus a sensor for the formation of micelles and the transition temperature is in agreement with the 23 ^{0}C reported in literature, Figure 4.4 B.[3b)] Figure 4.5 shows in more detail, how the CMT can be determined following the absorption at 412 nm in function of temperature. In contrast, at pH = 2.0 **AH**$^+$ is only slightly red shifted by increasing temperature (and hydrophobicity), Figure 4.4 B.

The *trans*-chalcone form may also be used as a probe for determination of the critical micellar concentration (CMC), by representing its shift in absorption maximum as a function of the polymer concentration, at different and constant temperatures, Figure 4.4 C. While at 39.2 ^{0}C the absorption maximum of **Ct** does not change by increasing polymer concentration (from 0.9 % to 30 %) because micelles are always present, at 9.2 ^{0}C the CMT can be detected, see Figure 4.4 C. On the other hand, it is not possible to sense the sol-gel transition, which is observed at 39.2 ^{0}C for polymer concentrations higher than 20 %.

In the case of the absorption wavenumber maximum of **AH**$^+$, it increases with increasing concentration of the polymer independently of the temperature, Figure 4.4 D. The red shift observed with increasing pluronic concentration can be due to the decreasing polarity afforded in the water phase by the micellar solubilization. This is as expected for flavylium compounds, characterized by π-π^* transitions with strong charge-transfer character, which present negative solvatochromism.[5] Nevertheless, this species is insensitive to the micelles or gel formation most probably because it remains in the water nanophase for all polymer concentrations.

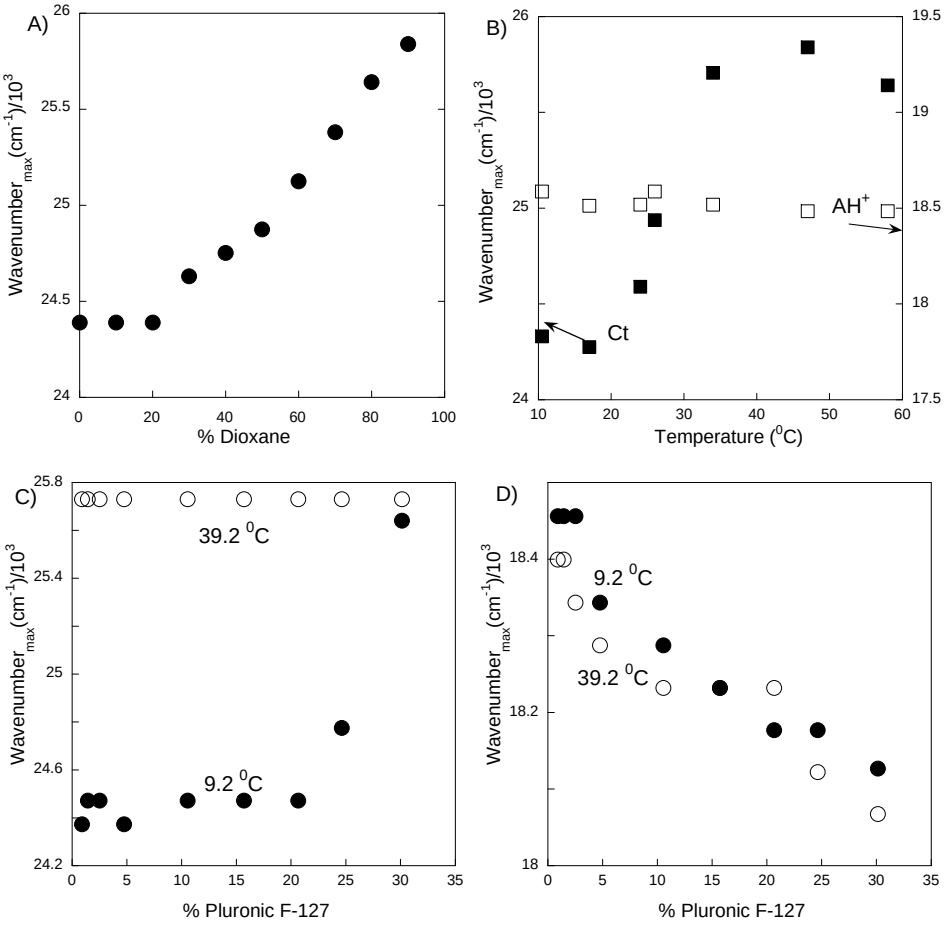

Figure 4.4 – Energy of the S_0->S_1 electronic transition of **Ct** and **AH**$^+$ of **DAF**: A) in mixtures water/1,4-dioxane; B) in the presence of Pluronic F127 (1.5%) as a function of the temperature, pH=6.0 (■) and pH=2.0 (□); C) **Ct** and D) **AH**$^+$, as a function of the pluronic concentration at 9.2^{0}C (●) and 39.2^{0}C (○).

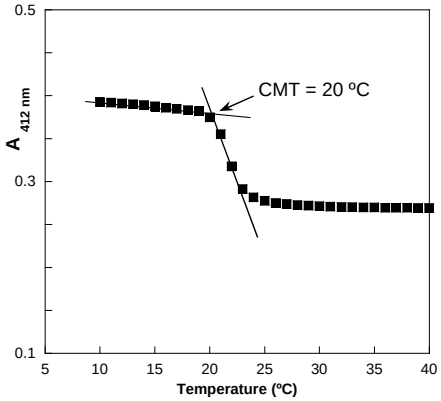

Figure 4.5 – Absorption at 412 nm (**Ct** in water) versus temperature in 5 % Pluronic F127 solution. Illustration of how can **Ct** absorption maximum be used to determine CMT, in this case 20 ºC.[3b]

In conclusion, according to the data reported in Figures 4.4 and 4.5 **Ct** is distributed in the micelles phases (for the moment without evidence for a specific location), while **AH**$^+$ remains most probably in the water phase.

The equilibrium distribution and the pK'_a are affected when preferential stabilization of one of the species takes place. The pK'_a in water is practically independent on the temperature (Supplementary Material section 9.4). In the presence of the pluronic (at any concentration) the acidity constant always increases because **Ct** is (relatively to **AH**$^+$) stabilized by the polymer. In

the case of 1.5% of Pluronic the dependence is approximately a sigmoid with a transition that is compatible with a critical micelle temperature (CMT) of 20 ^{0}C as previously reported.[2] At 30 % of Pluronic the pK'_a reaches a plateau which is only compatible with a sol-gel transition that was previously reported in literature to occur at ca. 18 ^{0}C.[2] However, the pK'_a in the presence of micelles formed at lower temperature for 30% of polymer is higher than the one observed at higher temperature for 1.5 % of polymer. This behavior can be explained if the decreasing of polarity in the water phase, by increasing polymer concentration is taken into account. It is known that flavylium cation is more soluble in ethanol than in water, and by consequence it could be expected a stabilization of $\mathbf{AH^+}$ at 30% of Pluronic when compared with 1.5 %, as shown in Figure 4.6 A.

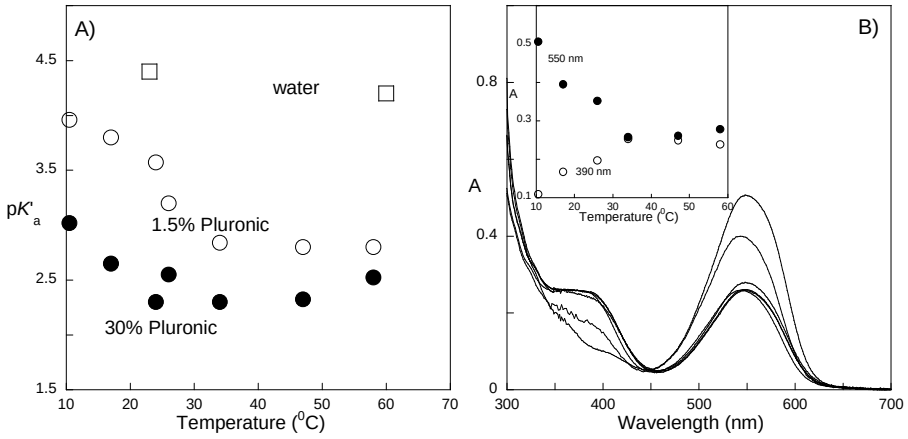

Figure 4.6 – A) pK'_a vs. temperature for water (□), 1.5 % (○) and 30% (●) of Pluronic F127. B) Spectral variations of **DAF** in the presence of Pluronic F127 30% at pH = 2.6, as a function of temperature.

However, at pH = 2.6 (30 % of Pluronic), Figure 4.6 B, the equilibrium that is established between $\mathbf{AH^+}$ and **Ct** is clearly shifted by raising the temperature, and the fraction of **Ct** is increased at the expenses of $\mathbf{AH^+}$/**A**. In other words, the shift of the equilibrium towards **Ct** is a result of the increasing of the less polar environment surrounding **Ct**, as expected if the gel is formed, the phase transition taking place at *ca.* 18 ^{0}C, see inset of Figure 4.6 B. At this polymer concentration the micelles are already formed at the lower temperature and by consequence the observed changes can be attributed to the gel formation. Inspection of the inset of Figure 4.6 B indicates that the equilibrium between **Ct** and $\mathbf{AH^+}$/**A** can be used as a sensor to determine the critical gel temperature.

Either in the presence of micelles of Pluronic F127 (1.5 %) or incorporated in a gel (30 %), the uncolored **Ct** species gives rise to the formation of the pink-red $\mathbf{AH^+}$ or **A** species, upon irradiation. The system is completely reversible in a time scale that depends on pH, temperature and percentage of polymer used. In Figure 4.7, some details of these photochromic reversible systems are shown.

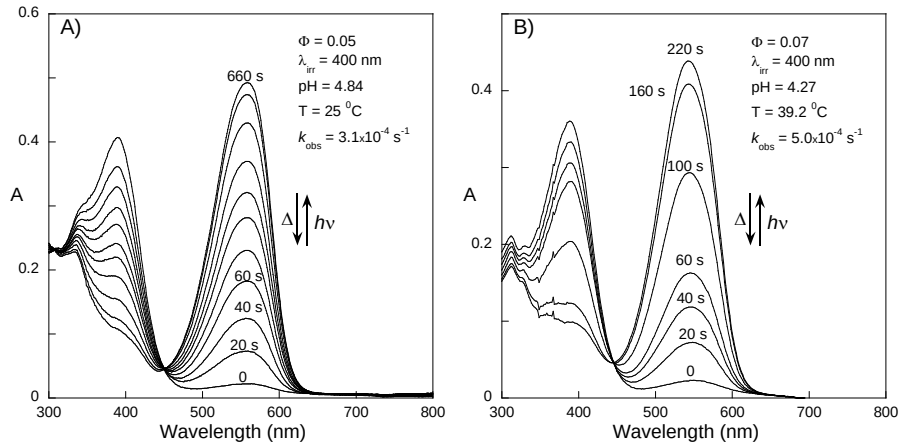

Figure 4.7 – A) Spectral variations of **DAF** incorporated in a 30 % Pluronic F127 gel. B) Spectral variations of **DAF** dissolved in micelles of Pluronic F127 (1.5%).

Traces of the transient absorptions after flash of **DAF** in the presence of the gel (Pluronic F127, 30 %, 45 ^{0}C,) are shown in Figure 4.8. Identical traces were obtained for micelles (1.5 % of the Pluronic F127, 45 ^{0}C). The transients were monitored at 400 nm (**Ct**) and 540 nm ($\mathbf{AH}^+$). Two parallel processes following the same first order rate constant take place: one leading to the formation of the photoproduct and the other recovering (partially) the **Ct**. As shown previously the experimental results can be accounted, in the simplest model, by equation 2.9:

$$k_{flash} = k_i{}^m \frac{K_t{}^m}{1+K_t{}^m} + k_{-h}{}^m \frac{\left[H^+\right]}{1+K_t{}^m} \qquad (2.9)$$

where the superscript *m* refers to micelle - all the events monitored by the flash photolysis occur inside the micellar environment.

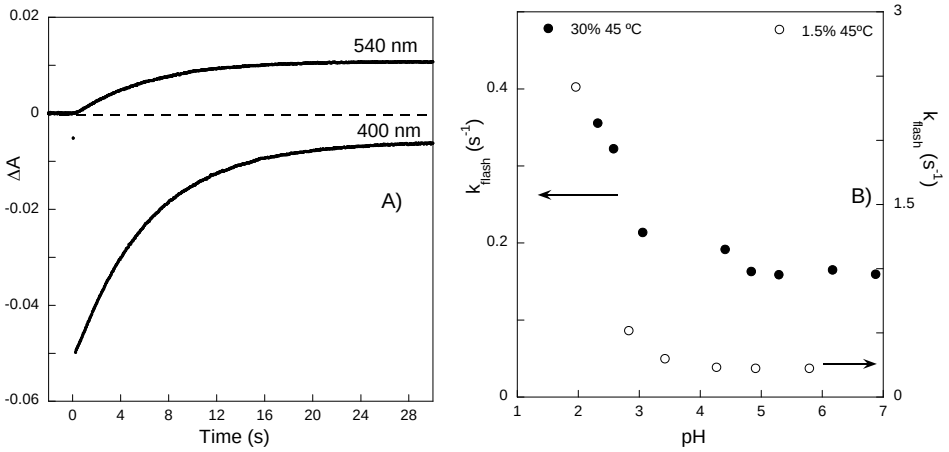

Figure 4.8 – A) Transient absorption traces of the **Ct** (400 nm) and $\mathbf{AH}^+$ species (540 nm), pH = 5.3 T = 45 ^{0}C for a gel 30 % Pluronic F127, both curves decay with the same rate constant. B) Plot of the rate constants obtained at 45 ºC, for 30 % Pluronic F127 (gel ●) and 1.5 % Pluronic F127 (micelles ○).

In equation 2.9 the first term accounts for the recovering of **Ct** while the second, which is proton dependent refers to the process leading to the photoproduct. According to the model, once $\mathbf{AH}^+$ is formed it is expelled to the hydrophobic environment where it is more soluble. Fitting of the date reported in Figure 4.8 allows constructing Table 4.1. The transient absorption traces obtained after flash the **Ct** species (leading to **Cc**) allowed us to conclude that the recovering reaction (**Cc**-**Ct**) is slightly faster in micelles than in gels which can be attributed to a higher viscosity in the gel. However, the formation of the photoproduct is significantly slower in the case of the gels, which is probably due to smaller water availability in the gels

Table 4.1 – Parameters from the fittings of experimental points in Fig. 4.8 with eq. 2.9.

T=45 ^{0}C	**1.5% F-127 micelles**	**30% F-127 gel**
$k_i^m \frac{K_t^m}{1+K_t^m}(\mathrm{s}^{-1})$	0.22	0.17
$\frac{k_{-h}^m}{1+K_t^m}(\mathrm{M}^{-1}\mathrm{s}^{-1})$	200	43

To summarize, the pK'_a was found to be a relatively good sensor for CMC and also for detection of the sol-gel critical gel temperature. In the presence of Pluronic F127 the equilibrium constant increases dramatically from pK'_a = 4.4 in water to pK'_a = 2.5 (in gels). So far, the results point out to those previously known for other compounds, extending and confirming published results.[2]

In order to get more insight regarding the photochromic mechanism, fluorescence and fluorescence anisotropy measurements were performed. A concentration of 20 % Pluronic was chosen, because micelles (at room temperature) and gels (at 40 ºC) are formed. The pH was set in all subsequent experiments to 6, because **A**, the most emissive species in the system, is formed in an appreciable amount and **Ct** is not yet deprotonated. In the subsequent sections of this paper, we will present a series of experimental results, obtained through independent techniques, which corroborate three main conclusions: 1) the **Ct** photochromism is enhanced in pluronic media compared with aqueous solutions because a competing non-radiative internal charge transfer state (ICT) is suppressed in less polar environments; 2) there is a non-uniform distribution of molecules in Pluronic micelles or gels and a selective photochemistry from the **Ct** species that are not in core could be detected; 3) there is a very small barrier in the excited state potential surface of **Ct** for the formation on the non-radiative ICT state.

4.3 Ct and A from DAF in pure solvents

In order to explain the different photochromic behaviors in aqueous solutions and in Pluronic micelles as well as in gels, the photophysics of *trans*-chalcone and its connection with the production of flavylium species was studied in different solvents. Evidence that photoisomerization occurs in the singlet excited state was reported in chapter 3. Therefore, the

photophysical studies carried out in this chapter were focused on the characterization of the **Ct** singlet excited state (mainly its fluorescence behavior).

The fluorescence of chalcone type molecules is not a straightforward issue. The electronic transition into the S_1 state is reported to be an Intramolecular Charge Transfer (ICT) band with a large change of dipole moment. Reported chalcones having a donor-acceptor (D/A) structure lead to an increase of negative charge density in the carbonyl group upon excitation. In some cases, dual fluorescence was observed and assigned to two excited states: a locally excited state (LE – short wavelength emission) exhibiting already some ICT character, and an ICT (long wavelength emission), that in some cases is assigned to a TICT state.[6,7] In other cases, the excited polar state is connected with a non-emissive ICT state.[7,8] The fluorescence behavior is strongly dependent on the nature and position of the substituents in the *trans*-chalcone structure and solvent polarity.[6] *Trans*-chalcones and related compounds also exhibit very large solvent-dependent Stokes shifts (e. g. more than 5000 cm^{-1}) which has been explained with large changes of dipole moment, formation of hydrogen bonds or vibrational relaxation in the singlet excited states of these compounds.[9,6,8] The ICT non-radiative channels are important because they are competitive with *trans-cis* photoisomerization, the first step of the photochromic effect.

The **Ct** species of the compound under study was isolated as a powder (see experimental part) and its absorption and fluorescence spectra in a series of solvents were measured. Although the ^{1}H-NMR spectroscopy showed no evidence for the presence of the **A** species after dissolving the powder, a certain quantity of **A** was always spectroscopically detected in the organic spectroscopic solvents, probably formed due to presence of trace amounts of water,[10] or the presence of <5 % of **A** in the isolated powder (not detectable in ^{1}H-NMR), or even its photochemical production in certain solvents. This presence is always interfering in absorption and, specially, fluorescence measurements because, as described below, **A** species has a fluorescence quantum yield significantly higher than **Ct**. However, a large separation between the two spectra is found in most of the solvents, decreasing the impact of this interference on the measurements of the **Ct** fluorescence quantum yields.

The absorption spectra of the **Ct** under study shows pronounced solvatochromic red-shift (about 2300 cm^{-1} on going from toluene to water), *see* Figure 4.9 A. Fluorescence spectra were measured in aprotic and protic solvents exciting the samples at 390 nm. The most evident result is the very weak fluorescence in the highly polar protic solvents (water) and the large Stokes shifts found in all solvents (about 5000 cm^{-1}), see Figure 4.9. In weakly polar solvents (tetrahydrofuran (THF), toluene and dioxane) it is possible to identify a small fluorescence peak, presumably of the LE state or appearance of vibrational structure (see the case of THF in Figure 4.9 B and the arrow pointing to this fluorescence peak).[6] The solvatochromic shifts found in emission are of the same order of magnitude of those found in absorption, see Figure 4.9 C, and both have a linear correlation with the empirical solvent polarity scale $E_T(30)$.[11] This polarity scale is a measure of both dipolar and proton donor ability aspects of the solvent used,

and from this correlation it is concluded that dipolar solute-solvent interactions and hydrogen-bond interactions play a major role on the **Ct** solvatochromism in both absorption and emission spectra. It is also known that in D/A chalcones the Stokes shifts are about 3000 cm^{-1} in apolar solvents and 7000 cm^{-1} in polar solvents[6], but in our case they are approximately constant, even in very different solvents. The poor solvent effect of the Stokes shifts was surprising, considering the charge transfer character of the electronic transitions and its large solvatochromic shift. A possible interpretation for this result is the D/A/D type structure of the molecule: two hydroxyl groups acting as donors from the olefinic side of the carbonyl, one dimethylamino group acting as a strong donor on the opposite side, and finally the carbonyl being the acceptor moiety at the center of the molecule. An increase of the charge density of the carbonyl group occurs in the electronic transition, but without a strong variation in the excited state dipolar moment. A significant change in the quadrupolar moment would justify the large solvatochromic shifts of the absorption and emission peaks, but without any significant changes of the Stokes shift. This lack of solvatochromic effect on the Stokes shifts has an additional implication: the possibility of finding time-dependent Stokes-shifts due to solvent reorganization (solvation dynamics) is reduced and could be important only on the femtosecond timescale. Therefore, possible time-dependent Stokes shift on a picosecond or nanosecond timescale of this molecule will be attributed to other photophysical features of **Ct**, not to solvation dynamics. This will be important for the discussion below regarding time-resolved fluorescence experiments in Pluronic media.

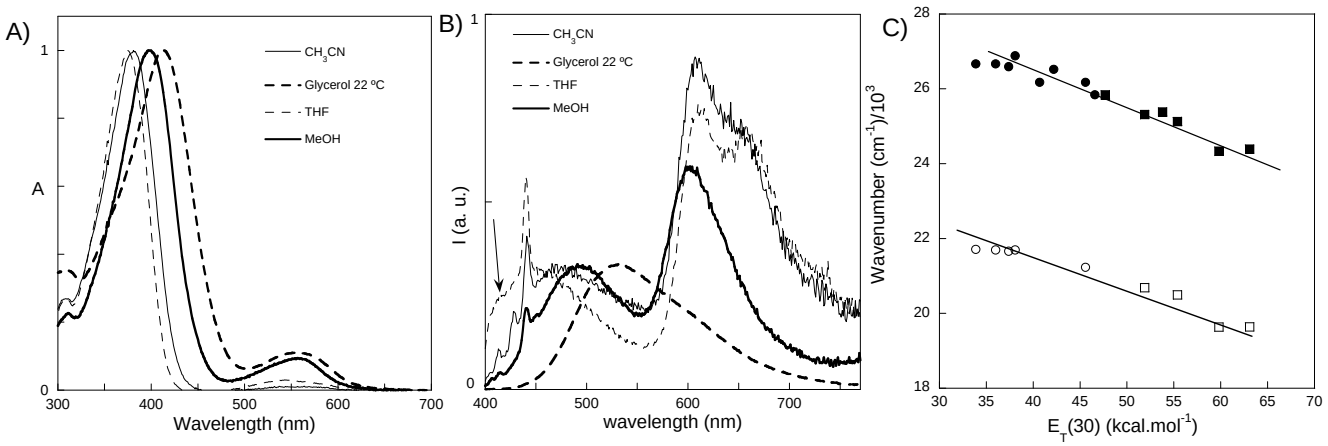

Figure 4.9 – A) Normalized absorption spectra of **Ct** and **A** species of **DAF** in tetrahydrofuran, acetonitrile, methanol and glycerol. B) Normalized emission spectra in the same set of solvents, exciting at 390 nm. C) Maximum wavenumber (cm^{-1}) in various solvents as a function of $E_T(30)$ of the solvent, open points refer to emission peaks (○ aprotic solvents, □ protic solvents) and filled ones to absorption peaks (● aprotic solvents, ■ protic solvents)

Another way to rationalize the solvatochromic dependence of absorption and emission spectra is the linear solvation correlations with Kamlet-Taft parameters.[12] This is a multiparametric empirical polarity scale, which takes the following form:

$$\bar{\nu} = \bar{\nu}_0 + p(\pi^* + d\delta) + a\alpha + b\beta \qquad (4.1)$$

in which π*, δ, α and β, are respectively measures of the solvent dipolarity, polarizibility, proton donor ability and proton acceptor ability.[12] The slopes *p, d, a* and *b* indicate the linear relationship between a given solute property and each solvent polarity parameter. The $E_T(30)$ polarity scale can, in fact, be a function of π* and α.

In the present case study, a dependence on π* and α was found as expected, which is similar in absorption and emission measurements and not significantly influenced by the β parameter, see Table 4.2, corroborating our previous conclusions from the correlation with $E_T(30)$.

Table 4.2 – Correlation of **Ct** absorption and emission maxima (exciting at 390 nm) with Kamlet-Taft parameters.

	$\bar{\nu}_0$ (cm^{-1})	*p* (cm^{-1})	*a* (cm^{-1})	r^2	number of solvents
Absorption	27180±260	-1020±390	-1530±140	0.94	15
Emission	22330±270	-1150±450	-1230±140	0.96	9[a)]

[a)] Please note that fewer solvents were used in the emission, because in some cases there is overlapping of emission spectra with Raman peaks or **A** fluorescence.

As mentioned above the quinoidal base species **A**, the final photochromic product of **Ct** (pH = 6.0), appears in our solutions with small intensity in the absorption spectra, but intense emission bands due to its much higher fluorescence quantum yields compared with **Ct**, even when exciting at 390 nm where its extinction coefficient is small see Figure 4.9 A and B. The species **A** exhibits a structured absorption and emission in aprotic solvents, with Stokes shifts around 2000 cm^{-1}, while in protic solvents both absorption and emission spectra lose the vibrational resolution, probably due to solute-solvent H-bonds formation.

The fluorescence quantum yields of all species are always very low, an exception being **A** in some protic solvents and aqueous Pluronic media (Table 4.3). **Ct** fluorescence quantum yields in a variety of protic solvents were calculated. The following Arrhenius law can be written:

$$\frac{1}{\Phi_f} - 1 = \frac{k_{nr}}{k_f} = \frac{k_{nr}^0}{k_f} e^{-\frac{E_a}{RT}} \qquad (4.2)$$

Considering that the non-radiative activation barrier is stabilized by solvent polarity, one expects a decrease of the activation energy with solvent polarity and consequently an increase of the non-radiative rate constant. Then one can write the following empirical formulation,[13] taking into account that k_f depends on the square of refractive index of the solvent:

$$\ln\left[\frac{1}{n^2}\left(\frac{1}{\Phi_f}-1\right)\right] = \ln\frac{k_{nr}^0}{k_f^0} - \left(\frac{E_a^0}{RT} - \gamma E_T(30)\right) \tag{4.3}$$

This equation implies a linear relationship between the non-radiative activation energy and the $E_T(30)$ polarity scale of the solvent, and was experimentally verified in protic solvents, Figure 4.10 A. In aprotic solvents (not shown) the results were not conclusive a problem that is still under study.

Table 4.3 – Fluorescence quantum yields in different media.

	AH^+	Ct	A	Ct^{2-}
water	0.05 %	0.05 %	0.3 %	0.2 %
Organic media		Methanol 0.1 %	Methanol 8 %	
		Ethanol 0.4 %	Ethanol 30 %	
		Decanol 0.8 %	Decanol 36 %	
Viscous Media	Sucrose (67 %)	Glycerol 2.5 %		
	aq. solution 2 %			
Pluronic 20 % (gel,40 ºC)	0.5 %	0.5 %	18 %	

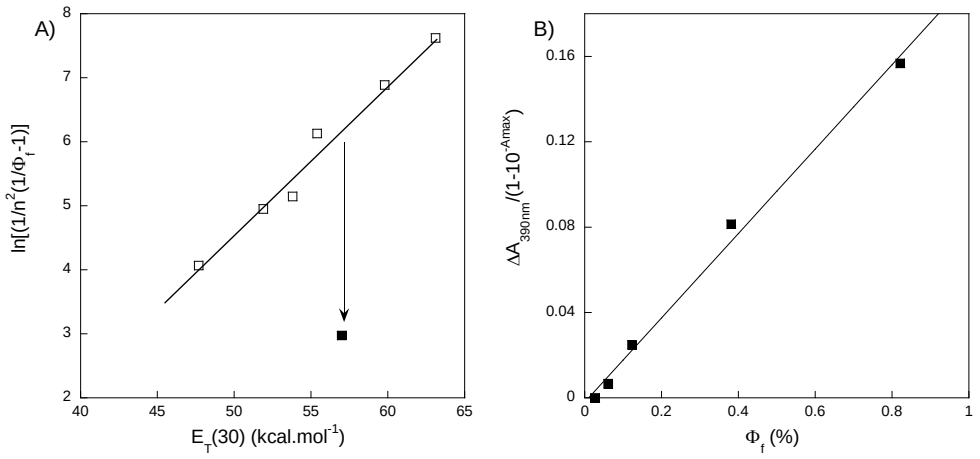

Figure 4.10 – A) $\ln[1/n^2(1/\Phi_f-1)]$ as a function of $E_T(30)$ of the solvent, □ protic solvents and ■ glycerol. B) Variation of absorbance at 390 nm immediately after the flash, corrected for the absorption of light, as a function of the fluorescence quantum yield in percentage, for protic solvents.

The positive solvatokinetic effect found in protic solvents indicates a strong solute/solvent hydrogen-bond interaction in the singlet excited state. It is known in the dimethylaminobenzonitrile (DMABN) molecule (the model compound of the TICT process) that strong hydrogen-bonding appears in protic solvents such as methanol.[14] This led to the conclusion that three states in DMABN exist in hydroxylic solvents: a LE state and the TICT state, but also a so-called HICT state due to hydrogen-bond interaction between the solvent and the solute amino group.[14] On this basis, a possible explanation for the data reported in Figure 4.10 A is the formation of HICT state.

Flash photolysis experiments were also performed in hydroxylic protic solvents (Figure 4.11).[15] The decreasing of the **Ct** absorption after the light flash, corrected for the initial absorbed light (since in this case, excitation is performed with white light, the correction was made with the maximum absorption), a quantity proportional to the isomerization quantum yield (Φ_{iso}), was represented *versus* the fluorescence quantum yield Φ_f, Figure 4.10 B. For each solvent equation 4.4 describes the relation between these two quantum yields.

$$\Phi_{iso} = \frac{k_{iso}}{k_f}\Phi_f \tag{4.4}$$

Therefore, the linear relationship found implies that the ratio k_{iso}/k_f is almost constant, and knowing that k_f is not expected to change significantly with the solvent (taking into account that the square of the refractive index within the solvents used does not vary significantly), the same is valid for k_{iso}. The following conclusions can be derived:

i) The *trans-cis* isomerization is almost solvent polarity independent and the solvent effect observed in the ϕ_{iso} should be attributed to the additional ICT non-radiative process. This striking result points out to a non-polar pathway for *trans-cis* isomerization process of this chalcone.

ii) Since the ICT non-radiative process dominates the solvent dependence of the **Ct** singlet-excited state deactivation, environments in which **Ct** has a higher ϕ_f are also expected to give rise to higher photochromism, provided the solvent viscosity is kept fairly constant.

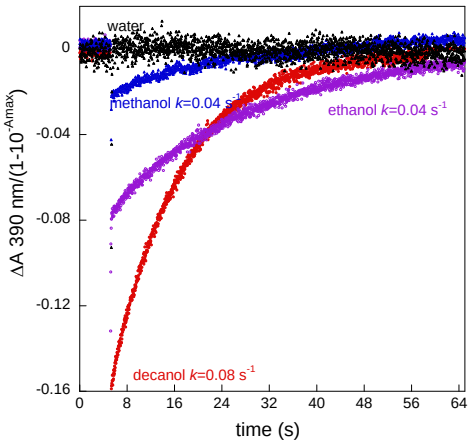

Figure 4.11 – Flash photolysis traces obtained in water, methanol, ethanol and decanol, following the variation in absorption at 390 nm. First order rate constants are shown.

Finally, the very high viscosity of glycerol suppresses non-radiative decays, including ICT and photoisomerization, enhancing significantly the fluorescence quantum yields of **A** and **Ct**, and does not correlate with the other solvents, see the experiment point for glycerol in Fig 4.10 A.

It is worth noting that both **Ct** and **A** present particularly low fluorescence quantum yield in water, and there is no photochemistry, which is an extreme case due to the high polarity of water (ICT deactivation), thus explaining why no significant photochromism is observed in aqueous solutions. Below, we discuss how the less polar environment of micelles or gels triggers photochromism.

The fluorescence quantum yields of the quinoidal base **A** have a similar trend with $E_T(30)$, and the conclusions presented for the **Ct** non-radiative processes could be also applied for **A**, Figure 4.12. However, **A** has much higher fluorescence quantum yields, which indicates the importance of the rigid structure of these molecules. The photophysics of **A** was not further explored in the context of this work, however previous studies support the existence of a non-radiative TICT state as well.[16]

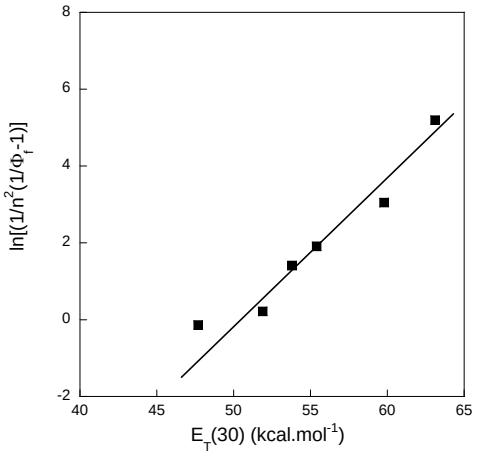

Figure 4.12 – $\ln[1/n^2(1/\Phi_f-1)]$ for **A** species in protic solvents as a function of $E_T(30)$.

4.4 Photophysics of Ct from DAF in Pluronic medium

In Figure 4.13, the absorption and emission spectra of **DAF** in a Pluronic gel before irradiation and in the photostationary state (PSS) are shown. The species **Ct** and **A** appear in both cases and do not change their spectral shape after irradiation. However, after irradiation the intensity of **A** increases at the expense of **Ct** in both absorption and emission measurements, indicating the photochromic reaction of **Ct** species in this medium. Evidence for the accumulation of **Cc**[17] or other species such as **B** is not found (although accumulation of **B** cannot completely be ruled out, since this species absorbs light in a spectral region in which Pluronic polymer absorbs light as well).

Fluorescence quantum yields of both species in Pluronic gel (20 %, 40 ºC) were calculated in the PSS. For **Ct** the value is equal to 0.5%, which is in keeping with values measured in *n*-decanol (0.8%), but still significantly lower than in glycerol (2.5 %). It is, nevertheless, one order of magnitude higher than in water (0.05 %). Viscous drag and polarity effects might play an important role on this result. For **A**, a fluorescence quantum yield equal to

18% (excitation at 530 nm) was measured, close to the values measured in alcohols (in methanol is 8 %) and orders of magnitude higher than in water (0.3 %). So like **Ct**, **A** also resides in a low polarity environment within the micelle, although the result also suggests that **A** is on a slightly more hydrophilic media.

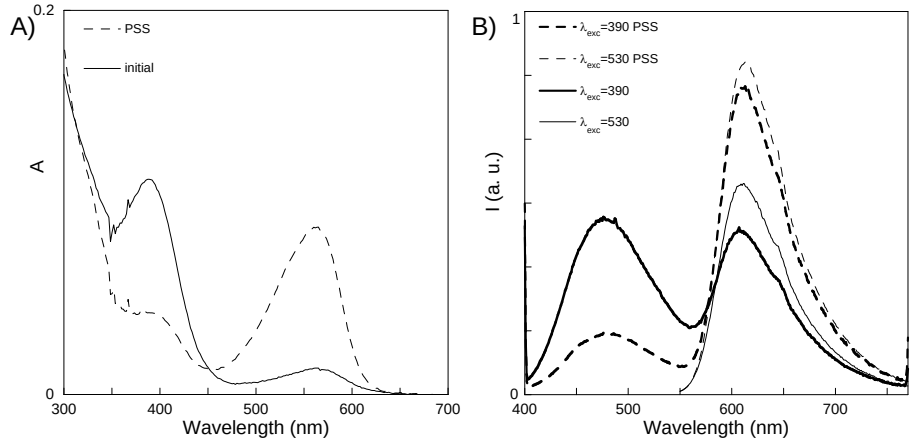

Figure 4.13 – A) Absorption of the Pluronic gel, F127 20 %, at 40 ºC pH = 5.9, containing **DAF**, before irradiation (full lines) and on the photostationary state (PSS, traced lines). B) The same for emission spectra exciting at 530 nm (thin lines) and at 390 nm (thick lines).

In the PSS, the change of the emission spectra as a function of the excitation wavelength was measured (see Figure 4.14). The emission peak shifts about 1500 cm^{-1} by changing the excitation wavelength from the blue to the red edge of the **Ct** absorption spectrum. From these spectra, the maxima emission were retrieved and plotted versus excitation wavenumber, Figure 4.14 B. It is clear that the emission spectra are strongly dependent on the excitation light, and three stages were found: for higher wavenumbers of excitation there is initially a steep red shift, followed by a less pronounced red shift, and finally at the red edge of the absorption spectra the red shift becomes again quite pronounced. In the **A** emission band this effect was not observed (Figure 4.15 B). The phenomenon observed in **Ct** is not exclusive to pluronic media, and is also observed, e.g., in methanol (Figure 4.15 A).

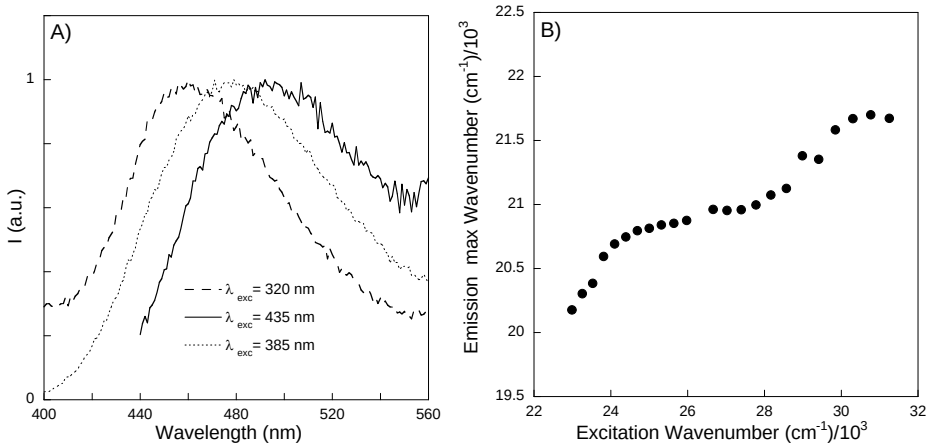

Figure 4.14 – A) Emission spectra of the compound **DAF** in Pluronic gel, F127 20 %, at 40 ºC, pH = 5.9 at different excitation wavelengths. B) Representation of the maximum wavenumber of the emission band (it was obtained through the fitting of a Lorentzian to the points near the maximum of the band) versus the excitation wavenumber.

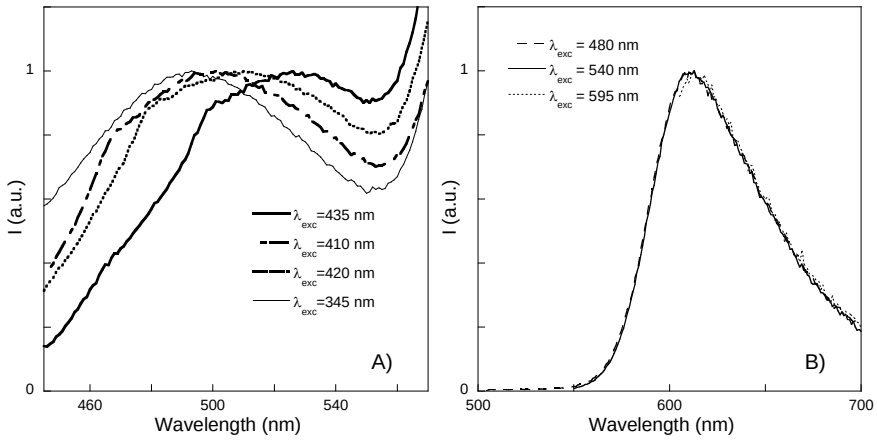

Figure 4.15 – A) Emission spectra of **Ct** from **DAF** in methanol at different excitation wavelengths. B) Emission spectra of **A** from **DAF** in Pluronic gel, F127 20 %, at 40 ºC, pH = 5.9 at different excitation wavelengths.

This type of effect is called Red Edge Effect (REE) and can be provoked by the following reasons extensively described in the literature:[18] i) the presence and simultaneous excitation of two or more species, either species in different environments or different conformers;[19] ii) the absence of an activation barrier in the excited state potential surface (barrierless process for the formation of a non-radiative excited-state species);[20] iii) slow solvation dynamics compared with the molecule fluorescence lifetime.[8]

The first reason can be easily applied in this case, since **Ct** molecules may be distributed in different environments of the polymer large size molecular aggregate (the Pluronic micelles present a hydrophobic core radius *ca* 4.4 nm and a more fluid and hydrophilic corona,[21] being the hydrodynamic radius of *ca* 10.2 nm,[3] and the aggregation number *ca* 50[21]). However, the presence of a nearly barrierless process cannot be excluded, due to the low fluorescence quantum yields of **Ct** and also because REE is observed in methanol as well. Solvation dynamics has been observed in Pluronic matrixes[22] of and also for a similar chalcone in alcoholic solvents.[8] However, this process is excluded based on our measurements in pure solvents (see previous section), in which no solvent-dependent Stokes shift is observed, a requirement for the observation of significant solvation dynamics on such a long timescale.

To gain information about the mechanism that gives rise to REE effect, fluorescence decays were measured (see Figure 4.16) at different emission wavelengths in Pluronic gel. The absence of a significant activation barrier in the excited state implies the observation of non-exponential fluorescence decays that are wavelength dependent and approach a monoexponential behavior at long wavelengths.[20] The results obtained have many of the features described for a barrierless process, see Figure 4.16 and Table 4.4, including fast decays at higher energies contemplated by this theory and an exponential tail *ca.* 2.6 ns present at all wavelengths. These fluorescence decays are also incompatible with pure multi-state decay kinetics, because in such case the emission at the red-edge would come from species in more polar/hydrophilic and fluid environment. In that case, the fluorescence decays would have an opposite trend with the emission wavelength. Indeed, for **Ct** in the core, blue shifts of

absorption and emission spectra are expected to occur, while in more aqueous environments red-shifted absorption and emission spectra would appear. The exponential long tail seems to be the same in all cases, which is again a sign of a nearly barrierless process. It is worth noticing, however, that at the red-edge there is still a significant amount of fast decay component, and no rise-time is observed. Such result is in agreement with the presence of **Ct** in hydrophilic environment, and while barrierless kinetics dominates the photophysics, multi-excited-state kinetics is operative as well. This effect will be more evident on time-resolved fluorescence anisotropy measurements shown below.

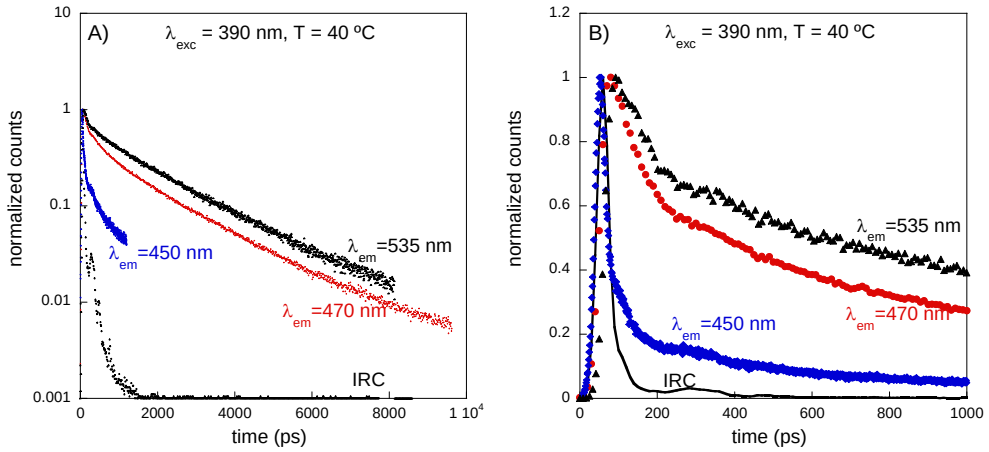

Figure 4.16 – A) Fluorescence decays 20 % Pluronic F127, pH = 5.9, λ_{exc} = 390 nm, after irradiation, T = 40 ºC, λ_{em} = 450 nm (1.3 ps/channel), λ_{em} = 470 nm (10 ps/channel), λ_{em} = 535 nm (8.4 ps/channel). IRC – Instrument Response Curve. B) Expansion of A) for shorter times. On A) the normalized counts are on logarithmic scale, while in B) the scale is linear (in order to visualize the shorter components of the fluorescence decay).

In conclusion, although the presence of multi-excited-states cannot be excluded, the **Ct** photophysics in pluronic media is dominated by the ICT non-radiative state described previously in pure solvents. In effect, the isomerization and fluorescence quantum yields account only for *ca.* 10% of the decay processes. The ICT process is nearly barrierless, as can be seen by the emission wavelength dependence of the fluorescence decays and from the REE phenomena. Considering that the ICT non-radiative process is strongly dependent of the solvent polarity, a completely barrierless process does not seem to be the case as well, which points out for a barrier around 10 kJ.mol^{-1} or less.[23] The striking effect of pluronic aqueous media on **Ct** photochromic behavior will be discussed in the next section.

4.5 Photochromic mechanism in Pluronic media

Continuous irradiation of **Ct** species in Pluronic media was achieved using the excitation light from the spectrofluorimeter. These experiments allowed the simultaneous determination of both fluorescence intensity and anisotropy at a given emission wavelength as a function of irradiation time. This is, therefore, a very useful technique to probe how **Ct** is transformed into **A** under irradiation. Irradiation (in these conditions) of **Ct** samples at 390 nm

leads to a strong decrease of **Ct** fluorescence with time. Simultaneously, an increase of **A** emission intensity is observed, as expected, confirming the photoconversion of **Ct** into **A**. Steady state fluorescence anisotropy, however, provides a different type of information. Its value depends of the fluorescence lifetime of the fluorophore and its rotational dynamics: fluorescence anisotropy increases with decrease of fluorescence lifetime or higher viscosity, and vice-versa, as can be seen for the simplest case of a fluorophore with a single fluorescence lifetime with an isotropic rotation:

$$\frac{r_0}{r_{ss}} = 1 + \frac{\tau}{\phi_R} \tag{4.6}$$

where r_0 is the fluorophore fundamental anisotropy, r_{ss} is the experimental steady state fluorescence anisotropy, τ is the fluorophore fluorescence lifetime and ϕ_R is the rotational correlation time.

Being independent of the solute concentration, it provides important information about the environment of the molecule under irradiation. Initially the anisotropy of **Ct** is close to 0.3, a consequence of its short fluorescence lifetime that does not allow rotation of the molecule, see Figure 4.17 A and results below. Then, as irradiation proceeds, the anisotropy decreases to 0.23, which is attributed to the increase in the lifetime of molecule, see below, and indicates different environments before and after irradiation for **Ct**. Meanwhile, **A** is being excited to its S_2 excited state and exhibits a much lower and constant value for anisotropy, a direct consequence of non-parallel absorption and emission transition moments. This result shows that **A** is always in the same medium during irradiation.

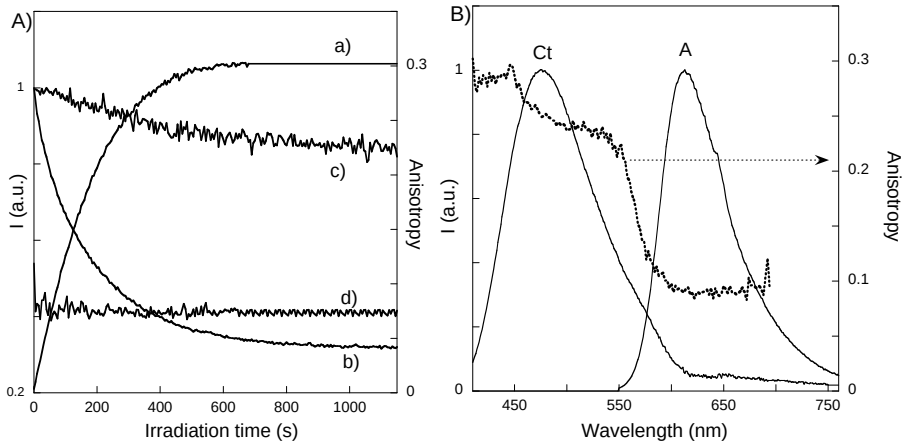

Figure 4.17 – A) 20 % Pluronic F127, pH = 5.9, T = 40 ºC, slits excitation-emission 10-2 nm, λ_{exc} = 390 nm a) emission intensity at the magic angle λ_{em} = 620 nm (**A**); b) emission intensity at the magic angle λ_{em} = 470 nm (**Ct**); c) anisotropy λ_{em} = 470 nm (**Ct**); d) anisotropy λ_{em}=620 nm (**A**). B) Fluorescence anisotropy of the photostationary state: 20 % Pluronic F127, pH = 5.9, T = 40 ºC, λ_{exc} = 390 nm on a previously irradiated cell as a function of the emission wavelength. Normalized emission spectra of the species **Ct** (obtained upon decomposition) and **A**.

Figure 4.17 B displays the anisotropy as a function of wavelength of emission at the PSS, and corroborates what was previously reported for **Ct** and **A**. Moreover, it shows that anisotropy of **Ct** is higher for shorter wavelengths, which is congruent with the results of Figure 4.16 where a shorter average fluorescence lifetime for shorter wavelengths is observed.

Figures 4.18 and 4.19 A indicate that the **Ct** fluorescence quantum yield is increasing upon irradiation. This result is only explainable if there is a non-uniform distribution of **Ct** molecules in Pluronic micelles/gels. Figure 4.18 shows an increasing emission intensity of **Ct**, corrected for the absorbed light, during irradiation as the PSS is approached. As reported in Figure 4.10 A the increasing on the fluorescence quantum yield occurs when the polarity decreases or the viscosity increases, as occur in the core of the Pluronic micelles. On this basis, as long as the irradiation takes place, the fraction of **Ct** molecules at the core increases. Moreover, the intensity of the **Ct** absorption and emission spectra decreases with irradiation time. This can only be explained if there is a selective photochemistry: the **Ct** molecules inside the rigid core of the micelle are essentially non-photoreactive (*trans-cis* photoisomerization is suppressed by the medium viscosity) and the **Ct** molecules in a more fluid environment originate **A** upon irradiation.

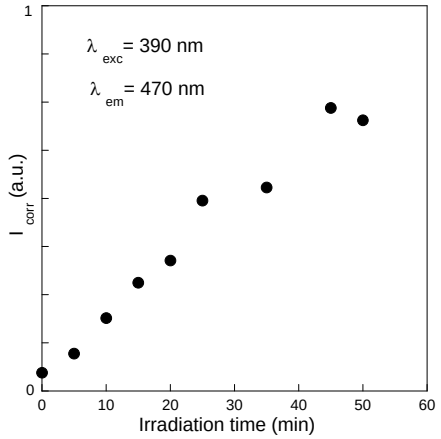

Figure 4.18 – Variation of the fluorescence emission intensity of the species **Ct** of **DAF**, λ_{exc}= 390 nm; λ_{em} =470 nm, upon correction for the absorbed light vs. irradiation time (λ_{irr}= 390 nm).

Figure 4.19 A constitutes an independent proof of this interpretation, as the fluorescence lifetime is shown to increase pronouncedly upon irradiation. Please note that it is rather cumbersome to obtain a lifetime before irradiation, since the measurement requires irradiation of the sample. In gels the irradiation area is small and stirring is not possible. Therefore, such measurement can only be performed in micelles. The fluorescence decays were analyzed with multiexponential kinetics (mainly tetra-exponential functions) Figure 4.19 A and B, Table 4.4. It is possible to see that upon irradiation the average lifetime of **Ct** increases from 0.42 ns to 1.69 ns, due to an increasing contribution from **Ct** species located in a more hydrophobic/viscous environment (*ca.* 2 ns). Also after irradiation the contribution from the shortest lifetime (*ca.* 15 ps) increases in agreement with emitting molecules located in a hydrophilic/fluid environment.

Upon gelation, the difference in the average lifetimes of **Ct** is not very pronounced. However, one can see from Table 4.4 that essentially the shorter lifetimes are affected, which might indicate that the water between the aggregates when the gel is formed increases its microviscosity.

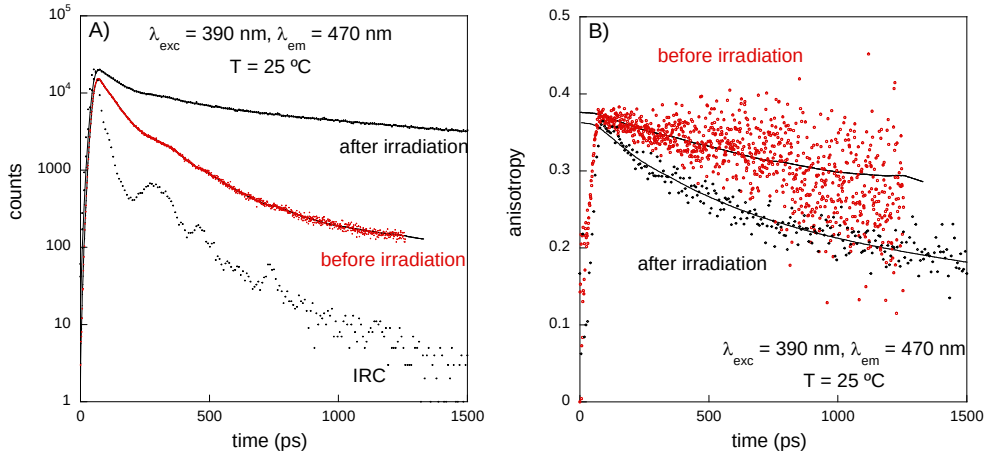

Figure 4.19 – A) Fluorescence decays 20 % Pluronic F127, pH =5.9, λ_{exc} = 390 nm, λ_{em} = 470 nm, T = 25 ºC, before irradiation (1.3 ps/channel) and after irradiation (7.5 ps/channel). IRC – Instrument Response Curve. B) Fluorescence anisotropy decays 20 % Pluronic F127, pH = 5.9, λ_{exc} = 390 nm, λ_{em} = 470 nm, T = 25 ºC, before irradiation (1.3 ps/channel) and after irradiation (6 ps/channel).

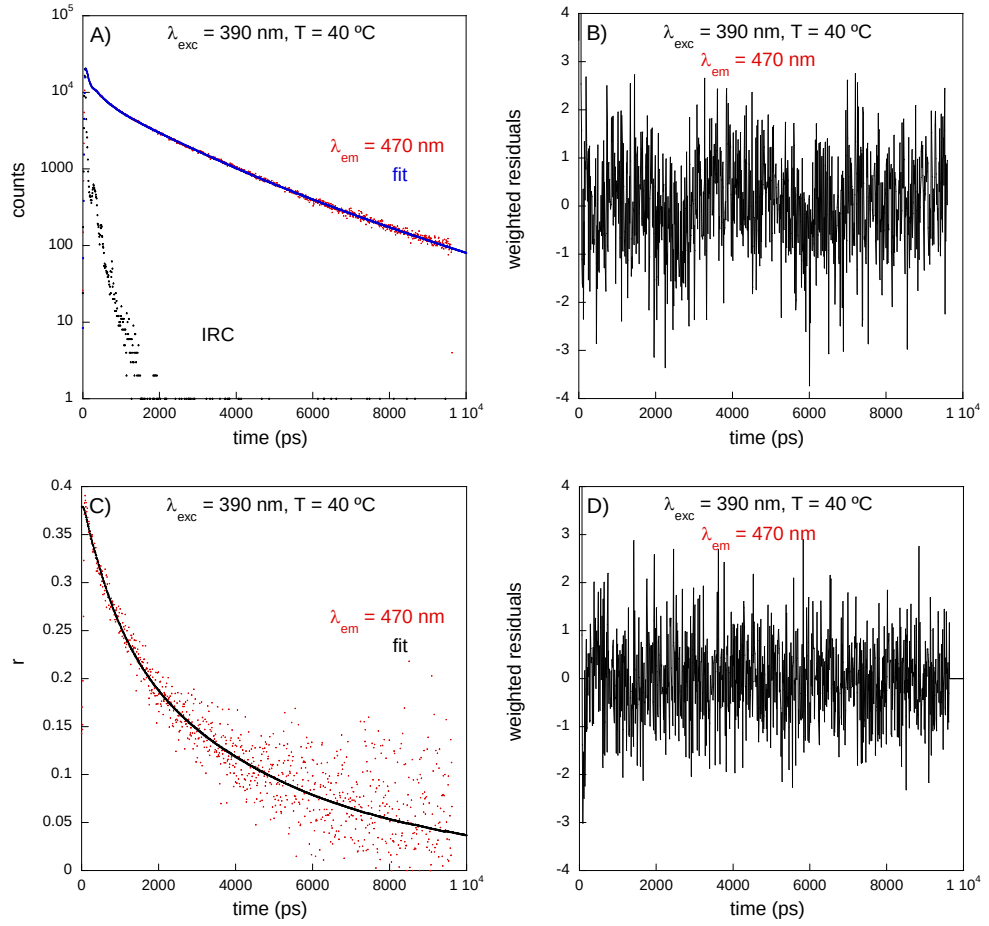

Figure 4.20 – Analysis of a fluorescence decay and a fluorescence anisotropy decay. A) Fluorescence decay 20 % Pluronic F127, pH = 5.9, λ_{exc} = 390 nm, λ_{em} = 470 nm, T = 40 ºC in PSS (10 ps/channel) and respective fitting. B) Weighted residuals for the fit in A). C) Fluorescence anisotropy decay 20 %

Pluronic F127, pH = 5.9, $\lambda_{ex\ c}$= 390 nm, λ_{em} = 470 nm, T = 40 ºC in PSS (10 ps/channel) and respective fitting. D) Weighted residuals for the fit in C) (for details see Table 4.4).

Time-resolved fluorescence anisotropy decays were performed in the Pluronic systems. In an isotropic medium, the anisotropy decay of a spherical solute can be described by:

$$r(t) = r_0 \exp\left(-\frac{t}{\phi_R}\right) \tag{4.7}$$

where the variables have the same meaning of equation 4.6. From these measurements, one has direct access to the values of r_0 and ϕ_R, which cannot be retrieved from the steady-state measurements, and therefore gain direct information about rotational relaxation processes within the micelle. Rotational relaxation of the whole micelle can be ignored, due to the large size of the molecular aggregate. Thus rotational processes can be attributed to the fluorophore inside the micelle, and its mechanism can be either isotropic rotational diffusion or a "wobble-in-cone" relaxation (when rotation is hindered in one of the directions of the polymer orientation within the micelle). Both effects give rise to an exponential relaxation formally equal to equation 4.7, but in hindered rotations a residual anisotropy value r_∞ is observed (the anisotropy decay does not go to zero). Multi-exponential anisotropy decays are observed when non-isotropic rotations are found or when there are more than one species in different environments.

According to our experimental results, the **Ct** fluorescence anisotropy decays in Pluronic micelles (T = 25 ºC) are bi-exponential (Figure 4.19 B and 4.20 C and D) in PSS conditions, with a fast component of 380 ps and a second slow component of about 4 ns. Before irradiation, however, the fast anisotropy relaxation is not observed, and the results can be fitted within experimental error with a single-exponential, leading to a rotational correlation lifetime of about 2.7 ns. Previously, bi-exponential anisotropy decays of coumarins and rhodamines in Pluronic matrixes were reported by other authors: the fast component was related to molecules in a more fluid environment that allows faster rotation, and the long component was attributed to the molecules more embedded within the micelles.[22,24] The same reasoning is applied to our work in PSS conditions, where no evidence of "wobble-in-cone" relaxation process is found (r_∞= 0). Before irradiation, the anisotropy decay displays very high experimental noise and it is difficult to unravel many details from this experiment, but the absence of the fast component is clear. It becomes evident that **Ct** molecules in a more fluid environment have an important contribution only after irradiation, while before irradiation the species residing in the micelle (probably in the corona) overshadow this fast component. When the gel is formed at 40 ºC, the fast component becomes slower, reflecting a viscosity enhancement of that environment.

Table 4.4 – Analysis of fluorescence decays 20 % Pluronic F127, pH = 5.9, λ_{exc} = 390 nm in the indicated conditions. 25 ºC = micelles, 40 ºC = gels.

Fluorescence Decays of Ct T=25ºC (470 nm)									
samples	a_1	τ_1 /ns	a_2	τ_2 /ns	a_3	τ_3 /ns	a_4	τ_4 /ns	χ^2
NI[1]	0.466	0.01[3]	0.381	0.05	0.148	0.15	0.005	1.96	1.06
I[2]	0.514	0.02	0.291	0.13	0.080	0.71	0.115	2.21	1.04
Fluorescence Decays of Ct T=40ºC (470 nm)									
λ_{em} /nm	a_1	τ_1 /ns	a_2	τ_2 /ns	a_3	τ_3 /ns	a_4	τ_4 /ns	χ^2
450	0.979	0.001[3]	0.012	0.05	0.006	0.32	0.003	2.62	0.96
470	0.547	0.05	0.210	0.27	0.187	1.45	0.056	2.96	1.05
535	0.040	0.01[3]	0.524	0.09	0.158	0.89	0.278	2.27	1.04
Fluorescence Anisotropy Decays of Ct T=25ºC (470nm)									
samples	r_0	a_1	ϕ_1 /ns	a_2	ϕ_2 /ns	$\langle\tau\rangle$ /ns	r_{ss}^{calc}	$r_{ss}^{exp\ 4}$	χ^2
NI	0.376	1.000	2.36	-	-	0.42	0.33	0.34	0.96
I	0.363	0.316	0.38	0.684	4.13	1.69	0.20	0.24	0.87
I 40ºC	0.379	0.324	0.79	0.676	4.97	1.74	0.23	0.22	0.86
Fluorescence Decays of A (620 nm)									
Temperature	a_1	τ_1 /ns	a_2	τ_2 /ns	a_3	τ_3 /ns	a_4	τ_4 /ns	χ^2
25	0.250	0.08	0.239	0.32	0.281	1.55	0.230	2.56	1.00
40	0.363	0.16	0.208	0.74	0.429	1.69	-	-	1.10
Fluorescence Anisotropy Decays of A (620 nm)									
Temperature	r_0	a_1	ϕ_1 /ns	a_2	ϕ_2 /ns	$\langle\tau\rangle$ /ns	r_{ss}^{calc}	$r_{ss}^{exp\ 4}$	χ^2
25	0.151	0.325	0.99	0.675	7.79	1.97	0.098	0.10	0.68
40	0.173	0.534	0.89	0.466	6.27	1.43	0.102	0.08	0.72

[1] non irradiated sample. [2] sample in the PSS. [3]Outside time resolution of equipment (FWHM=35 ps). [4] values from steady state measurements.

The fluorescence decays of **A** species were only measured in the PSS state and are multi-exponential as well, showing many similarities with **Ct** fluorescence decays, see Figure 4.21 A.[16] Fluorescence anisotropy decays are also bi-exponential in micelles and gels, Figure 4.21 B, Table 4.4 and Figure 4.22. The rotational relaxation constant of about 7 ns is attributed to **A** species located within the micelle core, while the component with 0.9 ns is attributed to **A** in the corona nanophase/water. It appears that as the aqueous nanophase becomes more viscous with gelation at 40 ºC, a higher number of **A** molecules reside in the more fluid environment, since the component of rotation relaxation around 0.9 ns has more weight. This is also apparent from the average fluorescence lifetime, which becomes smaller in the gel phase.

The calculated steady state anisotropies, from average fluorescence lifetimes and fluorescence anisotropy decays are all in reasonable agreement, within experimental error, with values obtained from steady state experiments. The obtained r_0 values are also according to what was expected, near 0.4 (0.36-0.38) for **Ct** (that is excited to S_1 state), and 0.15-0.17 for **A**, (excited to the S_2 state, λ_{ex} = 390 nm).

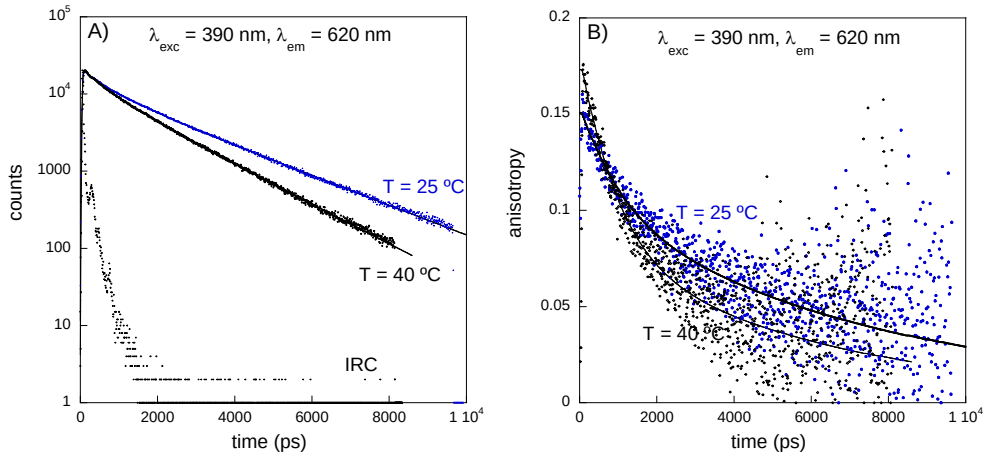

Figure 4.21 – A) Fluorescence decays 20 % Pluronic F127, pH = 5.9, λ_{exc} = 390 nm, λ_{em} = 620 nm, after irradiation, T = 25 ºC (10 ps/channel) and T = 40 ºC (8.4 ps/channel). IRC – Instrument Response Curve. B) Fluorescence anisotropy decays 20 % Pluronic F127, pH = 5.9, λ_{exc}= 390 nm, λ_{em} = 620 nm, T = 25 ºC, after irradiation, T = 25 ºC (10 ps/channel) and T = 40 ºC (8.4 ps/channel).

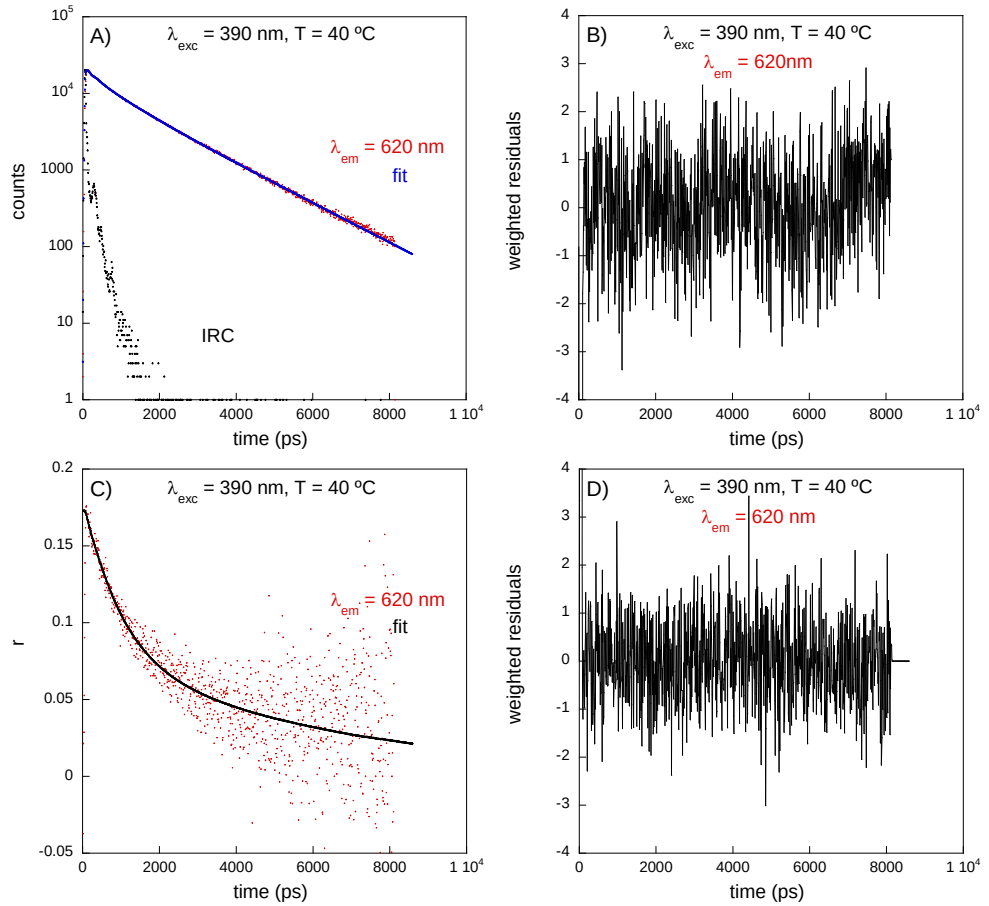

Figure 4.22 – Analysis of a fluorescence decay and a fluorescence anisotropy decay. A) Fluorescence decay 20 % Pluronic F127, pH = 5.9, λ_{exc} = 390 nm, λ_{em} = 620 nm, T = 40 ºC in PSS (10 ps/channel) and respective fitting. B) Weighted residuals for the fit in A). C) Fluorescence anisotropy decay 20 % Pluronic F127, pH = 5.9, λ_{exc}= 390 nm, λ_{em} = 620 nm, T = 40 ºC in PSS (10 ps/channel) and respective fitting. D) Weighted residuals for the fit in C) (for details see Table 4.4).

The kinetics of micelle formation in aqueous solution of Pluronic surfactants is still under discussion.[3] According to Linse and Malmsten and Malmsten and Lindman the residence time of the polymer molecules in the F127 PEO-PPO PEO micelles is extremely long (hours).[25] In order to get more insight and confirm the results that **Ct** located inside the core resides for

long time, a pH jump from equilibrated solutions at pH = 6 of **DAF** to 0.9 M HCl solution was carried out.

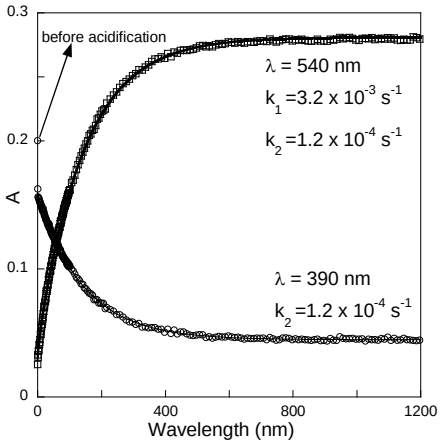

Figure 4.23 –Traces of the absorptions at 390 nm and 540 nm respectively from **Ct** and $\mathbf{AH^+}$ of **DAF** in Pluronic F127 upon a pH jump from pH = 6 to 0.9 M HCl at 25 ºC.

The trace of **Ct** in Figure 4.23 are in agreement with the data for the lifetimes measurements, considering the distribution of **Ct** before irradiation (pH = 6) in the core and in the corona of the Pluronic micelle, as well in aqueous phase. Immediately after the pH jump the absorption changes from 0.2 to 0.16, indicating that $\mathbf{CtH^+}$ was formed, from the protonation of the *trans*-chalcone molecules residing in the aqueous phase and in the corona. Sequentially $\mathbf{CtH^+}$ is transformed into $\mathbf{AH^+}$, a process that takes place with a lifetime of 5.14 min in agreement with the value observed in water, see section 9.4 in Supplementary Material. The equilibration occurs after a second and slower process with a lifetime of 144 min coincident in the **Ct** disappearance and $\mathbf{AH^+}$ formation. This process can be attributed to the micelle break-up, in accordance to a strong interaction of **Ct** in the core as well as a slow kinetics for micelle disruption as previously reported.[25] On this basis the ratio of the amplitudes of the two processes observed in the **Ct** trace, (immediate and process 2) reflects the relative distribution of **Ct** between the core and water phase/corona (3.5:1).

From these results, the following conclusions can be drawn:

1) **Ct** molecules distribute among different sites within the Pluronic aggregate: a) in a hydrophilic/fluid region where **Ct** has poor fluorescence and isomerization yields, bulk region; b) in the corona of the micelle, a less polar region where isomerization is maximized, and; c) in the hydrophobic/viscous region (probably the micelle core) where fluorescence quantum yield is higher, but photoisomerization is suppressed. This effect leads to a selective **Ct** photochemistry;

2) **Ct** fluorescence decays exhibit many features of a barrierless process, highlighting the effect of the ICT non-radiative pathway;

3) **A** species are always in the same environments: the corona of the micelle and the hydrophobic/viscous region;

4) Gelation gives rise to minor effects on the photochemistry of both **Ct** and **A**, probably because at the nanoscopic scale the large network of bounded Pluronic aggregates has also a minor effect.

4.6 Experimental Part

All reagents and solvents used were of analytical grade. ^{1}H-NMR spectra were run on a Bruker AMX 400 instrument operating at 400.13 MHz. Mass spectra were run on an Applied Biosystems Voyager-DE^{TM} PRO for MALDI. Elemental analyses were obtained on a Thermofinnigan Flash EA 1112 Series instrument.

4.6.1 Synthesis

4'-*N,N*-dimethylamino-7-hydroxyflavylium (**DAF**) perchlorate[26] was prepared by dissolving 2,4-dihydroxybenzaldehyde (2.76 g; 20.0 mmol) and 4'-*N,N*-dymethylaminoacetophenone (2.52 g; 19.1 mmol) in 25 ml of glacial acetic acid and 6 ml of concentrated sulphuric acid.[27] The reaction mixture was stirred overnight. On the following day, diethyl ether was added in excess and a reddish-brown solid was filtered off. It was dissolved in concentrated perchloric acid and then water was added. The purple solid thus obtained was filtered off, washed carefully with water and then diethyl ether and dried (5.74 g; 15.6 mmol). **Yield**: 82.2 %. **^{1}H-RMN** (CD_3OD/DCl, 400.13 MHz) δ (ppm): 8.57 (1H, d, ^{3}J = 9.1 Hz), 8.30 (2H, d, ^{3}J = 9.3 Hz), 8.02 (1H, d, ^{3}J = 9.1 Hz), 7.89 (1H, d, ^{3}J = 8.8 Hz), 7.30 (1H, d, ^{4}J = 2.0 Hz), 7.20 (1H, dd, ^{3}J = 8.8 Hz , ^{4}J = 2.0 Hz), 7.02 (2H, d, J^{3} = 9.3 Hz). It was impossible to see the protons corresponding to the dimethylamine in methanol. Nevertheless, they were observed when the NMR spectrum was done in acidified deuterated water at 3.30 ppm, corresponding to 6 protons. **EA** calcd for $C_{17}H_{16}ClNO_6 \cdot 1.5(H_2O)$: C 51.98, H 4.88, N 3.57; found: C 51.04, H 4.67, N 3.46. **MALDI-TOF/MS** 266.7 (100%) $[M]^{+}$.

The *trans*-chalcone species was isolated in the usual way.[28] 1 g of 4'-*N,N*'-dimethylamino-7-hydroxyflavylium perchlorate was dissolved in a mixture of ethanol and 10 M NaOH. The solid that does not dissolve was filtered out and discarded. The solution was left to equilibrate for a few hours, and then it was acidified to pH 7 by the addition of HCl. The precipitate was filtered, carefully washed with water and with diethyl ether. **Yield**: 40.0 %. **^{1}H-RMN** (CD_3OD, 400.13 MHz) δ (ppm): 7.98 (3H, m), 7.68 (1H, d, ^{3}J = 15.6 Hz), 7.49 (1H, d, ^{3}J = 8.2 Hz), 6.77 (2H, d, ^{3}J = 9.0 Hz), 6.35 (2H,m), 3.30 (6H, s).

4.6.2 Measurements

All flavylium aqueous solutions were prepared using acidified (HCl) water and universal buffer was used to control pH.[29] Absorption spectra were run on a Shimadzu UV-2501PC or a CARY 100Bio and fluorescence spectra on a Jobin Yvon Spex, Fluorolog FL3-22.

Pluronic F127 was kindly donated by BASF Corp. and was used without further purification. All other reagents used were of analytical grade. Solutions of Pluronic F127 containing of the desired concentration (w/v %) were prepared in the presence of acetate buffer 0.01M or by adding the proper amounts of HCl. The concentration of the flavylium compound was always lower or equal to 2.1×10^{-5} M. For each pH value and concentration of flavylium the respective solutions were transferred to plastic cells. Measurements were carried out upon complete equilibration which was controlled by measuring the absorption as a function of time.

Temperature control was performed with a water bath, connected to the spectrophotometer, with an approximate accuracy of ± 1°C. Plastic cuvettes, with an optical path of 1 cm, and 0.5 cm large were often used. Photochemical measurements in all the cases were performed in these cells, with no stirring. While being irradiated the cuvette's temperature was controlled, but the spectrophotometer was not under thermic control, so the maximum speed of the instrument was used. Ferrioxalate actinometry was performed in the same conditions.[30] In the case of gels, the irradiated area is determined easily after irradiation, because one can directly measure the irradiated area (pink on a colorless background). Flash photolysis experiments were performed as described elsewhere.[15]

Fluorescence measurements were performed in quartz cuvettes with 1 cm optical path, in specified conditions. Fluorescence quantum yields were determined using Rhodamine 6G in ethanol as standard when exciting at 530 nm; perylene in toluene was used as standard when exciting at 390 nm. Standard fluorescence quantum yields and refractive indexes were taken from literature.[31, 32]

Time-resolved fluorescence decays were performed at IST with Doctor A. Federov. Picosecond resolution fluorescence decays were obtained by the single-photon timing technique using laser excitation at 390 nm and recording the emission at the referred wavelength. The set up consisted of a The Ti: Sapphire laser Tsunami (Spectra Physics) pumped with a solid state laser Millennia Xs (Spectra Physics), delivering 70 fs pulses at a repetition rate of 80 MHz. The laser repetition rate was reduced to 4 MHz using a pulse-picker (APE), and the output was frequency doubled to 390 nm (~1nJ per pulse) and vertically polarized. The fluorescence passed through a polarizer set at the magic angle and was selected by a Jobin-Yvon HR320 monochromator with a grating of 100 lines/mm and detected by a Hamamatsu 2809U-01 microchannel plate photomultiplier. The experimental excitation pulse (FWHM = 35 ps) was measured using a LUDOX scattering solution in water. The decays were stored in a multichannel analyzer working with 1024 channels. The fluorescence emission was observed using a cutoff filter to effectively eliminate the scattered light from the sample. The experimental decay curves were fitted to simulated curves using a non linear least-squares reconvolution method. In the case of anisotropy measurements, the polarized fluorescence components parallel ($I_{\parallel}$) and perpendicular ($I_{\perp}$) to the direction of polarization of the excitation light were recorded. For the setup used the instrumental correction factor G, which takes into

account the sensitivity of the monochromator to the polarization of the light, is equal to 1 because the polarized fluorescence light components were depolarized before the entrance slit of the monochromator.

4.7 Conclusions

The red flavylium ion (**AH**$^+$), or the quinoidal base (**A**) depending on pH, is the irradiation product of the colorless *trans*-chalcone (**Ct**). At moderately acidic to neutral pH values the **Ct** species is distributed between the core and corona of the Pluronic micelle, as well as in the aqueous phase. On the other hand, at acidic pH values **AH**$^+$ remains most probably in the water phase. The **Ct** maximum absorption wavelength constitutes a good sensor for the critical micelle concentration (CMC) or critical micelle temperature (CMT). The apparent acidity constant pK'_a was found to be a relatively good sensor for CMC and also for detection of the sol-gel critical temperature.

The **Ct** photochromic mechanism was analyzed by comparing the photophysics in pure solvents and the Pluronic media. Solvatochromic effects show lack of solvent polarity dependence of the Stokes shift, indicating low dipolar moment change between ground and the locally excited state. An internal charge transfer non-radiative process (ICT) competes with **Ct** photoisomerization and is the dominant process in high polar solvents, preventing the appearance of photochromism, in contrast with lower polar environments, such as micelles and ethanol. In highly viscous environments as those found in the core of the Pluronic F127 micelles or glycerol both ICT and photoisomerization are reduced enhancing the **Ct** fluorescence quantum yield.

According to the data from fluorescence measurements and pH jumps, evidence for **Ct** distribution among different sites within the Pluronic aggregate was found:

i) a hydrophilic/fluid region where **Ct** has poor fluorescence and isomerization yields, bulk region;

ii) the corona of the micelle where photoisomerization is maximized;

iii) the hydrophobic/viscous region where fluorescence quantum yield is higher (and photoisomerization lower).

This effect leads to a selective **Ct** photochemistry.

4.8 References

[1] M. C. Moncada, D. Fernandez, J. C. Lima, A. J. Parola, C. Lodeiro, F. Folgosa, M. J. Melo, F. Pina, *Org. Biomol. Chem.*, **2004**, 2, 2802-2808.
[2] F. Pina, T. A. Hatton, *Langmuir* **2008**, 24, 2356-2364.
[3] a) P. Alexandridis, T. A. Hatton, *Colloids Surfaces A: Physicochem. Eng. Aspects* **1995**, 96, 1-46. b) P. Alexandridis, J. F. Holzwarth, T. A. Hatton, *Macromolecules* **1994**, 27, 2414-2425.
[4] H. Langhals, *Angew. Chem. Int. Ed. Engl.***1982**, *21*, 724.
[5] a) G. Haucke, P. Czerney, C. Igney, *Ber. Bunsenges. Phys. Chem.* **1989**, 93, 805-815; b) G. Haucke, P. Czerney, F. Cebulla, *Ber. Bunsenges. Phys. Chem.* **1992**, 96, 880-886.
[6] T. A Fayed, M. K. Awad, *Chemical Physics* **2004**, 317-326.
[7] K.Rurack, M. L. Dekhtyar, J. L. Bricks, U. Resch-Genger, W. Rettig, *J. Phys. Chem. A* **1999**, 103, 9626-9635.
[8] K. Rurack, J. L. Bricks, G. Reck, R.Radeglia, U. Resch-Genger, *J. Phys. Chem. A* **2000**, 104, 3087-3109.
[9] A.Espagne, D. H. Paik, P. Changenet-Barret, M. M. Martin, A. H Zewail, *ChemPhysChem* **2006**, 7, 1717-1726.
[10] C. Cazeau-Dubroca, S. A. Lyazidi, P. Cambou, A. Peirigua, P. Cazeau, M. Pesquer, *J. Chem. Phys.* **1989**, 93, 2347-2358.
[11] C. Reichardt, *Solvents and Solvent Effects in Organic Chemistry*; Wiley VCH, **1998**, Chapter 7, 339-405.
[12] M. J. Kamlet, J.-L. M. Abboud, M. H. Abraham, R. W. Taft, *J. Org. Chem* **1983**, 48, 2877-2887.
[13] J. Hicks, M.Vandersall, Z. Babarogic, K. B. Eisenthal, *Chem. Phys. Lett.* **1985**, 116, 18-24.
[14] a) W.-M. Kwok, M. W. George, D. C. Grills, C. Ma, P. Matousek, A. W. Parker, D. Phillips, W. T. Toner, M. Towrie, *Angew. Chem, Int. Ed*. **2003**, 42, 1826-1830; b) W.-M Kwok, C. Ma, M. W. George, D. C. Grills, P. Matousek, A. W. Parker, D. Phillips, W. T. Toner, M. Towrie, *Photochem. Photobiol. Sci.* **2007**, 6, 987-994.
[15] F. Pina, M. J. Melo, R. Ballardini, L. Flamigni, M. Maestri, *New. J. Chem.* **1997**, 21, 969-976.
[16] G. Haucke, P. Czerney, D. Steen, W. Rettig, H. Hartmann, *Ber. Bunsenges. Phys. Chem.* **1993**, 97, 561-570.
[17] R. Matsushima, H. Mizuno, H.Itoh, J. Photochem. *Photobiol. A: Chem.* **1995**, 89, *251-256*; b) R. Matsushima, S. Fujimoto, K. Tokumura, *Bull. Chem. Soc. Jpn.* **2001**, 74, 827-832.
[18] A. P. Demchenko, *Luminescence* **2002**, 17, 19-42.
[19] J. R. Lakowicz, S. K. Nakamoto, *Biochemistry* **1984**, 23, 3013-3021.
[20] B. Bagchi, G. R. Fleming, D. W. Oxtoby, *J. Chem. Phys.* **1983**, 78, 7375-7385.
[21] R. Prud'homme, G. Wu, D. Schneider, *Langmuir* **1996**, 12, 4651.
[22] S. Ghosh, A. Adhikari, U. Mandal, S. Dey, K. Bhattacharyya *J. Phys. Chem. C* **2007**, 111, 8775-8780
[23] L. Nikowa, D. Schwarzer, J. Troe, J. Schroeder, *J. Chem. Phys.* **1992**, 97, 4827-4835.
[24] S. Jeon, S. Granick, K. Kwon, K. Char, *Microviscosity* **2002**, 2883-2888.
[25] a) P. Linse, M. Malmsten, *Macromolecules* **1992**, 25, 5434-5439. b) M. Malmsten, B. Lindman, *Macromolecules* **1992**, 25, 5440-5445.
[26] Previous reference to this compound in the paper M. C Moncada, F. Pina, A. Roque, A. J. Parola, M. Maestri, V. Balzani, *Eur. J. Org. Chem.* **2004**, *2*, 304 – 312, was corrected in *Eur. J. Org. Chem.* **2006**, 4761. The present compound was synthesized for the first time for this work.
[27] a) R. Robinson, D. D. Pratt, *J. Chem. Soc. Trans.*, **1922**, 121, 1577-1585; b) A. Robertson, R. Robinson, *J. Chem. Soc,* **1926**, 1713-1720.
[28] A. Roque, J. C. Lima, A. J. Parola, F. Pina, *Photochem. Photobiol. Sci.* **2007**, *6*, 381-385.
[29] F. W. Küster, A. Thiel, *Tabelle per le Analisi Chimiche e Chimico- Fisiche*, 12th ed.; Hoepli, Milano, Italy, **1982**, 157-160.
[30] C. G. Hatchard, C. A. Parker, *Proc R Soc A* **1956**, 235, 518-536.
[31] J. Olmsted, *J. Phys. Chem.* **1979**, 83, 2581-2584.
[32] M. Montalti, A. Credi, L. Prodi, M. T. Gandolfi, *Handbook of Photochemistry*, 3rd ed., Taylor & Francis, CRC Press, Boca Raton, **2006**.

5. Host-guest interactions between molecular clips and multistate systems based on flavylium salts

In this chapter we investigate the effect of the water-soluble molecular clips substituted by hydrogenphosphate and sulphate groups on the stability and network of reactions of the flavylium salts by the use of UV-Vis absorption, fluorescence, and NMR spectroscopy as well as of the time-resolved pH-jump and flash-photolysis methods.

5.1 Introduction

Among the reactions from the characteristic network of reactions described in Scheme 1.8, the hydration reaction is particularly relevant. The hydration reaction (and the coupled fast tautomerization) is important in the establishment of color in the vacuoles of plant cells, since it is the key step for color loss of these dyes at moderately acidic pH values. The pH inside the vacuoles of plant cells, where anthocyanins are located in vivo, ranges roughly between 3 and 6. At these pH values, anthocyanin solutions in vitro are essentially colorless and Nature had to develop strategies for stabilizing the color of anthocyanins inside the vacuoles[1] These strategies involve the association of flavylium cations and their quinoidal bases with other polyphenols (co-pigmentation) and complexation with metal ions, giving rise to beautifully organized supramolecular structures.[2] It is usually believed that co-pigmentation is driven by hydrophobic stacking and that hydration is reduced mainly by exclusion of water from the vicinity of the reactive center, but recent work[3] shows that hydration is actually very efficient in low dielectric media suggesting the existence of other stabilization effects, such as charge transfer interactions.[4] The study of flavylium salts upon host-guest complexation could in principle contribute to uncover the thermodynamic and kinetic contributions to the co-pigmentation effect in Nature.

During the past few years, Klärner *et al.* have introduced various molecular tweezers and clips designed for the inclusion of electron-poor guests such as aromatics with –M substituents, pyridinium cations, or even sulfonium cations.[5] These guests were mainly bound by π–π, CH–π, and π–cation interactions inside their electron-rich concave cavity. However, due to the lipophilic nature of these hosts, molecular recognition was restricted to organic solvents. On a later development, the molecular clips were decorated with phosphonate monoester anions, leading to water-soluble host molecules, flanked by two negatively charged functionalities for hydrogen bonding and/or additional ion pairing with cationic guests.[6] More recently, the hydrogenphosphate- and sulphate-functionalized clips **C1** and **C2** (see Figure 5.1), were synthesized presenting superior inclusion properties for electron-poor guests.[7] Flavylium salts, with their positive 1-benzopyrylium moieties, seem excellent candidates to be hosted by these molecular clips.

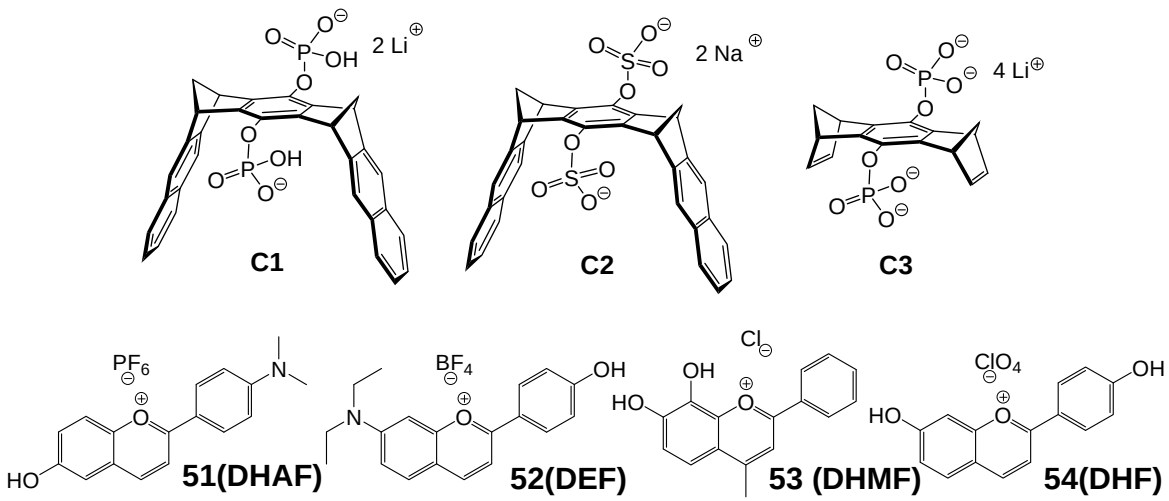

Scheme 5.1 –Structure of the molecular clips (**C1** and **C2**), model compound **C3** (phosphate-substituted bridge) and flavylium salts **51**-**54** used throughout this chapter.

Scheme 5.1 shows the structures of the flavylium salts and the water soluble molecular clips **C1** and **C2** substituted with hydrogenphosphate or sulphate groups in the central bridging unit, and the phosphate-substituted bridge **C3** to be used as guest and host molecules, respectively. In this study, 6-hydroxy-4'-(*N,N*-dimethylamino)flavylium hexafluorophosphate (**51**, **DHAF**)[8] and 7-(*N,N*-diethylamino)-4'-hydroxyflavylium tetrafluoroborate (**52**, **DEF**),[9] both flavylium salts with amino substituents, were chosen on the basis of their stability until pH 4-5 where they start to be hydrated; they are in principle suitable to study the interaction of these flavylium salts with the hydrogenphosphate-substituted clip **C1** in a pH range where **C1** remains unprotonated, whereas the phosphate groups (OPO_3^{2-}) of bridge **C3** are certainly protonated to the corresponding hydrogenphosphate groups ($OP(OH)O^{2-}$) under these slightly acidic conditions. 7,8-dihydroxy-4-methyl flavylium chloride (**DHMF**, **53**)[10] is hardly hydrated in aqueous solutions due to the methyl group in position 4 (that reduces positive charge on position 2); **DHMF** was chosen to allow NMR studies on both states $\mathbf{AH^+}$ and **A**, with no worries with the hydration reaction. 7,4'-dihydroxyflavylium (**DHF**, **54**),[11] a very well studied compound, is hydrated at pH 2-3 and the resulting chalcones are photochromic. It was chosen to test the effect of host-guest complex formation on the network of reactions. Particularly, we were interested in the following two questions:

i) does the host molecule in the host-guest complex protect the flavylium core of the guest molecule from water attack?

ii) is the *trans-cis* isomerization of the chalcones affected upon complexation?

5.2 Host-guest formation with molecular clip C1

Throughout this work, the mass spectroscopy, NMR studies and calculations were performed by Professor Klärner's group from Duisburg-Essen University, and its explanation, in the context of this thesis, will be reduced to the essential parameters needed for the comprehension of the system.

When aqueous acidic solutions of clip **C1** and flavylium salts **51-53** are mixed together, a red shift in color and precipitation of solid materials are observed. ^{1}H-NMR spectra of the precipitates dissolved in [D_6]DMSO suggest the formation of (1:1) complexes between clip **C1** and the corresponding flavylium salt. The (1:1) complex stoichiometry was also confirmed by ESI MS spectra, Table 5.1. In each case, the ion peaks corresponding to the free clip and the (1:1) complex with the flavylium cation (without the counter-ions) were observed in the negative spectral mode, while in the positive spectral mode only the ion peaks corresponding to the free flavylium cations were detected.

Table 5.1 – ESI-MS data found for the precipitates of the 1:1 mixtures of molecular clip **C1** with the flavylium salts **51-53** from water (dissolved in methanol).

Ion	$(m/z)_{exp}$	$(m/z)_{calc}$
$[\mathbf{C1} - 2\ Li^+]^{2-}$	298.0347	298.0400
$[\mathbf{51} + \mathbf{C1} - PF_6^- - 2\ Li^+]^-$	862.1909	862.1965
$[\mathbf{51} - PF_6^-]^+$	619.0641	619.0699
$[\mathbf{C1} - 2\ Li^+]^{2-}$	298.0360	298.0400
$[\mathbf{52} + \mathbf{C1} - BF_4^- - 2\ Li^+]^-$	890.2230	890.2289
$[\mathbf{52} + \mathbf{C1} - BF_4^- - 2\ Li^+ - H^+]^{2-}$	444.6075	444.6108
$[\mathbf{52} - BF_4^-]^+$	294.1495	294.1498
$[\mathbf{C1} - 2\ Li^+]^{2-}$	298.0367	298.0400
$[\mathbf{C1} - 2\ Li^+ + H^+]^-$	597.0837	597.0874
$[\mathbf{53} + \mathbf{C1} - Cl^- - 2\ Li^+]^-$	849.1598	849.1660
$[\mathbf{53} - Cl^-]^+$	253.0848	253.0859

The mixture of clip **C1** and the flavylium salts **51-53** was soluble in methanol. Thus, the host-guest interactions between these compounds could be studied in methanol by UV-Vis absorption spectroscopy, steady-state and time-resolved spectrofluorimetry, and ^{1}H-NMR dilution titrations.

5.2.1 UV-Vis and fluorescence and studies in methanol

The color of the solution of 4'-dimethylamino-6-hydroxyflavylium hexafluoro-phosphate (**DHAF**), **51**, and 7-diethylamino-4'-hydroxyflavylium tetrafluoroborate (**DEF**), **52**, in methanol, is intensely purple and pink, respectively. In both cases the observed color corresponds to the presence of the flavylium cation, $\mathbf{AH^+}$, which is stable in solution for days. The maximum in the UV-Vis absorption spectrum of flavylium salt **51** and **52** in methanol is at 547 and 551 nm, respectively. These maxima are red-shifted relative to the values observed in acidic aqueous solution (540 nm for **51**[8] and 530 nm for **52**[9]), as expected for flavylium compounds characterized by π-π* transitions with strong charge-transfer character, which present negative solvatochromism.[12]

The addition of increasing amounts of molecular clip **C1** to methanolic solutions of **51** and **52** was followed by UV-Vis absorption spectroscopy and spectrofluorimetry (Figure 5.1). Figure 5.1 A shows that the addition of clip **C1** to flavylium salt **51** causes a red shift in the absorption maxima as well as a small decrease in the absorption intensity. In the case of the addition of **C1** to flavylium salt **52** the red shift is observed in the shoulder at *ca*. 585 nm and not at λ_{max}. The red shifts of the absorption maxima or shoulder indicate the positioning of the flavylium ions into a less polar medium than the original methanol and, hence, the interaction of the flavylium cations with the molecular clip. Further evidence for this interaction comes from the finding that the intensity of the emission band at 616 and 613 nm, respectively, for flavylium salts **51** and **52**, strongly increases upon addition of clip **C1**. This result suggests that each flavylium cation is bound inside the cavity of clip **C1**, since in the more rigid environment of the clip cavity the non-radiative transitions become less important, leading to an increase in the fluorescence quantum yield. Table 5.2 resumes the relevant photophysical data for **51**-**53**, **C1** and their complexes in methanol.

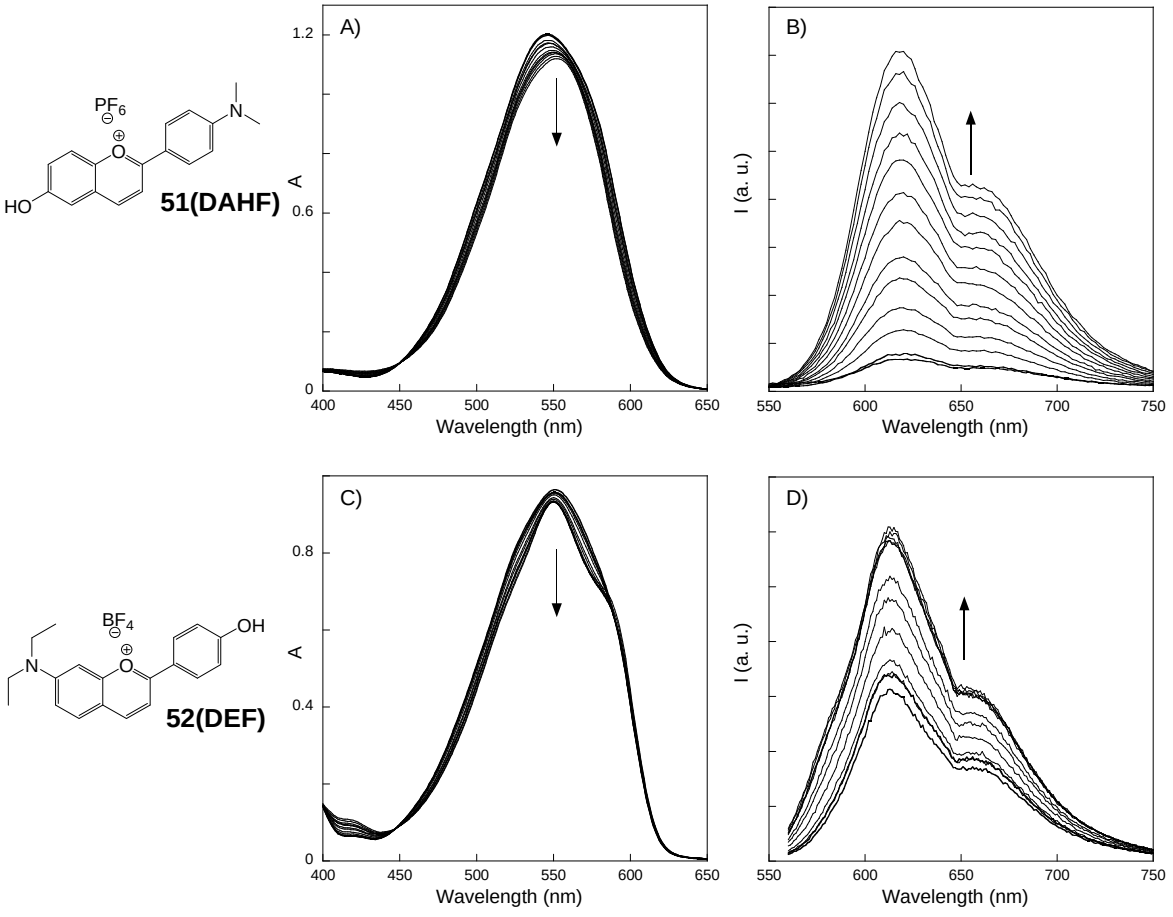

Figure 5.1 – Spectral modifications observed upon addition of molecular clip, [**C1**] = 0 - 7×10^{-4} M, to methanolic solutions of **DAHF**, [**51**] = 1.92×10^{-5} M, followed by absorption (A) and fluorescence emission (B, 2 nm slits, λ_{exc} = 545 nm); and to methanolic solutions of **DEF**, [**52**] = 2.26×10^{-5} M, followed by absorption (C) and fluorescence emission (D, 2 nm slits, λ_{exc}= 550 nm).

Table 5.2 – Photophysical properties of **51**-**53**, **C1** and their complexes in methanol.

Compound	Absorption	Luminescence		
	λ_{max}/nm (ε/$M^{-1}cm^{-1}$)	λ/nm	Φ_f [a]	τ/ns
C1	252 sh (33300) 308 (2000) 322 (2300)	331		
51	547 (62600)	618	0.0002	0.08
52	551 (42700)	613	0.03	0.6
53	383 (25583) 462 (9223)	<650	$<10^{-5}$	
53A	335 (11300) 545 (5300)	641	0.0004	
51@C1	553 (58300)	616	0.002	
52@C1	550 (41300) [b]	613	0.07	1.8
53A@C1	545 (5300)	653	0.0008	

[a] estimated error of ± 20%; [b] when molecular clip **C1** is added to **52**, a shoulder at *ca*. 590 nm is evidenced.

The concentration-dependent spectral evolutions shown in Figure 5.1 were used to obtain the association constants, *K*, between molecular clip **C1** and flavylium salts **51** and **52**. A 1:1 stoichiometry was assumed, as suggested by ESI-MS data and confirmed by ^{1}H NMR (see below). The emission data was fitted using equation 5.1 [13] (see Supplementary Material, section 9.6), where I_0 is the emission intensity of the flavylium in the absence of host **C1**, I_{lim} is the emission intensity of the complex of the flavylium salt with clip **C1**, *S* refers to the flavylium salt, *R* to the clip **C1,** and *K* is the association constant. The UV-Vis data were fitted using a similar equation. The simultaneous fitting of absorption and emission data for each host-guest complex are shown in Figure 5.2 and allowed us to obtain log *K* values of 4.2 ± 0.1 and 4.7 ± 0.1 for **51@C1** and **52@C1**, respectively.

$$I = I_0 + (I_{lim} - I_0) \times \frac{([R]_0 + [S]_0 + 1/K) - \sqrt{([R]_0 + [S]_0 + 1/K)^2 - 4[R]_0[S]_0}}{2[S]_0} \qquad (5.1)$$

For flavylium salt **52** in the absence and presence of clip **C1**, fluorescence lifetimes were measured, Figure 5.3. The decay of **52** in methanol is monoexponential with a lifetime of 0.6 ns. When clip **C1** is added, the decay becomes biexponential with lifetimes of 0.6 ns and 1.8 ns. This longer lifetime corroborates the emission data, where the intensity increases upon addition of clip **C1**, which was assigned to complexed **52**. The weighed amplitudes of these lifetimes are in reasonable agreement with the mole fractions of **52** and **52@C1** calculated on the basis of the association constant log *K* = 4.7; accordingly, a solution of clip **C1** (1.5×10^{-4} M) and flavylium salt **52** (1.8×10^{-5} M) contains 16% of free salt **52** and 84% of complex **52@C1** and a contribution of 76% of the longer lifetime is calculated from the amplitudes.

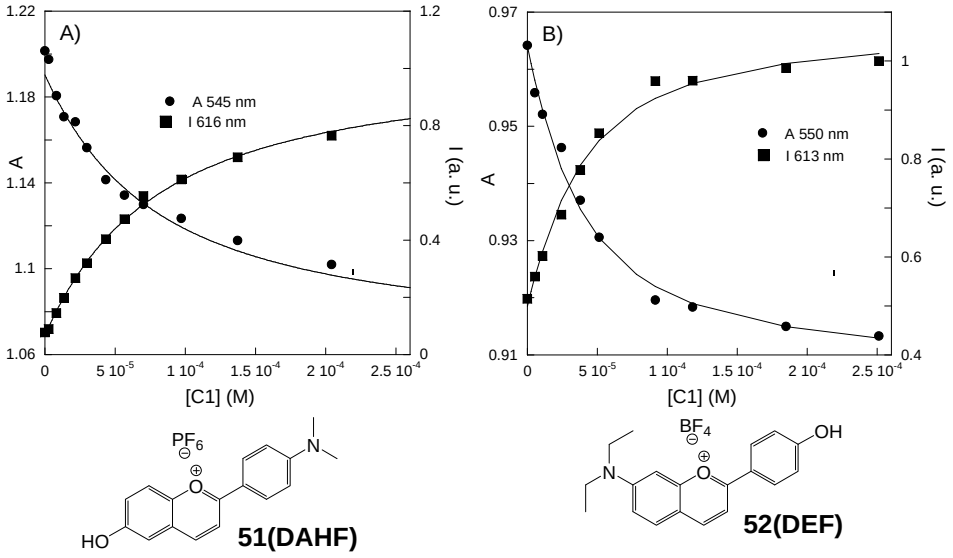

Figure 5.2 – Fitting of the data in Figure 5.1 using eq. 5.1 for the emission data and a similar equation for absorption data. A) **51**@**C1**, log $K = 4.2 \pm 0.1$; B) **52**@**C1**, log $K = 4.7 \pm 0.1$.

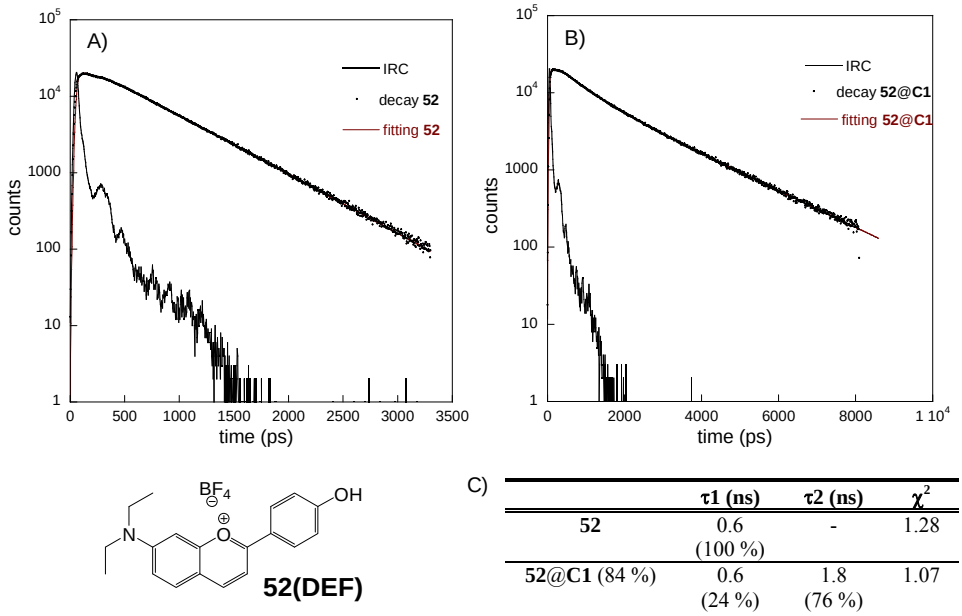

C)

	τ1 (ns)	τ2 (ns)	χ^2
52	0.6 (100 %)	-	1.28
52@**C1** (84 %)	0.6 (24 %)	1.8 (76 %)	1.07

Figure 5.3 – Fluorescence decays of flavylium **DEF**, **52** (A) and **52**@**C1** (84 % complexation, B) in methanol. Excitation at 390 nm, emission at 650 nm, scale 3.44 ps/channel for **52**, 8.4 ps/channel for **52**@**C1**. C) Table with fitting parameters for flavylium salt **52** in the absence (lifetime 0.6 ns) and in presence of clip **C1** (lifetime 1.8 ns).

The quinoidal bases of flavylium salts **51** and **52** can be easily obtained by adding a drop of NaOH (1 M) to a previously prepared solution in methanol. However, these species are not stable. They undergo subsequent reactions to the more stable *trans*-chalcone species as final products, as could be easily detected by the color evolution of the solutions. For this reason, it was not possible to study the interaction between the molecular clip **C1** and these quinoidal bases.

Contrary to **51** and **52**, flavylium salt **53** does not hydrate and in the presence of methanol **53** exists in its flavylium form $\mathbf{AH}^+$ and/or its quinoidal base **A**. When flavylium salt

53 is dissolved in methanol a color between yellow and purple may be observed indicating a mixture of both forms. This is certainly due to the presence of acid or base trace impurities in the solvent or in the flask. To overcome these problems, small aliquots of dilute HCl (0.1 M) or NaOH (0.1 M) were added until constant absorption spectra of **53** were observed, in order to obtain either the flavylium cation, $\mathbf{AH^+}$, or the quinoidal base, **A**. The interaction between the flavylium salt $\mathbf{53AH^+}$ (obtained by addition of small amounts of dilute HCl to the methanolic solution) and clip **C1** is very weak (see Figure 5.4) contrary to that with quinoidal base **53A**. The association constant for the formation of complex $\mathbf{53AH^+@C1}$ in methanol was determined by ^{1}H-NMR titration to be log $K = 2.0 \pm 0.1$ (see below). Figure 5.5 shows the spectral changes observed upon addition of **C1** to methanolic solutions of the quinoidal base **53A**. The absorption spectra show no changes on the flavylium absorption band while a small increase is observed in the fluorescence intensity. These changes, although small, are reproducible and allowed us to determine the association constant for the formation of complex **53A@C1** to be log $K = 5.6 \pm 0.2$. This result of a highly stable host-guest complex **53A@C1** is in agreement with the findings of the ^{1}H-NMR titration experiments which only gave a lower limit of the association constant of log $K \geq 4.2$.

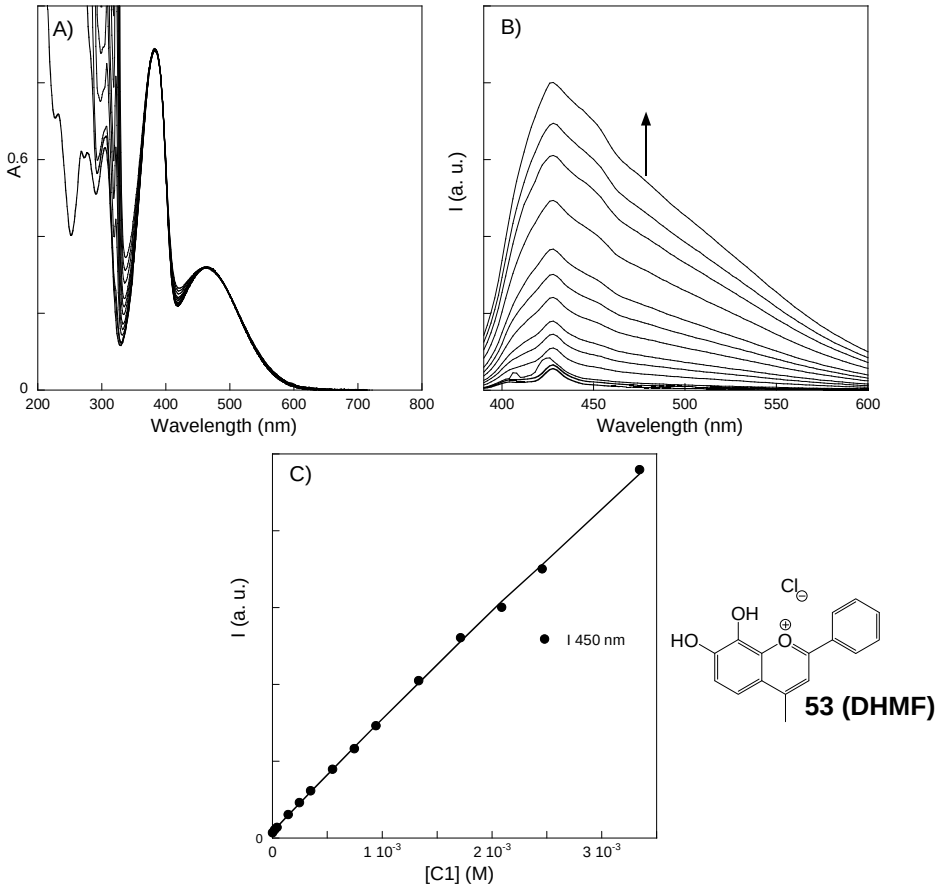

Figure 5.4 – Spectral modifications observed upon addition of clip **C1**, $0 - 3.3 \times 10^{-3}$ M, to methanolic solutions of the flavylium salt **DHMF**, **53**, 3.45×10^{-5} M, followed by absorption (A) and fluorescence emission (B, $\lambda_{exc} = 380$ nm); Fitting of the data in B) using eq. 5.1, log $K = 1.4 \pm 0.5$.

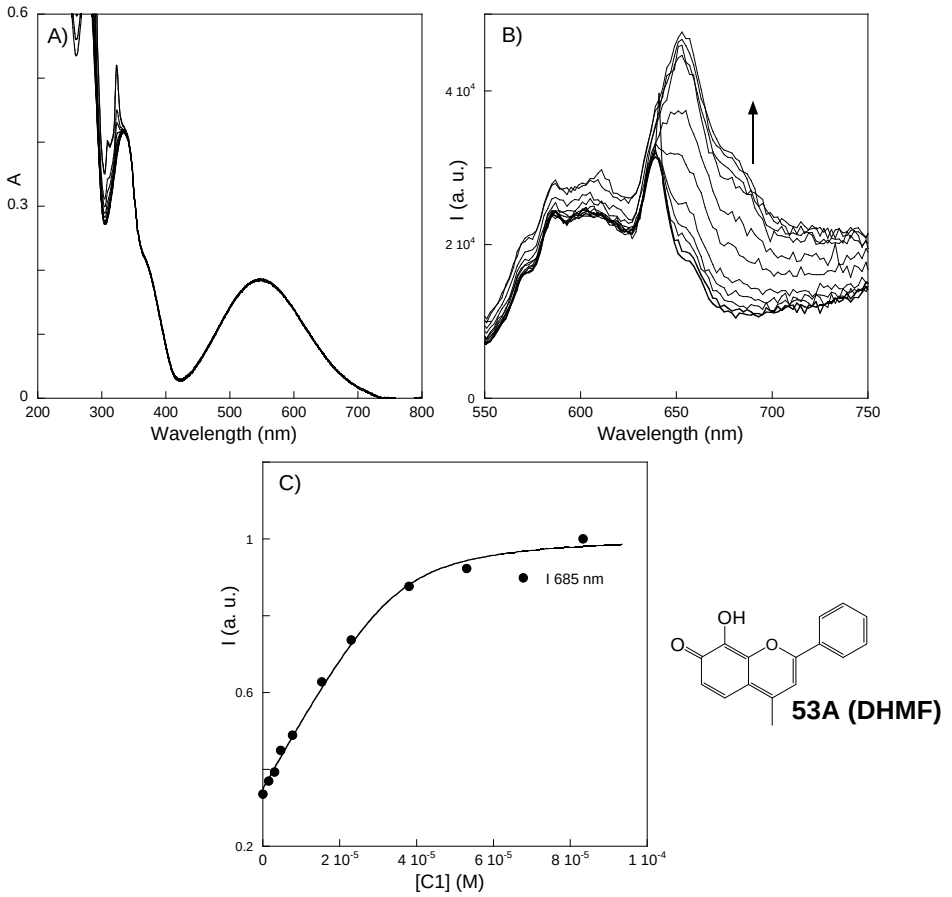

Figure 5.5 – Spectral modifications observed upon addition of clip **C1**, [**C1**] = 0 – 8.3 × 10^{-5} M, to a methanolic solution of **DHMF**, [**53A**] = 3.46 × 10^{-5} M, followed by absorption (A) and fluorescence emission (B, λ_{exc}= 520 nm); C) Fitting of the data in B) using eq. 5.1 leads to log *K* = 5.6 ± 0.2.

5.2.2 NMR studies in methanol

The host-guest complex formation between clip **C1** and flavylium salts **51**-**53** could be also detected by ^{1}H-NMR (by Professor F.-G. Klärner's group). In the spectra of a methanol solution containing clip **C1** and one of the flavylium salts either **51**, **52**, or **53**, pronounced upfield shifts of the signals assigned to the flavylium as well as to the clip arene protons are observed, as it is illustrated for clip **C1** and flavylium salt **52** in Figure 5.6. The ^{1}H-NMR signals of host **C1** and guests **51**-**53** could be assigned by the use of two-dimensional ^{1}H-NMR experiments. The observation of upfield shifts of the guest and host ^{1}H-NMR signals indicate that both species are facing each other's aromatic regions and, hence, the flavylium guest is bound inside the clip cavity. In the ^{1}H-NMR spectra of the mixture between clip **C1** and flavylium salt **51**, **52**, or **53** the signals of the guest protons are broad (Figure 5.6). This finding indicates that the mutual host-guest complex formation and dissociation is slow compared to the time which is required to observe sharp NMR signals resulting from an averaging between the signals of complexed and free guest. However, this mutual interconversion is still too fast to observe separate signals for complexed and free guest. Professor F.-G. Klärner and co-workers tried to determine the association constants *K* and the maximum complexation-induced shifts of

the guest ^{1}H-NMR signals, $\Delta\delta_{max}$, by means of ^{1}H-NMR dilution titration experiments. In these experiments, the guest concentration of the flavylium salt was kept constant and the host concentration of clip **C1** was varied. In the range of concentrations which could be studied, the observed complexation-induced ^{1}H-NMR shifts of the guest signals, $\Delta\delta_{obs}$, of the flavylium salts **51, 52** and quinoidal base **53A** did not vary significantly (Figure 5.7). This small concentration dependence of $\Delta\delta_{obs}$ indicates that the complexes of clip **C1** with these guest molecules are very stable. For each guest signal, the dependence of the chemical shift, $\Delta\delta_{obs}$, on the clip concentration was fitted with equation 5.2 (similar to equation 5.1), as exemplified in Figure 5.7 for one kind of protons of each flavylium salt **51**, **52**, **53A**, or **53AH**$^+$. These fittings allowed us to determine the $\Delta\delta_{max}$ values very accurately (Figure 5.8) but not the association constants, K. These experiments only provide lower limiting values for the association constants, log $K \geq 4.3$. In the case of **53** the formation of the stable complex with clip **C1** in methanolic solution was only observed for the deprotonated quinoidal **53A** form but not for salt **53AH**$^+$ which can be produced by the addition of dilute DCl to the methanol solution of **53A.** The association constant (determined by ^{1}H-NMR titration for the complex formation of **53AH**$^+$ with clip **C1** in an acidified methanolic solution is with log $K = 2.0 \pm 0.1$ surprisingly small.

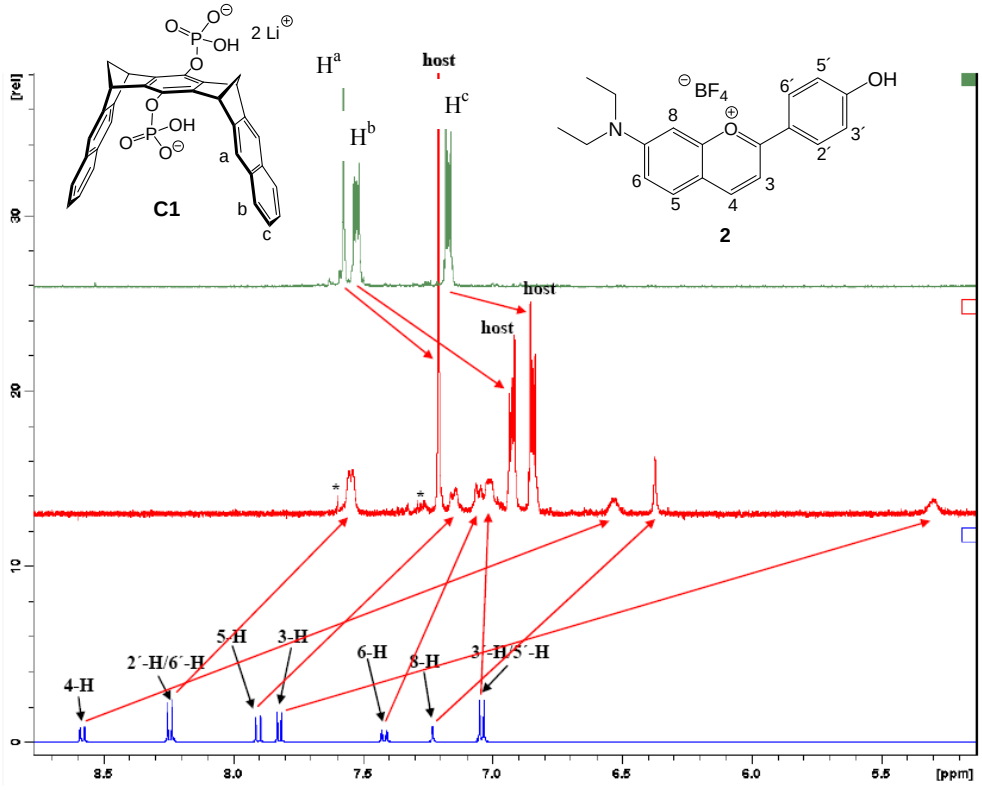

Figure 5.6 – ^{1}H-NMR spectra (500 MHz, CD_3OD, 25°C) of clip **C1** (5.07 mM, top), a mixture of **C1** (1.53 mM) and flavylium salt **52** (1.50 mM, middle), and flavylium salt **52** (1.50 mM, bottom) (aromatic range); * impurities.

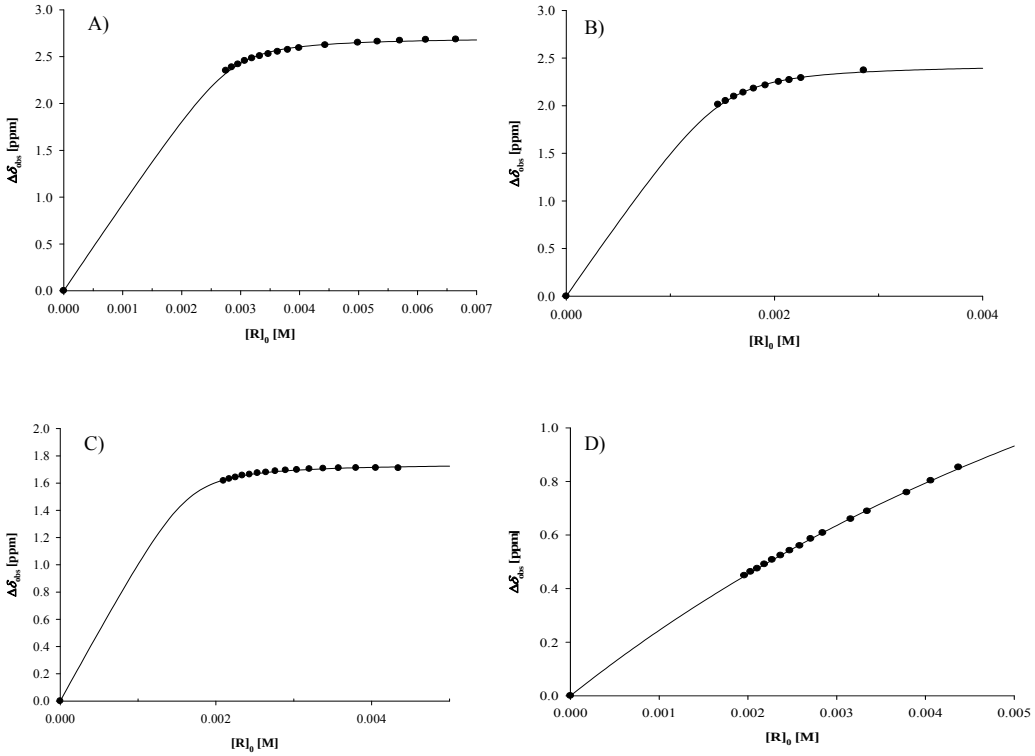

Figure 5.7 – Dependence of $\Delta\delta_{obs}$ (flavylium salt) from the concentration of clip **C**1 (≡ $[R]_0$): A) $\Delta\delta_{obs}$ (4-H) of **51**, B) $\Delta\delta_{obs}$ (4-H) of **52**, C) $\Delta\delta_{obs}$ (4-H) of **53A**, and D) $\Delta\delta_{obs}$ (4-H) of **53AH**$^+$.

$$\Delta\delta_{\max} = \frac{\Delta\delta_{obs}[S]_0}{(1/2)([R]_0 + [S]_0 + 1/K) - \sqrt{(1/4)([R]_0 + [S]_0 + 1/K)^2 - [R]_0[S]_0}} \qquad (5.2)$$

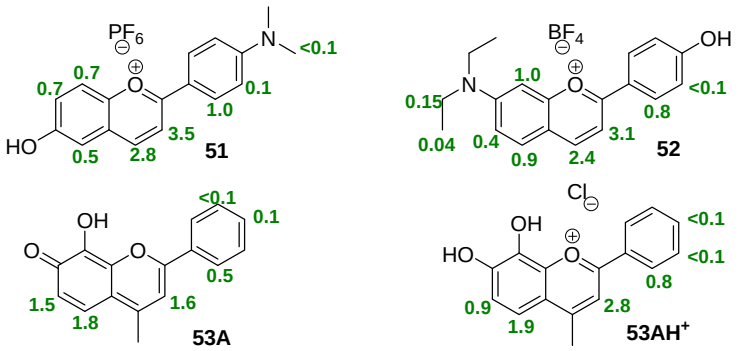

Figure 5.8 – Complexation-induced maximum ^{1}H-NMR shifts, $\Delta\delta_{max}$ (= $\delta_{complex}$ -δ_0) in ppm, determined by ^{1}H-NMR titrations for the flavylium protons of **51**, **52** and **53AH**$^+$ and the quinoidal base **53A** in the host-guest complexes with clip **C1**.

The large complexation-induced maximum upfield shifts, $\Delta\delta_{max}$, observed for the signals of the aromatic protons show that all flavylium cations are bound inside the clip cavity. For flavylium cations **51** and **52**, the signals of the protons 3-H and 4-H show the highest $\Delta\delta_{max}$ values indicating that the positively charged pyrylium ring is positioned inside the clip cavity presumably with the protons 3-H and 4-H pointing toward the central spacer-unit of clip **C1**. In the complex of **C1** with the flavylium salt **53AH**$^+$, the methyl group at C-4 evidently prevents this position of the pyrylium ring inside the clip cavity. In this case, the $\Delta\delta_{max}$ value of proton

3-H is 2.8 ppm, smaller than that of flavylium salt **51** ($\Delta\delta_{max}$ = 3.5 ppm) and **52** ($\Delta\delta_{max}$ = 3.1 ppm), on the other hand, the $\Delta\delta_{max}$ value of 5-H and 6-H (1.9 and 0.9 ppm, respectively) of **53AH**$^+$ are larger than those of **51** ($\Delta\delta_{max}$ (5-H) = 0.5 ppm) and **52** ($\Delta\delta_{max}$ (5-H, 6-H) = 0.9 and 0.4 ppm, respectively). These findings suggest that the methyl group at C-4 in **53AH**$^+$ points toward the tips of the clip naphthalene sidewalls and causes a shift of the guest position in the direction of the inclusion of the terminal dihydroxy-substituted benzene ring inside the clip cavity. In the complex of clip **C1** with the quinoidal base **53A** the large value of $\Delta\delta_{max}$ for proton 6-H (1.5 *vs*. 0.9 ppm in **53AH**$^+$) and the low value for 3-H (1.6 *vs*. 2.8 ppm in **53AH**$^+$) suggest that the *o*-hydroxy-quinone ring of **53A** is encapsulated in the clip cavity.

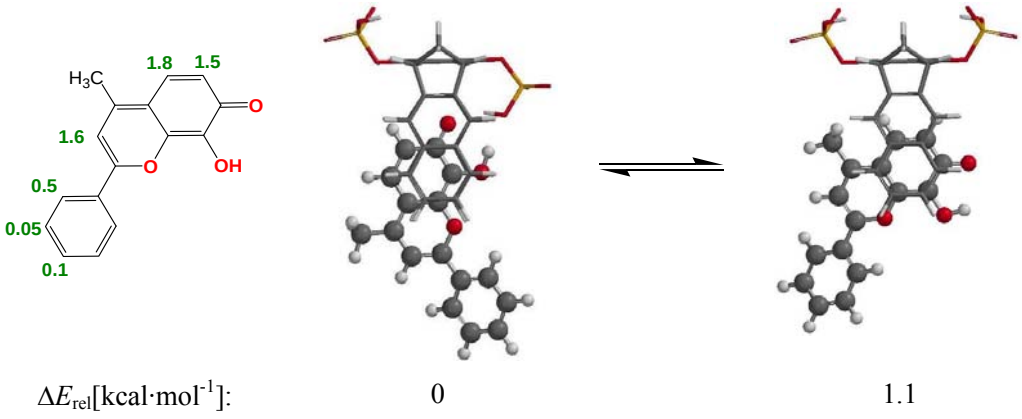

Figure 5.9 – Comparison of the $\Delta\delta_{max}$ values (determined by ^{1}H-NMR titration) with lowest-energy structures of the host-guest complex of the quinoidal base **53A** with clip **C1** calculated by a Monte-Carlo conformer search (force field: AMBER*/H_2O, 5000 structures implemented in Macromodel 9.0).[14]

Attempts to model the host-guest complex structures of the flavylium salts by the use of force-field methods (MMFF94, Monte-Carlo conformer search implemented in SPARTAN)[15] were not very successful because these gas-phase calculations overestimate the ion-ion interaction between the differently charged flavylium salts and clip **C1** and the hydrogen bonds. Since in Macromodel the oxonium ion parameters are missing in the force fields (AMBER*, MMFF, MM2*, MM3*, OPLS), it was not possible to perform calculations. However, successful force field calculations could be run for the complex between the quinoidal form **53A** and clip **C1** (Figure 5.9), by Professor Klärner's group. The Monte-Carlo conformer search gave several structures in which the guest molecule is positioned inside the clip cavity. In the structure which is calculated to be only 1.1 kcal/mol higher in energy than the energy-minimum structure, the guest protons attached to the terminal *o*-hydroxyquinone ring point toward the central aromatic spacer-unit of clip **C1**. This finding suggests that these protons are particularly strongly influenced by the magnetic anisotropy of the clip arene-units and is in good agreement with the large $\Delta\delta_{max}$ values determined for these protons by ^{1}H-NMR titration experimentally. The large $\Delta\delta_{max}$ value observed for guest proton 3-H (attached to the pyrane ring) indicates,

however, that several conformers (equilibrating rapidly with respect to the NMR timescale) are involved in the overall complex structure.

Table 5.3 – The association constants, log *K*, determined for the host-guest complex formation of clip **C1** with flavylium salts **51**, **52**, **53AH**$^+$ and the quinoidal base **53A** in methanol, at 298 K determined by a) UV-Vis spectroscopic and/or fluorometric titration, b) ^{1}H-NMR titration in a methanolic solution acidified by addition of DCl.

complex	**51@C1**	**52@C1**	**53AH$^+$@C1**	**53A@C1**
log *K*	4.1 ± 0.1 [a)]	4.7 ± 0.1 [a)]	2.0 ± 0.1 [b)]	5.6 ± 0.2 [a)]

The host-guest complexes of hydrogenphosphate-substituted clip **C1** with the flavylium salts **51** and **52** as guest molecules are highly stable, Table 5.3. ^{1}H-NMR structural analysis (described above) suggests the positively charged guest pyrylium ring to be bound inside the clip cavity in both complexes. Thus, cation-π interactions between the pyrylium ring and the clip arene-units seem to provide a significant contribution to the stability and structure of these complexes besides the Coulombic forces (between the negatively charged clip hydrogenphosphate groups and positively charged flavylium salt), dispersive, and solvophobic interactions. The result of the surprisingly high stability of the complex of **C1** with neutral quinoidal base **53A**, however, suggests that the arene-arene (CH-π) and the solvophobic interactions are major factors for the stability observed for this complex. Quantum chemical calculation of the electrostatic potential surface of clip **C1** substituted by dihydrogenphosphate groups (-$OPO(OH)_2$ instead of -$OPO_2(OH)^-$ Li^+) and quinoidal base **53A** indicate attractive electrostatic forces between the positively polarized hydrogen atoms 5- and 6-H attached to the *o*-hydroxyquinone ring of **53A** and the negatively polarized clip arene-units (Figure 5.10).

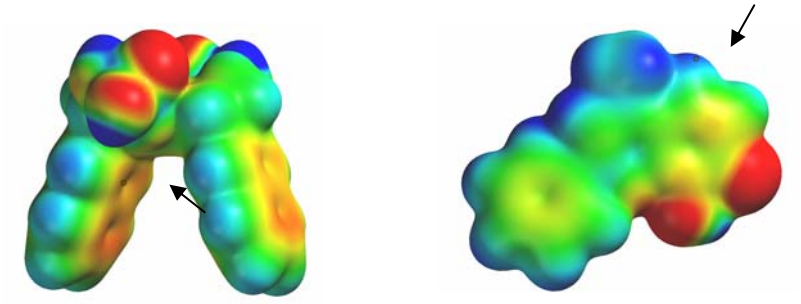

Figure 5.10 –The electrostatic potential surface (EPS) calculated for clip **C1** substituted by dihydrogenphosphate groups ($OPO(OH)_2$ instead of $OPO_2(OH)^-$ Li^+, *left*) and quinoidal base **53A**, *right*) by the use of density functional B3LYP/6-31G**//AM1 (implemented in SPARTAN)[16] The color code ranges from -25 kcal/mol (red) to +25 kcal/mol (blue). The molecular electrostatic potential (MEP) was calculated at the marked position to be -19 kcal/mol at the clip naphthalene sidewalls and +18 kcal/mol at hydrogen atom 5-H of **53A**.

The finding that clip **C1** only forms a very weak complex with the flavylium salt **53AH**$^+$, is surprising and not well understood. Speculatively, we assume that the addition of DCl to the mixture of clip **C1** and **53A** in methanol causes concomitant deuteration of the

hydrogenphosphate groups of **C1** and the quinoidal base **53A**. Evidently, the non charged neutral clip substituted by dihydrogenphosphate groups ($OPO(OH)_2$ or $OPO(OD)_2$) binds the flavylium salt **53AH**$^+$ (or **53AD**$^+$) only weakly. Since phosphoric acid is a weak acid compared to sulphuric acid, we examined the complex formation of flavylium salt **53AH**$^+$ with the sulphate-substituted clip **C2** in the presence of a small amount of DCl with the hope that under these conditions only the quinoidal base **53A** is deuterated and not the clip's sulphate groups. But also under these conditions only the formation of a weak complex was observed in methanol at 25°C by ^{1}H-NMR titration (log K = 2.2 ± 0.1). The large complexation-induced shifts of the guest signals ($\Delta\delta_{max}$ = 2.8 (3-H), 1.5 (5-H), and 0.4 (6-H) again indicate that the guest is bound inside the clip cavity. The small association constant suggests that the sulphate groups of clip **C2** were protonated (respectively deuterated) concomitantly with the protonation/deuteration of the quinoidal base comparable to the hydrogenphosphate groups of clip **C1**.

5.2.3 Studies in water

The study of the host-guest interactions of flavylium salts **51** and **52** in aqueous solutions could not be performed because the complexes precipitate from water. However, water is by far the most interesting medium to study the effects of host-guest formation on the network of reactions of flavylium salts.

The compound **DHMF**, **53AH**$^+$, does not suffer hydration in aqueous solution to give the hemiketal species. The only observed processes are the acid-base reactions to form the neutral quinoidal base **3A** with pK_a = 4.0 and the anionic deprotonated species **3A**$^-$ with pK_{a2} = 6.8.[10]

Flavylium salt **53** could be associated with clip **C1** in aqueous media, under dilute conditions. The addition of clip **C1** to an acidic solution of the flavylium salt at pH = 2 gives rise to a red shift from 380 nm to 387 nm accompanied by a decrease of the absorption intensity. This red shift was also observed upon addition of **C1** to flavylium salts **51** and **52** in methanol and is an indicator for the flavylium salts entering into the clip cavity. Although the host-guest complex that is being formed (1:1) slowly precipitates, it was possible to determine the association constant for the complex formation between the flavylium salt **53AH**$^+$ and clip **C1** by UV-Vis titration (log K = 4.9 ± 0.1), Figures 5.11 A and B.

When clip **C1** is added to a solution of the quinoidal base of **53A** at pH = 5.3, a decrease in the absorption band centered at 512 nm is observed with no shift in λ_{max} (Figure 5.11 C). The association constant was determined (log K = 4.9 ± 0.1, Figure 5.11 D) for the host-guest complex formation between **53A** and the clip **C1** which was identical within the limits of the experimental error with that obtained for the formation of **53AH**$^+$**@C1**. This finding suggests that the hydrophobic interactions are the major force in aqueous solution that determines the host-guest complex stability here. Evidently, the loss of the attractive

electrostatic interactions (which are present in **53AH$^+$@C1**) has no apparent consequences in the binding constant of **53A@C1**.

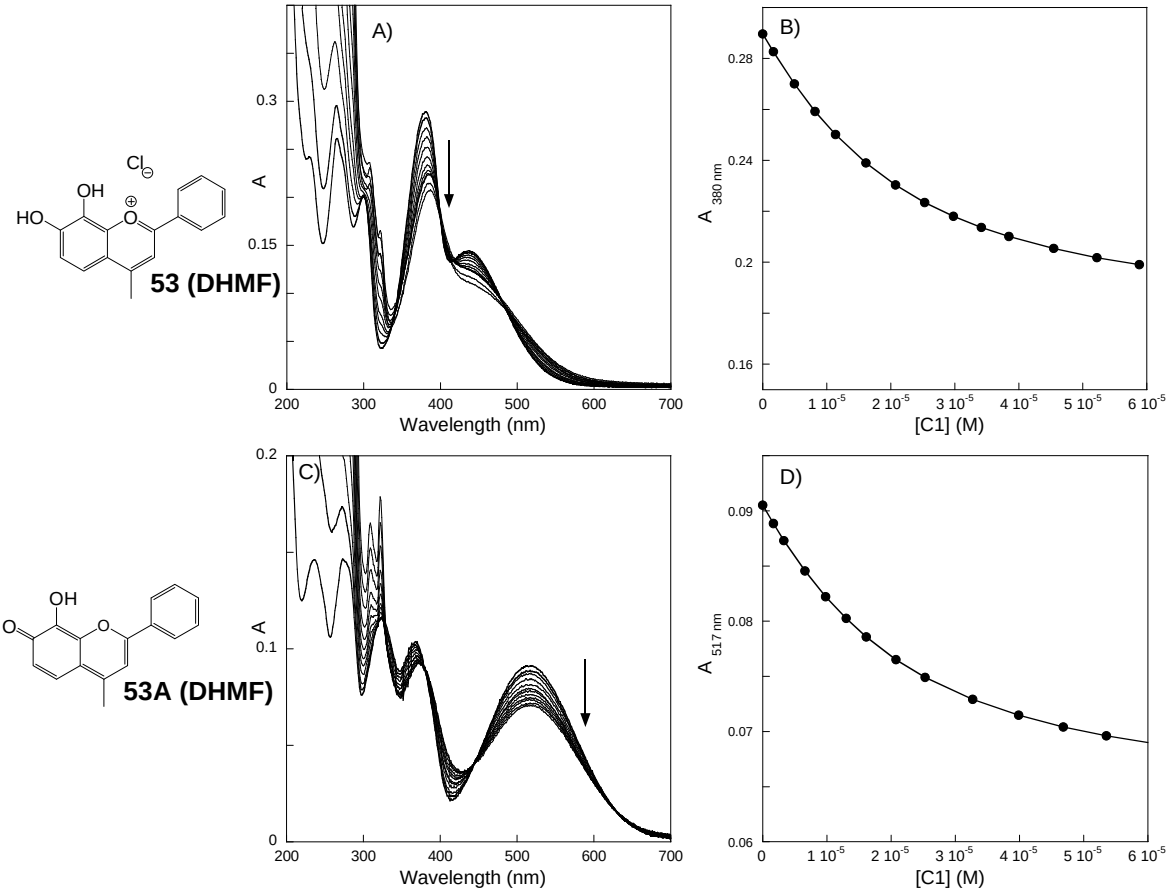

Figure 5.11 – The dependence of the UV-Vis spectra of compound **DHMF**, **53** ([**53**] = 1.3 × 10^{-5} M) from the concentration of clip **C1** ([**C1**] = 0 – 6 × 10^{-5} M) in aqueous solution: A) and B) at pH = 2; C) and D) at pH = 5.3. The association constants were determined from theses concentration dependencies by UV-Vis titration to give the same value of log K = 4.9 ± 0.1 for the formation of both complexes **53AH$^+$@C1** and **53A@C1**. At both pH values, clip **C1** exists in its negatively charged hydrogenphosphate form whereas **53** exist as **53AH$^+$** at pH = 2 and as **53A** at pH = 5.3.

A confirmation of the importance of naphthalene sidewalls in clip **C1** for the binding of the flavylium salt **53AH$^+$** comes from a UV-Vis titration experiment of **53AH$^+$** ([**53AH$^+$**] = 4.2 ×10^{-5} M) with the phosphate-substituted bridge **C3** ([**C3**] = 0 - 1.2 × 10^{-3} M, lacking the naphthalene sidewalls) at pH = 2.0. The phosphate groups (OPO_3^{2-}) of **C3** are certainly protonated to the hydrogenphosphate groups ($OP(OH)O_2^-$) under these acidic conditions. No change in the spectra of **53AH$^+$** was observed upon the addition of **C3** indicating that here the electrostatic interaction between the positively and negatively charged systems is not sufficient to observe the host-guest complex formation.

The high association constants of **53AH$^+$@C1** and **53A@C1** allowed us to study the influence of the molecular clip on the acid-base behavior of flavylium salt **53** through a pH titration ([**C1**] = 5.9 × 10^{-5} M, [**53**] = 1.3 × 10^{-6} M; 81 % association). Figure 5.12 A shows the pH dependence of UV-Vis spectral changes in the acidic pH range resulting from the evolution of complex **53AH$^+$@C1** to **53A@C1**, equation 5.3. A further increase in the pH value leads to

the deprotonation of the quinoidal base **53A** to **53A**$^-$ in the complex with clip **C1** (Figure 5.12 B). These data could be fitted to obtain pK_{a1} = 4.8 and pK_{a2} = 7.0 (Figure 5.12 C). The increase in pK_{a1} of **53** from 4.0 to 4.8, when clip **C1** is present, can be explained by the "intrasupramolecular" charge compensation in the complex between the positively charged flavylium salt inside the negatively charged host cavity. The slight increase in pK_{a2} from 6.8 to 7.0 in the presence of clip is explainable with a destabilization of negatively charged unprotonated quinoidal base in the presence of the negatively charged clip **C1** relative to the neutral quinoidal base. Furthermore, in this pH region, the deprotonation of the hydrogenphosphate to the phosphate groups of clip **C1** also occurs[6] which contributes to such a destabilization.

53AH$^+$**@C1** + H_2O ⇆ **53A@C1** + H_3O^+ (5.3)

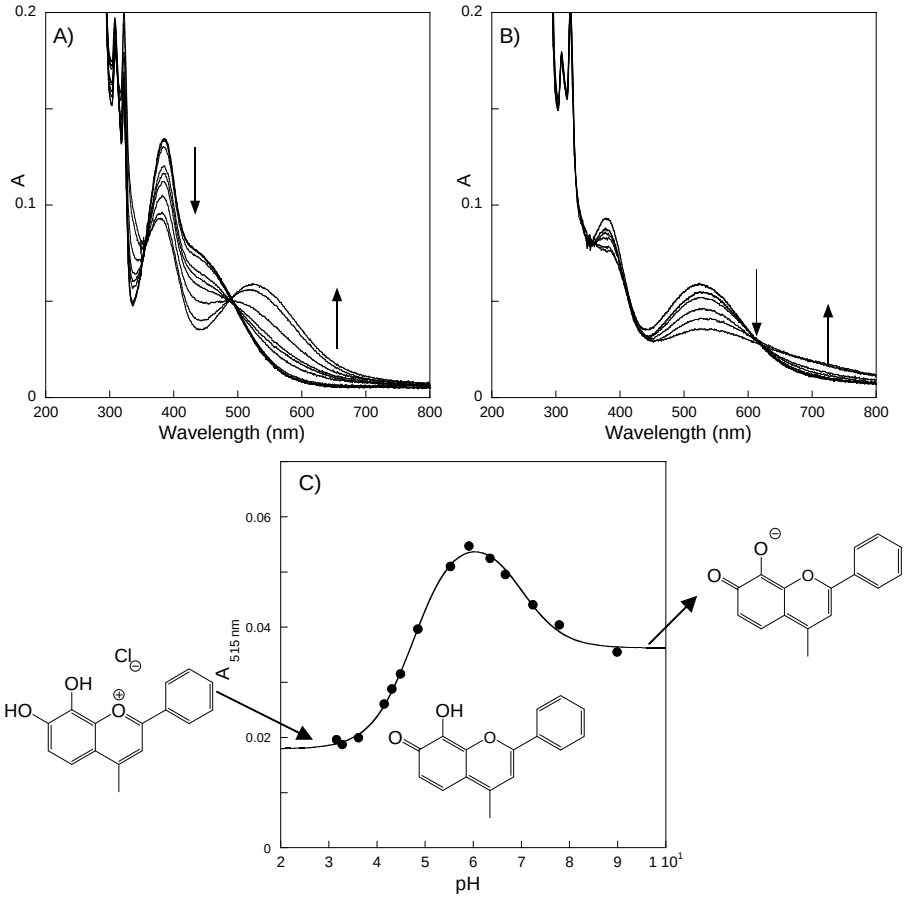

Figure 5.12 – pH titration of the host-guest complex **53@C1** ([**C1**] = 5.9 × 10^{-5} M, [**53**] = 1.3 × 10^{-5} M) in aqueous solution. A) Change in the UV-Vis spectra of **53@C1** observed in the range from pH = 3.2 to pH = 5.9. B) pH = 5.9 to pH = 9.0. C) The pH dependence of the absorption intensity at 515 nm. The continuous curve presents the fit of these data points leading to the pK_a values of 4.8 and 7.0.

5.3 Host-guest formation with molecular clip C2 in aqueous solutions

Molecular clip **C2,** containing two sulphate groups in the central spacer-unit, led to host-guest complexes with flavylium salts that are more soluble in water than the corresponding

complexes with hydrogenphosphate-substituted clip **C1**. The solubility is however limited to the range of concentrations used in absorption and fluorescence measurements. In aqueous solution the compound **DHF**, **54**, undergoes a network of reactions that is well characterized in both thermodynamic and kinetic terms.[11] It also exhibits photochromic behavior in water that has been exploited in liquid solutions as well as in organized media, as discussed in the chapter 2 of this thesis.[11] For these reasons this flavylium salt was chosen to study the influence of host-guest complex formation with molecular clips on the thermal and photochemical behavior of flavylium salts.

At acidic pH values, the flavylium cation **54AH$^+$** is the thermodynamically stable species, Scheme 1.8. By increasing the pH value, the quinoidal base **54A** is only formed as a transient in the equilibrium with cation **54AH$^+$** (pK_a = 4.1) and then **Ct** is obtained in the final thermodynamic equilibrium (pK'_a = 3.1), equations 1.22 and 1.26/1.27.[11] The reaction pathways have already been described, as well the photoisomerization of **Ct** to form **Cc** (and consequently **AH$^+$**/**A**, depending on pH), a reaction that occurs in aqueous solutions as well as in heterogeneous media.[11]

When sulphate clip **C2** is added to an aqueous solution of **54** at pH = 2, the UV-Vis absorption band corresponding to the flavylium cation decreases and the maximum wavelength of absorption is shifted to higher wavelengths, from 457 nm to 465 nm (Figure 5.13 A), similar to the observation for host-guest complex formation between clip **C1** and the flavylium salts **51** and **52** described above. Upon addition of clip **C2** the emission spectra show no wavelength change in the emission maximum but a quenching of the emission intensity. It is known that flavylium salt **54** exhibits excited state proton transfer (ESPT) in protic solvents,[17] so that the emission spectra shown in Figure 5.13 B has features of the quinoidal base **54A**. Taking into account the results observed above for **51**@**C1**, **52**@**C1** and **53A**@**C1**, we expected that the inclusion of flavylium cation **54AH$^+$** into the clip cavity would lead to an increase in the emission quantum yield. The observed quenching shown in Figure 5.13 B is not fully understood and might be correlated with the ESPT process that is not present in the other flavylium salts or with a quenching process of **54AH$^+$** or **54A** encapsulated by the sulphate clip. Assuming a 1:1 stoichiometry, the observed spectral changes lead to an association constant for the formation of **54**@**C2** of log K = 4.3 ± 0.1, Figure 5.13 C.

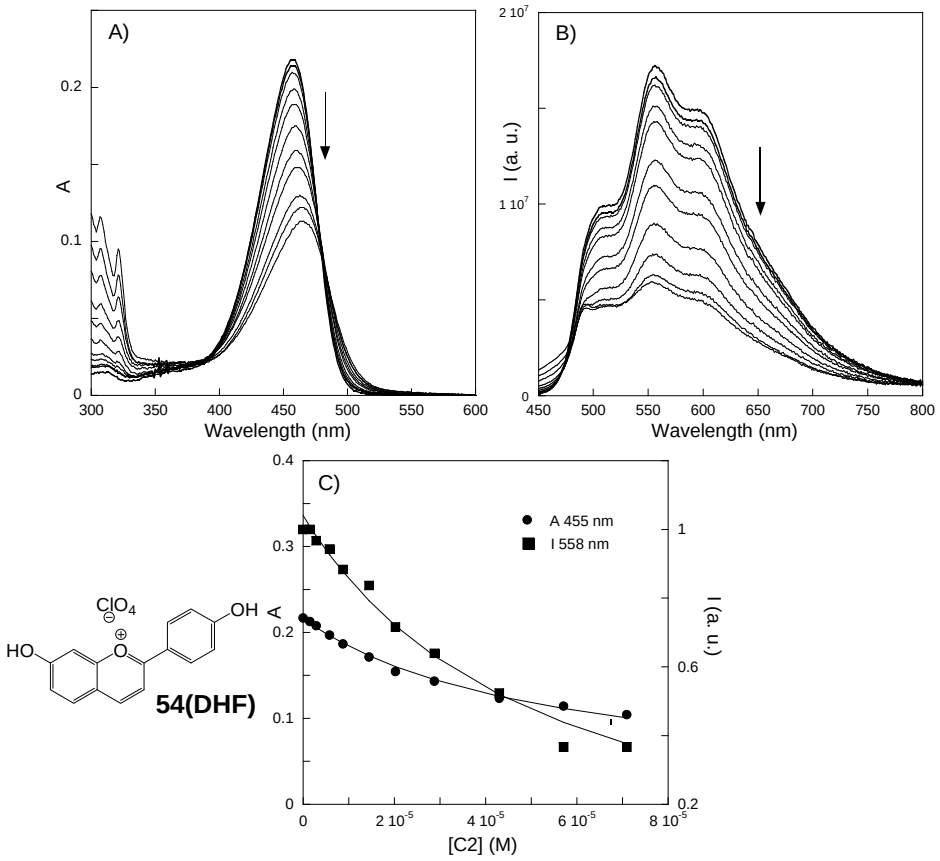

Figure 5.13 – Spectral modifications observed upon addition of clip **C2**, [**C2**] = 0 – 7.2 × 10^{-5} M, to an aqueous solution of **54** at pH = 2, [**54**] = 6.9 × 10^{-6} M, in the presence of buffer,[18] followed by absorption (A) and fluorescence emission (B, λ_{exc} = 420 nm). C) The dependence of the absorption data on A at 455 nm and emission data on B) at 558 nm from the clip concentration were fitted by the use of eq. 5.1 to give log K = 4.3 ± 0.1 for **54AH**$^+$**@C2**.

The thermodynamics of the network of reactions in the presence of clip **C2** was assessed by determining the value of pK'_a= 4.0 ± 0.2, Figure 5.14. The comparison of this value with that of pK'_a = 3.1 obtained for the free flavylium salt in water[11c] shows that the association of **54** with clip **C2** extends the pH stability region of the flavylium cation. The value of pK'_a is a measure of the effective color loss of solution of a flavylium salt, defining the pH range in which its color exists. In nature, anthocyanins often participate into supramolecular structures that also extend the color of the flavylium cations to the pH region of the vacuoles where they accumulate in plant cells.[2]

The fact that the pK'_a for **54@C2** is higher than for free **54** proves that the complexation of **C2** with **AH**$^+$ is stronger than with the other species comprised in **CB**. Among these species, the quinoidal base **A** results from deprotonation of **AH**$^+$ and can be observed upon pH jumps to higher pH values from an acidic solution, where only **AH**$^+$ exists. This experimental approach allowed us to determine the pK_a = 4.5 ± 0.2 for **54@C2**, Figure 5.15.

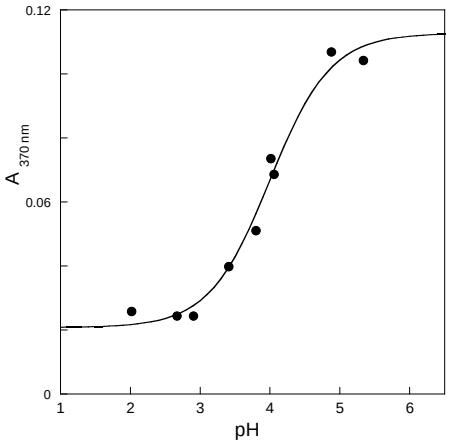

Figure 5.14 –Variation of the absorbance at 370 nm (λ_{max} of **Ct**) of equilibrated aqueous solutions of flavylium salt **54** (7.2×10^{-6} M) and clip **C2** (8.7×10^{-5} M) as a function of pH. Fitting was obtained with $pK'_a = 4.0 \pm 0.2$; T = 21 ± 1 ºC.

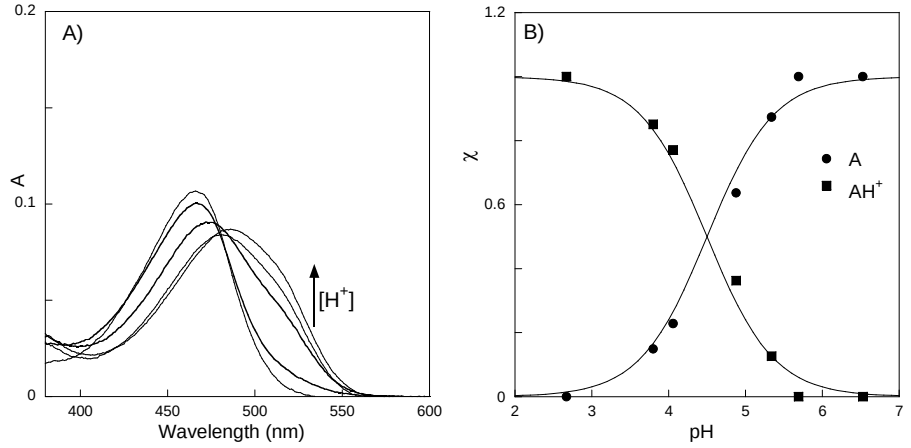

Figure 5.15 – A) The change in the UV-Vis spectra of **54** in the presence of **C2** observed upon pH jumps from pH=2.0 to higher pH values with final concentrations of [**54**] = 7.2×10^{-6} M and [**C2**] = 8.7×10^{-5} M; B) simultaneous fitting of the mole fractions of $\mathbf{AH^+}$ and **A** calculated from the spectral data leads to pK_a=4.5±0.2 for **54**@**C2**, at 21 ± 1 ºC, aqueous solution.

The association constant for the formation of complex **54A**@**C2** could be determined from the values of log K(**54AH**$^+$@**C2**) = 4.3 ± 0.1, pK_a(**54**@**C2**) = 4.5 ± 0.2 and pK_a(**54**) = 4.1[11c]: log K(**54A**@**C2**) = 4.3-4.5-(-4.1) = 3.9; this value is slightly lower than log K(**54A**H$^+$@**C2**) = 4.3 ± 0.1 as expected for the case that the electrostatic interaction between the charged host and guest system is important. But the relatively small difference between these two association constants indicates that other effects (such as the hydrophobic interactions) are responsible for the comparable stability of the host-guest complexes of sulphate-substituted clip **C2** with the charged flavylium salt $\mathbf{54AH^+}$ and neutral quinoidal base **54A** in agreement with the results obtained for the host-guest complexes of the hydrogenphosphate-substituted clip **C1** with $\mathbf{53AH^+}$ and **53A**. The association constants for **C2** with the hemiketal **B** and with the *cis*-chalcone **Cc** could not be determined because they only exist as transient species during the period when $\mathbf{AH^+}$ (which is with the quinoidal base **A** in a fast acid-base equilibrium) reacts to the final equilibrium mixture at slightly acidic to neutral pH values. For free flavylium salt **54** in aqueous solution, the final equilibrium mixture in this pH range contains *ca*. 90% **54Ct** and

10% **54A**.[11a] Adding clip **C2** to such an equilibrated mixture of **54** at pH = 5.19 leads to a change in the UV-Vis spectrum of **54** which is constant after few hours (see Figure 5.16). This spectral change indicates that the final equilibrium mixture in the presence of clip **C2** contains *ca*. 80% **54Ct** and 20% **54A**, showing that **C2** binds **54A** more strongly than it binds **54Ct**. A fast titration of an equilibrated mixture at pH = 5.7 was carried out in order to determine the association constant for complex formation between **C2** and **54Ct**. However, the changes in UV-Vis absorption were too small to allow the determination of this association constant. Furthermore, emission spectroscopy could not be used to determine this constant since the incident light (used for the electronic excitation of **54Ct**) led to a *trans-cis* photoisomerization of **4Ct**, as verified by UV-Vis spectroscopy.

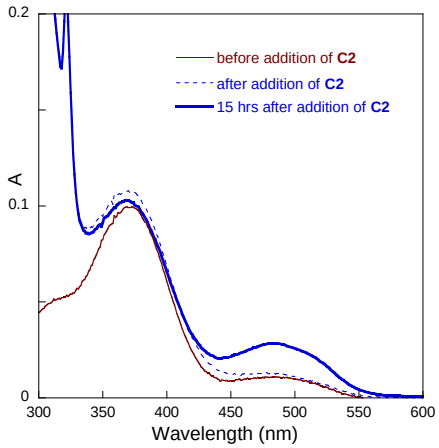

Figure 5.16 – Absorption spectral modifications observed upon addition of sulphate clip **C2**, 8.7×10^{-5} M, to a pre-equilibrated aqueous solutions of the **Ct** of **54**, 7.2×10^{-6} M, in the presence of 10 % of buffer,[19] at pH 5.19. Spectra before addition of the clip **C2** (red), immediately after addition of the clip (traced blue line) and fifteen hours after addition of the clip (bold blue line, in the final equilibrium) are shown. A percentage of *ca* 20% is obtained in the final equilibrium after the addition of clip.

^{1}H-NMR titration experiments confirmed the assumed host-guest complex formation between clip **C2** and *trans*-chalcone **54Ct**. Since the solubility of **54Ct** is not sufficient in water for a NMR analysis, the association constant was determined in methanol to be $\log K = 3.2 \pm 0.3$ (not shown). The small complexation-induced ^{1}H-NMR shifts of the guest signals assigned to the aromatic protons ($\Delta\delta_{max} \leq 0.3$ ppm) and the protons attached to the C=C double bond ($\Delta\delta_{max}$ = 0.14 (2-H), and -0.04 (3-H)) indicate that in this complex neither the aromatic rings nor the double bond of **54Ct** is included inside the clip cavity to a major extend. According to a Monte-Carlo conformer search by the use of force field calculations (SPARTAN, MMFF94, gas phase) there are many low-energy conformers where either the aromatic rings or the C=C double bond of **54Ct** are positioned outside the clip cavity. The mutual exchange between these conformers certainly is a rapid process with respect to the NMR timescale, so that only averaged NMR signals are observed. Therefore, the overall effect of the clip arene-units on the shifts of the ^{1}H NMR guest signals may be small in this case.

The kinetics of the system consisting of flavylium salt **54** and clip **C2** was studied by carrying out pH jumps from solutions at pH = 2 to higher pH values, using UV-Vis absorption spectroscopy to follow the course of reaction. At all pH values, the time dependence of the changes observed in the spectra of **54** in the presence and absence of clip **C2**, until the equilibrium between the different forms of **54** was reached, could be fitted as monoexponential processes. The observed rate constants, k_{obs}, as a function of pH are plotted in Figure 5.17.

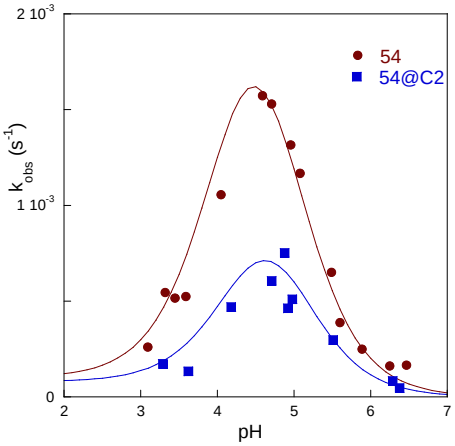

Figure 5.17 – k_{obs} as a function of pH for **54** in aqueous solution (red) and in the presence of clip (blue, **54@C2**), using [**54**] = 7.2×10^{-6} M and [**C2**] = 8.7×10^{-5} M. Fitting was obtained with eq. 1.45, for pK_a = 4.2 for **54** and pK_a = 4.5 for **54@C2**; T = 21 ± 1 ºC.

To describe the observed kinetics, equation 1.45 was used (Supplementary Material, section 9.1.1). The fitting of equation 1.45 to the experimental data in the presence and absence of clip is represented in Figure 5.17. The value of K_a was determined independently (Figure 5.15) and used in the fitting where the following three parameters were adjusted (see equation 1.45): $k_iK_tK_h$, k_{-i} and k_iK_t/k_{-h}. Table 5.4 resumes the thermodynamic and kinetic data for both systems (k_h was calculated through $k_iK_tK_h/(k_iK_t/k_{-h})$).

Table 5.4 – Thermodynamic and kinetic constants for the reactions of free **54** and complexed **54@C2** at 21 ± 1 ºC.

	54	**54@C2**
pK_a	4.1[11c]	4.5 ± 0.2
pK'_a	3.1[11c]	4.0 ± 0.2
$k_iK_tK_h$ / s^{-1} M^{-1}	$(2.1 \pm 0.4) \times 10^{-7}$	$(6 \pm 2) \times 10^{-8}$
k_{-i} / s^{-1}	$(1.0 \pm 0.3) \times 10^{-4}$	$(8 \pm 0.3) \times 10^{-5}$
$\frac{k_i K_T}{k_{-h}}$/M	$(1.8 \pm 0.4) \times 10^{-5}$	$(1.6 \pm 0.4) \times 10^{-5}$
k_h / s^{-1}	$(1.2 \pm 0.4) \times 10^{-2}$	$(4 \pm 1) \times 10^{-3}$

The data for free **54** are in reasonable agreement within the limits of experimental error with previously published data.[11c] Most importantly, Figure 5.17 shows that the binding of **54** to clip **C2** causes a *ca*. 60% reduction of the overall rate constants determined for the conversion of **54AH**$^+$ into the species comprised in **CB**. When the pH of a solution containing the flavylium salt is increased, the first (kinetic) product is the quinoidal base **A** which then equilibrates to **Ct** passing through **AH**$^+$, **B** and **Cc** as transient intermediates. Table 5.4 evidences that the rate constant for the hydration reaction, k_h, is reduced by a factor of 3 in the presence clip **C2**. This might happen because the complexed flavylium cation **54AH**$^+$ is more protected against the attack of a water molecule at C-2 than the free cation.

To gain further insight into the effect of the molecular clip **C2** on the network of reactions of the various forms of **54** we performed flash photolysis experiments in aqueous solutions of equilibrated **4** at various pH values in the presence and absence of clip **C2**. These rate constants display the usual linear dependency with [H$^+$] (equation 1.46, see Figure 5.18), but for higher proton concentrations the rate becomes constant, because the rate determining step is no longer the pH dependent dehydration rate, k_{-h}[H$^+$], and the steady state approach for B and Cc is no longer valid. The results indicate an effect of the clip on the various reactions of **54**. Since some of the parameters are missing, for example the equilibrium constant K_t, this effect cannot be unambiguously assigned to the single reaction steps. With the assumption that K_t is not affected by the presence of the clip, the proton-mediated H_2O elimination of hemiketal **54B** is calculated from the data in Figure 5.18 B to be faster in the complex with **C2** by a factor of 1.4 than in free **54B**. This suggests that the certainly positively polarized transition state of this reaction is stabilized by binding to the clip comparable to that of the flavylium cation **54AH**$^+$.

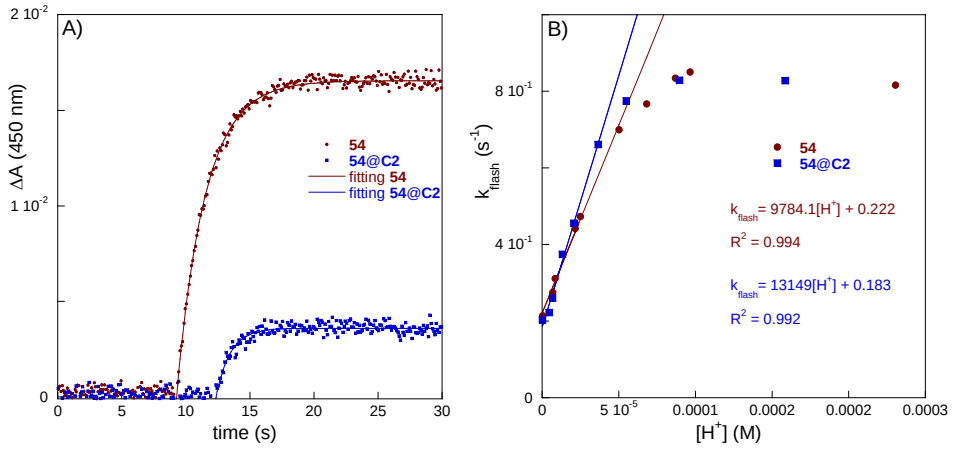

Figure 5.18 –A) Differential absorbance at 450 nm *versus* time in seconds in the absence (red, **54**, pH = 4.66) and in presence of **C2** (blue, **54@C2**, pH = 4.06), [**54**] = 7.2 × 10^{-6} M [**C2**] = 8.7 × 10^{-5} M. Fitting was obtained using an exponential function with k_{flash} = 0.91 s^{-1} in the presence of clip pH = 4.06 and 0.45 s^{-1} without clip pH = 4.66. B) Rates of flash photolysis *versus* [H$^+$], for **54** (red) and **54@C2** blue. Linear regressions and obtained equations and correlation coefficients are shown.

The photoisomerization of the *trans*-chalcone **54Ct** was studied in the presence of clip **C2** to gain further information about the effect of the clip on the network of reactions. To an

aqueous solution of equilibrated **54** at pH = 5.7, containing *ca*. 90% of **54Ct** and 10% of **54A**, clip **C2** was added and the solution irradiated at 390 nm (where clip **C2** no longer absorbs), Figure 5.19. A solution of equilibrated **54** in the absence of clip was also irradiated.

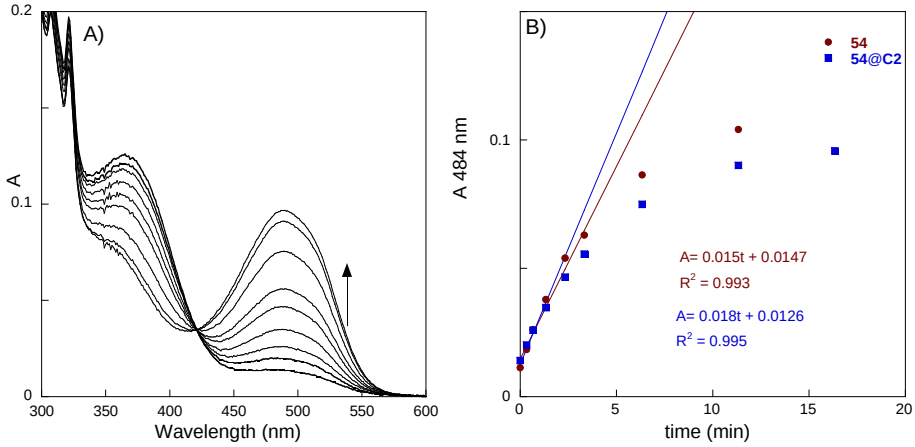

Figure 5.19 – A) Spectral modifications that occur upon irradiation at 390 nm of an aqueous solution of equilibrated [**54**] = 6.3×10^{-6} M at pH = 5.7 in presence of clip [**C2**] = 4.0×10^{-5} M. b) Changes in absorbance at 484 nm in the absence (red circles, **54**) and in presence of **C2** (blue squares, **54@C2**) with time at pH = 5.7.

Figure 5.19 A shows that irradiation of **54Ct** at pH = 5.7 in the presence of clip leads to the formation of **54A**, as expected at this pH (pK_a = 4.2). The presence of a clean isosbestic point in the spectra shows that no degradation accompanies the photoisomerization reaction and also that the reactions passing through **54Cc**, **54B**, **54AH**$^+$ as intermediates to **54A** occur in the subsecond timescale. The solutions in the absence and in presence of clip have the same absorbance at λ_{irr} = 390 nm, so that the slopes in Figure 5.19 B are a direct measure of the *trans-cis* photoisomerization quantum yields and these are the same for both experiments within the limits of the experimental error indicating that the clip **C2** has no significant effect on the photochemical *trans-cis* isomerization of **54Ct** to **54Cc**.

$$\Phi = \Phi_{Ct-Cc}\frac{\left[H^+\right]}{\left[H^+\right]+\frac{k_i K_t}{k_{-h}}} \qquad (1.48)$$

The quantum yield is given by equation 1.48 (Supplementary material, section 9.1.3). Since Table 5.4 shows that the ratio k_iK_t/k_{-h} is the same within the limits of experimental error independently of the presence of clip, the pH-dependent factor is also the same. The similarity of slopes in Figure 5.19 B would then mean that $\Phi_{Ct\rightarrow Cc}$, the intrinsic quantum yield of the reaction, is not much affected by the addition of clip. This conclusion is however to be taken with caution since the measured quantum yields are actually a combination of the quantum yield

of the **Ct** inside the clip and in bulk solution and there is large uncertainty in the association constant between **54Ct** and **C2**.

5.4 Experimental Part

All reagents and solvents used were of analytical grade. The synthesis of water soluble molecular clips, the mass spectroscopy, the NMR studies and calculations were performed by Professor F-G. Klärner's group in Duisburg-Essen University.

5.4.1 Synthesis

Synthesis of water-soluble clip **C1** and **C2** and the bridge **C3** was described in the literature.[6,7] Flavylium salts **51**-**54** were available from previous studies.[8,9,10,11] ESI mass spectra were recorded on a Bruker BioTOF II-Mass spectrometer.

5.4.2 Measurements

All flavylium solutions were freshly prepared using acidified (HCl) water or methanol. The association constants were determined by adding increasing amounts of a stock solution of the clip to 2 ml of the flavylium. After each addition the absorption and emission spectra were taken. Absorption spectra were run on a Shimadzu UV-2501PC or a CARY 100Bio and fluorescence spectra on a Jobin Yvon Spex, Fluorolog FL3-22. Fluorescence quantum yields were determined using Rhodamine 6G in ethanol as standard for flavylium salts **51** and **52** (**AH**$^+$ form) and **53** (**A** form); perylene in toluene was used as standard for **53** (AH^+ form). Standard fluorescence quantum yields and refractive indexes were taken from literature.[19,20]

Time-resolved fluorescence decays with picosecond resolution were obtained by the single-photon time technique using laser excitation at 390 nm and recording the emission at 510 nm. The setup consisted of a Ti:Sapphire laser Tsunami (Spectra Physics) pumped with a solid state laser Millennia Xs (Spectra Physics), delivering 70 fs pulses at a repetition rate of 80 MHz. The laser repetition rate was reduced to 4 MHz using a pulse-picker, and the output was frequency doubled to 390 nm (~ 1 nJ per pulse) and vertically polarized. The fluorescence passed through a polarizer set at the magic angle and was selected by a Jobin-Yvon HR320 monochromator with a grating of 100 lines/mm and detected by a Hamamatsu 2809U-01 microchannel plate photomultiplier. The experimental excitation pulse (FWHM = 35 ps) was measured using a LUDOX scattering solution in water. The decays were stored in a multichannel analyzer working with 1024 channels. The fluorescence emission was observed at 510 nm using a cutoff filter to effectively eliminate the scattered light from the sample. The experimental decay curves were fitted to simulated curves using a non linear least-squares reconvolution method.

pH jumps were carried out by mixing 100 µl of universal buffer at desired pH,[19] 400 µl of NaOH 0.01 M and 500 µl of a stock solution of the flavylium **54** at pH 2.0 (1.4×10^{-5} M) or

200 µl of NaOH 0.01 M, 200 µl of a stock solution of the flavylium cation at pH 2.0 (3.4×10^{-5} M) and 500 µl of water. In the cases where the clip is present, 30 µl of clip **C2** 2.9×10^{-3} M or 28.5 µl of clip **C2** 3.1×10^{-3} M were previously mixed with the used amount of the flavylium ion. The absorption spectrum was read immediately after the pH jump and followed along the time.

Flash photolysis experiments were performed as described elsewhere,[11b] using a CARY 5000 with fiber optics adapter and a head to which the flash was adapted. A filter was used in the reference beam (neutral density, T = 0.01) in order to maximize the signal. The kinetics was followed at 450 nm, average time 0.1 s and 5 nm slits.

The photoisomerization reaction of **54Ct** was studied by irradiating 3 ml of an aqueous solution of equilibrated [**54**] = 6.3×10^{-6} M at pH = 5.7 in presence and in absence of clip [**C2**] = 4.0×10^{-5} M, following the reaction by UV-Vis spectroscopy. The irradiations were carried out using as light source the 450 W Xenon lamp of a Fluorolog FL3-22, with 5 nm slits in both monochromators.

5.5 Conclusions

It was possible to demonstrate, that UV-Vis absorption and fluorescence spectroscopy, on one hand, and ^{1}H-NMR spectroscopy, on the other hand, are complementary techniques for the investigation of host-guest complexes. Due to the different range of concentrations required for the measurements, the electronic spectroscopic methods are particularly suited for the determination of high binding constants, *K*, while NMR is better suited for the determination of lower *K* values. NMR provides, however, valuable information about the structures of host-guest complexes which cannot be gained by the other methods.

The hydrogenphosphate-substituted molecular clip **C1** forms highly stable host-guest complexes with the flavylium salts **DHAF**, **51** (6-hydroxy-4'-(*N,N*-dimethylamino)flavylium hexafluorophosphate) and **DEF**, **52** (7-(*N,N*-diethylamino)-4'-hydroxyflavylium tetrafluoroborate) in methanol. The large binding constants (log *K* = 4.1 and 4.7 determined by fluorometric titration for the formation of **51@C1** and **52@C1**, respectively) and the large complexation-induced ^{1}H-NMR shifts of the guest signals assigned to the protons 3- and 4-H of **51** or **52** allow the conclusion that in each complex the positively charged pyrylium ring of **51** or **52** is bound inside the clip cavity and, hence, cation-π interactions provide an important contribution to the host-guest complex formation besides other noncovalent bonds, for example the Coulombic ion-ion and the solvophobic interactions. To explain the surprising result, that the neutral quinoidal base **53A** (quinoidal base from 7,8-dihydroxy-4-methyl flavylium chloride, **DHMF**) forms an even more stable complex with clip **C1** in methanol (log *K* = 5.6), we assume that the solvophobic interactions contribute to the noncovalent host-guest binding substantially. In water the solvophobic effect (in this case the hydrophobic effect) should be even stronger than in methanol. Indeed, clip **C1** forms stable (1:1) complexes with the flavylium

salts **51**, **52**, and **53AH**$^+$ and the quinoidal base **53A**, but these complexes are insoluble in water and precipitate during the mixing of aqueous solutions containing both the clip and one of guest compounds. In highly diluted aqueous solution the association constants for the complex formation of clip **C1** with the flavylium salt **53AH**$^+$ at pH = 2 and the quinoidal base **53A** at pH = 5.3 could be determined by UV-Vis titration experiments to be log $K = 4.9$ for the formation of both complexes. The finding that the complexes of the positively charged flavylium salt and the neutral quinoidal base are of the same stability, indicates that here the hydrophobic interactions are dominating for the host-guest binding. The increase in the pK_a value of the acid-base reaction in the presence of clip **C1** from 4.0 to 4.8 shows, that the proton dissociation from **53AH**$^+$ is more difficult inside the negatively charged clip cavity than in the free flavylium salt. As a consequence of this finding, the pH stability region of the flavylium cation is extended in the clip cavity to higher pH values.

Host-guest complexes of the sulphate-substituted clip **C2** with the flavylium salt **DHF**, **54** (7,4'-dihydroxyflavylium) and the other network species are slightly more soluble in water. Therefore, thermodynamic and kinetics analyses could be performed in the presence of the clip **C2** by a combination of UV-Vis and fluorescence spectroscopy, pH jump and flash photolysis methods. The finding, that clip **C2** forms complexes with **54AH**$^+$ and **54A** of comparable stability, confirms the results obtained for the complex formation of clip **C1** with **53AH**$^+$ and **53A** and provides further evidence for the importance of the hydrophobic interaction for the host-guest binding observed here. The *trans*-chalcone **54Ct** is also bounded inside the clip cavity, which could be confirmed by ^{1}H NMR titration experiments independently. Since the solubility of **54Ct** is not sufficient in water for a NMR analysis, the association constant was determined in methanol to be log $K = 3.2 \pm 0.3$.

According to the kinetic data, the H_2O addition to **54AH**$^+$ followed by H^+ elimination leading to **54B**, that is the hydration reaction, is retarded in the presence of clip **C2**. This is presumably due to the steric constraints of the clip cavity in which the bimolecular H_2O addition to **54AH**$^+$ has to proceed and it might be correlated with the mechanism that Nature indeed uses to perverse the color at physiological pH values. On the other hand, the photochemically-induced *trans-cis* isomerization of the chalcones seems essentially not affected by encapsulation.

5.6 References

[1] a) R. Brouillard, *Flavonoids and Flower Colour* in *The Flavonoids*; ed. J. B. Harborne, Chapman and Hall, New York, Chapter 16, pp 525-538; b) C. A. Mazza, H. E. Boccalandro, C. V. Geordano, D. Battista, A. L. Scopel, C. L. Ballaré, *Plant Physiology* **2000**, 122, 117-126.

[2] a) T. Hondo, K. Yoshida, A. Nakagawa, T. Kawai, H. Tamura, T. Goto, *Nature* **1992**, 358, 515-518; b) T. Hondo, K. Yoshida, A. Nakagawa, T. Kawai, H. Tamura, T. Goto, T. Kondo, *Angew. Chem.* **1991**, 103, 17–33; *Angew. Chem. Int. Ed. Engl.* **1991**, 30, 17-33; c) T. Kondo, M. Ueda, K. Yoshida, K. Titani, M. Isobe, T. Goto, *J. Am.Chem. Soc.* **1994**, 116, 7457-7458; d) T. Kondo, K.-I. Oyama, K. Yoshida,

Angew. Chem. **2001**, 113, 918-922; *Angew. Chem. Int. Ed.* **2001**, 40, 894-897; e) M. Shiono, N. Matsugaki, K. Takeda, *Nature* **2005**, 436, 791.
[3] R. Gomes, A. J. Parola, J. C. Lima, F. Pina, *Chem. Eur. J.* **2006**, 12, 7906-7912.
[4] P. F. da Silva, J. C. Lima, A. A. Freitas, K. Shimizu, A. L. Maçanita, F. H. Quina, *J. Phys. Chem. A* **2005**, 109, 7329-7338.
[5] a) F.-G. Klärner, B. Kahlert, *Acc. Chem. Res.* **2003**, 36, 919-932; b) F.-G. Klärner, M. C. Kuchenbrandt, In *Strategies and Tactics in Organic Synthesis,* Vol. *7*, ed. M. Harmata, Academic Press - Elsevier, Amsterdam, **2008**, Chapter 4, vol. 7, page 99-153.
[6] a) M. Fokkens, C. Jasper, T. Schrader, F. Koziol, C. Ochsenfeld, J. Polkowska, M. Lobert, B. Kahlert, F.-G Klärner, *Chem. Eur. J*., **2005**, *11*, 477-494; b) J. Polkowska, F. Bastkowski, T. Schrader, F.-G. Klärner, J. Zienau, F. Koziol, C. Ochsenfeld, *J. Phys. Org. Chem*., **2009**, 22, 779-790; c) M. Kirsch, P. Talbiersky, J. Polkowska, F. Bastkowski, T. Schaller, H. de Groot, F.-G. Klärner, T. Schrader, *Angew. Chem. Int. Ed. Engl.*, **2009**, 48, 2886-2890.
[7] a) T. Schrader, M. Fokkens, F.-G Klärner, J.Polkowska, F. Bastkowski, *J. Org. Chem*. **2005**, 70, 10227-10237; b) B. Branchi, P. Ceroni, V. Balzani, M. C. Cartagena, F.-G. Klärner, T. Schrader, F. Vögtle, *New J. Chem.* **2009***,* 33, 397-407.
[8] C. A. T. Laia, A. J. Parola, ,F. Folgosa, F. Pina, *Org. Biomol. Chem*. **2007**, 5, 69-77.
[9] M. C. Moncada, D. Fernández, J. C. Lima, A. J. Parola, C. Lodeiro, F. Folgosa, M. J. Melo, F. Pina,, *Org. Biomol. Chem.* **2004**, 2, 2802-2808.
[10] M. C. Moncada, S. Moura, M. J. Melo, A. Roque, C. Lodeiro, F. Pina, *Inorg. Chim. Acta* **2003**, 356, 51-61.
[11] a) P. Figueiredo, J. C. Lima, H. Santos, M. C. Wigand, R. Brouillard, A. L. Maçanita, F. Pina, *J. Am. Chem. Soc.* **1994**, 116, 1249-1254; b) F. Pina, M. J. Melo, R. Ballardini, L. Flamigni, M. Maestri, *New. J. Chem.* **1997***, 21*, 969-976; c) F. Pina, L. Benedito, M. J. Melo, A. J. Parola, J. C. Lima, A. L. Maçanita, *Anales De Quimica* **1997**, 93, 111-118; d) F. Pina, M. J. Melo, A. J. Parola, M. Maestri, V. Balzani, *Chem. Eur. J.*, **1998,** 4*,* 2001-2007; e) F. Pina, M. Maestri, V. Balzani, *Chem.Commun.* **1999**, 107-114; f) Pina, F.; Lima, J. C.; Parola, A. J. C.; Afonso, A. M. *Angew. Chem. Int. Ed.* **2004**, 43, 1525-1527; g) F. Galindo, J. C. Lima, S. V. Luis, A. J. Parola, F. Pina, *Adv. Funct. Mat.* **2005**, 15, 541-545.
[12] a) G. Haucke, P. Czerney, C. Igney, *Ber. Bunsenges. Phys. Chem.* **1989**, 93, 805-815; b) G. Haucke, P. Czerney, F. Cebulla, *Ber. Bunsenges. Phys. Chem.* **1992**, 96, 880-886.
[13] P. Cudic, M. Zinic, V. Tomisic, V. Simeon, J.-P. Vigneron, , J.-M. Lehn *J. Chem. Soc., Chem. Commun.* **1995**, 1073-1075.
[14] SPARTAN 04 version 1.0.0; Wave Function Inc.; Irvine, CA, **2004**.
[15] F. Mohamadi, N. G. J. Richards, W. C. Guida, R. Liskamp, M. Lipton, C. Caufield, G. Chang, T. Hendrickson, W. C. Still, *J. Comput. Chem*. **1990**, 11, 440 –467. Macromodel, v. 7.1, Schrödinger, 1500 SW First Ave., Ste. 1180, Portland, OR 97201.
[16] The electrostatic potential surfaces (EPS) shown in Figure 5.10 were calculated by the use of computer program SPARTAN 04 Version 1.0.0 (Wavefunction Inc.) as described by a) M. Kamieth, F.-G. Klärner, F. Diederich, *Angew. Chem. Int. Ed.* **1998**, 37, 3303-3306; b) F.-G. Klärner, J. Panitzky, D. Preda, L. Scott, *J. Mol. Mode* **2000**, 6, 318-327.
[17] F. Pina, M. J. Melo, H. Santos, J. C. Lima, I. Abreu, R. Ballardini, M. Maestri, *New J. Chem.* **1998**, 22, 1093-1098.
[18] F. W. Küster, A. Thiel*, Tabelle per le Analisi Chimiche e Chimico- Fisiche*, 12th ed.; Hoepli, Milano, Italy, **1982**, 157-160.
[19] J. Olmsted, *J. Phys. Chem.***, 1979**, 83, 2581-2584.
[20] M. Montalti, A. Credi, L. Prodi, M. T. Gandolfi, *Handbook of Photochemistry*, CRC Press, Boca Raton, FL, **2006**, 3rd ed, Chapter 12, 601-616.

6. Supramolecular host-guest flavylium-loaded zeolite L hybrid materials: network of reactions of encapsulated 7,4'-dihydroxyflavylium (DHF)

In this chapter a preliminary spectroscopic study of the network of reactions of a flavylium dye encapsulated into the one-dimensional channels of zeolite L is reported.

6.1 Introduction

The importance of flavylium salts as colorants, as well as the complex pH and light dependent network of reactions that these compounds exhibit in water, leading to several species with different chemical properties[1] has been already stressed throughout this thesis. Many interesting photochemical applications of this type of dyes in solution or in gels have been reported in the literature and were also outlined previously.[2,3,4] In particular, flavylium based systems are well-known for their ability to behave as models for optical memories capable of performing *write-read-erase* cycles or even mimicking some elementary properties of neurons.[5,6] The role of flavylium in the field of optical memory may become more evident and even appealing if one encapsulates it into versatile nano containers, such as zeolite L (see Scheme 6.1).

Zeolite L is an aluminosilicate that forms crystals with parallel one-dimensional channels with pore openings of about 7.1 Å in diameter, which is therefore able to accommodate a large variety of small dyes, Scheme 6.1.[7] Additionally, zeolite L crystals can be assembled into oriented monolayers forming highly anisotropic materials,[8] can be assembled with bio-systems[9] and can be used for bio-imaging.[10]

The aim of this chapter is studying the optical properties of flavylium-loaded zeolite L crystals and investigating the photoisomerization of this hybrid system. The different forms that flavylium species can assume in aqueous solution depend on several factors, such as the nature and position of the groups linked to the basic 2-phenylbenzopyrylium ring.[1] As seen previously, it is very common that at neutral or basic pH values the *trans*-chalcones are the most stable species, and that **Ct** (or its deprotoned form $\mathbf{Ct^{n-}}$) can be reverted by the action of light to **Cc** (or $\mathbf{Cc^{n-}}$), **B** or even $\mathbf{AH^+}$ and **A**, depending on the final pH and on the existence or absence of thermal barrier for *cis-trans* isomerization.[1] The formation of the most colored species $\mathbf{AH^+}$ and **A** from the usually colorless **Ct** results in the best color contrast. However, this general picture might be very different in intra-zeolite environment.

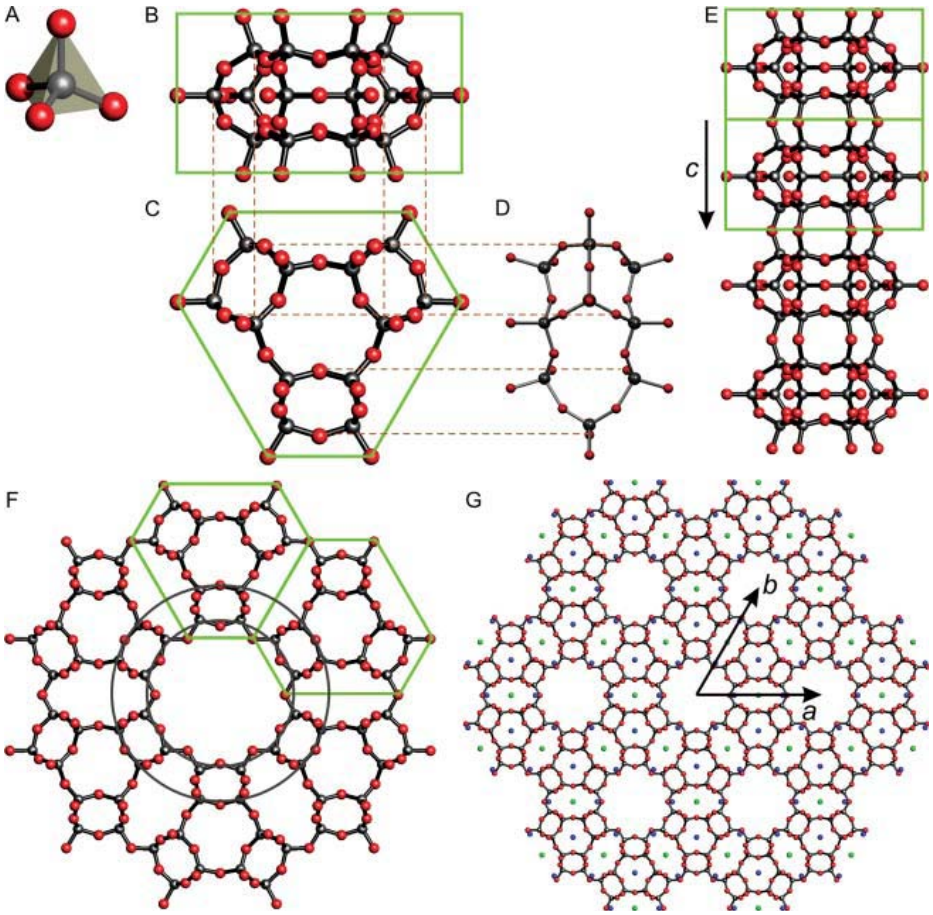

Scheme 6.1 –Structure of zeolite L. A) Primary building unit, grey spheres are Si or Al atoms, red are oxygen atoms. B)–D) Secondary building unit, cancrinite cage (18 corner-sharing tetrahedra). E) Stacking the cages along the *c*-axis of the crystal. The length of the vector *c* is 7.5 Å. F) Top view of a 1D channel; cancrinite cages are connected in a plane perpendicular to the *c*-axis (*a*,*b*-plane). The two grey circles mark the shortest and the largest channel openings, 7.1 and 12.6 Å, respectively. G) Channel system, blue and green balls represent charge compensating cations. The length of the vectors *a* and *b* is 18.4 Å.[11]

Kohno *et al.*[12] have recently proved that encapsulation of flavylium dyes, by cationic exchange, in protonated zeolites (Y and Mordenite), enhances significantly the thermal and chemical stability of the flavylium dye.[12] The authors, however, did not show any experimental evidence of the encapsulation of the neutral species (such as **Ct**) and were not concerned with the possibility of the occurrence of isomerization inside the zeolites.[12] This is exactly what we intend to address in the work developed in this chapter.

Isomerization inside the cavities of zeolites is still a hot topic in the literature. Intrazeolite chemistry and, photoisomerization in a particular way, can be radically different from those found in solution, due to geometrical constraints (that can be the reason for transition state selectivities) and particular interactions, for instance, with cations (that can cause various alterations of the photophysical and photochemical properties).[13,14] Azobenzene,[15,16,17] stilbene,[18,19,20] thioindingo[13] and α,ω-diphenyl allyl cations[21] have been shown to photoisomerize inside the cavities of zeolites.

For azobenzene, the thermal isomerization from *cis* to *trans* in the cavity of zeolite Y (K and Na)[14] is 20 fold slower than in benzene, if solvent is excluded from the cavities and cannot

stabilize the transition state.[15] However, there is no significant difference between the photochemical behavior of azobenzene in NaY, compared to the solution photochemical behavior.[16] Nevertheless, in the smaller cavities of Na-Mordenite[14] the photostationary state has more non photoisomerized *trans*-isomer, illustrating that steric effects play a role on the photoreaction.[16]

Stilbene one way isomerization from *cis* to *trans* was reported on silicalite,[20] Na-Y, H-Y, H-ZSM-5 and H-Mordenite thermally,[18] and *trans*-*cis* photochemically in Na-Y and K-Y.[19] The mechanisms for the isomerization are discussed.[18,19,20]

Thioindigo in NaX[14] was shown to exhibit photoinduced *cis*-*trans* isomerization only for NaX-encaged thioindigo molecules which are not closely coordinated to sodium cations.[13] Moreover, the thermal back reaction is slower for the encaged dye (increase of energy barrier). Schulz-Ekloff *et al.* indeed illustrated how zeolite-dye composites can represent an improved system for optical data storage, comparatively to systems in solution.[13]

1,3-diphenylpropenylium and 1,5-diphenylpentadienylium ions have been generated within acid ZSM-5 and Mordenite zeolites as persistent species (by adsorption of precursors) and irradiation of these allylic cations led to *cis*-*trans* isomerization.[21] This work from Garcia *et al.* proves that there is enough space, even in the small ZSM-5, to accommodate the planar and the non planar stereoisomers of these cations, even if *cis*-stilbene is reported to be excluded by its pores.[21]

6.2 Incorporation of the flavylium dyes in zeolite L

The flavylium salt used in this study, 7,4'-dihydroxyflavylium (Scheme 1.8, **DHF**), was synthesized according to a well-known procedure[22,23] and its **Ct** form was also isolated according to published procedures, from the flavylium ion.[24] In a first approach, **DHF** was inserted inside the zeolite by cation exchange in water at pH = 2, using [**DHF**] = 6.4 x 10^{-5} M and loading overnight at 70 ºC. While this procedure allows the encapsulation of $\mathbf{AH^+}$, it prevents the formation of **Ct** species. Our attempts to increase the pH of the zeolite loaded with $\mathbf{AH^+}$, through equilibration with buffers, were not successful to observe formation of **Ct** inside the zeolite, as expected due to the great affinity of the zeolite cavity for protons. Moreover, addition of NaOH is not advisable since it destroys the crystalline structure of zeolite L.[25] Therefore, a possible approach would be the direct incorporation of the neutral **Ct** species. The gas-phase insertion was not successful due to thermal instability of **Ct**. Encapsulation of **Ct** was finally achieved from a saturated solution of the compound in toluene with triethylamine (20 %), used to capture protons and keep the pH more basic. We employed zeolite L 0.7-1.2 μm in width: 1-1.4 μm in length, in order to have relatively large zeolite to be visible in an optical microscope, but still small enough to have uniform suspensions, and therefore improved the quality of the spectra obtained. The main pores of the potassium exchanged zeolite L have been reported to exhibit a proton activity similar to that of an aqueous solution with pH 3.4.[25] After

inserting the dye into the K^+-exchanged zeolite L, the loaded crystals were washed and centrifuged several times with ethanol and acetone, until no more color was observed in the supernatant. The dye loading *p* inside the zeolite L was calculated by dissolving the zeolite framework in HF and measuring the absorbance of the released dye, as previously described.[26] A loading of 2 % was obtained.

6.3 Evidences for the incorporation

The loaded crystals were then suspended in water (1.1 mg/L) and its spectroscopic behavior was investigated. For comparison purposes, the spectra of free **AH**$^+$ and **Ct** in water are shown in Figure 6.1, together with the loaded K^+-exchanged zeolite L.

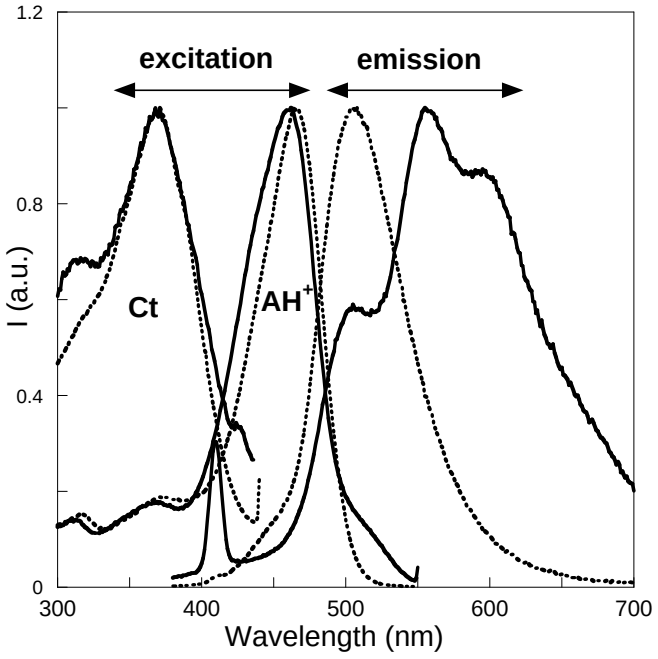

Figure 6.1 – Normalized emission and excitation spectra of free **DHF** in water (full lines) and encapsulated inside the K^+-exchanged zeolite L (pointed lines) at room temperature – aqueous suspension, 1.1 mg / ml, after preparation (*ca.* 32 min, Figure 6.3). The emission spectrum of the free compound (full line) was obtained by excitation at 360 nm at pH = 3.0, where both **AH**$^+$ and **Ct** are in equilibrium. The excitation spectrum of free **AH**$^+$ was performed at 555 nm at pH = 3.0, while the excitation spectrum of free **Ct** was carried out by recording the emission at 500 nm at pH = 5. The concomitant excitation spectra of the aqueous suspension of the compound encapsulated in zeolite L were obtained by recording the emission at 450 nm (**Ct**) and 555 nm (**AH**$^+$), and the respective emission spectrum was obtained exciting at 360 nm.

The emission of free **DHF** in water was previously reported and is shown in Figure 6.1, full line. Three contributions can be observed; i) **AH**$^+$ (λ_{max} = 507 nm), **A** (λ_{max} = 555 nm, shoulder at ca 600 nm) and a contribution from the **Ct** (λ_{max} = 502 nm) superimposed with the emission of **AH**$^+$). The emission from **A** was attributed to excited state proton transfer (ESPT, $pK^*_a \sim 0$)[27], a common phenomenon observed in the spectroscopy of hydroxyflavylium compounds. On the other hand, the emission from **Ct**, which is in part coincident with the one of the flavylium cation, is confirmed by the excitation spectra recording emission at 500 nm,

Figure 6.1. The large Stokes shift observed for the **Ct** species in aqueous solution (7160 cm^{-1}) can be explained on the basis of a large geometry change in the excited state.

Regarding the emission of **DHF** loaded zeolite L, only the $\mathbf{AH^+}$ species (λ_{max} = 508 nm) and **Ct** (λ_{max} ca 480 nm, see below) are detected, suggesting that ESPT does not occur inside the zeolite, probably due to the small availability of water to accept protons. On the other hand, the Stokes shift for the **Ct** species is significantly smaller (by 1040 cm^{-1}) inside the zeolite. One possible explanation for this behavior can be the existence of space restrictions for the distortion of the excited state. In conclusion, the fluorescence emission of the dye changes dramatically in the zeolite in comparison with water, and this is only compatible with the encapsulation.

Upon encapsulation, the excitation spectra of $\mathbf{AH^+}$ and **Ct** exhibit a red shift (5 nm and 2 nm respectively), which is frequently found for some encapsulated compounds and can be due to the interaction with the framework of the zeolite. [12,28] The smaller red shift observed for the neutral species, almost imperceptible in Figure 6.1, is expected on the basis of a smaller interaction with the negative framework of zeolite L, in comparison with the positively charged species.[29] Despite this small change in the maximum of the excitation spectra, one can see clearly that its shape is modified upon encapsulation: the band becomes sharper and the contribution of the shoulder at *ca* 315 nm is smaller by a factor of *ca* 0.8. The most interesting feature of this result is the detection of the **Ct** species inside the zeolite L. This was achieved because K^+ was used as counter-ion to keep the proton activity of the zeolite L channels similar to that of a solution with pH 3.4.[25]

The emission from dyes encapsulated inside the one-dimensional channels of zeolite L can be extremely anisotropic depending on the length *d* of the dye and the relative orientation of the transition moments and *c*-axis: small dyes ($d \approx 9$ Å) can be aligned perpendicularly to the *c*-axis, emitting with maximum intensity when the polarizer is perpendicular to the *c*-axis and disappearing when it is parallel to the axis. On the hard, larger dies ($d \approx 19$ Å) have no choice but to align along the *c*-axis, and the opposite situation is verified, giving rise also to a strongly polarized emission. Zeolite L loaded with dyes of intermediate sizes can exhibit any behavior between these two extremes and even exhibit no polarized emission if the transition lies at the magic angle. Dyes having lengths around 12 Å, exhibit a very weak polarization, because the relation between this size and the internal dimensions of the zeolite L channels forces the dye to be oriented in an angle close to the magic angle.[7] The emission of the flavylium-loaded zeolite L crystals prepared in this work is very weakly polarized, which is in agreement with the above discussions, since the main emitting species $\mathbf{AH^+}$, as well as **Ct**, have both d ≈ 12 Å, Figure 6.2.

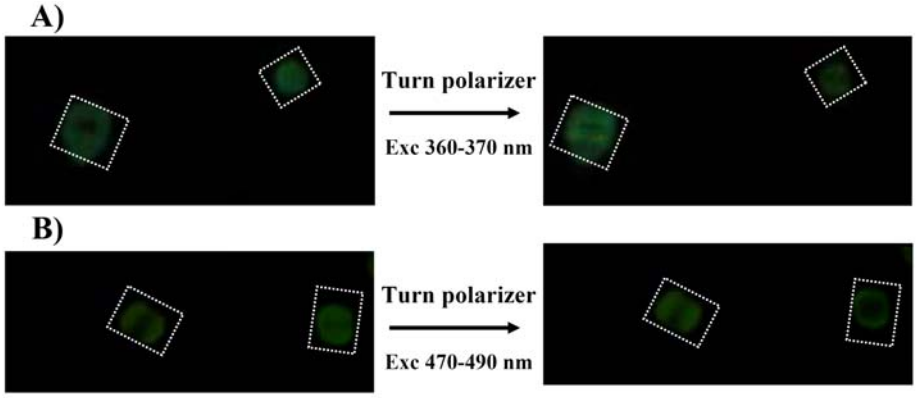

Figure 6.2 – Polarized fluorescence microscope pictures of single crystals of flavylium-loaded K^+ exchanged zeolite L. The size of the crystals is *ca* 1 μm and in every picture their long axis are approximately perpendicular to each other; λ_{exc} = 360-370 nm for A) and λ_{exc} = 470-490 nm for B).

6.4 Network of reactions inside the zeolite

When the crystals of K^+-zeolite L loaded with **Ct** are suspended in water, its fluorescence emission evolves with time, an increasing on the emission of $\mathbf{AH}^+$ being observed, Figure 6.3 A. It is worth of note that the method used for loading the zeolite L crystals is carried out in toluene, but before performing the fluorescence emission measurements it is necessary to ultrasonicate the water suspension, a process that implies approximately 32 min of water contact before the first fluorescence measurement. If this delay time is introduced into the kinetic curve representing the flavylium cation emission as a function of time, Figure 6.3 B, the kinetic process is compatible with **Ct** being the main species at zero time, see Figure 6.3 B. The initial emission spectra reported in Figure 6.3 A, after 32 min delay, at the excitation wavelength of 360 nm, (also reported in Figure 6.1) is already a mixture of *ca.* 50% of **Ct** and 50% of $\mathbf{AH}^+$. On this basis, the final spectrum $\mathbf{AH}^+$, λ_{max} = 508 nm, could be used to obtain, upon decomposition, the emission spectrum of **Ct**, λ_{max} = 480 nm. This value compares with λ_{max} = 501 nm in water, showing that the Stokes shift is reduced (by 1040 cm^{-1}), probably due to a confinement effect. This process reaches equilibrium in *ca* 1.5 hours and is only possible if a series of consecutive reactions take place inside the zeolite:

i) thermal isomerization to give **Cc**,

ii) ring closure of **Cc** to afford **B**;

iii) dehydration of **B** to give $\mathbf{AH}^+$.

In water the pK'_a of the equilibrium between $\mathbf{AH}^+$ and **Ct** (90%) plus **A** (10%) (**B** and **Cc** are negligible) is 3.1,[30] meaning that at the natural pH of the water (pH *ca* 6), **Ct** is expected to be the thermodynamically stable species and the mole fraction of $\mathbf{AH}^+$ is negligible (0.12%). Consequently, the diffusion of **Ct** to the outside of the zeolite L channels to form $\mathbf{AH}^+$ (adsorbed outside the channels or in solution) can be excluded taking into account the last argument, as well as the following reasons:

i) the emission spectrum shown in Figure 6.3 A is very different from the emission of $\mathbf{AH}^+$ in aqueous solution (see Figure 6.1, solid line);

ii) the interaction between $\mathbf{AH}^+$ and the negatively charged framework of the zeolite L is expected to be much stronger than that involving the neutral **Ct** species, stabilizing the former to a greater extent inside the zeolite and most likely raising the pK'_a value.

The latter argument may even increase the driving force to convert **Ct** into $\mathbf{AH}^+$ inside the zeolite L, besides internal changes in pH caused by $\mathbf{H}^+$ diffusing into the channels. This is according to our best knowledge, the first report of a *cis-trans* isomerization inside the zeolite L.

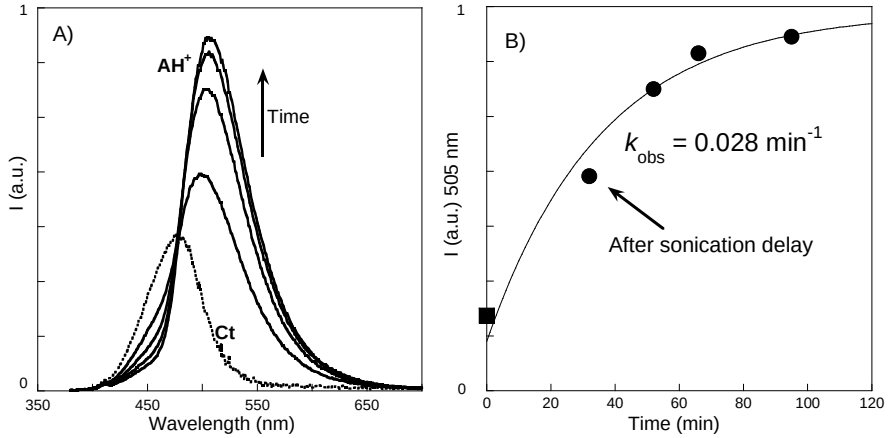

Figure 6.3 – A) Time evolution of the emission spectra of a suspension of **Ct** loaded in K^+-exchanged zeolite L (1.1 mg /ml) at room temperature. λ_{exc} = 360 nm. The **Ct** spectrum was obtained upon decomposition of the $\mathbf{AH}^+$ contribution. B) Representation of the kinetic processes (normalized emission intensity at 505 nm *versus* time in min) taking into account the delay time of 32 min to prepare the aqueous suspension of the loaded crystals.

In conclusion, $\mathbf{AH}^+$ is the thermodynamically stable species inside the zeolite L crystals suspended in water and it is not possible to isomerize **Ct** by the action of light, since **Ct** is not available at the equilibrium.

6.5 Experimental Part

The zeolite L crystals have been synthesized according to a well-known procedure described in the literature, in Professor De Cola's group (University of Münster).[31] The zeolites L used were 0.7-1.2 μm in width and 1-1.4 μm in length. Polarized fluorescence pictures were made with a confocal microscope MicroTime 200 (PicoQuant).

The flavylium dye[22,23] and its *trans*-chalcone[24] were available from previous experiments and their solutions were freshly prepared using water (acidified with HCl or buffered to the pretended pH value)[32] or spectroscopic toluene and triethylamine. Encapsulation of **Ct** was achieved from a saturated solution of the compound in toluene with triethylamine (20 %).

Absorption spectra were measured on a Varian Cary 100 Bio double-beam UV-Vis spectrometer and baseline corrected. Fluorescence spectra were run on a Jobin Yvon Spex, Fluorolog FL3-22. Measurements on zeolite aqueous suspensions were carried out under

constant stirring. Moreover, it was confirmed that the observed fluorescence was due to species incorporated (or adsorbed) in zeolites performing blank spectra of only zeolite suspensions and spectra of filtrates, after removal of zeolites.

6.6 Conclusions

It was shown for the first time that *trans*-chalcones derived from flavylium dyes can be isomerized inside the channels of zeolite L. It was proved that neutral *trans*-chalcones can be encapsulated into zeolite L with K^+ counterions and reasonable loadings were achieved by dissolving it in a mixture toluene/triethylamine (80/20), which is demonstrated by the good quality of the spectra obtained. Variations in excitation and emission spectra for $\mathbf{AH^+}$ (red shift in excitation, absence of ESPT in emission) and **Ct** (different shape in excitation spectra and much smaller Stokes shift) were found. This behavior suggests that both forms from the network of reactions of 7,4'-dihydroxyflavylium (**DHF**) were successfully encapsulated. The *trans*-chalcone originates the flavylium ion (also encapsulated) in zeolite aqueous suspension, which is only possible if isomerization, tautomerization and dehydration reactions take place inside zeolite L.

This work is only a first step towards the understanding of the behavior of encapsulated flavylium salts and further work is under course. Particularly, the stabilization of *trans*-chalcone species encapsulated inside the zeolite L, would allow the photoisomerization to occur inside the zeolite L, since it was proved that there are no space restrictions.

6.7 References

[1] F. Pina, M. Maestri, V. Balzani, *in Handbook of Photochemistry and Photobiology*, American Scientific Publishers, Stevenson Ranch, CA, USA, **2003**, Chapter 9, vol. 3, 411-449.
[2] P. Figueiredo, J. C. Lima, H. Santos, M. C. Wigand, R. Brouillard, A. L. Macanita, F. Pina, *J. Am. Chem. Soc.* **1994**, 116, 1249-1254.
[3] F. Pina , J. C. Lima, A. J. Parola, C. A. M. Afonso , *Angew. Chem. Int. Ed.* **2004**, 43, 1525-1527.
[4] F. Pina, T. A. Hatton, *Langmuir* **2008**, 24, 2356-2364.
[5] F. Pina, M. J. Melo, M. Maestri, P. Passaniti, V. Balzani*, J. Am. Chem. Soc.* **2000**, 122, 4496-4498.
[6] L. Giestas, F. Folgosa, J. C. Lima, A. J. Parola , F. Pina, *Eur. J. Of Org. Chem.* **2005**, 4187-4200.
[7] G. Calzaferri, S. Huber, H. Maas, C. Minkowski, *Angew. Chem. Int. Ed.* **2003**, 42, 3732 –3758
[8] F. Cucinotta, Z. Popovic, E. Weiss, G. Whitesides, L. De Cola, *Adv. Mat.* **2009**, 21, 1142-1145.
[9] Z. Popovic, M. Otter, G. Calzaferri, L. De Cola, *Angew. Chem. Int. Ed.* **2007**, 46, 6188-6191.
[10] M. Tsotsalas, M. Busby, E. Gianolio, S. Aime, L. De Cola, *Chem. Mater.* **2008**, 20, 5888-5893.
[11] G. Calzaferri, K. Lutkouskaya, *Photochem. Photobiol. Sci*. **2008**, 7, 879–910.
[12] Y. Kohno, Y. Shibata, N. Oyaizu, K. Yoda, M. Shibata, R. Matsushima, *Microporous and Mesoporous Materials* **2008**, 114, 373-379.
[13] R. Hoppe, G. Schulz-Ekloff, D. Wöhrle, C. Kirschhock, H. Fuess, *Langmuir* **1994**, 10, 1517-1523.
[14] S. Hashimoto, *J. Photochem. Photobiol. C* **2003**, 4, 19-49.
[15] Y. Kuriyama, S. Oishi, *Chem. Lett.* **1999**, 1045-1046.
[16] M. Kojima, T. Takagi, T. Goshima, *Mol. Cryst. Liq. Cryst* **2000**, 344, 179-184.
[17] K. Hoffmann, F. Marlow, J. Caro, *Adv. Mater.* **1997**, 9, 567-570.
[18] M. Kojiama, H. Takeya, Y. Kuriyama, S. Oishi, *Chem. Lett.* **1997**, 997-998.
[19] Y. Kuriyama, H. Takeya, S. Oishi, M. Kojima, *Chem. Lett.* **1998**, 843-844.
[20] F. Guessner, A. Olea, J. H. Lobaugh, L. J. Johnston, J. C. Scaiano, *J. Org. Chem.* **1989**, 259-261.
[21] H. Garcia, S. Garcia, J. Perez-Prieto, J. C. Scaiano, *J. Phys. Chem.* **1996**, 100, 18158-18164 and references 24 and 25 therein.

[22] R. Robinson, D. D. Pratt, *J. Chem. Soc. Trans.* **1922**, 121, 1577-1585.
[23] A. Robertson, R. Robinson, *J. Chem. Soc.* **1926**, 1713-1720.
[24] A. Roque, J. C. Lima, A. J. Parola, F. Pina, *Photochem. Photobiol. Sci.* **2007**, *6*, 381-385.
[25] R. Q. Albuquerque, G. Calzaferri, *Chem. Eur. J.* **2007**, 13, 8939-8952.
[26] K. Lutkouskaya, G. Calzaferri, *J. Phys. Chem. B* **2006,** *110,* 5633-5638
[27] F. Pina, M. J. Melo, H. Santos, J. C. Lima, I. Abreu, R. Ballardini, M. Maestri, *New J. Chem.* **1998**, 22, 1093-1098.
[28] M. G. Neumann, C. C. Schmitt, F. Gessner, *J. Colloid Interface Sci.* **1996**, 177, 495-501.
[29] B. Bussemer, D. Munsel, H. Wünscher, G. J. Mohr, U.-W. Grummt, J. *Phys. Chem. B* **2007**, 111, 8-15.
[30] F. Pina, L. Benedito, M. J. Melo, A. J. Parola, J. C. Lima, A. L. Maçanita *Anales De Quimica* **1997**, 93, 111-118
[31] A. Z. Ruiz, H. Li, G. Calzaferri, *Angew. Chemie Int. Ed.* **2006**, 45, 5282-5287.
[32] F. W. Küster, A. Thiel*, Tabelle per le Analisi Chimiche e Chimico- Fisiche*, 12th ed.; Hoepli, Milano, Italy, **1982**, 157-160.

7. Conclusions

In this thesis, the kinetics from the network of flavylium ions in aqueous solutions was firmly established and extended for heterogeneous media, such as CTAB micelles. A better understanding of the fluorescence behavior of flavylium salts, and particularly *trans*-chalcones, **Ct** was also achieved.

A general strategy to obtain photochromism from the network of chemical reactions originated by flavylium compounds was achieved, even when photochromism cannot be detected in aqueous solutions. Introduction of CTAB micelles shifts the equilibrium to lower pH values, stabilizing **Ct**. At such pH values in the bulk, $\mathbf{AH^+}$ is still more stable than **Ct** and is slowly converted into $\mathbf{Ct^m}$ (**Ct** adduct with the micelle). Under thermodynamic equilibrium, irradiation of $\mathbf{Ct^m}$ leads to the production of $\mathbf{AH^+}$, which is quickly ejected to the bulk, that is, the system switches to a colored state giving rise to a pronounced photochromism. This approach was demonstrated for 7-(*N,N*-diethylamino)-4'-hydroxyflavylium and 7,4'-dihydroxyflavylium, whose kinetics and thermodynamics have been studied. These photochromic systems work with no need of changing pH, which constitutes an important improvement over previously described systems dependent on pH jumps.

A series of 2-styryl-1-benzopyrylium salts were synthesized and thoroughly studied in comparison with flavylium analogues. This new family of compounds results from the introduction of a double bond between benzopyrylium and phenyl units. The network of reactions of flavylium salts could be applied to styryl compounds, but the absorption maxima are pronouncedly red shifted compared with flavylium analogues (up to 90 nm). 2-Styryl-1-benzopyrylium salts are also more stable towards color loss at slightly higher pH values and kinetically more inert towards hydration than their corresponding flavylium ions. However, photochemistry in water from styryl derivatives is very poor. In the presence of CTAB micelles, new photochromic systems were obtained, with significant color contrasts. In particular, a photochromic system switching from yellow to blue based on derivatives of natural anthocyanins is for the first time documented. Evidence for a singlet state isomerization process was given by studying chalcones lacking a hydroxyl group in position 2 in water/ethanol mixed solvents, where no *trans*-*cis* isomerization is found in the triplet state.

The study of Pluronic F127 micelles and gels with 4'-*N,N'*-dimethylamino-7-hydroxyflavylium allowed confirming previously reported results: the **Ct** maximum absorption wavelength constitutes a good sensor for the critical micelle concentration (CMC) or critical micelle temperature (CMT). The **Ct** photochromic mechanism was analyzed by comparing the photophysics in pure solvents and the Pluronic media. An intramolecular charge transfer (ICT) non-radiative process competes with **Ct** photoisomerization and is the dominant process in high polar solvents, preventing the appearance of photochromism, in contrast with lower polar

environments, such as micelles and ethanol. It this therefore explained why no photochromism in water is observed for the compound under study. In high viscous environments, as those found in the core of the Pluronic F127 micelles or glycerol, both ICT and photoisomerization are reduced enhancing the **Ct** fluorescence quantum yield. According to the data from fluorescence measurements and pH jumps, evidence for **Ct** distribution among different sites within the Pluronic aggregate was found: a hydrophilic/fluid region where **Ct** has poor fluorescence and isomerization yields, bulk region; the corona of the micelle where photoisomerization is maximized; the hydrophobic/viscous region where fluorescence quantum yield is higher (and photoisomerization lower). This effect leads to a selective **Ct** photochemistry.

In the last two chapters of this thesis, encapsulation of flavylium salts was studied. The association constants of host-guest complexes formed by molecular clips and flavylium salts were determined by ^{1}H-NMR spectroscopy as well as absorption and fluorescence spectroscopies. NMR provided information on the structures of host-guest complexes. The finding that the complexes of the positively charged flavylium salt and the neutral quinoidal base are of the same stability indicates that here the hydrophobic interactions are dominating for the host-guest binding. The main achievements for the study of this interaction were reached when host-guest complexes of the sulphate-substituted clip with the flavylium salts and their derivatives were found to be better soluble in water than the corresponding complexes of the hydrogenphosphate clip. We could subsequently prove that the **Ct** and **A** species are also bound inside the clip cavity and that the hydration reaction is slower in the presence of clip. On the other hand, the photochemically-induced *trans*-*cis* isomerization of the chalcones seems essentially unaffected by encapsulation.

Finally, neutral *trans*-chalcones could be encapsulated in zeolite L with K^{+} counterions. The *trans*-chalcone originates the flavylium ion (also encapsulated) in aqueous suspension, which is only possible if isomerization, tautomerization and dehydration reactions take place inside zeolite L. It was therefore proven that there are no space restrictions for the isomerization of *trans*-chalcones inside the channels of zeolite L.

8. Publications

List of publications originated by the work in this thesis:

1. Raquel Gomes, A. Jorge Parola, César A. T. Laia, Fernando Pina, "Efficient Photochromism From the Network of Chemical Reactions of 7,4'-Dihydroxyflavylium in CTAB Micelles", *Photochem. Photobiol. Sci* **2007**, 6, 1003-1009.

2. Raquel Gomes, A. Jorge Parola, César A. T. Laia, Fernando Pina, "Promoting Photochromism on Flavylium Derived 2-Hydroxychalcones in Aqueous Solutions by Addition of CTAB Micelles", *J. Phys. Chem. B*, **2007** 111, 12059-12065.

3. Raquel Gomes, Ana M. Diniz, Alexandre Jesus, A. Jorge Parola, Fernando Pina, "The Synthesis and Reaction Network of 2-styryl-1-benzopyrylium Salts: An Unexploited Class of Potential Colorants", *Dyes and Pigments* **2009**, 81, 69-79.

4. Ana M. Diniz, Raquel Gomes, César A. T. Laia, A. Jorge Parola, Fernando Pina, "Photochemistry of 7-hydroxy-2-(4-hydroxystyryl)-1-benzopyrylium and Related Compounds", *J. Phys. Chem. B* **2009**, 113, 719-727.

5. Raquel Gomes, César A. T. Laia, Fernando Pina, "On the Mechanism of Photochromism of 4'-*N,N*-Dimethylamino-7-Hydroxyflavylium in Pluronic F127", *J. Phys. Chem. B* **2009**, 113, 11134-11146.

6. Raquel Gomes, A. Jorge Parola, Frank Bastkowski, Jolanta Polkowska, Frank-Gerrit Klärner, "Host-guest Interactions Between Molecular Clips and Multistate Systems Based on Flavylium Salts", *J. Am. Chem. Soc.* **2009**, 131, 8922–8938.

7. Raquel Gomes, Rodrigo Q. Albuquerque, Fernando Pina, A. Jorge Parola, Luisa De Cola, "Supramolecular Host-Guest Flavylium-Loaded Zeolite L Hybrid Materials: Network of Reactions of Encapsulated 7,4'-Dihydroxyflavylium", Manuscript in preparation.

9. Supplementary Material

9.1 Water network of flavylium ions with low barrier

9.1.1 Kinetics of thermal reaction – deduction of equations 1.45 and 2.14

$$A \underset{}{\overset{K_a}{\rightleftharpoons}} AH^+ \underset{k_{-h}[H^+]}{\overset{k_h}{\rightleftharpoons}} B \overset{K_t}{\rightleftharpoons} Cc \underset{k_{-i}}{\overset{k_i}{\rightleftharpoons}} Ct \tag{1.44}$$

Assuming that **B** and **Cc** are in fast equilibrium, we can simplify the problem:

$$A \underset{}{\overset{K_a}{\rightleftharpoons}} AH^+ \underset{k_{-h}[H^+]}{\overset{k_h}{\rightleftharpoons}} X \underset{k_{-i}}{\overset{k_i}{\rightleftharpoons}} Ct \tag{S1}$$

$$[X] = [B] + [Cc] \tag{S2}$$

$$[X] = [B] + K_t[B] \tag{S3}$$

$$\chi_B = \frac{1}{1+K_t}\,;\, \chi_{Cc} = \frac{K_t}{1+K_t} \tag{S4,S5}$$

And we obtain the following differential equations:

$$\frac{d([AH^+]+[A])}{dt} = -k_h \frac{[H^+]}{[H^+]+K_a}([AH^+]+[A]) + k_{-h}[H^+]\chi_B[X] \tag{S6}$$

$$\frac{d([X])}{dt} = k_h \frac{[H^+]}{[H^+]+K_a}([AH^+]+[A]) + k_{-i}[Ct] - (k_{-h}[H^+]\chi_B + k_i\chi_{Cc})[X] \tag{S7}$$

$$\frac{d([Ct])}{dt} = k_i\chi_{Cc}[X] - k_{-i}[Ct] \tag{S8}$$

Applying the steady state approximation:

$$[X] = \frac{k_h \frac{[H^+]}{[H^+]+K_a}([AH^+]+[A]) + k_{-i}[Ct]}{k_{-h}[H^+]\chi_B + k_i\chi_{Cc}} \tag{S9}$$

And finally, substituting [X] one obtains,

$$\frac{d([AH^+]+[A])}{dt} = -k_h \frac{[H^+]}{[H^+]+K_a}([AH^+]+[A]) + k_{-h}[H^+]\chi_B \frac{k_h \frac{[H^+]}{[H^+]+K_a}([AH^+]+[A]) + k_{-i}[Ct]}{k_{-h}[H^+]\chi_B + k_i\chi_{Cc}}$$

$$\frac{d([AH^+]+[A])}{dt} = -\frac{k_i \chi_{Cc} k_h \dfrac{[H^+]}{[H^+]+K_a}([AH^+]+[A])}{k_{-h}[H^+]\chi_B + k_i \chi_{Cc}} + \frac{k_{-i}k_{-h}[H^+]\chi_B[Ct]}{k_{-h}[H^+]\chi_B + k_i \chi_{Cc}} \quad \text{(S10)}$$

$$\frac{d([Ct])}{dt} = k_i \chi_{Cc} \frac{k_h \dfrac{[H^+]}{[H^+]+K_a}([AH^+]+[A]) + k_{-i}[Ct]}{k_{-h}[H^+]\chi_B + k_i \chi_{Cc}} - k_{-i}[Ct]$$

$$\frac{d([Ct])}{dt} = \frac{k_i \chi_{Cc} k_h \dfrac{[H^+]}{[H^+]+K_a}([AH^+]+[A])}{k_{-h}[H^+]\chi_B + k_i \chi_{Cc}} - \frac{k_{-i}k_{-h}[H^+]\chi_B[Ct]}{k_{-h}[H^+]\chi_B + k_i \chi_{Cc}} \quad \text{(S11)}$$

Now it is easy to account for first order kinetic constant observed:

$$k_{obs} = \frac{\dfrac{[H^+]}{[H^+]+K_a} k_i \chi_{Cc} k_h + k_{-i}k_{-h}[H^+]\chi_B}{k_{-h}[H^+]\chi_B + k_i \chi_{Cc}} \quad \text{(S12)}$$

$$k_{obs} = \frac{\dfrac{[H^+]}{[H^+]+K_a} k_i \dfrac{K_T}{1+K_T} k_h + k_{-i}k_{-h}[H^+]\dfrac{1}{1+K_T}}{k_{-h}[H^+]\dfrac{1}{1+K_T} + k_i \dfrac{K_T}{1+K_T}} \quad \text{(S13)}$$

Rearranging, one obtains:

$$k_{obs} = \frac{\dfrac{[H^+]}{[H^+]+K_a} k_i K_t k_h + k_{-i}k_{-h}[H^+]}{k_{-h}[H^+] + k_i K_t}$$

$$k_{obs} = \frac{\dfrac{[H^+]}{[H^+]+K_a} k_i K_t K_h + k_{-i}[H^+]}{[H^+] + \dfrac{k_i K_t}{k_{-h}}} \quad \textbf{(1.45)}$$

When an amino group is present protonated chalcone species can be formed **CtH$^+$** that give **AH$^+$** the thermodynamic product at relatively acidic pH values. The observed rate constants can be accounted for by considering a sum of two components, one involving the species **AH$^+$/Ct**, as usual, (eq. 1.45) and the other, the species **AH$^+$/CtH$^+$**, eq. 2.13, in which **X'** is composed by **B** and **Cc** species in their protonated and/or unprotonated forms and K_t, is the equilibrium constant between these species. This second rate constant is derived in a similar way to what was done in eq. 1.45, except that k_{h+} can be ignored, because there is no reversibility from **AH$^+$**.

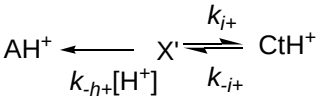

(2.13)

$$k_{obs} = \frac{\frac{[H^+]}{[H^+]+K_a} k_i K_t K_h + k_{-i}[H^+]}{[H^+]+\frac{k_i K_t}{k_{-h}}} + \frac{\frac{[H^+]}{[H^+]+K_{Ct+}} k_{-i+}[H^+]}{[H^+]+\frac{k_{i+} K_t'}{k_{-h+}}} \quad \textbf{(2.14)}$$

9.1.2 Flash photolysis kinetics – equation 1.46

After the flash, two processes exhibiting the same lifetime are observed at different wavelengths, when there is no barrier for *cis-trans* isomerization: i) recovery of **Ct** absorption and ii) formation of $\mathbf{AH^+}$. The global kinetics is given by equation 1.46, in which the first term accounts for the recovery of **Ct** and the second term for the formation of $\mathbf{AH^+}$, once again assuming **B** and **Cc** in fast equilibrium.

$$k_{flash} = k_i \frac{K_t}{1+K_t} + k_{-h} \frac{[H^+]}{1+K_t} \quad \textbf{(1.46)}$$

9.1.3 Quantum yields – equation 1.48

The quantum yield of formation of $\mathbf{AH^+}$ is pH dependent, and in the case of a low thermal barrier it can be given by equation 1.48, in which the numerator accounts for the formation of $\mathbf{AH^+}$ and the denominator is simply a sum of the two processes. That is, the observed quantum yield is given by the product of the intrinsic quantum yield of the reaction by the efficiency of formation of $\mathbf{AH^+}$.

$$\Phi = \Phi_{Ct-Cc} \frac{k_{-h}[H^+]}{k_{-h}[H^+]+k_i K_t} = \Phi_{Ct-Cc} \frac{[H^+]}{[H^+]+\frac{k_i K_t}{k_{-h}}} \quad \textbf{(1.48)}$$

9.2 DHF in CTAB micelles - deduction of equations 2.2, 2.4, 2.5 and 2.6

The system can be generically represented by Scheme 2.2, and the thermodynamics and kinetics can be derived on its basis.

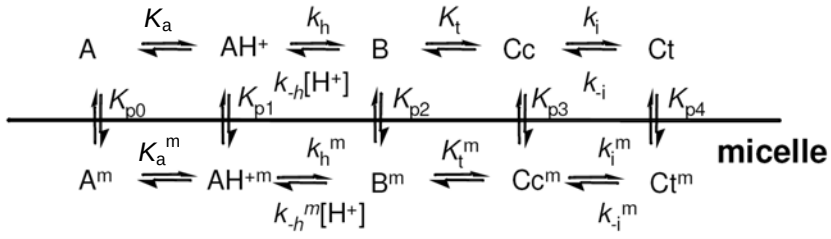

Scheme 2.2

9.2.1 Thermodynamic equilibrium

The total concentration of flavylium species is given by:

$$C_0 = [A] + [AH^+] + [B] + [Cc] + [Ct] + [A^m] + [AH^{+m}] + [B^m] + [Cc^m] + [Ct^m] \quad \text{(S14)}$$

And the concentration of each species can be expressed as a function of [**AH**$^+$]:

$$[AH^{+m}] = K_{p1}[AH^+] \quad \text{(S15)}$$

$$[A] = \frac{K_a}{[H^+]}[AH^+] \quad \text{(S16)}$$

$$[A^m] = K_{p0}\frac{K_a}{[H^+]}[AH^+] \quad \text{(S17)}$$

$$[B] = \frac{K_h}{[H^+]}[AH^+] \quad \text{(S18)}$$

$$[Cc] = K_t\frac{K_h}{[H^+]}[AH^+] \quad \text{(S19)}$$

$$[Ct] = K_i K_t\frac{K_h}{[H^+]}[AH^+] \quad \text{(S20)}$$

$$[B^m] = K_{p2}\frac{K_h}{[H^+]}[AH^+] \text{ or } [B^m] = K_{p1}\frac{K_h^{\,m}}{[H^+]}[AH^+] \quad \text{(S21)}$$

$$[Cc^m] = K_{p3}K_t\frac{K_h}{[H^+]}[AH^+] \text{ or } [Cc^m] = K_{p1}K_t^{\,m}\frac{K_h^{\,m}}{[H^+]}[AH^+] \quad \text{(S22)}$$

$$\left[Ct^{m}\right] = K_{p4}K_{i}K_{t}\frac{K_{h}}{\left[H^{+}\right]}\left[AH^{+}\right] \text{ or } \left[Ct^{m}\right] = K_{p1}K_{i}{}^{m}K_{t}{}^{m}\frac{K_{h}{}^{m}}{\left[H^{+}\right]}\left[AH^{+}\right] \quad \text{(S23)}$$

Substituting equations S15 to S23 on S14:

$$C_{0} = \frac{\left[AH^{+}\right]}{\left[H^{+}\right]}\left((1+K_{p1})\left[H^{+}\right] + K_{a} + K_{po}K_{a} + K_{h} + K_{t}K_{h} + K_{i}K_{t}K_{h} + K_{p2}K_{h} + K_{p3}K_{t}K_{h} + K_{p4}K_{i}K_{t}K_{h}\right) \quad \text{(S24)}$$

or

$$C_{0} = \frac{\left[AH^{+}\right]}{\left[H^{+}\right]}\left((1+K_{p1})\left[H^{+}\right] + K_{a} + K_{po}K_{a} + K_{h} + K_{t}K_{h} + K_{i}K_{t}K_{h} + K_{p1}K_{h}{}^{m} + K_{p1}K_{t}{}^{m}K_{h}{}^{m} + K_{p1}K_{i}{}^{m}K_{t}{}^{m}K_{h}{}^{m}\right) \quad \text{(S25)}$$

Now it is possible to evaluate mole fractions:

$$\chi_{AH^{+}} = \frac{\left[AH^{+}\right]}{C_{0}} = \frac{\left[H^{+}\right]}{\left((1+K_{p1})\left[H^{+}\right] + K_{a} + K_{po}K_{a} + K_{h} + K_{t}K_{h} + K_{i}K_{t}K_{h} + K_{p2}K_{h} + K_{p3}K_{t}K_{h} + K_{p4}K_{i}K_{t}K_{h}\right)} \quad \text{(S26)}$$

or

$$\chi_{AH^{+}} = \frac{\left[AH^{+}\right]}{C_{0}} = \frac{\left[H^{+}\right]}{\left((1+K_{p1})\left[H^{+}\right] + K_{a} + K_{po}K_{a} + K_{h} + K_{t}K_{h} + K_{i}K_{t}K_{h} + K_{p1}K_{h}{}^{m} + K_{p1}K_{t}{}^{m}K_{h}{}^{m} + K_{p1}K_{i}{}^{m}K_{t}{}^{m}K_{h}{}^{m}\right)} \quad \text{(S27)}$$

Since K_{p1}~0, because $\mathbf{AH^{+}}$ resides in the bulk due to electrostatic repulsion, S26 and S27 can be simplified:

$$\chi_{AH^{+}} = \frac{\left[AH^{+}\right]}{C_{0}} = \frac{\left[H^{+}\right]}{\left(\left[H^{+}\right] + K'_{a}{}^{m}\right)} \quad \textbf{(2.2)}$$

where:

$$K'_{a}{}^{m} = K'_{a} + K_{p0}K_{a} + K_{p2}K_{h} + K_{p3}K_{t}K_{h} + K_{p4}K_{i}K_{t}K_{h} \quad \textbf{(2.4)}$$

or

$$K'_{a}{}^{m} = K'_{a} + K_{p0}K_{a} + K_{p1}K_{h}{}^{m} + K_{p1}K_{t}{}^{m}K_{h}{}^{m} + K_{p1}K_{i}{}^{m}K_{t}{}^{m}K_{h}{}^{m} \quad \text{(S28)}$$

and:

$$K'_{a} = K_{a} + K_{h} + K_{t}K_{h} + K_{i}K_{t}K_{h} \quad \text{(S29)}$$

It is known that $K'_a = 10^{-3.1}$ M and $K'^{m}_{a} = 10^{0.16}$ M, therefore K'_a can be neglected from the calculations. Also all species that are not **AH**$^+$ or **Ct** are not present in significant quantities at equilibrium, therefore the terms that come from **A**, **B** and **Cc** species (in the bulk and in the micellar phase) may be neglected. The only term that remains is therefore $K_{p4}K_hK_tK_i$ or $K_{p1}K_t^mK_i^mK_h^m$. It turns out that the product $K_hK_tK_i$ is known from experiments in water, and therefore the following relation can be used as seen in the text:

$$K'^{m}_{a} = K_{p4}K_iK_tK_h \qquad \textbf{(2.5)}$$

9.2.2 Thermal kinetics – equation 2.6

The kinetics of the thermal part follows a similar route of thinking. The only detectable species are, again, **AH**$^+$ and **Ct**. But the intermediate species should play a role as well. The sum of the intermediate species **X** in fast equilibrium may be given by:

$$[X] = [B] + [B^m] + [Cc] + [Cc^m] \qquad \text{(S30)}$$

Assuming the above mentioned intermediates are in fast equilibrium, the molar fractions for the steady state species are easily calculated as for the network in water:

$$[X] = [B](1 + K_{p2} + K_t + K_tK_{p3}) \qquad \text{(S31)}$$

$$\chi_B = \frac{1}{(1 + K_{p2} + K_t + K_tK_{p3})} \qquad \text{(S32)}$$

$$\chi_{B^m} = \frac{K_{p2}}{(1 + K_{p2} + K_t + K_tK_{p3})} \qquad \text{(S33)}$$

$$\chi_{Cc} = \frac{K_t}{(1 + K_{p2} + K_t + K_tK_{p3})} \qquad \text{(S34)}$$

$$\chi_{Cc^m} = \frac{K_tK_{p3}}{(1 + K_{p2} + K_t + K_tK_{p3})} \qquad \text{(S35)}$$

The following set of differential equations can now be defined:

$$\frac{d([AH^+]+[A])}{dt} = -k_h \frac{[H^+]}{[H^+]+K_a}([AH^+]+[A]) + [H^+][X]\left(k_{-h}{}^m \chi_{B^m} + k_{-h}\chi_B\right) \quad \text{(S36)}$$

$$\frac{d([X])}{dt} = k_h \frac{[H^+]}{[H^+]+K_a}([AH^+]+[A]) + k_{-i}{}^m[Ct^m] - \left(k_{-h}[H^+]\chi_B + k_{-h}{}^m[H^+]\chi_{B^m} + k_i\chi_{Cc} + k_i{}^m\chi_{Cc^m}\right)[X] \quad \text{(S37)}$$

$$\frac{d([Ct]+[Ct^m])}{dt} = \left(k_i\chi_{Cc} + k_i{}^m\chi_{Cc^m}\right)[X] - k_{-i}{}^m[Ct^m] \quad \text{(S38)}$$

Since K_{p4} is very large, the concentration of **Ct** may be neglected. Applying the steady approximation to S37 one obtains:

$$[X] = \frac{k_h \frac{[H^+]}{[H^+]+K_a}([AH^+]+[A]) + k_{-i}{}^m[Ct^m]}{k_{-h}[H^+]\chi_B + k_{-h}{}^m[H^+]\chi_{B^m} + k_i\chi_{Cc} + k_i{}^m\chi_{Cc^m}} \quad \text{(S39)}$$

Substituting on the other differential equations:

$$\frac{d([AH^+]+[A])}{dt} = \frac{-k_h(k_i\chi_{Cc} + k_i{}^m\chi_{Cc^m})\frac{[H^+]}{[H^+]+K_a}([AH^+]+[A]) + [H^+]\left(k_{-h}{}^m\chi_{B^m} + k_{-h}\chi_B\right)k_{-i}{}^m[Ct^m]}{\left(k_{-h}\chi_B + k_{-h}{}^m\chi_{B^m}\right)[H^+] + k_i\chi_{Cc} + k_i{}^m\chi_{Cc^m}} \quad \text{(S40)}$$

$$\frac{d([Ct]+[Ct^m])}{dt} = \frac{k_h\left(k_i\chi_{Cc} + k_i{}^m\chi_{Cc^m}\right)\frac{[H^+]}{[H^+]+K_a}([AH^+]+[A]) - [H^+]\left(k_{-h}\chi_B + k_{-h}{}^m\chi_{B^m}\right)k_{-i}{}^m[Ct^m]}{\left(k_{-h}\chi_B + k_{-h}{}^m\chi_{B^m}\right)[H^+] + k_i\chi_{Cc} + k_i{}^m\chi_{Cc^m}} \quad \text{(S41)}$$

Finally, the solution of the set of differential equations is now easy to achieve, and the observed rate constants for the first order kinetics is given by:

$$k_{obs} = \frac{k_h\left(k_i\chi_{Cc} + k_i{}^m\chi_{Cc^m}\right)\dfrac{[H^+]}{[H^+]+K_a} + [H^+]\left(k_{-h}\chi_B + k_{-h}{}^m\chi_{B^m}\right)k_{-i}{}^m}{\left(k_{-h}\chi_B + k_{-h}{}^m\chi_{B^m}\right)[H^+] + k_i\chi_{Cc} + k_i{}^m\chi_{Cc^m}} =$$

$$= \frac{\dfrac{[H^+]}{[H^+]+K_a}k_hK_t\left(k_i + k_i{}^mK_{p3}\right) + [H^+]k_{-i}{}^m\left(k_{-h} + k_{-h}{}^mK_{p2}\right)}{\left(k_{-h} + k_{-h}{}^mK_{p2}\right)[H^+] + (k_i + k_i{}^mK_{p3})K_t} = \quad \textbf{(2.6)}$$

$$= \frac{\dfrac{[H^+]}{[H^+]+K_a}\dfrac{k_hK_t\left(k_i + k_i{}^mK_{p3}\right)}{\left(k_{-h} + k_{-h}{}^mK_{p2}\right)} + [H^+]k_{-i}{}^m}{[H^+] + \dfrac{(k_i + k_i{}^mK_{p3})K_t}{\left(k_{-h} + k_{-h}{}^mK_{p2}\right)}}$$

9.2.3 Flash photolysis kinetics – equation 2.9

Assuming that **Ct** is in the micellar medium and $\mathbf{AH^+}$ is formed within the micelle as well (followed by its fast exit), a similar form of eq. 1.46 is obtained:

$$k_{flash} = k_i{}^m\frac{K_t{}^m}{1+K_t{}^m} + k_{-h}{}^m\frac{[H^+]}{1+K_t{}^m} \quad \textbf{(2.9)}$$

9.2.4 Quantum yields – equation 2.12

Considering the same pathway as before, it is possible to obtain eq. 2.12 for the quantum yield of formation of Cc^m from Ct^m, being $\Phi_{Ct^m\rightarrow Cc^m}$ the respective intrinsic quantum yield.

$$\Phi = \Phi_{Ct^m\rightarrow Cc^m}\frac{[H^+]}{[H^+] + \dfrac{k_i{}^mK_t{}^m}{k_{-h}{}^m}} \quad \textbf{(2.12)}$$

9.3 DEF in CTAB micelles - deduction of equations 2.27-2.32

9.3.1 Thermal kinetics

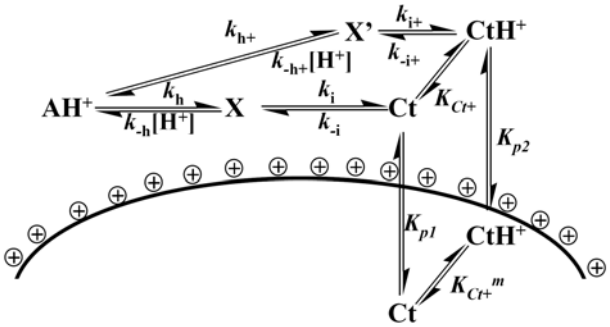

Scheme 2.4

The rate of $\mathbf{AH^+}$ conversion to $\mathbf{Ct^m}$ and $\mathbf{CtH^{+m}}$ follows a first-order kinetics, which means that a great number of approximations may be done, despite the fact that many intermediate species are involved. First one must write the differential equations.

$$\frac{d[AH^+]}{dt} = -(k_h + k_{h+})[AH^+] + (k_{-h}\chi_B[X] + k_{-h+}\chi_{B'}[X'])[H^+] \quad \text{(S42)}$$

$$\frac{d[X]}{dt} = k_h[AH^+] - (k_{-h}[H^+]\chi_B + k_i\chi_{Cc})[X] + k_{-i}[Ct] \quad \text{(S43)}$$

$$\frac{d[X']}{dt} = k_{h+}[AH^+] - (k_{-h+}[H^+]\chi_{B'} + k_{i+}\chi_{Cc'})[X'] + k_{-i+}[CtH^+] \quad \text{(S44)}$$

$$\frac{d([Ct]+[Ct^m]+[CtH^+]+[CtH^{+m}])}{dt} = k_i\chi_{Cc}[X] + k_{i+}\chi_{Cc'}[X'] - k_{-i}[Ct] - k_{-i+}[CtH^+] \quad \text{(S45)}$$

Three fast equilibriums are needed to define this kinetic scheme. One between **Ct** and **B**, similar to what was defined in S1 to S5, the other similar involving the **X'** species (equations S46-S50) and one involving, **Ct**, $\mathbf{Ct^m}$, $\mathbf{CtH^+}$ and $\mathbf{CtH^{+m}}$, equations 2.19, 2.20, S51.

$$AH^+ \underset{k_{-h+}[H^+]}{\overset{k_{h+}}{\rightleftharpoons}} X' \underset{k_{-i+}}{\overset{k_{i+}}{\rightleftharpoons}} CtH^+ \quad \text{(S46)}$$

$$[X'] = [B'] + [Cc'] \quad \text{(S47)}$$

$$[X'] = [B'] + K_{t'}[B'] \quad \text{(S48)}$$

$$\chi_{B'} = \frac{1}{1+K_{t'}}\,;\, \chi_{Cc'} = \frac{K_{t'}}{1+K_{t'}} \quad \text{(S49,S50)}$$

Defining:

$$C_0 = [Ct] + [Ct^m] + [CtH^+] + [CtH^{+m}] = [CtH^+]\left(1 + K_{p2} + \frac{K_{Ct+}(1+K_{p1})}{[H^+]}\right) \tag{2.19}$$

One obtains:

$$\chi_{CtH^+} = \frac{[CtH^+]}{C_0} = \frac{1}{\left(1 + K_{p2} + \frac{K_{Ct+}(1+K_{p1})}{[H^+]}\right)} = \frac{\frac{[H^+]}{(1+K_{p2})}}{[H^+] + \frac{K_{Ct+}(1+K_{p1})}{(1+K_{p2})}} \tag{2.20}$$

$$\chi_{Ct} = \frac{[Ct]}{C_0} = \frac{\frac{K_{Ct+}}{(1+K_{p2})}}{[H^+] + \frac{K_{Ct+}(1+K_{p1})}{(1+K_{p2})}} \tag{S51}$$

If the molar fractions are introduced in the set of differential equations:

$$\frac{d[X]}{dt} = k_h[AH^+] - (k_{-h}[H^+]\chi_B + k_i\chi_{Cc})[X] + k_{-i}\chi_{Ct}C_0 \tag{S52}$$

$$\frac{d[X']}{dt} = k_{h+}[AH^+] - (k_{-h+}[H^+]\chi_{B'} + k_{i+}\chi_{Cc'})[X'] + k_{-i+}\chi_{CtH^+}C_0 \tag{S53}$$

$$\frac{dC_o}{dt} = k_i\chi_{Cc}[X] + k_{i+}\chi_{Cc'}[X'] - k_{-i}\chi_{Ct}C_0 - k_{-i+}\chi_{CtH^+}C_0 \tag{S54}$$

Now steady state approximations are made for intermediates **X** and **X'**:

$$[X] = \frac{k_h[AH^+] + k_{-i}\chi_{Ct}C_0}{k_{-h}[H^+]\chi_B + k_i\chi_{Cc}} \tag{S55}$$

$$[X'] = \frac{k_{h+}[AH^+] + k_{-i+}\chi_{CtH^+}C_0}{k_{-h+}[H^+]\chi_{B'} + k_{i+}\chi_{Cc'}} \tag{S56}$$

After substitution on differential equations for $\mathbf{AH^+}$ and $\mathbf{C_0}$:

$$\frac{d[AH^+]}{dt} = -\left(\frac{k_i \chi_{Cc} k_h}{k_{-h}[H^+]\chi_B + k_i \chi_{Cc}} + \frac{k_{i+} \chi_{Cc'} k_{h+}}{k_{-h+}[H^+]\chi_{B'} + k_{i+} \chi_{Cc'}}\right)[AH^+] + \\ + \left(\frac{k_{-h} \chi_B k_{-i} \chi_{Ct}}{k_{-h}[H^+]\chi_B + k_i \chi_{Cc}} + \frac{k_{-h+} \chi_{B'} k_{-i+} \chi_{CtH^+}}{k_{-h+}[H^+]\chi_{B'} + k_{i+} \chi_{Cc'}}\right)[H^+]C_0 \quad \text{(S57)}$$

$$\frac{dC_o}{dt} = \left(\frac{k_i \chi_{Cc} k_h}{k_{-h}[H^+]\chi_B + k_i \chi_{Cc}} + \frac{k_{i+} \chi_{Cc'} k_{h+}}{k_{-h+}[H^+]\chi_{B'} + k_{i+} \chi_{Cc'}}\right)[AH^+] - \\ - \left(\frac{k_{-h} \chi_B k_{-i} \chi_{Ct}}{k_{-h}[H^+]\chi_B + k_i \chi_{Cc}} + \frac{k_{-h+} \chi_{B'} k_{-i+} \chi_{CtH^+}}{k_{-h+}[H^+]\chi_{B'} + k_{i+} \chi_{Cc'}}\right)[H^+]C_0 \quad \text{(S58)}$$

And therefore the observed rate constant for the thermal process will be given by:

$$k_{obs} = \frac{[H^+]}{[H^+] + K_a}\left(\frac{k_i \chi_{Cc} k_h}{k_{-h}[H^+]\chi_B + k_i \chi_{Cc}} + \frac{k_{i+} \chi_{Cc'} k_{h+}}{k_{-h+}[H^+]\chi_{B'} + k_{i+} \chi_{Cc'}}\right) + \\ + \left(\frac{k_{-h} \chi_B k_{-i} \chi_{Ct}}{k_{-h}[H^+]\chi_B + k_i \chi_{Cc}} + \frac{k_{-h+} \chi_{B'} k_{-i+} \chi_{CtH^+}}{k_{-h+}[H^+]\chi_{B'} + k_{i+} \chi_{Cc'}}\right)[H^+] \quad \text{(S59)}$$

$$k_{obs} = \frac{[H^+]}{[H^+] + K_a}\left(\frac{k_i K_t k_h}{k_{-h}[H^+] + k_i K_T} + \frac{k_{i+} K_{t'} k_{h+}}{k_{-h+}[H^+] + k_{i+} K_{t'}}\right) + \left(\frac{k_{-h} k_{-i} \chi_{Ct}}{k_{-h}[H^+] + k_i K_t} + \frac{k_{-h+} k_{-i+} \chi_{CtH^+}}{k_{-h+}[H^+] + k_{i+} K_{t'}}\right)[H^+] \quad \text{(S60)}$$

In which the first term appears in order to correct the [$\mathbf{AH^+}$], similarly to what was seen in other cases, due to its acid base equilibrium **A**. It turns out that $\chi_{Ct} \sim 0$ at all pH values and equation S60 can be thus simplified to eq. 2.27.

$$k_{obs} = \frac{[H^+]}{[H^+] + K_a}\left(\frac{k_i K_t k_h}{k_{-h}[H^+] + k_i K_T} + \frac{k_{i+} K_{t'} k_{h+}}{k_{-h+}[H^+] + k_{i+} K_{t'}}\right) + \left(\frac{k_{-h+} k_{-i+} \chi_{CtH^+}}{k_{-h+}[H^+] + k_{i+} K_{t'}}\right)[H^+] \quad \textbf{(2.27)}$$

9.3.2 Flash photolysis kinetics

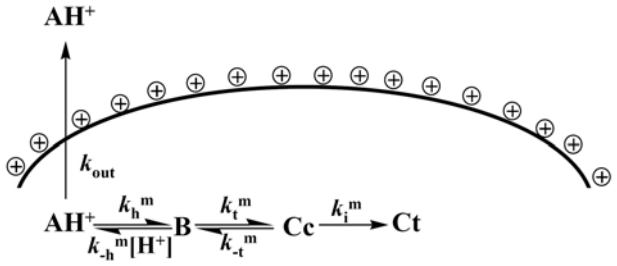

Scheme 2.5

The differential equations that describe the kinetics according to the scheme are

$$\frac{d\left[Ct^{m}\right]}{dt} = k_{i}^{m}\left[Cc^{m}\right] \tag{S61}$$

$$\frac{d\left[Cc^{m}\right]}{dt} = k_{t}^{m}\left[B^{m}\right] - (k_{i}^{m} + k_{-t}^{m})\left[Cc^{m}\right] \tag{S62}$$

$$\frac{d\left[B^{m}\right]}{dt} = k_{h}^{m}\left[AH^{+m}\right] + k_{-t}^{m}\left[Cc^{m}\right] - (k_{t}^{m} + k_{-h}^{m}\left[H^{+}\right])\left[B^{m}\right] \tag{S63}$$

$$\frac{d\left[AH^{+m}\right]}{dt} = k_{-h}^{m}\left[H^{+}\right]\left[B^{m}\right] - (k_{h}^{m} + k_{out})\left[AH^{+m}\right] \tag{S64}$$

$$\frac{d\left[AH^{+}\right]}{dt} = k_{out}\left[AH^{+m}\right] \tag{S65}$$

Since $\mathbf{Ct^{m}}$ and $\mathbf{AH^{+}}$ are products, the respective differential equations are not necessary for the explanation of the observed rate constants. In order to solve the other equations, one can apply steady-state approximations for some of the intermediate products, namely $\mathbf{B^{m}}$ and $\mathbf{AH^{+m}}$. The experimental kinetics can be solved with biexponential functions, which gives two observed rate constants ($k_{\text{flash}}^{\text{I}}$ and $k_{\text{flash}}^{\text{II}}$). Now one can envisage Scheme 2.5 as two sequential steps. The first step occurs immediately after the photochemical production of $\mathbf{Cc^{m}}$, and can be attributed to the fast formation of the hemiketal species $\mathbf{B^{m}}$. The second step occurs on a larger timescale, and deals with the production of $\mathbf{AH^{+}}$ and $\mathbf{Ct^{m}}$. Under such circumstances, it might be feasible to apply the steady-state approximation to all intermediate products, as long as their concentrations are always very low. If one makes such approximation, the following expressions are derived:

$$\left[AH^{+m}\right] = \frac{k_{-h}^{m}\left[H^{+}\right]}{k_{h}^{m} + k_{out}}\left[B^{m}\right] \tag{S66}$$

$$\left[B^m\right] = \frac{k_{-t}{}^m\left(k_h{}^m + k_{out}\right)}{k_t{}^m\left(k_h{}^m + k_{out}\right) + k_{-h}{}^m\left[H^+\right]k_{out}}\left[Cc^m\right] \tag{S67}$$

Substituting in eq. S67 on S62:

$$\frac{d\left[Cc^m\right]}{dt} = -k_i{}^m\left[Cc^m\right] - \frac{\dfrac{k_{-t}{}^m k_{-h}{}^m k_{out}}{\left(k_h{}^m + k_{out}\right)}\left[H^+\right]}{k_t{}^m + \dfrac{k_{-h}{}^m k_{out}}{\left(k_h{}^m + k_{out}\right)}\left[H^+\right]}\left[Cc^m\right] \tag{S68}$$

Considering:

$$\beta = \frac{k_{-h}{}^m k_{out}}{k_h{}^m + k_{out}} \tag{2.30}$$

It is now easy to account for the rate constant

$$k_{flash}{}^I = k_i{}^m + \frac{k_{-t}{}^m \beta\left[H^+\right]}{k_t{}^m + \beta\left[H^+\right]} \tag{2.28}$$

On the other hand, the fast component would be the fast equilibration between $\mathbf{B^m}$ and $\mathbf{Cc^m}$:

$$k_{flash}{}^{II} = k_t{}^m + k_{-t}{}^m \tag{2.29}$$

The two steady-state approximations are feasible if the tautomeric step is very fast and the decays are well separated events. Clearly this is not the case of the compound under study in the presence of CTAB micelles. Therefore only one steady-state approximation is made (eq. S66). Under such circumstances, the following set of differential equations is obtained:

$$\frac{d\left[B^m\right]}{dt} = +k_{-t}{}^m\left[Cc^m\right] - \left(k_t{}^m + \beta\left[H^+\right]\right)\left[B^m\right] \tag{S69}$$

$$\frac{d\left[Cc^m\right]}{dt} = k_t{}^m\left[B^m\right] - \left(k_i{}^m + k_{-t}{}^m\right)\left[Cc^m\right] \tag{S70}$$

The set of equations can be solved using the matrix method:

$$\begin{vmatrix} -(k_t^m + \beta[H^+]) - \lambda & k_{-t}^m \\ k_t^m & -(k_i^m + k_{-t}^m) - \lambda \end{vmatrix} = 0 \quad \text{(S71)}$$

And therefore the two constants can be evaluated:

$$k_{flash}^{I} = \frac{(k_t^m + \beta[H^+] + k_i^m + k_{-t}^m) - \sqrt{(k_t^m + \beta[H^+] + k_i^m + k_{-t}^m)^2 - 4k_i^m k_t^m - 4(k_i^m + k_{-t}^m)\beta[H^+]}}{2}$$

(2.31)

$$k_{flash}^{II} = \frac{(k_t^m + \beta[H^+] + k_i^m + k_{-t}^m) + \sqrt{(k_t^m + \beta[H^+] + k_i^m + k_{-t}^m)^2 - 4k_i^m k_t^m - 4(k_i^m + k_{-t}^m)\beta[H^+]}}{2}$$

(2.32)

9.3.3 Quantum yields – equation 2.36

The observed quantum yield is given by the product of the intrinsic quantum yield of the reaction by the efficiency of formation of $\mathbf{AH}^+$. This efficiency is the given by the ratio of rate of the reaction leading to $\mathbf{AH}^+$ by the sum of this process plus the rate of **Ct** formation. This means the hydration and back isomerization processes are not taken into account. k_{out} is also assumed to be very fast. So the formation of $\mathbf{AH}^+$ is given by:

$$\frac{d[AH^{+m}]}{dt} = k_{-h}^m [H^+][B^m] \quad \text{(S72)}$$

and the formation of **Ct** is given by:

$$\frac{d[Ct^m]}{dt} = k_i^m [Cc^m] \quad \text{(S73)}$$

and:

$$\frac{d[B^m]}{dt} = k_{-t}^m [Cc^m] - (k_t^m + k_{-h}^m [H^+])[B^m] \quad \text{(S74)}$$

Now the steady state for **B** is assumed (as seen before, a too strong assumption for the time scale of flash photolysis, but this might not be the case for continuous irradiation).

$$\left[B^m\right] = \frac{k_{-t}{}^m \left[Cc^m\right]}{(k_t{}^m + k_{-h}{}^m \left[H^+\right])} \tag{S75}$$

Substituting on S75 on S72:

$$\frac{d\left[AH^{+m}\right]}{dt} = \frac{k_{-h}{}^m \left[H^+\right] k_{-t}{}^m \left[Cc^m\right]}{(k_t{}^m + k_{-h}{}^m \left[H^+\right])} \tag{S76}$$

Then one can account for the quantum yield:

$$\Phi = \Phi_{Ct^m - Cc^m} \frac{\frac{k_{-h}{}^m \left[H^+\right] k_{-t}{}^m}{(k_t{}^m + k_{-h}{}^m \left[H^+\right])}}{\frac{k_{-h}{}^m \left[H^+\right] k_{-t}{}^m}{(k_t{}^m + k_{-h}{}^m \left[H^+\right])} + k_i{}^m} = \Phi_{Ct^m - Cc^m} \frac{k_{-h}{}^m \left[H^+\right] k_{-t}{}^m}{k_{-h}{}^m \left[H^+\right] k_{-t}{}^m + k_i{}^m (k_t{}^m + k_{-h}{}^m \left[H^+\right])}$$

$$= \Phi_{Ct^m - Cc^m} \frac{k_{-h}{}^m \left[H^+\right] k_{-t}{}^m}{k_{-h}{}^m \left[H^+\right](k_{-t}{}^m + k_i{}^m) + k_t{}^m k_i{}^m} \tag{S77}$$

assuming that $\beta \sim k_{\text{-h}}{}^{\text{m}}$:

$$\Phi = \Phi_{Ct^m - Cc^m} \frac{\beta \left[H^+\right] k_{-t}{}^m}{\beta \left[H^+\right](k_{-t}{}^m + k_i{}^m) + k_t{}^m k_i{}^m} \tag{2.36}$$

In order to confirm the approximations that were made, the same equation was deduced, assuming only steady state for $\mathbf{AH^{+m}}$. In this case, one can write the following set of differential equations:

$$\frac{d\left[AH^+\right]}{dt} = \beta \left[H^+\right]\left[B^m\right] \tag{S78}$$

$$\frac{d\left[Cc^m\right]}{dt} = k_t{}^m \left[B^m\right] - (k_i{}^m + k_{-t}{}^m)\left[Cc^m\right] \tag{S62}$$

$$\frac{d\left[B^m\right]}{dt} = k_{-t}{}^m\left[Cc^m\right] + \left(\frac{k_h{}^m k_{-h}{}^m\left[H^+\right]}{k_h{}^m + k_{out}} - k_t{}^m - k_{-h}{}^m\left[H^+\right]\right)\left[B^m\right] = k_{-t}{}^m\left[Cc^m\right] + d\left[B^m\right] \quad \text{(S79)}$$

On the other hand:

$$\left[AH^{+m}\right] = a_1 e^{-k_{flash}{}^I t} + a_2 e^{-k_{flash}{}^{II} t} + a_3 \quad \text{(S80)}$$

$$\left[B^m\right] = a_4 e^{-k_{flash}{}^I t} + a_5 e^{-k_{flash}{}^{II} t} + a_6 \quad \text{(S81)}$$

$$\left[Cc^m\right] = a_7 e^{-k_{flash}{}^I t} + a_8 e^{-k_{flash}{}^{II} t} + a_9 \quad \text{(S82)}$$

$$\left[Ct^m\right] = a_{10} e^{-k_{flash}{}^I t} + a_{11} e^{-k_{flash}{}^{II} t} + a_{12} \quad \text{(S83)}$$

Two boundary conditions can be written:

t=0 s

$$\left[AH^{+m}\right] = 0 \Rightarrow a_1 + a_2 + a_3 = 0 \quad \text{(S84)}$$

$$\left[B^m\right] = 0 \Rightarrow a_4 + a_5 + a_6 = 0 \quad \text{(S85)}$$

$$\left[Cc^m\right] = \left[Cc^m\right]_{t=0} \quad \text{(S86)}$$

and t = ∞

$$\left[B^m\right] = 0 \Rightarrow a_6 = 0, a_5 = -a_4 \quad \text{(S87)}$$

$$\left[Cc^m\right] = 0 \Rightarrow a_9 = 0, a_8 = \left[Cc^m\right]_{t=0} - a_7 \quad \text{(S88)}$$

Solving equations S80-S82 with these two conditions:

$$\left[AH^{+m}\right] = a_1 e^{-k_{flash}{}^I t} + a_2 e^{-k_{flash}{}^{II} t} + a_3 \quad \text{(S80)}$$

$$\left[B^m\right] = a_4 (e^{-k_{flash}{}^I t} - e^{-k_{flash}{}^{II} t}) \quad \text{(S89)}$$

$$\left[Cc^m\right] = a_7 e^{-k_{flash}{}^I t} + (\left[Cc^m\right]_{t=0} - a_7) e^{-k_{flash}{}^{II} t} \quad \text{(S90)}$$

Deriving these equations:

$$\frac{d\left[AH^{+m}\right]}{dt} = -a_1 k_{flash}{}^I e^{-k_{flash}{}^I t} - a_2 k_{flash}{}^{II} e^{-k_{flash}{}^{II} t} \quad \text{(S91)}$$

$$\frac{d\left[B^m\right]}{dt} = a_4 (-k_{flash}{}^I e^{-k_{flash}{}^I t} + k_{flash}{}^{II} e^{-k_{flash}{}^{II} t}) \quad \text{(S92)}$$

$$\frac{d[Cc^m]}{dt} = -k_{flash}{}^{I} a_7 e^{-k_{flash}{}^{I} t} - k_{flash}{}^{II}([Cc^m]_{t=0} - a_7) e^{-k_{flash}{}^{II} t} \quad \text{(S93)}$$

On the other hand, it is possible to define the mass balance:

$$[Cc^m]_{t=0} = [AH^{+m}] + [B^m] + [Cc^m] + [Ct^m] \quad \text{(S94)}$$

When t = ∞

$$[Cc^m]_{t=0} = [AH^{+m}] + [Ct^m] = a_3 + a_{12} \quad \text{(S95)}$$

And the quantum yield can also de defined as:

$$\Phi = \Phi_{Ct^m - Cc^m} \frac{a_3}{a_3 + a_{12}} = \Phi_{Ct^m - Cc^m} \frac{a_3}{[Cc^m]_{t=0}} \quad \text{(S96)}$$

So, we must only determine a_3. One can equal equations S91 and S78:

$$\beta[H^+] a_4 (e^{-k_{flash}{}^{I} t} - e^{-k_{flash}{}^{II} t}) = -a_1 k_{flash}{}^{I} e^{-k_{flash}{}^{I} t} - a_2 k_{flash}{}^{II} e^{-k_{flash}{}^{II} t} \quad \text{(S97)}$$

From equations S97, two equations can be obtained:

$$\beta[H^+] a_4 = -a_1 k_{flash}{}^{I} \Leftrightarrow a_1 = \frac{-\beta[H^+] a_4}{k_{flash}{}^{I}} \quad \text{(S98)}$$

$$\beta[H^+] a_4 = a_2 k_{flash}{}^{II} \Leftrightarrow a_2 = \frac{\beta[H^+] a_4}{k_{flash}{}^{II}} \quad \text{(S99)}$$

Substituting equations S99 and S98 on S84:

$$\frac{\beta[H^+] a_4}{k_{flash}{}^{I}} - \frac{\beta[H^+] a_4}{k_{flash}{}^{II}} = a_3 \Leftrightarrow a_3 = \frac{\beta[H^+] a_4 (k_{flash}{}^{II} - k_{flash}{}^{I})}{k_{flash}{}^{I} k_{flash}{}^{II}} \quad \text{(S100)}$$

To determine a_4 equations S92 and S79 were used

$$k_{-t}{}^{m}(a_7 e^{-k_{flash}{}^{I} t} + ([Cc^m]_{t=0} - a_7) e^{-k_{flash}{}^{II} t}) + d a_4 (e^{-k_{flash}{}^{I} t} - e^{-k_{flash}{}^{II} t}) = a_4 (-k_{flash}{}^{I} e^{-k_{flash}{}^{I} t} + k_{flash}{}^{II} e^{-k_{flash}{}^{II} t}) \quad \text{(S101)}$$

$$k_{-t}{}^{m} a_7 + d a_4 = -a_4 k_{flash}{}^{I} \Leftrightarrow a_7 = \frac{a_4 (-k_{flash}{}^{I} - d)}{k_{-t}{}^{m}} \quad \text{(S102)}$$

$$k_{-t}{}^{m}[Cc^m]_{t=0} - k_{-t}{}^{m} a_7 = a_4 (k_{flash}{}^{II} + d) \Leftrightarrow [Cc^m]_{t=0} - \frac{a_4 (k_{flash}{}^{II} + d)}{k_{-t}{}^{m}} = a_7 \quad \text{(S103)}$$

$$[Cc^m]_{t=0} - \frac{a_4 (k_{flash}{}^{II} + d)}{k_{-t}{}^{m}} = \frac{a_4 (-k_{flash}{}^{I} - d)}{k_{-t}{}^{m}} \Leftrightarrow \frac{[Cc^m]_{t=0} k_{-t}{}^{m}}{(k_{flash}{}^{II} - k_{flash}{}^{I})} = a_4 \quad \text{(S104)}$$

Substituting S104 on S100,

$$a_3 = \frac{\beta\left[H^+\right]\left[Cc^m\right]_{t=0} k_{-t}{}^m}{k_{flash}{}^I k_{flash}{}^{II}} \tag{S105}$$

And finally the quantum yield (S96) is given by:

$$\Phi = \Phi_{Ct^m - Cc^m} \frac{\beta\left[H^+\right] k_{-t}{}^m}{k_{flash}{}^I k_{flash}{}^{II}} \tag{S106}$$

From equations 2.31 and 2.32 the product of the constants is equal to:

$$k_{flash}{}^I k_{flash}{}^{II} = k_i{}^m k_t{}^m + (k_i{}^m + k_{-t}{}^m)\beta\left[H^+\right] \tag{S107}$$

And equation 2.36 is again obtained:

$$\Phi = \Phi_{Ct^m - Cc^m} \frac{\beta\left[H^+\right] k_{-t}{}^m}{\beta\left[H^+\right](k_{-t}{}^m + k_i{}^m) + k_t{}^m k_i{}^m} \tag{2.36}$$

9.4 Water network of 4'-*N,N*-dimethylamino-7-hydroxyflavylium (DAF)

At very acidic pH values, aminoflavylium cations $\mathbf{AH^+}$ can protonate to form a dipositive flavylium ion $\mathbf{AH_2^{2+}}$. In the particular case of 4'-*N,N*-dimethylamino-7-hydroxyflavylium (**DAF**), the $\mathbf{AH_2^{2+}}$ absorbs at 430 nm and $\mathbf{AH^+}$ at 535 nm, which makes possible to observe a very strong color transition from yellow to pink when the pH is changed from -1 to 2, *see* Figure 1S. The pK_{a+} determined is - 0.24.

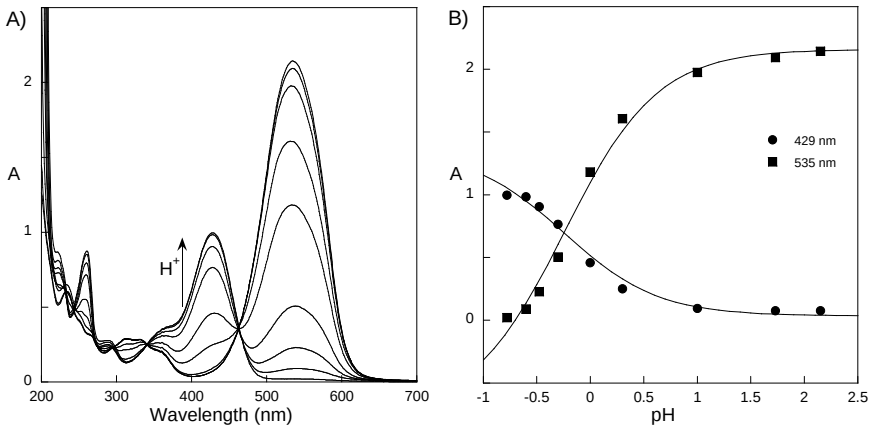

Figure 1S – A) Spectra of solutions of [**DAF**] = $5x10^{-5}$M at 6M, 4M, 3M, 2M, 1M HCl and at pH 1.0, 1.73 and 2.15. B) Fitting of the absorptions at 535 and 429 nm was achieved with pK_{a+} value of - 0.24.

When the pH is increased, deprotonation of the aminoflavylium cation $\mathbf{AH^+}$ to form the quinoidal base **A** takes place. The spectra of both species is highly overlapped making difficult the determination of the pK_a value, *see* Figure 2S. Although the experimental error is significative, a pK_a value around 5.4 ± 0.2, can be determined.

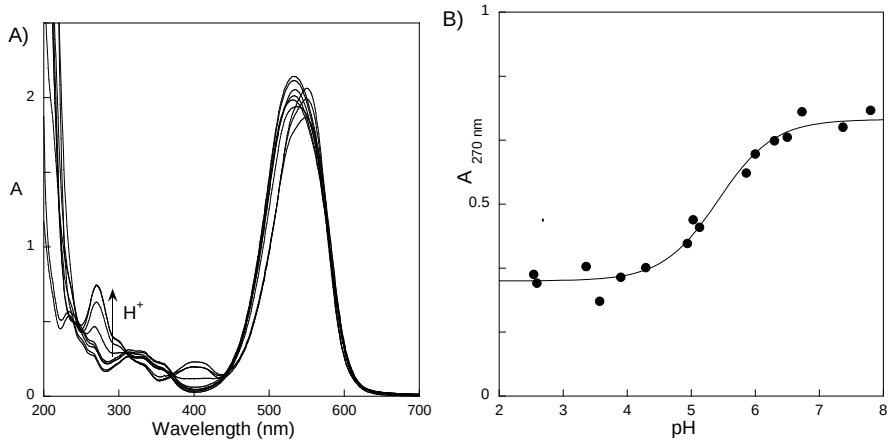

Figure 2S – A) Immediate spectra of solutions of [**DAF**] = $5x10^{-5}$ M after a pH jump from 1 to 4.29,4.94, 5.03, 5.13, 5.86, 6.00, 6.30, 6.50, 6.73, 7.37, 7.80 and 8.20 (not all spectra shown). B) Fitting of the absorptions at 500 nm was achieved with pK_a value of approximately 5.4.

At very basic pH values the thermodynamic stable species are the ionized *trans*-chalcones. If the titration of a dionized chalcone $\mathbf{Ct^{2-}}$ to acidic pH values is performed, the species $\mathbf{Ct^-}$ and **Ct** are obtained, *see* Figure 3S. In this case values of pK_{Ct1} and pK_{Ct2} are 8.1 and

9.6, respectively, *see* Fig 3S. The **Ct** species has maximum absorption at 410 nm and the $\mathbf{Ct}^{2-}$ species at 490 nm.

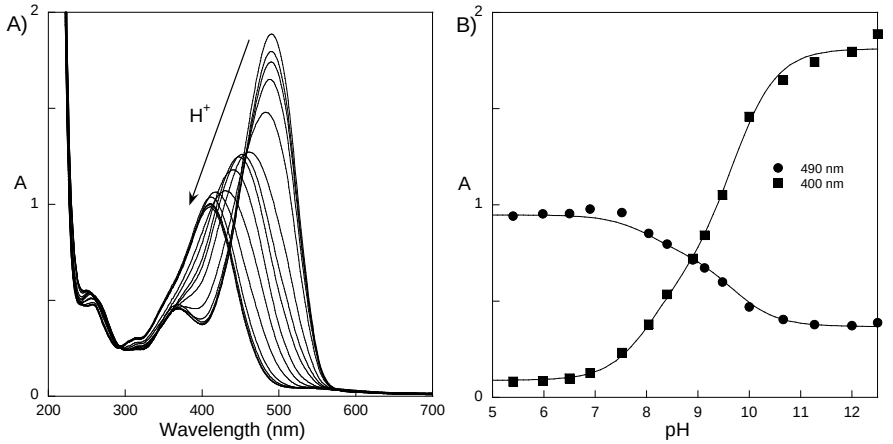

Figure 3S – A) Spectra of solutions of [**DAF**] = $5x10^{-5}$ M from pH 12.5 to pH 4, obtained by successive acidification of the thermally equilibrated solution at pH 12.5. B) Fitting of the absorptions at 400 and 490 nm was achieved with pK_{Ct1} and pK_{Ct2} values of 8.1 and 9.6.

The **Ct** species, in the case of aminoflavylium compounds can also protonate to give a $\mathbf{CtH}^+$ species whose absorption spectrum exhibits a maximum *ca.* 370 nm. However, this not the thermodynamically stable species giving rise to the flavylium ion in water. In order to obtain the respective pK_{Ct+} value, a series of pH jumps from very basic (equilibrated) solutions was performed and the spectra registered immediately after (before significant conversion into $\mathbf{AH}^+$), allowing to obtain an estimative of the pK_{Ct+} of 2.3, Figure 4S.

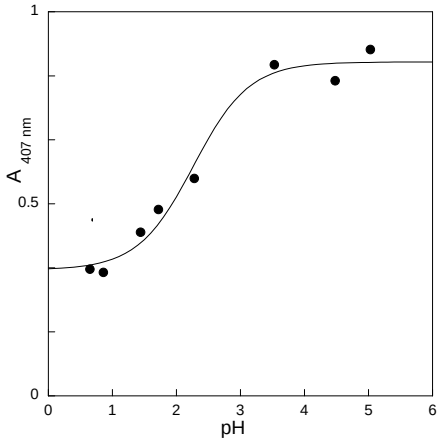

Figure 4S –Fitting of the absorptions at 407 nm (**Ct** species) as a function of the final pH value of a pH jump from a stock solution at pH around 13 was achieved with pK_{Ct+} of 2.3.

The final equilibrated solutions show the presence of two species $\mathbf{AH}^+$ and **Ct**, as well as **A**, thus being possible to define an equilibrium K'_a (eq. 1.26). This **Ct** species presents a great tendency to precipitate in water solutions, and the pK'_a value had to be evaluated in very diluted solutions. This value was determined at room temperature 20 ± 1ºC (pK'_a = 4.4, *see* Figure 5S) and at 60 ºC (pK'_a = 4.2).

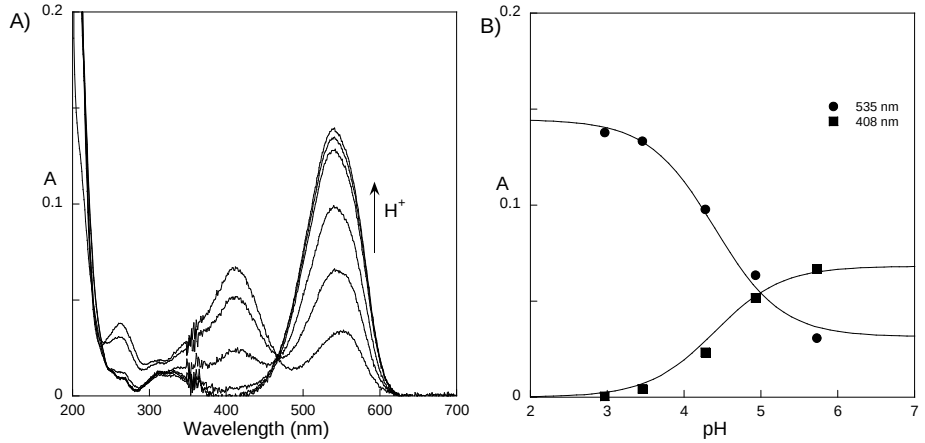

Figure 5S – A) Spectra of equilibrated solutions of [**DAF**] = 3.6×10^{-6} M at pH 2.22, 2.97, 3.46, 4.28, 4.93, 5.73 at room temperature. B) Fitting of the absorptions at 535 and 408 nm was achieved with pK'_a of 4.4.

In order to confirm the previous pK_a (**AH**$^+$/**A**) value a pH jump from 1 to 6.9 was performed and ratio of the amplitudes of the initial and final absorption at 550 nm was found to be 0.159. Taking into account that % A = K_a/K'_a and pK'_a = 4.4, a value of pK_a of 5.2 is obtained, which is in a very reasonable agreement with the experimental data depicted in Figure 2S.

In order to get some insight into the kinetics of the process, the kinetics of pH jumps from a stock solution at very basic pH values (**Ct**$^{2-}$) to acidic pH values were followed at room temperature. The results obtained are plotted in Figure 6S and can be interpreted considering two regimes: i) one that gives the **AH**$^+$ from **Ct** (moderately acidic pH values) and with which a bell shaped curve is predicted, ii) other that gives the **AH**$^+$ from **CtH**$^+$, at very acidic pH values, as was shown before:

$$k_{obs} = \frac{\dfrac{[H^+]}{[H^+]+K_a} k_i K_t K_h + k_{-i}[H^+]}{[H^+]+\dfrac{k_i K_t}{k_{-h}}} + \frac{\dfrac{[H^+]}{[H^+]+K_{Ct+}} k_{-i+}[H^+]}{[H^+]+\dfrac{k_{i+}K_t'}{k_{-h+}}} \qquad (2.14)$$

The expected trend is obtained and it is possible to evaluate the order of magnitude of the kinetics of the process under study, Figure 6S.

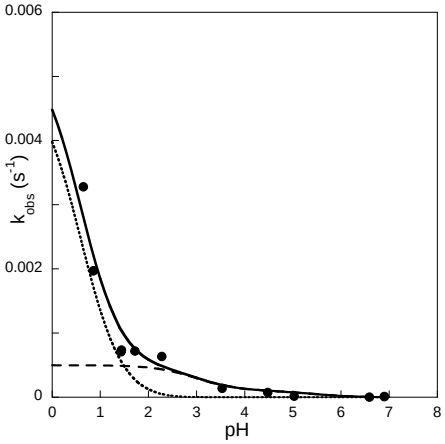

Figure 6S – Kinetics of pH jumps from a stock solution at very basic pH values (**Ct^{2-}**) to acidic pH values were followed at room temperature**.** Fitting, full line, was achieved using eq. 2.14 – pK_{Ct+}=2.3, $k_{-i+} = 5x10^{-3}\ s^{-1}$, $k_{i+}K_{t'}/k_{-h+} = 0.25$ M, p$K_a = 5.45$, $k_iK_tK_h = 1x10^{-7}\ M.s^{-1}$, $k_{-i} = 5x10^{-4}\ s^{-1}$, $k_{-i}K_t/k_{-h} = 1x10^{-3}$ M.

Fluorescence studies were also performed on equilibrated solutions. A fluorescence maximum, when exciting at 540 nm, is obtained at 608 nm that could be due to the flavylium cation or the base. However, the increasing intensity of this fluorescence with increasing pH values discards the **AH^+** emission. The trend of the emission can thus be attributed to the **A** species that is in equilibrium with **Ct**. The observed pK = 4.3 corroborates this interpretation (pK'_a = 4.4), *see* Figure 7S.

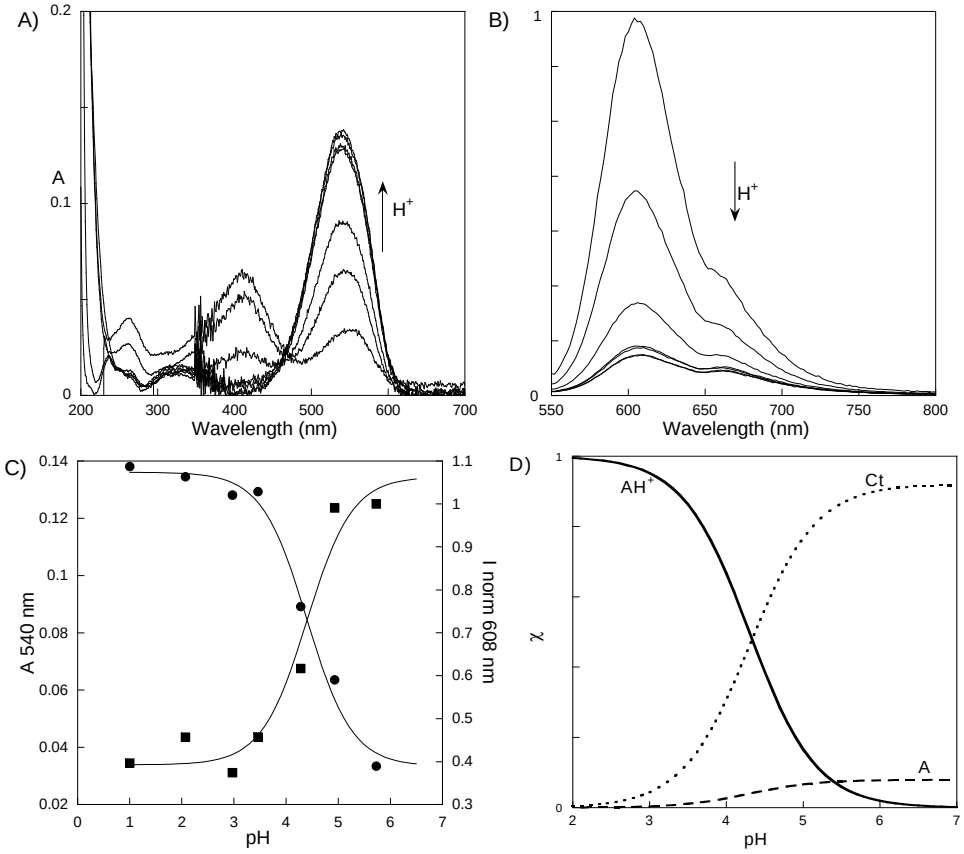

Figure 7S – A) Absorption spectra of equilibrated solutions at pH 1, 2.07, 2.97, 3.46, 4.28, 4.93 and 5.73. B) Emission spectra of the same solutions exciting at 540 nm. C) Plot of the absorbance at 540 nm and intensity of fluorescence versus pH. D) Molar Fractions of **Ct**, **AH^+** and **A** in equilibrium – the low percentage of **A** is responsible for the emission observed.

9.5 Deduction of equations 3.4-3.6.

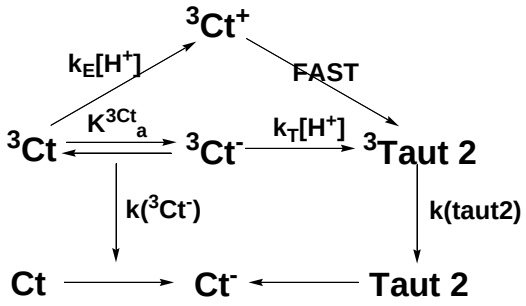

Scheme 3.5

Taking into account Scheme 3.5, the following equations can be written:

$$\frac{d\left(\left[{}^3Ct\right]+\left[{}^3Ct^-\right]\right)}{dt}=-\left[\left(k_E\chi_{{}^3Ct}+k_T\chi_{{}^3Ct^-}\right)\left[H^+\right]+k\left({}^3Ct^-\right)\chi_{{}^3Ct^-}\right]\left(\left[{}^3Ct\right]+\left[{}^3Ct^-\right]\right) \quad \text{(S108)}$$

$$\frac{d\left(\left[{}^3Taut2\right]\right)}{dt}=\left(k_T\chi_{{}^3Ct^-}+k_E\chi_{{}^3Ct}\right)\left[H^+\right]\left(\left[{}^3Ct\right]+\left[{}^3Ct^-\right]\right)-k\left(taut2\right)\left[{}^3Taut2\right] \quad \text{(S109)}$$

Double exponential decays are predicted with this model, with the following decay constants:

$$\kappa_1=\left(k_E\chi_{{}^3Ct}+k_T\chi_{{}^3Ct^-}\right)\left[H^+\right]+k\left({}^3Ct^-\right)\chi_{{}^3Ct^-} \quad \text{(S110)}$$

$$\kappa_2=k\left(taut2\right) \quad \text{(S111)}$$

Now, one can write:

Two boundary conditions can be written:

t=0 s

$$\left(\left[{}^3Ct\right]+\left[{}^3Ct^-\right]\right)=\left(\left[{}^3Ct\right]+\left[{}^3Ct^-\right]\right)_{t=0} \quad \text{(S112)}$$

$$\left[{}^3Taut2\right]=0 \quad \text{(S113)}$$

and t=∞

$$\left(\left[{}^3Ct\right]+\left[{}^3Ct^-\right]\right)=0 \quad \text{(S114)}$$

$$\left[{}^3Taut2\right]=0 \quad \text{(S115)}$$

Based on these boundary conditions, one can write:

$$\left(\left[{}^3Ct\right]+\left[{}^3Ct^-\right]\right)=a_1e^{-\kappa_1t}+\left(\left(\left[{}^3Ct\right]+\left[{}^3Ct^-\right]\right)_{t=0}-a_1\right)e^{-\kappa_2t} \quad \text{(S116)}$$

$$\left[{}^3Taut2\right]=a_4\left(e^{-\kappa_1t}-e^{-\kappa_2t}\right) \quad \text{(S117)}$$

The problem is therefore greatly simplified, and the task is now to find a_1 and a_4. Differentiating equations S116 and S117, one obtains:

$$\frac{d\left(\left[{}^3Ct\right]+\left[{}^3Ct^-\right]\right)}{dt} = -a_1\kappa_1 e^{-\kappa_1 t} - \left(\left(\left[{}^3Ct\right]+\left[{}^3Ct^-\right]\right)_{t=0} - a_1\right)\kappa_2 e^{-\kappa_2 t} \tag{S118}$$

$$\frac{d\left[{}^3Taut2\right]}{dt} = a_4\left(-\kappa_1 e^{-\kappa_1 t} + \kappa_2 e^{-\kappa_2 t}\right) \tag{S119}$$

Taking equations S108, S116, S118, S109 and S117 the following equations may be written:

$$-a_1\kappa_1 e^{-\kappa_1 t} - \left(\left(\left[{}^3Ct\right]+\left[{}^3Ct^-\right]\right)_{t=0} - a_1\right)\kappa_2 e^{-\kappa_2 t} = -\kappa_1\left[a_1 e^{-\kappa_1 t} + \left(\left(\left[{}^3Ct\right]+\left[{}^3Ct^-\right]\right)_{t=0} - a_1\right)e^{-\kappa_2 t}\right] \tag{S120}$$

$$a_4\left(-\kappa_1 e^{-\kappa_1 t} + \kappa_2 e^{-\kappa_2 t}\right) = \left(k_T\chi_{{}^3Ct^-} + k_E\chi_{{}^3Ct}\right)\left[H^+\right]\left[a_1 e^{-\kappa_1 t} + \left(\left(\left[{}^3Ct\right]+\left[{}^3Ct^-\right]\right)_{t=0} - a_1\right)e^{-\kappa_2 t}\right] - \kappa_2 a_4\left(e^{-\kappa_1 t} - e^{-\kappa_2 t}\right) \tag{S121}$$

Equation S120 does not lead to a solution for a_1. But from equation S121 two equations can be written:

$$-a_4\kappa_1 = \left(k_T\chi_{{}^3Ct^-} + k_E\chi_{{}^3Ct}\right)\left[H^+\right]a_1 - \kappa_2 a_4 \tag{S122}$$

$$a_4\kappa_2 = \left(k_T\chi_{{}^3Ct^-} + k_E\chi_{{}^3Ct}\right)\left[H^+\right]\left(\left(\left[{}^3Ct\right]+\left[{}^3Ct^-\right]\right)_{t=0} - a_1\right) + \kappa_2 a_4 \tag{S123}$$

The solutions are:

$$a_1 = \left(\left[{}^3Ct\right]+\left[{}^3Ct^-\right]\right)_{t=0} \tag{S124}$$

$$a_4 = \frac{\left(k_T\chi_{{}^3Ct^-} + k_E\chi_{{}^3Ct}\right)\left[H^+\right]}{\left(\kappa_2 - \kappa_1\right)}\left(\left[{}^3Ct\right]+\left[{}^3Ct^-\right]\right)_{t=0} \tag{S125}$$

The solution becomes:

$$a_4 = -\alpha\left(\left[{}^3Ct\right]+\left[{}^3Ct^-\right]\right)_{t=0} \tag{S126}$$

If α is defined:

$$\alpha = \frac{\left(k_T\chi_{{}^3Ct^-} + k_E\chi_{{}^3Ct}\right)\left[H^+\right]}{\left(\kappa_1 - \kappa_2\right)} = \frac{\left(k_T\chi_{{}^3Ct^-} + k_E\chi_{{}^3Ct}\right)\left[H^+\right]}{\left(\left(k_E\chi_{{}^3Ct} + k_T\chi_{{}^3Ct^-}\right)\left[H^+\right] + k\left({}^3Ct^-\right)\chi_{{}^3Ct^-} - k\left(taut2\right)\right)} \tag{S127}$$

The molar fractions can be given by:

$$\chi_{{}^3Ct} = \frac{\left[H^+\right]}{\left[H^+\right] + K_a^{{}^3Ct}} \tag{S128}$$

$$\chi_{^3Ct^-} = \frac{K_a^{^3Ct}}{\left[H^+\right] + K_a^{^3Ct}} \tag{S129}$$

So α is given by equation 3.6 in the text:

$$\alpha = \frac{\left[H^+\right]^2 + \frac{k_T K_a^{^3Ct}}{k_E}\left[H^+\right]}{\left[H^+\right]^2 + \left(\frac{k_T K_a^{^3Ct}}{k_E} - \frac{k(taut2)}{k_E}\right)\left[H^+\right] + \frac{K_a^{^3Ct}}{k_E}\left(k\left({}^3Ct^-\right) - k(taut2)\right)} \tag{3.6}$$

And now it is possible to write the final solutions of equation S116 and S117:

$$\left(\left[{}^3Ct\right] + \left[{}^3Ct^-\right]\right) = \left(\left[{}^3Ct\right] + \left[{}^3Ct^-\right]\right)_{t=0} e^{-\kappa_1 t} \tag{S130}$$

$$\left[{}^3Taut2\right] = \alpha\left(\left[{}^3Ct\right] + \left[{}^3Ct^-\right]\right)_{t=0}\left(e^{-\kappa_2 t} - e^{-\kappa_1 t}\right) \tag{S131}$$

Equation S130 can now be splitted:

$$\left[{}^3Ct\right] = \chi_{^3Ct}\left(\left[{}^3Ct\right] + \left[{}^3Ct^-\right]\right)_{t=0} e^{-\kappa_1 t} = \frac{\left[H^+\right]}{\left[H^+\right] + K_a^{^3Ct}}\left(\left[{}^3Ct\right] + \left[{}^3Ct^-\right]\right)_{t=0} e^{-\kappa_1 t} \tag{S132}$$

$$\left[{}^3Ct^-\right] = \chi_{^3Ct^-}\left(\left[{}^3Ct\right] + \left[{}^3Ct^-\right]\right)_{t=0} e^{-\kappa_1 t} = \frac{K_a^{^3Ct}}{\left[H^+\right] + K_a^{^3Ct}}\left(\left[{}^3Ct\right] + \left[{}^3Ct^-\right]\right)_{t=0} e^{-\kappa_1 t} \tag{S133}$$

In Laser Flash Photolysis experiments, however, one obtains transient absorptions at several monitoring wavelengths. So one must write:

$$\Delta A_\lambda = \Delta\varepsilon_{^3Ct\lambda}\left[{}^3Ct\right] + \Delta\varepsilon_{^3Ct^-\lambda}\left[{}^3Ct^-\right] + \Delta\varepsilon_{^3Taut2\lambda}\left[{}^3Taut2\right] \tag{S134}$$

Substituting equations S133, S132 and S131, one obtains equations 3.4 and 3.5:

$$\begin{aligned}\Delta A_\lambda = {} & \Delta\varepsilon_{^3Ct\lambda}\frac{\left[H^+\right]}{\left[H^+\right] + K_a^{^3Ct}}\left(\left[{}^3Ct\right] + \left[{}^3Ct^-\right]\right)_{t=0} e^{-\kappa_1 t} + \Delta\varepsilon_{^3Ct^-\lambda}\frac{K_a^{^3Ct}}{\left[H^+\right] + K_a^{^3Ct}}\left(\left[{}^3Ct\right] + \left[{}^3Ct^-\right]\right)_{t=0} e^{-\kappa_1 t} \\ & - \Delta\varepsilon_{^3Taut2\lambda}\alpha\left(\left[{}^3Ct\right] + \left[{}^3Ct^-\right]\right)_{t=0} e^{-\kappa_1 t} + \Delta\varepsilon_{^3Taut2\lambda}\alpha\left(\left[{}^3Ct\right] + \left[{}^3Ct^-\right]\right)_{t=0} e^{-\kappa_2 t}\end{aligned} \tag{S135}$$

So the amplitudes:

$$a_{1\lambda} = \left(\left[{}^3Ct\right] + \left[{}^3Ct^-\right]\right)_{t=0}\left(\Delta\varepsilon_{^3Ct\lambda}\frac{\left[H^+\right]}{\left[H^+\right] + K_a^{^3Ct}} + \Delta\varepsilon_{^3Ct^-\lambda}\frac{K_a^{^3Ct}}{\left[H^+\right] + K_a^{^3Ct}} e^{-\kappa_1 t} - \Delta\varepsilon_{^3Taut2\lambda}\alpha\right) \tag{3.4}$$

$$a_{\lambda 2} = \left(\left[{}^3Ct\right] + \left[{}^3Ct^-\right]\right)_{t=0}\Delta\varepsilon_{^3Taut2\lambda}\alpha \tag{3.5}$$

9.6 Association constant - deduction of equation 5.1.

Consider the formation of a complex *RS* from receptor *R* and substrate *S*:

$$R + S \rightleftharpoons RS \tag{S136}$$

So the association constant *K* will be given by:

$$K = \frac{[RS]}{[R][S]} \tag{S137}$$

And the emission *I* (or absorbance) at each point of the titration, if followed at the substrate's emission, will be given by:

$$I = I_0 + (I_{\lim} - I_0)\frac{[RS]}{[S_0]} \tag{S138}$$

where I_0 is the emission intensity of substrate (the flavylium in the absence of host), $I_{\lim}$ is the emission intensity of the complex (of the flavylium salt with clip), *S* refers to the substrate (flavylium salt), *R* to the receptor (clip)**,** and *K* is the association constant.
It is necessary to determine [RS]. Considering the mass balances:

$$[R_0] = [R] + [RS] \Leftrightarrow [R_0] = \frac{[RS]}{K[S]} + [RS] \tag{S139}$$

$$[S_0] = [S] + [RS] \Leftrightarrow [S] = [S_0] - [RS] \tag{S140}$$

Substituting S140 on S139:

$$[R_0] = \frac{[RS]}{K([S_0] - [RS])} + [RS] \Leftrightarrow [RS]^2 - (\frac{1}{K} + [S_0] + [R_0])[RS] + [R_0][S_0] = 0 \tag{S141}$$

Solving the quadratic equation and substituting on S138, one obtains equation 5.1:

$$I = I_0 + (I_{\lim} - I_0) \times \frac{([R]_0 + [S]_0 + 1/K) - \sqrt{([R]_0 + [S]_0 + 1/K)^2 - 4[R]_0[S]_0}}{2[S]_0} \tag{5.1}$$